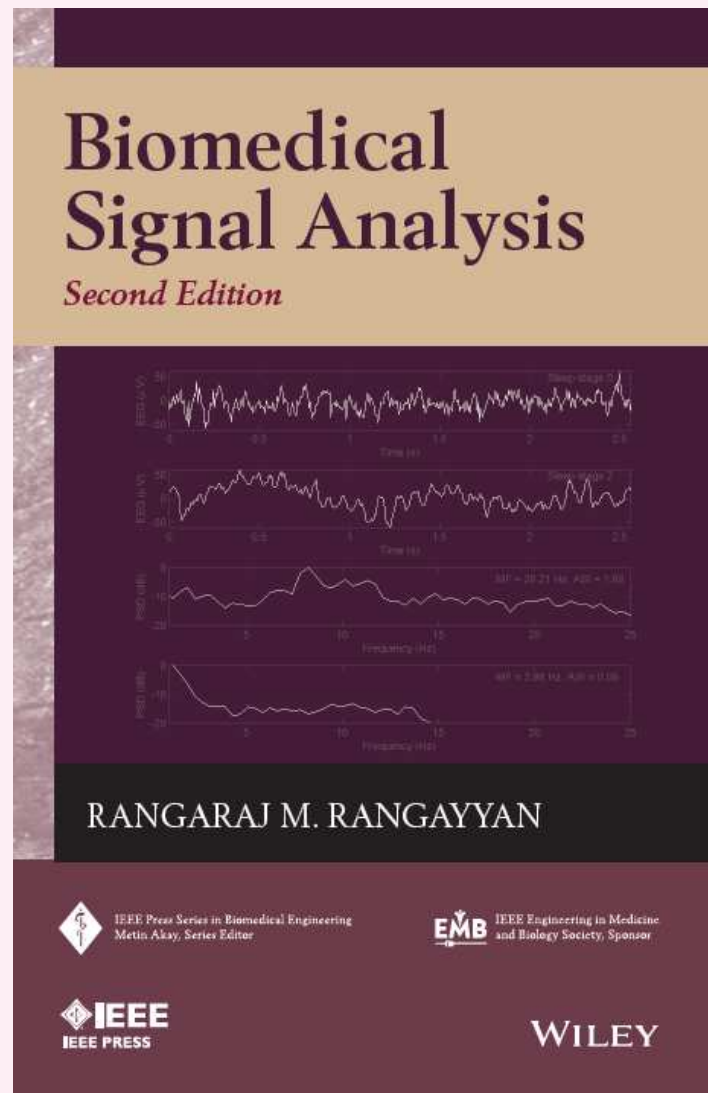# BIOMEDICAL SIGNAL ANALYSIS

Rangaraj M. Rangayyan

Professor
Department of Electrical and Computer Engineering
Schulich School of Engineering
Adjunct Professor, Departments of Surgery and Radiology
University of Calgary
Calgary, Alberta, Canada T2N 1N4

Phone: +1 (403) 220-6745
e-mail: ranga@ucalgary.ca

Web: `http://people.ucalgary.ca/~ranga/enel563`

Biomedical Signal Analysis

Second Edition

RANGARAJ M. RANGAYYAN

IEEE/ Wiley, New York, NY, 2nd Edition, 2015
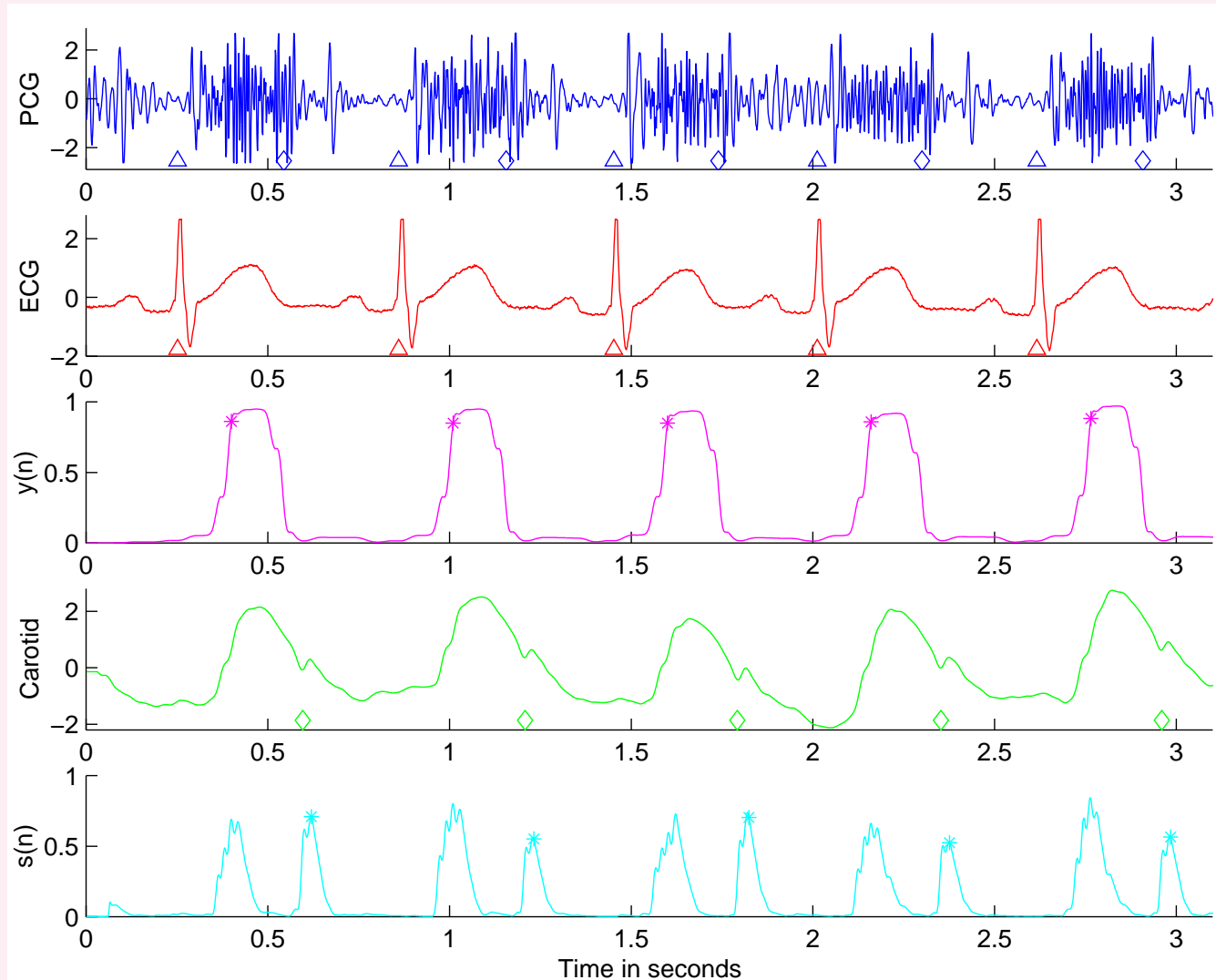
Illustration of various stages of
biomedical signal processing and analysis

18   CHAPTER 1. INTRODUCTION TO BIOMEDICAL SIGNALS

1.2 Examples of Biomedical Signals

1.2.1 The action potential

The action potential (AP) is the electrical signal that accompanies

the mechanical contraction of a single cell when

stimulated by an electrical current (neural or external).

Cause: flow of sodium (Na^+), potassium (K^+), chloride (Cl^-),

and other ions across the cell membrane.

- The nature of biomedical signals
- Examples of biomedical signals
- Resting potential
- Depolarization
- Repolarization
- The electroneurogram

08:05 / 42:04

Video of course given at
Ragnar Granit Institute of Biomedical Engineering
Tampere University of Technology, Tampere, Finland
www.evicab.eu
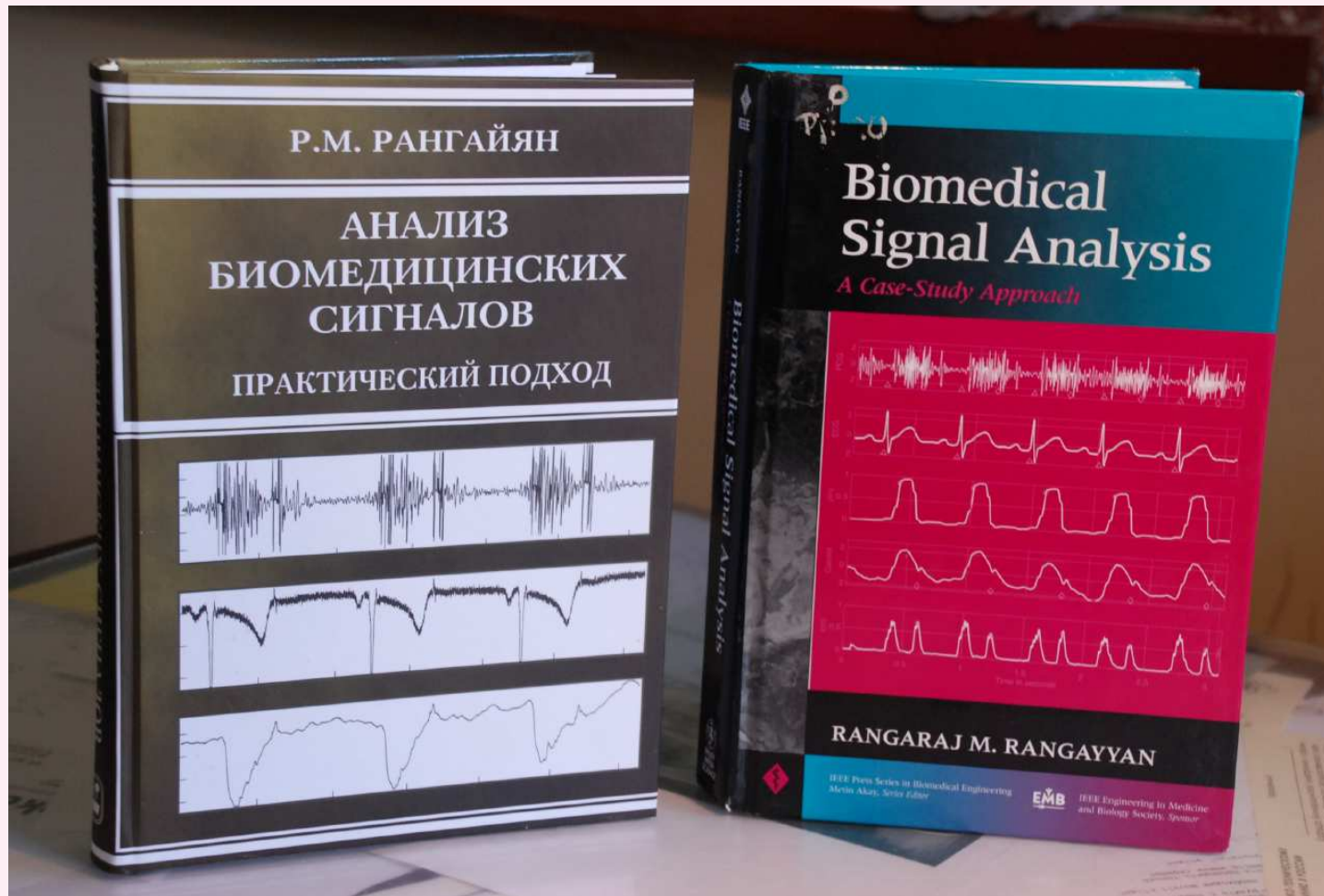
Russian translation of 1st Edition by A. Kalinichenko, 2007
Physmathlit, Moscow, Russia

4

Detection of Events

Biomedical signals carry signatures of physiological events.

Epoch: part of a signal related to a specific event.

The analysis of a signal requires the identification of epochs and investigation of the corresponding events.

4.1   Problem Statement

Given a biomedical signal, identify discrete signal epochs and correlate them with events in the related physiological process.

Solution: Development of signal processing techniques to

emphasize, detect, segment, and analyze epochs.

4.2   Illustration of the Problem with Case Studies

4.2.1   The P, QRS, and T waves in the ECG

Epochs in an ECG waveform:

- **The P wave:**

  Contraction of the atria triggered by the SA node.

- **The PQ segment:**

  AV node provides delay to facilitate completion of atrial contraction and transfer of blood to ventricles before ventricular contraction is initiated.

  Normally flat or isoelectric.

- **The QRS wave:**

  Purkinje fibers stimulate contraction of ventricles.

- **The ST segment:**

  Normally flat or isoelectric – related to the plateau

  in the action potential of ventricular muscle cells.

  Myocardial ischemia or infarction could change the

  action potentials of ventricular muscle cells:

  ST segment depressed or elevated.

- **The T wave:**

  Related to the last phase of the

  action potential of ventricular muscle cells:

  ventricular repolarization or relaxation.

4.2.2   The first and second heart sounds

- **The first heart sound S1:**

  S1 reflects a sequence of events related to

  ventricular contraction —

  closure of the atrioventricular valves,

  isovolumic contraction,

  opening of the semilunar valves, and

  ejection of the blood from the ventricles.

- **The second heart sound S2:**

  S2 is related to the end of ventricular contraction —

  closure of the aortic and pulmonary valves (A2 and P2).

- **Murmurs:**

  Systolic murmur of aortic stenosis —

  turbulent ejection of blood from the left ventricle

  through a restricted opening of the aortic valve.

  Diastolic murmur in case of aortic insufficiency —

  regurgitation of blood from the aorta back into the

  left ventricle through a leaky aortic valve.

4.2.3 *The dicrotic notch in the carotid pulse*

Closure of the aortic valve causes a sudden drop in

aortic pressure on a downward slope at end of systole.

Dicrotic notch in the carotid pulse is a delayed, upstream

manifestation of the incisura in the aortic pressure wave.

4.2.4 EEG rhythms, waves, and transients

EEG rhythms: α, β, δ, θ, and γ waves.

Additional waves and events:

- **K-complex:** transient waveform with slow waves,
  sometimes associated with sharp components,
  often followed by $14\ Hz$ waves.
  Occurs spontaneously or in response to a sudden stimulus
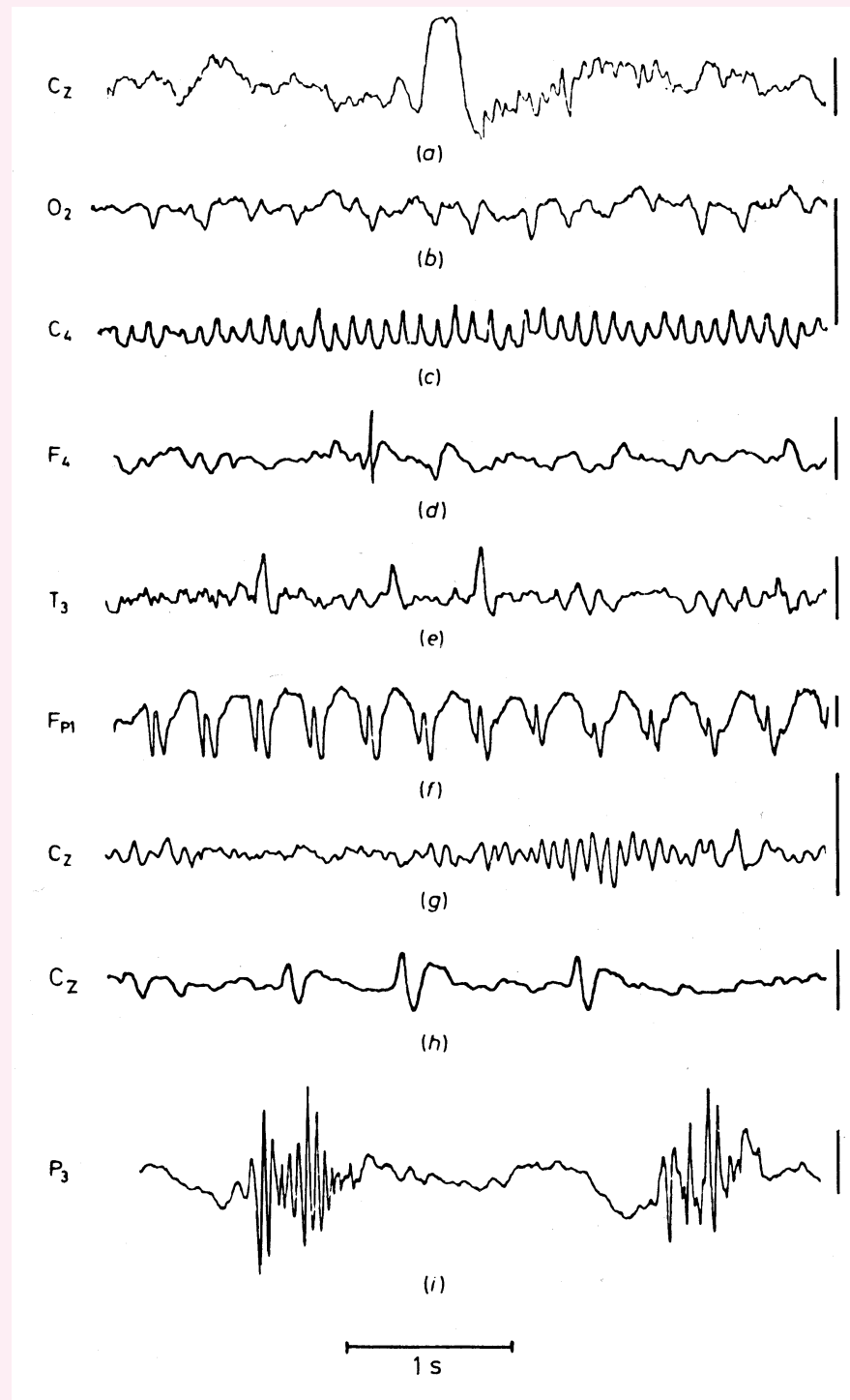 during sleep; amplitude $\sim 200\ \mu V$.

Figure 4.1: From top to bottom: (a) the K-complex; (b) the lambda wave; (c) the mu rhythm; (d) a spike; (e) sharp waves; (f) spike-and-wave complexes; (g) a sleep spindle; (h) vertex sharp waves; and (i) polyspike discharges. The horizontal bar at the bottom indicates a duration of $1\ s$; the vertical bars at the right indicate $100\ \mu V$. Reproduced with permission from R. Cooper, J.W. Osselton, and J.C. Shaw, EEG Technology, 3rd Edition, 1980. ©Butterworth Heinemann Publishers, a division of Reed Educational & Professional Publishing Ltd., Oxford, UK.

- **Lambda waves:** monophasic, positive, sharp waves;

  occur in the occipital location with amplitude $< 50\ \mu V$.

  Related to eye movement;

  associated with visual exploration.

- **Mu rhythm:** group of waves, $7 - 11\ Hz$,

  arcade or comb shape in the central location.

  Amplitude $< 50\ \mu V$.

  Attenuated by contralateral movement,

  thought of movement,

  readiness to move, or tactile stimulation.

- **Spike:** transient with a pointed peak, duration $20 - 30 \ ms$.

- **Sharp wave:** transient with a pointed peak,
  longer duration than a spike of $70 - 200 \ ms$.

- **Spike-and-wave rhythm:** sequence of surface-negative
  slow waves, $2.5 - 3.5 \ Hz$,
  spike associated with each wave.
  Spike amplitude up to $1,000 \ \mu V$ in each complex.

- **Sleep spindle:** episodic rhythm, $14\ Hz$, $50\ \mu V$, occurring maximally over the frontocentral regions during certain stages of sleep.

- **Vertex sharp transient** or **V-wave:**

  sharp potential maximal at the vertex at about $300\ \mu V$, negative in relation to the EEG in other areas.

  Occurs spontaneously during sleep or

  in response to a sensory stimulus during sleep

  or wakefulness.

EEG record is described in terms of:

- most persistent rhythm (for example, α);

- presence of other rhythmic features,
  such as δ, θ, or β;

- discrete features of relatively long duration,
  such as an episode of spike-and-wave activity;

- discrete features of relatively short duration,
  such as isolated spikes or sharp waves;

- activity remaining when all of the above
  have been described: background activity; and

- artifacts; ambiguity in interpretation.

Each EEG wave or activity is described

in chronological sequence in terms of amplitude;

frequency, in the case of rhythmic features;

waveform, for both rhythmic and transient features;

location or spatial distribution;

incidence or temporal variability;

right – left symmetry in location of activity;

responsiveness to stimuli, e.g., eye opening and closure.

EEG record at rest is first described as above;

the effects of evocative techniques

are then specified in the same terms.

Behavioral changes, such as the subject

becoming drowsy or falling asleep, are also noted.

4.3 Detection of Events and Waves

4.3.1 Derivative-based methods for QRS detection

Problem: *Develop signal processing techniques*

to facilitate detection of the QRS complex,

given that it is the sharpest wave in an ECG cycle.

■ ■ ■ ■ ■

Solution 1: QRS complex has the largest slope

or rate of change of voltage in a cardiac cycle —

rapid conduction and depolarization of the ventricles.

Rate of change: derivative operator $\frac{d}{dt}$.

The derivative operator enhances the QRS;

the result has no resemblance to a typical QRS complex.

The slow P and T waves are suppressed.

Result is noisy: significant smoothing required.

Algorithm of Balda et al. for QRS detection:

Smoothed three-point first derivative $y_0(n)$

of the given signal $x(n)$ approximated as

$$y_0(n) = |x(n) - x(n-2)|. \qquad (4.1)$$

The second derivative approximated as

$$y_1(n) = |x(n) - 2x(n-2) + x(n-4)|. \qquad (4.2)$$

The two results are weighted and combined to obtain

$$y_2(n) = 1.3\, y_0(n) + 1.1\, y_1(n). \qquad (4.3)$$

The result $y_2(n)$ is scanned with a threshold of 1.0.

Whenever threshold is crossed, the subsequent eight

samples are also tested against the same threshold.

If at least six of the eight points pass the threshold test,

the segment of eight samples taken to be a part of a QRS.

Result: pulse with width proportional to QRS width.

Illustration of application: Figure 4.2.

Two cycles of a filtered version of the

ECG signal shown in Figure 3.5:

eighth-order Butterworth lowpass filter, $f_c = 90 \ Hz$,

down-sampled by a factor of five,

notch filter with $f_o = 60 \ Hz$.

Effective sampling rate is $200 \ Hz$.

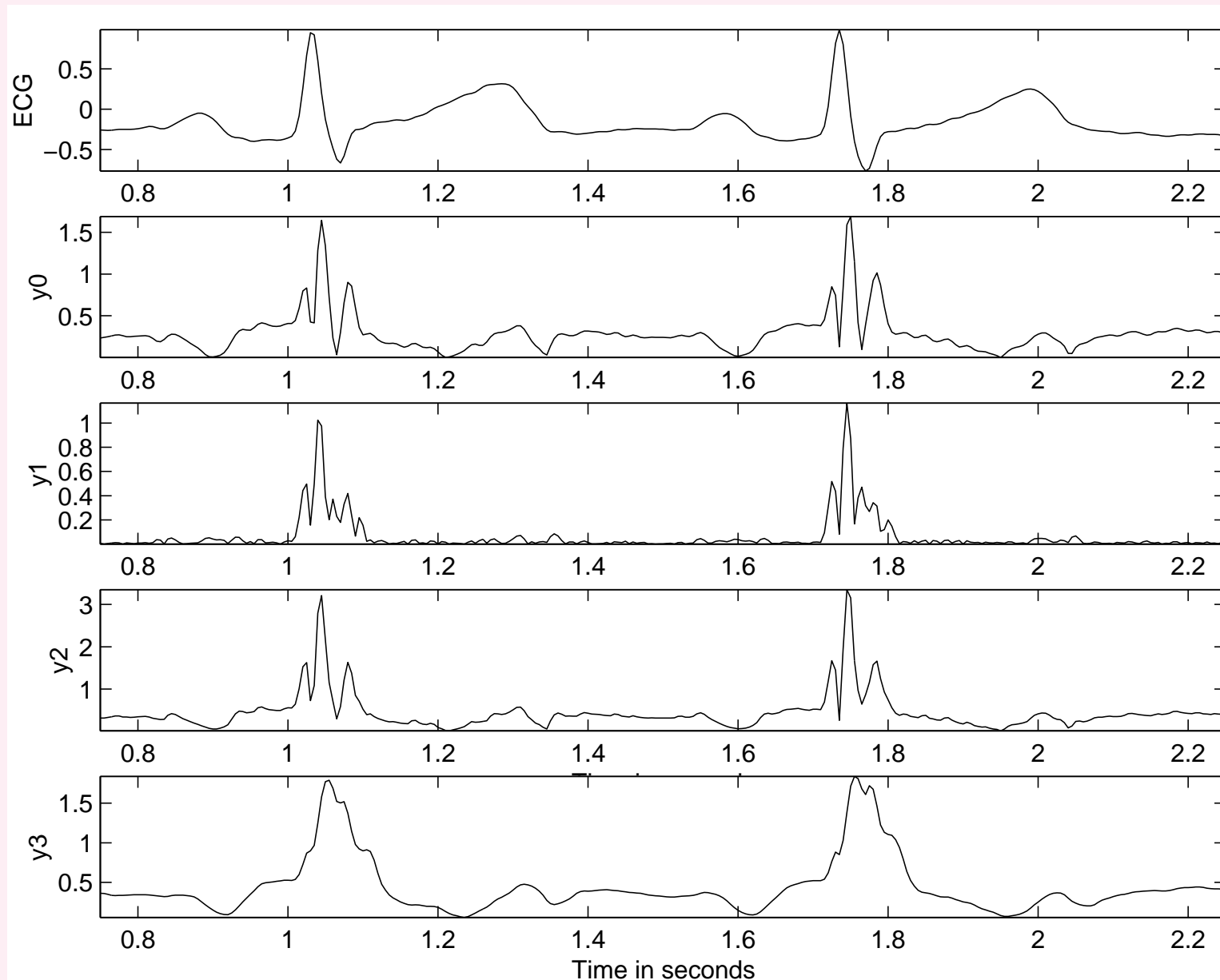Signal normalized by dividing by its maximum value.

Figure 4.2: From top to bottom: two cycles of a filtered version of the ECG signal shown in Figure 3.5; output $y_0(n)$ of the first-derivative-based operator in Equation 4.1; output $y_1(n)$ of the second-derivative-based operator in Equation 4.2; the combined result $y_2(n)$ from Equation 4.3; and the result $y_3(n)$ of passing $y_2(n)$ through the 8-point MA filter in Equation 3.107.

Solution 2:

Algorithm of Murthy and Rangaraj —

squared first-derivative and MA filter.

$$g_1(n) = \sum_{i=1}^{N} |x(n-i+1) - x(n-i)|^2 \, (N-i+1), \quad (4.4)$$

$$g(n) = \frac{1}{M} \sum_{j=0}^{M-1} g_1(n-j). \quad (4.5)$$

Sampling rate $100 \, Hz$, $M = N = 8$.

Peak-searching algorithm:

1. Scan a portion of the signal $g(n)$ expected to contain a peak; determine maximum value $g_{\max}$.

2. Define a threshold as a fraction of the maximum, for example, $Th = 0.5\ g_{\max}$.

3. For all $g(n) > Th$, select those samples for which the corresponding $g(n)$ values are greater than a predefined number M of preceding and succeeding samples of $g(n)$:

$$\{p\} = [\ n\ |\ g(n) > Th\ ]\ AND \hspace{2cm} (4.6)$$
$$[\ g(n) > g(n-i), i = 1, 2, \ldots, M\ ]\ AND$$
$$[\ g(n) > g(n+i), i = 1, 2, \ldots, M\ ].$$

The set $\{p\}$ contains the indices of the peaks in $g(n)$.

Illustration of application: Figure 4.3.

Two cycles of a filtered version of the

ECG signal shown in Figure 3.5:

eighth-order Butterworth lowpass filter, $f_c = 40\ Hz$,

down-sampled by a factor of ten.

Effective sampling rate is $100\ Hz$.

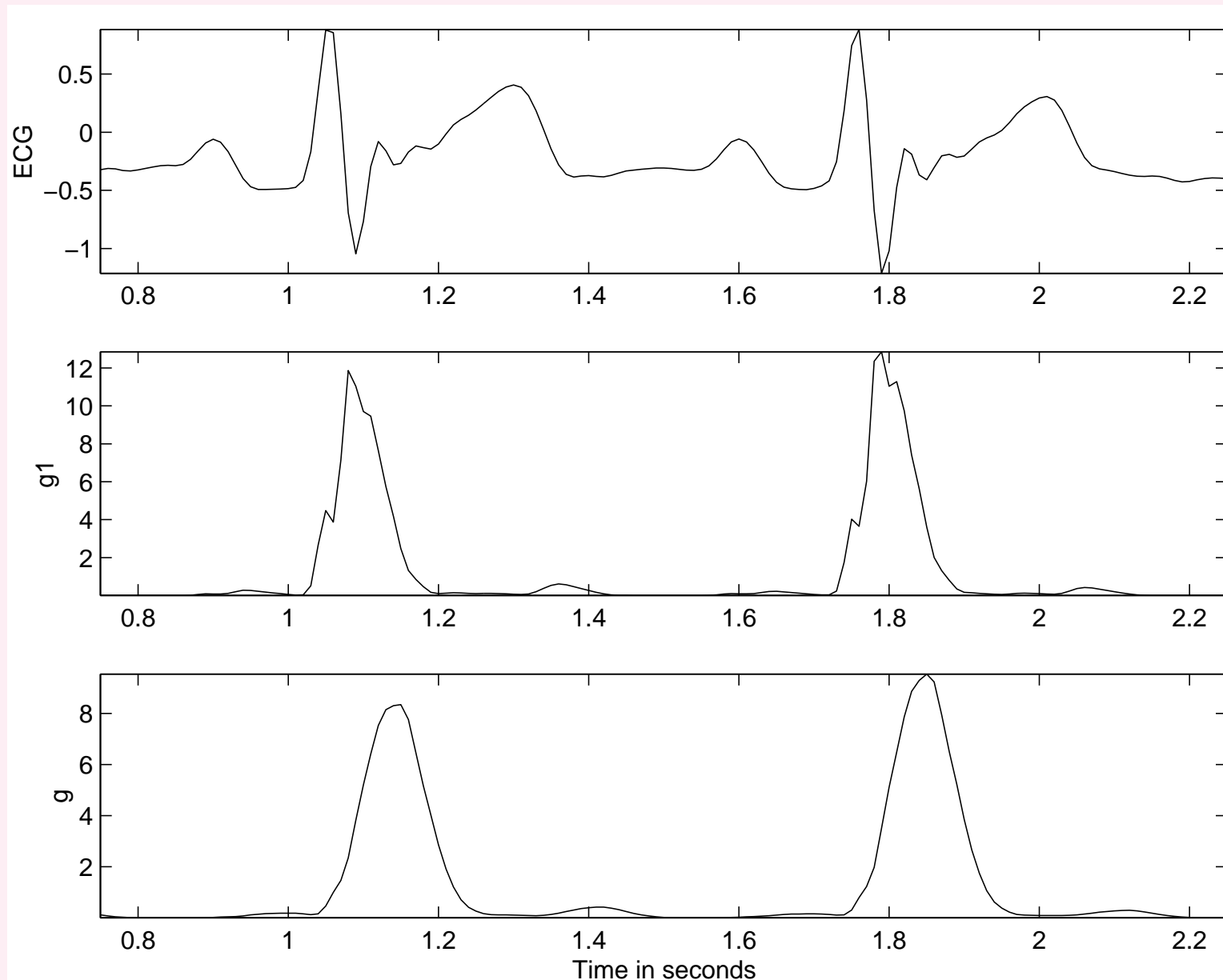Signal normalized by dividing by its maximum value.

Figure 4.3: From top to bottom: two cycles of a filtered version of the ECG signal shown in Figure 3.5; output $g_1(n)$ of the weighted and squared first-derivative operator in Equation 4.4; output $g(n)$ of the smoothing filter in Equation 4.5.

4.3.2 The Pan–Tompkins algorithm for QRS detection

Problem: *Propose an algorithm to detect QRS complexes in an ongoing ECG signal.*

Solution: Pan–Tompkins real-time QRS detector.

Analysis of slope, amplitude, and width of QRS complexes.

Algorithm includes a series of filters and methods:

lowpass, highpass, derivative, squaring, integration,

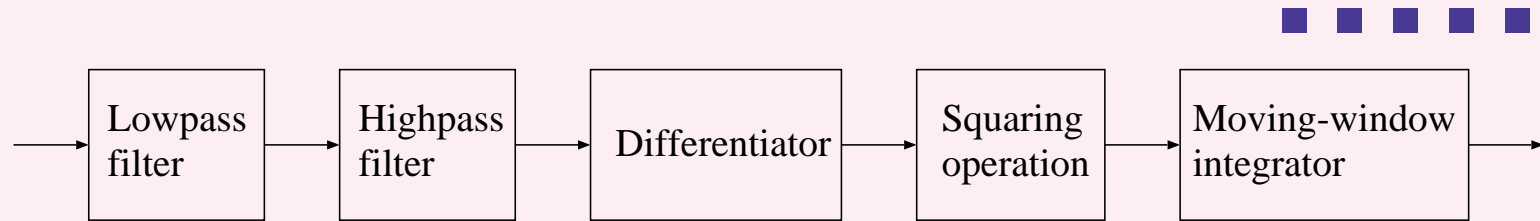adaptive thresholding, and search procedures.

Figure 4.4: Block diagram of the Pan–Tompkins algorithm for QRS detection.

Lowpass filter: Recursive filter with integer coefficients.

$$H(z) = \frac{1}{32} \frac{(1 - z^{-6})^2}{(1 - z^{-1})^2}. \qquad (4.7)$$

$$y(n) = 2y(n-1) - y(n-2) + \frac{1}{32}\left[x(n) - 2x(n-6) + x(n-12)\right].$$
$$(4.8)$$

Sampling rate $200\ Hz$, $f_c = 11\ Hz$,

delay of 5 samples or $25\ ms$.

Attenuation greater than $35\ dB$ at $60\ Hz$,

effectively suppresses power-line interference.

Highpass filter: allpass filter minus a lowpass filter.

Lowpass component:

$$H_{lp}(z) = \frac{(1 - z^{-32})}{(1 - z^{-1})} \; ; \qquad (4.9)$$

$$y(n) = y(n-1) + x(n) - x(n-32). \qquad (4.10)$$

Transfer function $H_{hp}(z)$ of the highpass filter:

$$H_{hp}(z) = z^{-16} - \frac{1}{32} \, H_{lp}(z) \, . \qquad (4.11)$$

Output $p(n)$ of the highpass filter:

$$p(n) = x(n-16) - \frac{1}{32}\left[y(n-1) + x(n) - x(n-32)\right], \quad (4.12)$$

$x(n)$ and $y(n)$ related as in Equation 4.10.

Input–output relationship of the overall highpass filter:

$$p(n) = p(n-1) - \frac{1}{32}x(n) + x(n-16) - x(n-17) + \frac{1}{32}x(n-32). \quad (4.13)$$

Highpass cutoff $5\ Hz$, delay of $80\ ms$.

Derivative operator:

$$y(n) = \frac{1}{8} \left[2x(n) + x(n-1) - x(n-3) - 2x(n-4) \right]. \quad (4.14)$$

Approximates the ideal $\frac{d}{dt}$ operator up to $30\ Hz$.

Suppresses the low-frequency components of P and T,

provides a large gain to the high-frequency components

arising from the high slopes of the QRS complex.

Squaring: makes the result positive and emphasizes

large differences resulting from QRS complexes;

small differences from P and T waves are suppressed.

Nonlinear operation.

Integration:

Output of a derivative-based operation will exhibit

multiple peaks within the duration of a single QRS complex.

Smoothing with a moving-window integration filter:

$$y(n) = \frac{1}{N}\left[x(n-(N-1)) + x(n-(N-2)) + \cdots + x(n)\right].$$
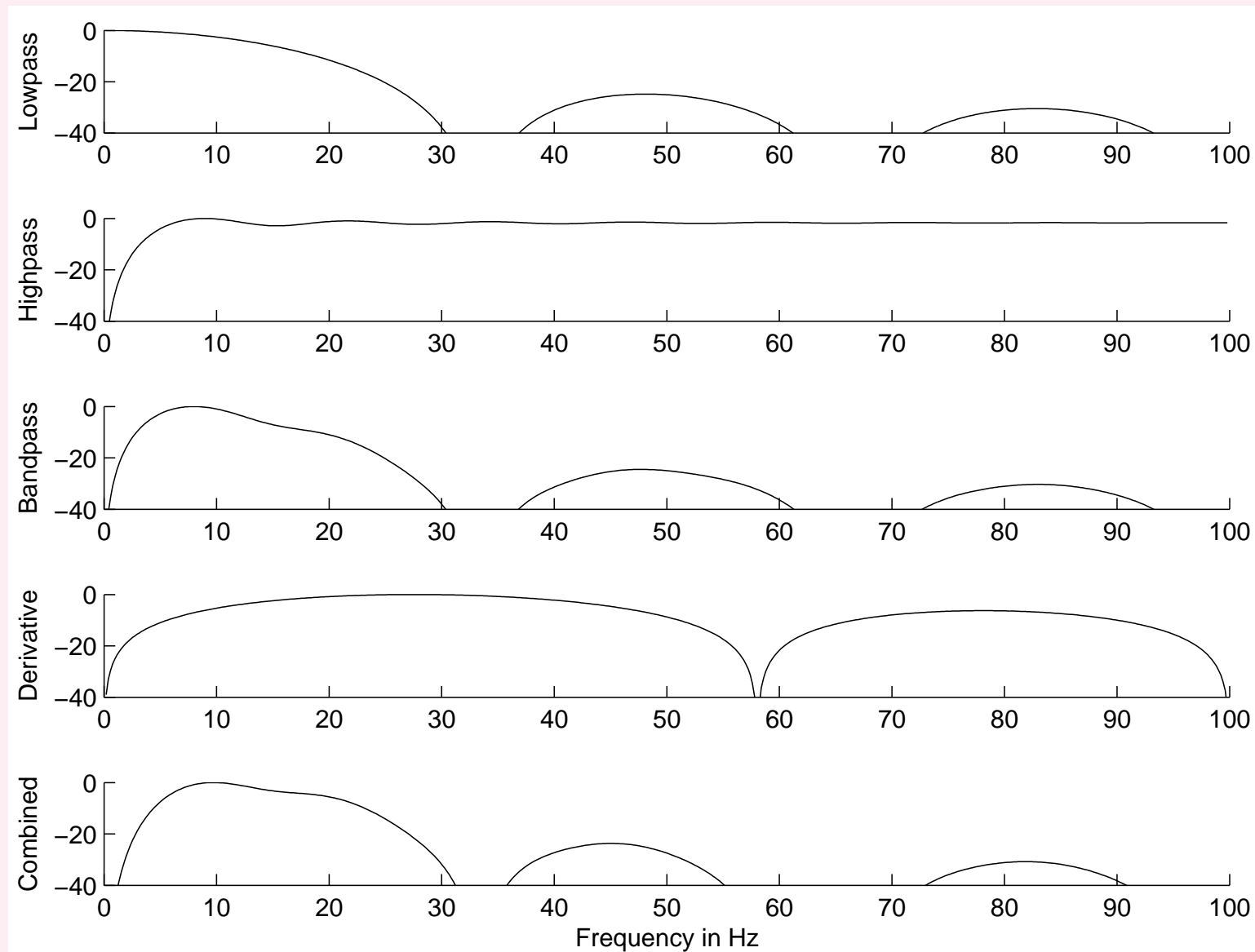$$(4.15)$$

$N = 30$ for $f_s = 200\ Hz$.

Figure 4.5: Frequency response (magnitude, in dB) of the filters used in the Pan–Tompkins algorithm for QRS detection. Top to bottom: the initial lowpass filter, the highpass filter, the bandpass filter resulting from the combination of the two filters, the derivative operator, and the combination of the bandpass filter and the derivative operator. The bandpass nature of the combined procedure is evident from the final response.
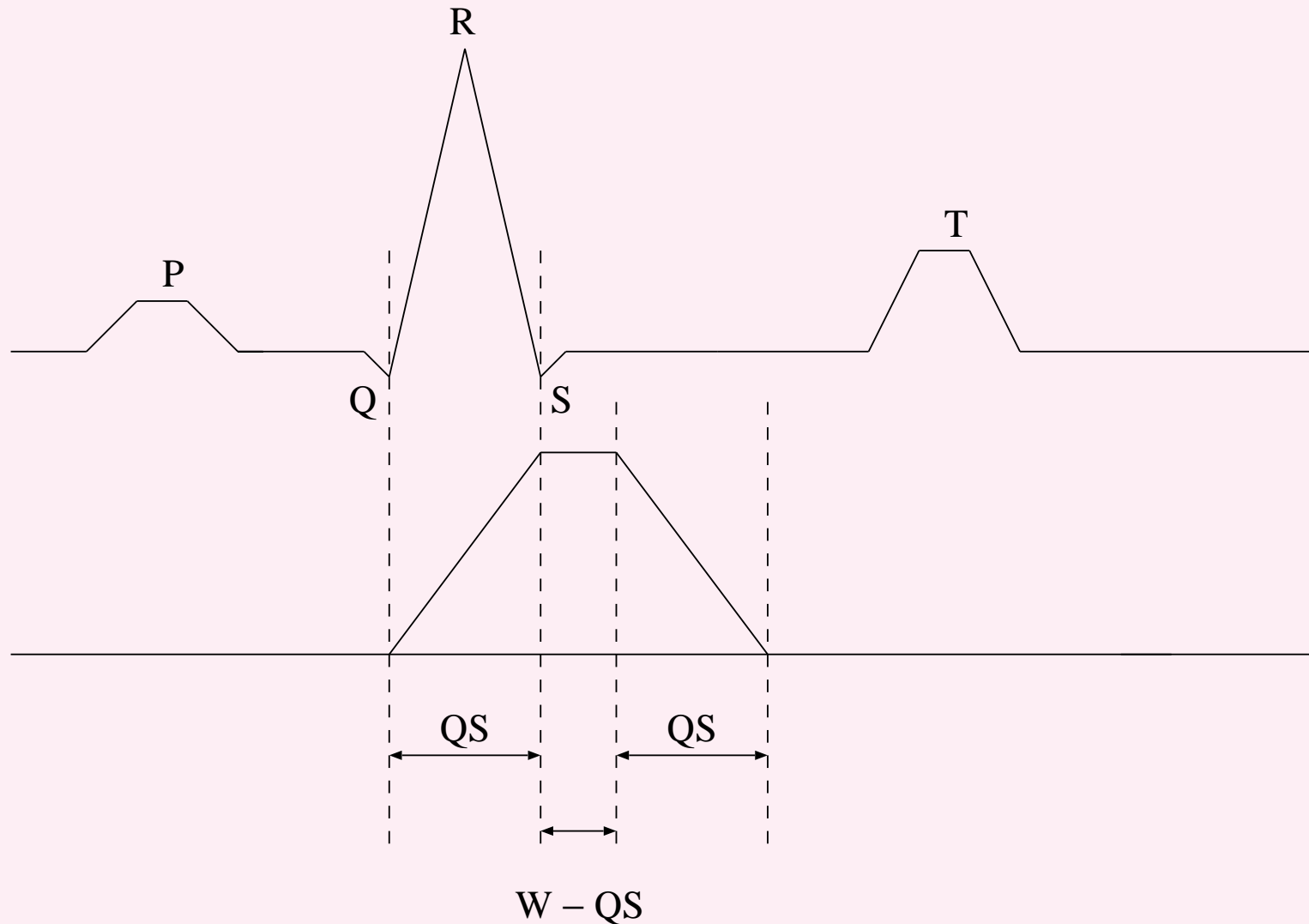
Figure 4.6: The relationship of a QRS complex to the moving-window integrator output. Upper plot: Schematic ECG signal. Lower plot: Output of the moving-window integrator. QS: QRS complex width. W: width of the integrator window, given as N/f_s s. Adapted from Tompkins.

Adaptive thresholding:

Running estimates of signal and noise peaks maintained.

$SPKI$: peak level the algorithm has learned for a QRS.

$NPKI$: peak level related to non-QRS events (noise).

$THRESHOLD\ I1$ and $THRESHOLD\ I2$:

to categorize peaks detected as signal (QRS) or noise.

Every new peak detected categorized as signal peak or noise.

If a peak exceeds $THRESHOLD\ I1$ during the

first step of analysis: classified as a QRS (signal) peak.

If the searchback technique is used,

the peak should be above $THRESHOLD\ I2$

to be called a QRS.

Peak levels and thresholds updated

after each peak is detected and classified.

$$SPKI = 0.125\,PEAKI + 0.875\,SPKI \qquad (4.16)$$

$$\text{if } PEAKI \text{ is a signal peak;}$$

$$NPKI = 0.125\,PEAKI + 0.875\,NPKI$$

$$\text{if } PEAKI \text{ is a noise peak;}$$

$$THRESHOLD\ I1 = NPKI + 0.25(SPKI - NPKI);$$

$$THRESHOLD\ I2 = 0.5\,THRESHOLD\ I1. \qquad (4.17)$$

The updating formula for $SPKI$ is changed to

$$SPKI = 0.25 \, PEAKI + 0.75 \, SPKI \qquad (4.18)$$

if a QRS is detected in the searchback procedure

using $THRESHOLD \ I2$.

Searchback procedure:

Maintains two RR-interval averages.

$RR\ AVERAGE1$: average of the eight most-recent beats;

$RR\ AVERAGE2$: average of the eight most-recent beats

having RR intervals within the range specified by

$RR\ LOW\ LIMIT = 0.92 \times RR\ AVERAGE2$ and

$RR\ HIGH\ LIMIT = 1.16 \times RR\ AVERAGE2.$

If a QRS is not detected for the interval

$$RR\ MISSED\ LIMIT = 1.66 \times RR\ AVERAGE2,$$

the QRS is taken to be the peak between the established

thresholds applied in the searchback procedure.

Low error rate of 0.68%, or 33 beats per hour

on a database of about $116,000$ beats obtained from

24-hour records of the ECGs of 48 patients.

If N_B QRS complexes or beats are detected in an ECG signal over a duration of $T\ s$

$$HR = 60\,\frac{N_B}{T} \qquad\qquad (4.19)$$

in bpm (on the average).

If the average RR interval over several beats is $RR_a\ s$

$$HR = \frac{60}{RR_a} \qquad\qquad (4.20)$$

in bpm (on the average).

In an ECG monitoring system, it is desirable to update and display the average heart rate a few times per minute.
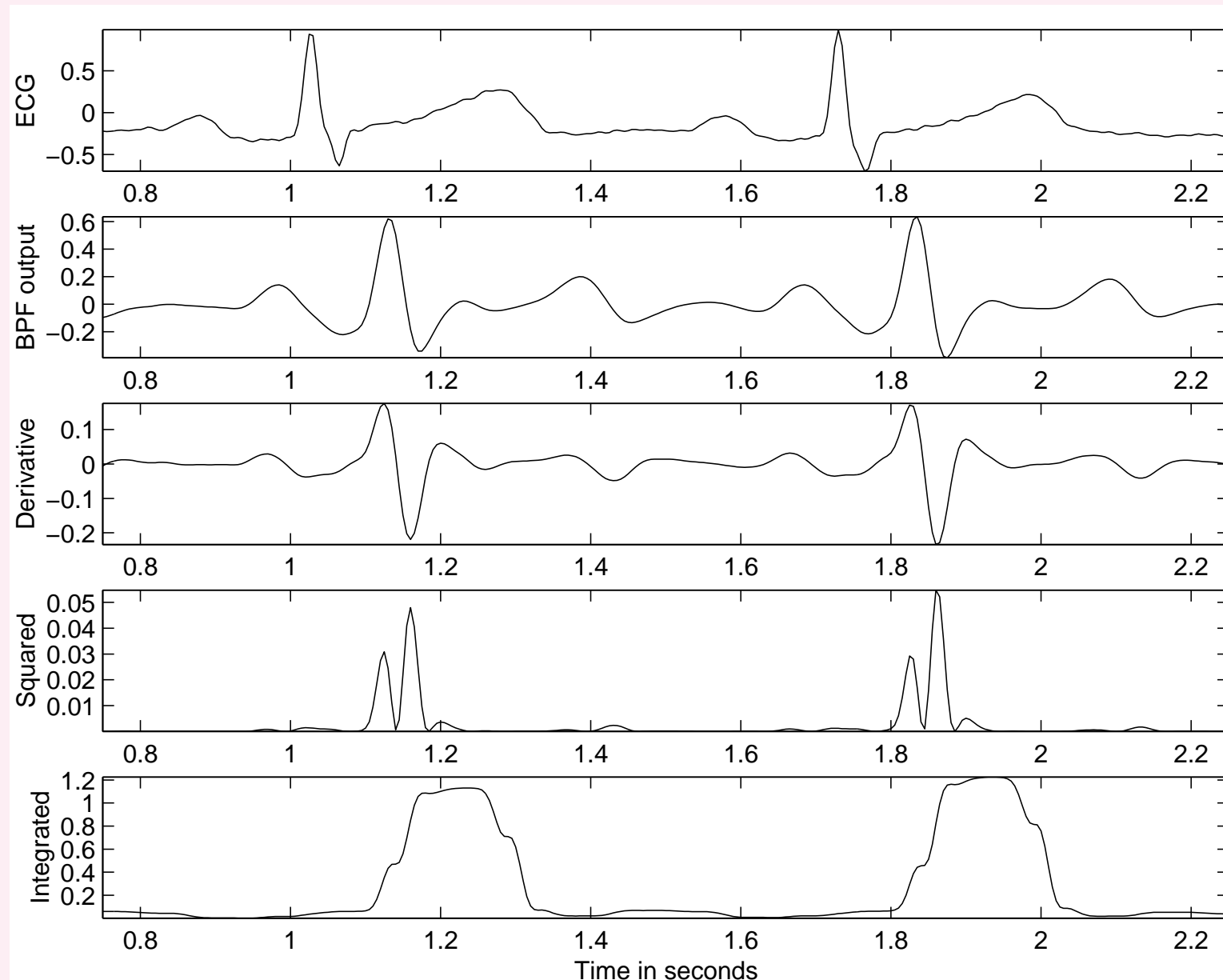
■ ■ ■ ■ ■

Figure 4.7: Results of the Pan–Tompkins algorithm. From top to bottom: two cycles of a filtered version of the ECG signal shown in Figure 3.5 (the same as that in Figure 4.2); output of the bandpass filter (BPF, a combination of lowpass and highpass filters); output of the derivative-based operator; the result of squaring; and $100\times$ the result of the final integrator.

4.3.3   Detection of the dicrotic notch

Problem: *Propose a method to detect the*

dicrotic notch in the carotid pulse signal.

Solution: Lehner and Rangayyan method.

Dicrotic notch: short wave on downward slope

of the carotid pulse.

Use the second derivative.

Least-squares estimate of the second derivative:

$$p(n) = 2y(n-2) - y(n-1) - 2y(n) - y(n+1) + 2y(n+2).$$
$$(4.21)$$

Noncausal; made causal by adding a delay of two samples.

Second derivative removes effect of downward slope;

enhances the notch itself.

Result squared and smoothed:

$$s(n) = \sum_{k=1}^{M} p^2(n - k + 1)\, w(k), \qquad (4.22)$$

where $w(k) = (M - k + 1)$ is a linear weighting function,

$M = 16$ for $f_s = 256\ Hz$.

Two peaks for each period of the carotid pulse signal:

first peak represents the onset of the carotid upstroke;

second peak is due to the dicrotic notch.

To locate the dicrotic notch:

search for the local minimum in the carotid pulse

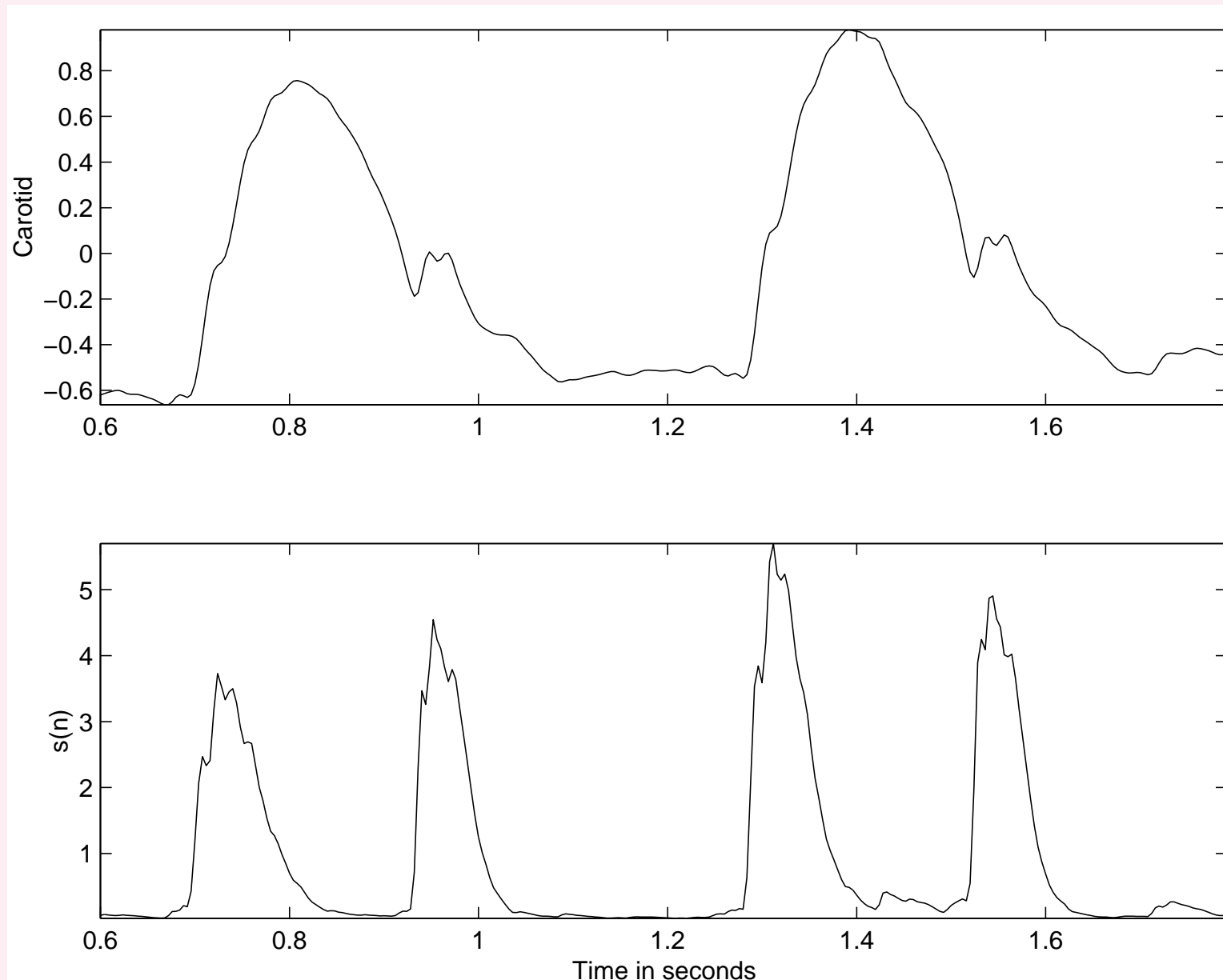within a $\pm 20\ ms$ interval of the second peak.

Figure 4.8: Two cycles of a carotid pulse signal and the result of the Lehner and Rangayyan method for detection of the dicrotic notch. Signal lowpass filtered at $100\ Hz$ and sampled at $250\ Hz$.

4.4   Correlation Analysis of EEG channels

4.4.1   Detection of EEG rhythms

Problem: *Propose a method to detect the*

presence of the α rhythm in an EEG channel.

How would you extend the method to detect the presence of

the same rhythm simultaneously in two EEG channels?

Solution: Two signals may be compared

to detect common characteristics between them via their

dot product (inner or scalar product).

$$x \cdot y = \langle x, y \rangle = \sum_{n=0}^{N-1} x(n)\, y(n). \qquad (4.23)$$

Dot product: projection of one signal onto the other,

with each signal being viewed as an N-dimensional vector.

Dot product normalized by the geometric mean of the

energies of the two signals to get a correlation coefficient:

$$\gamma_{xy} = \frac{\sum_{n=0}^{N-1} x(n)\, y(n)}{\left[\sum_{n=0}^{N-1} x^2(n)\, \sum_{n=0}^{N-1} y^2(n)\right]^{1/2}}. \qquad (4.24)$$

The means of the signals may be subtracted out, if desired.

In the case of two continuous-time signals $x(t)$ and $y(t)$,

the projection of one signal onto the other is defined as

$$\theta_{xy} = \int_{-\infty}^{\infty} x(t) \, y(t) \, dt. \qquad (4.25)$$

When a shift or time delay may be present in the

occurrence of the epoch of interest in the two signals,

it becomes necessary to introduce a time-shift parameter.

Cross-correlation function (CCF) for a shift or delay of

τ seconds or k samples:

$$\theta_{xy}(\tau) = \int_{-\infty}^{\infty} x(t)\, y(t + \tau)\, dt. \qquad (4.26)$$

$$\theta_{xy}(k) = \sum_n x(n)\, y(n+k). \qquad (4.27)$$

Range of summation limited to range of

available overlapped data.

Scale factor: depending upon the number of

data samples used.

In the case of random signals: need to take the expectation

or sample average of the outer product of the vectors.

Let $\mathbf{x}(n) = [x(n), x(n-1), \ldots, x(n-N+1)]^T$

and $\mathbf{y}(n) = [y(n), y(n-1), \ldots, y(n-N+1)]^T$

represent the N-dimensional vectorial form of

$x(n)$ and $y(n)$ with the most-recent N samples

in each signal at the time instant n.

If $\mathbf{x}(n)$ and $\mathbf{y}(n)$ are sample observations of

random processes, their CCF is defined as

$$\mathbf{\Theta}_{xy} = E[\mathbf{x}(n)\,\mathbf{y}^T(n)]. \qquad (4.28)$$

This outer product, which is an $N \times N$ matrix,

provides cross-terms that include all possible delays

or shifts within the duration of the signals.

The ACF displays peaks at intervals corresponding to

the period and integral multiples thereof

of any periodic or repetitive pattern present in the signal.

Facilitates detection of rhythms in signals such as the EEG:

α rhythm indicated by a peak near $0.1\ s$.

ACF of most signals decays and reaches negligible values

after delays of a few milliseconds,

except for periodic signals of infinite or indefinite duration

for which the ACF will also exhibit periodic peaks.

ACF will also exhibit multiple peaks when the same event

repeats itself at regular or irregular intervals.

CCF displays peaks at the period of any periodic pattern

present in *both* of the signals being analyzed.

CCF may be used to detect common rhythms present

between two signals: α rhythm in two EEG channels.

When one of the functions is a template of an event,
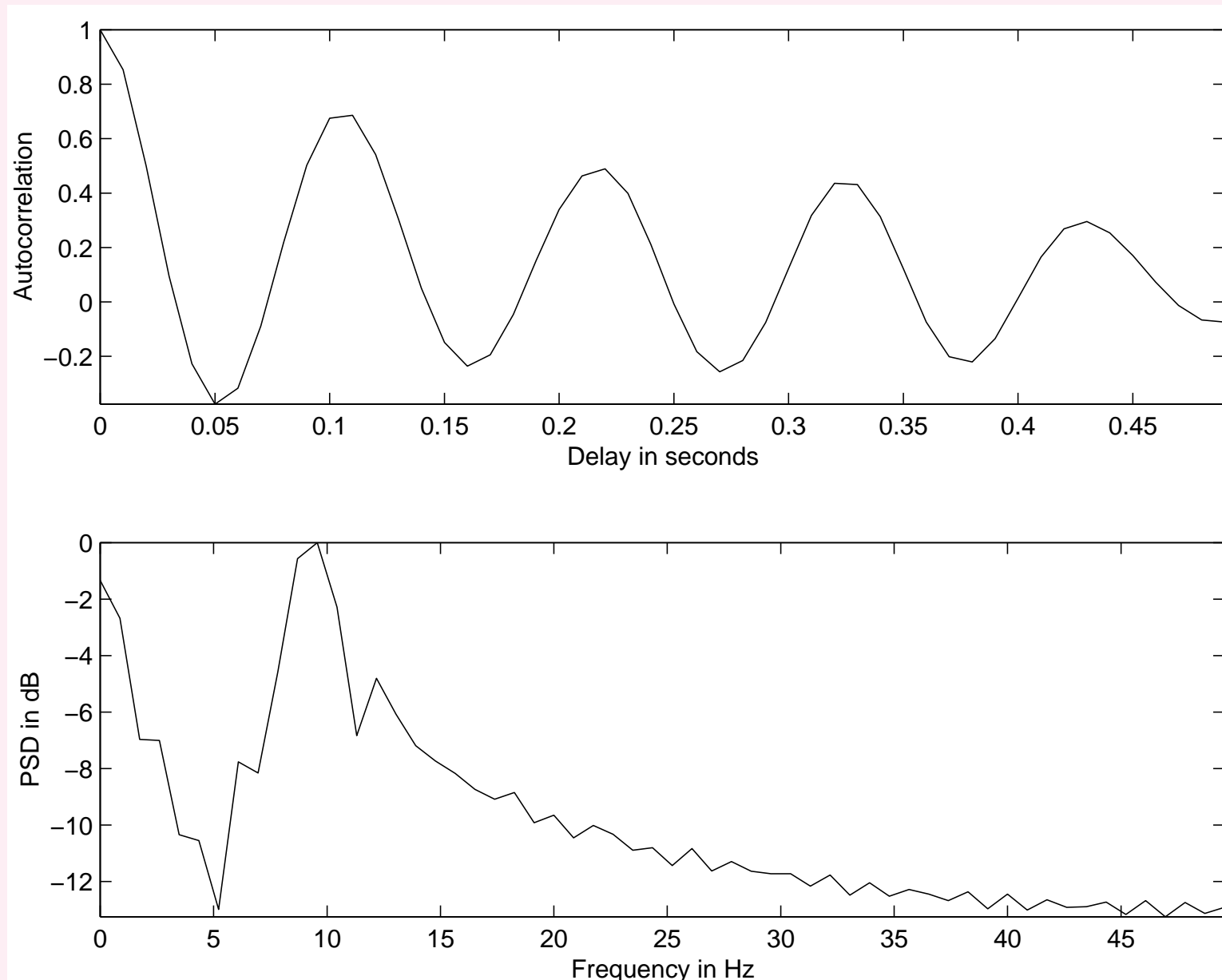
the procedure is known as *template matching.*

Figure 4.9: Upper trace: ACF of the $4.67-5.81\ s$ portion of the p4 channel of the EEG signal shown in Figure 1.39. Lower trace: The PSD of the signal segment in dB, given by the Fourier transform of the ACF.
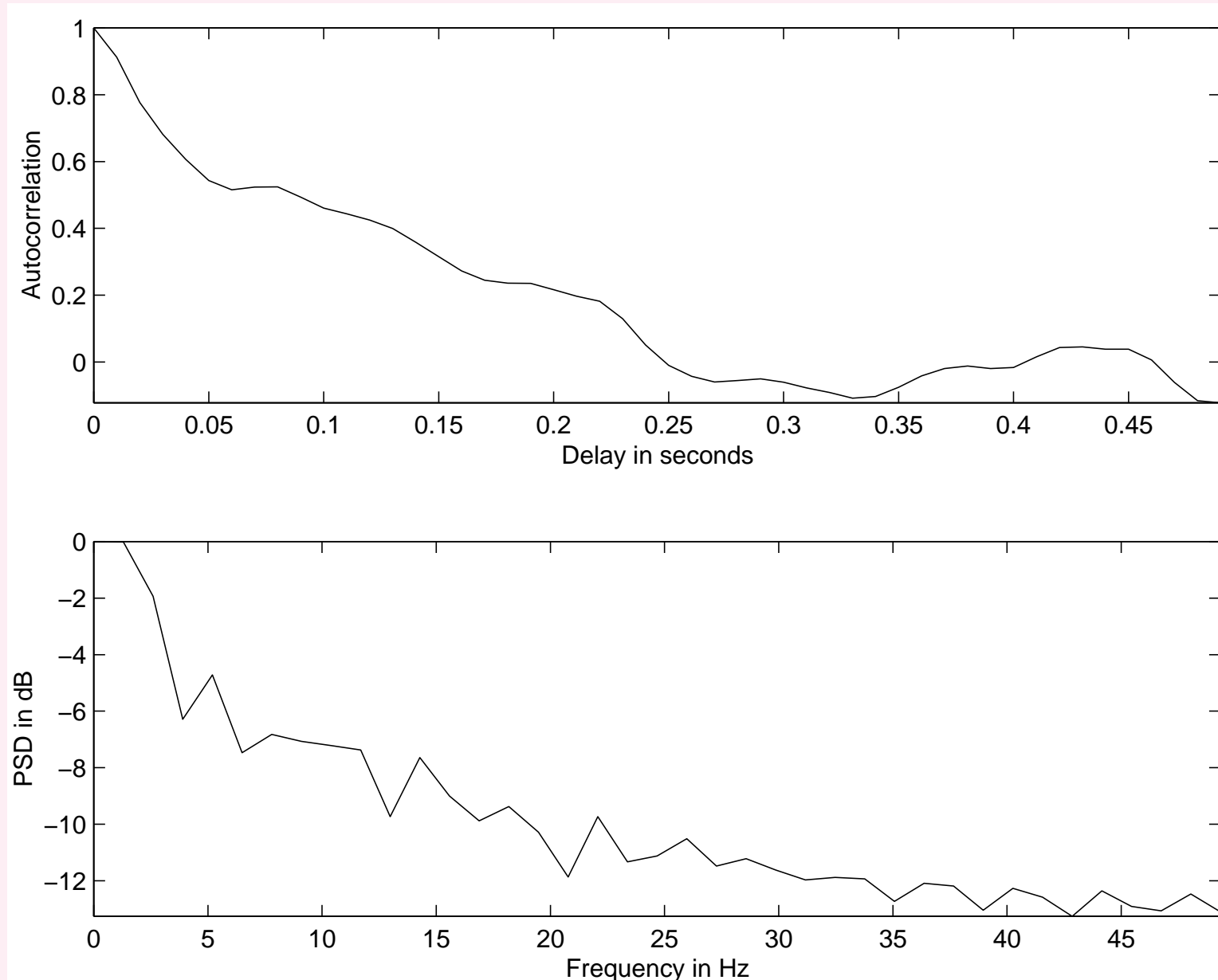
Figure 4.10: Upper trace: ACF of the $4.2-4.96\ s$ portion of the f3 channel of the EEG signal shown in Figure 1.39. Lower trace: The PSD of the signal segment in dB.
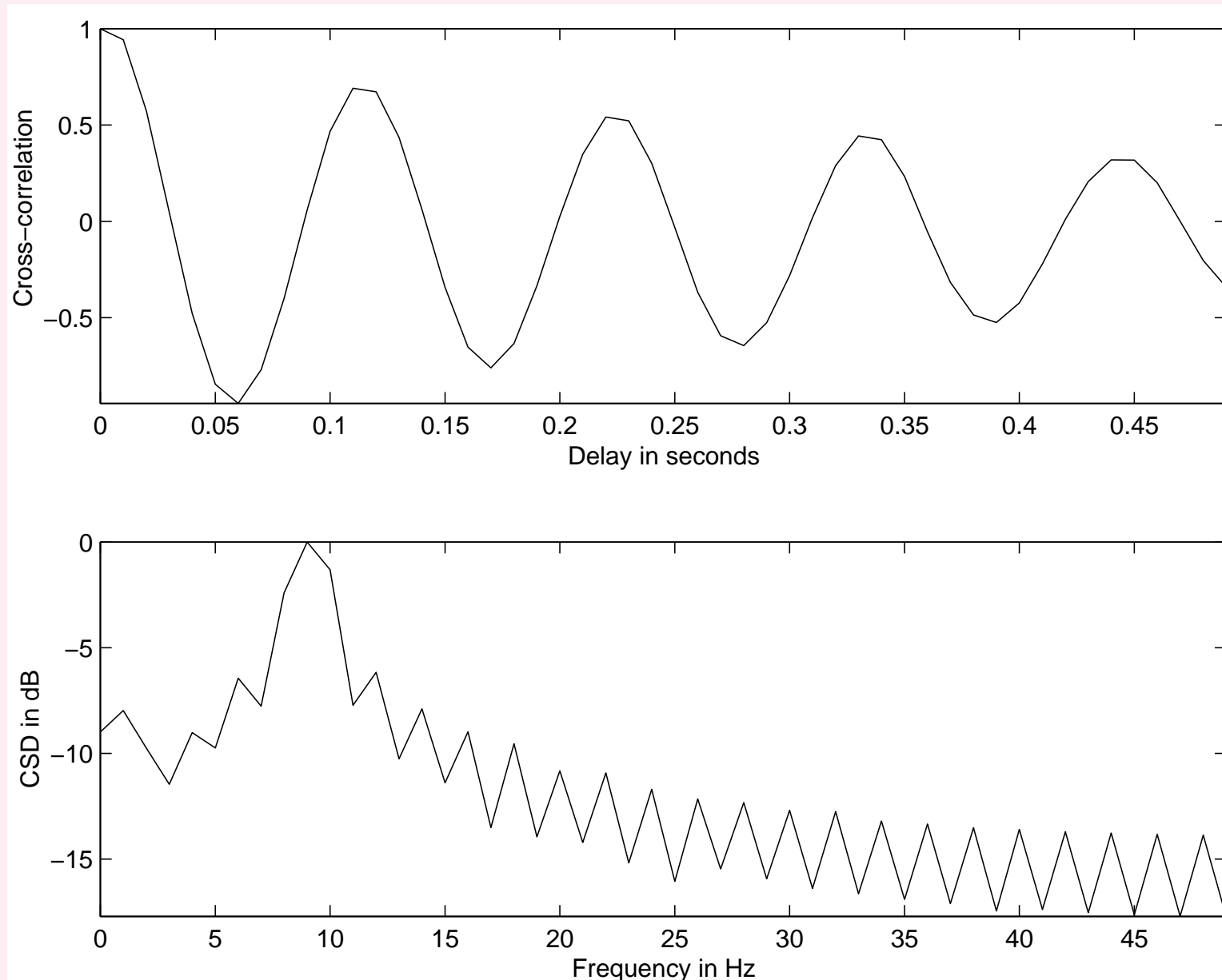
Figure 4.11: Upper trace: CCF between the $4.72 - 5.71 \ s$ portions of the p3 and p4 channels of the EEG signal shown in Figure 1.39. Lower trace: The CSD of the signal segments in dB, computed as the Fourier transform of the CCF.
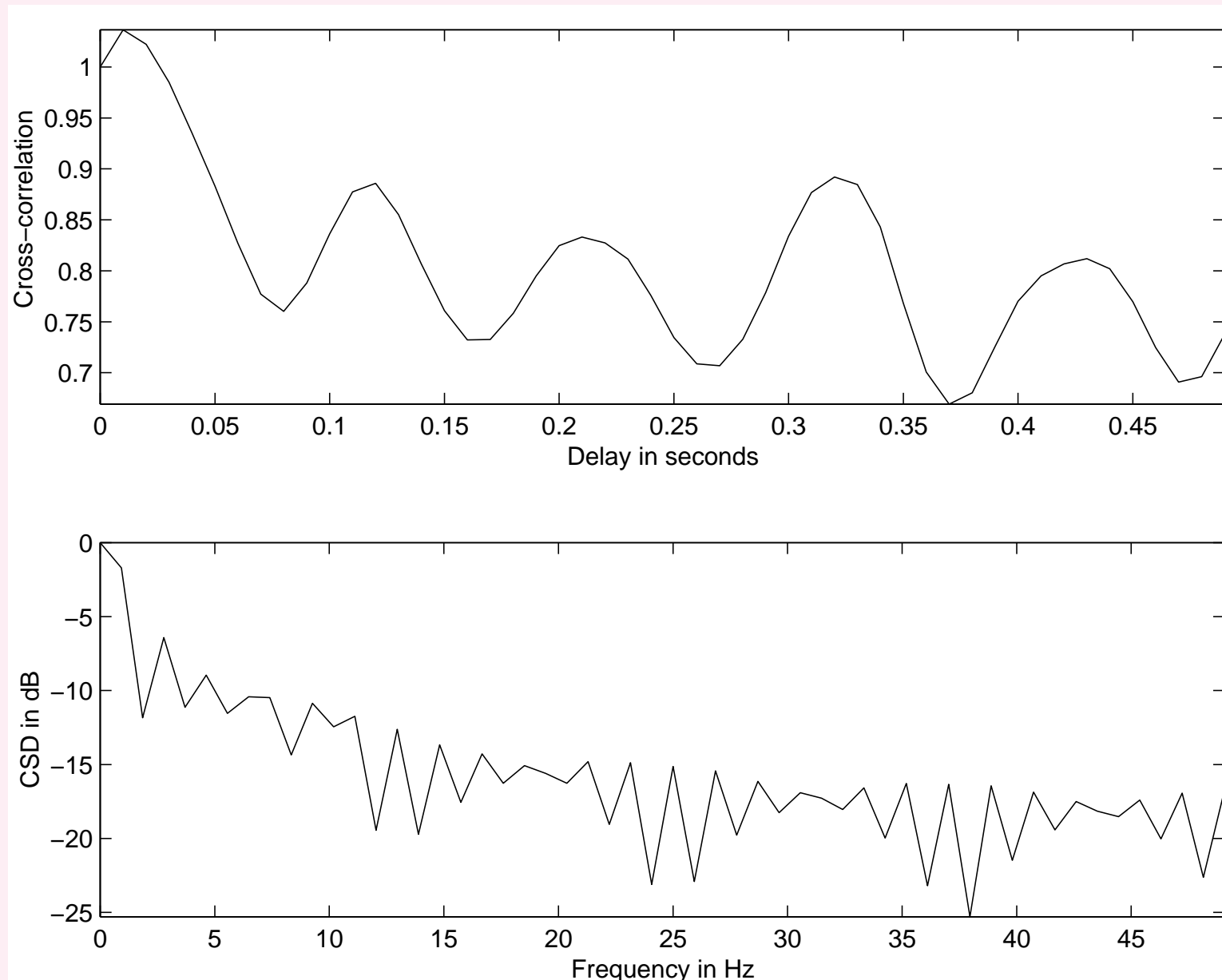
Figure 4.12: Upper trace: CCF between the $5.71 - 6.78\ s$ portions of the o2 and c4 channels of the EEG signal shown in Figure 1.39. Lower trace: The CSD of the signal segments in dB.
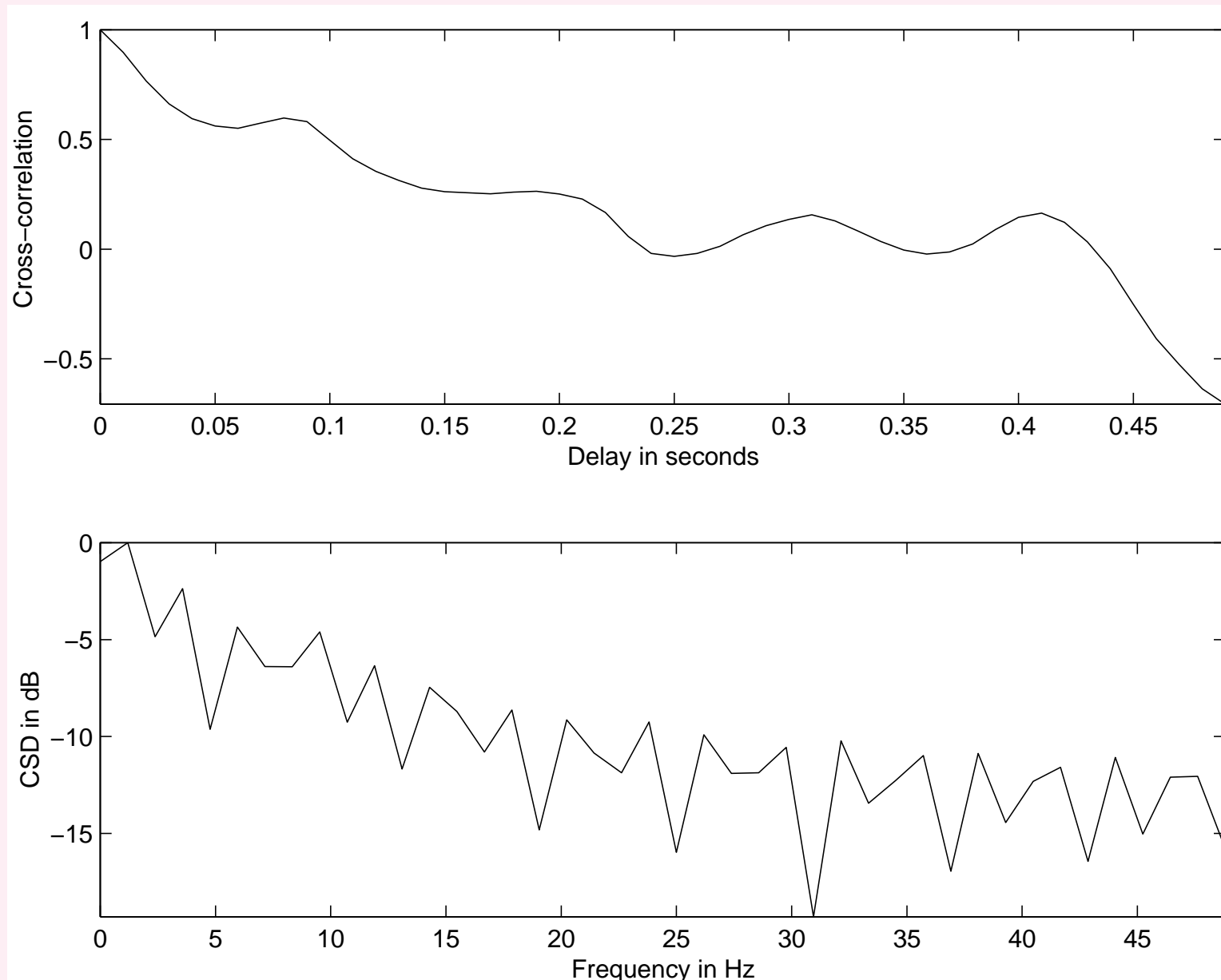
Figure 4.13: Upper trace: CCF between the $4.13 - 4.96\ s$ portions of the f3 and f4 channels of the EEG signal shown in Figure 1.39. Lower trace: The CSD of the signal segments in dB.

4.4.2   Template matching for EEG spike-and-wave detection

Problem: *Propose a method to detect*

spike-and-wave complexes in an EEG signal.

You may assume that a sample segment of

a spike-and-wave complex is available.

Solution:

A spike-and-wave complex is a well-defined event,

composed of a sharp spike followed by a wave

with a frequency of about $3\ Hz$;

the wave may contain a half period or a

full period of an almost-sinusoidal pattern.

Extract an epoch of a spike-and-wave complex

from an EEG channel and use it for template matching.

Figure 4.14: Upper trace: the c3 channel of the EEG signal shown in Figure 1.40. Lower trace: result of template matching. The spike-and-wave complex between $0.60\ s$ and $0.82\ s$ in the signal was used as the template.
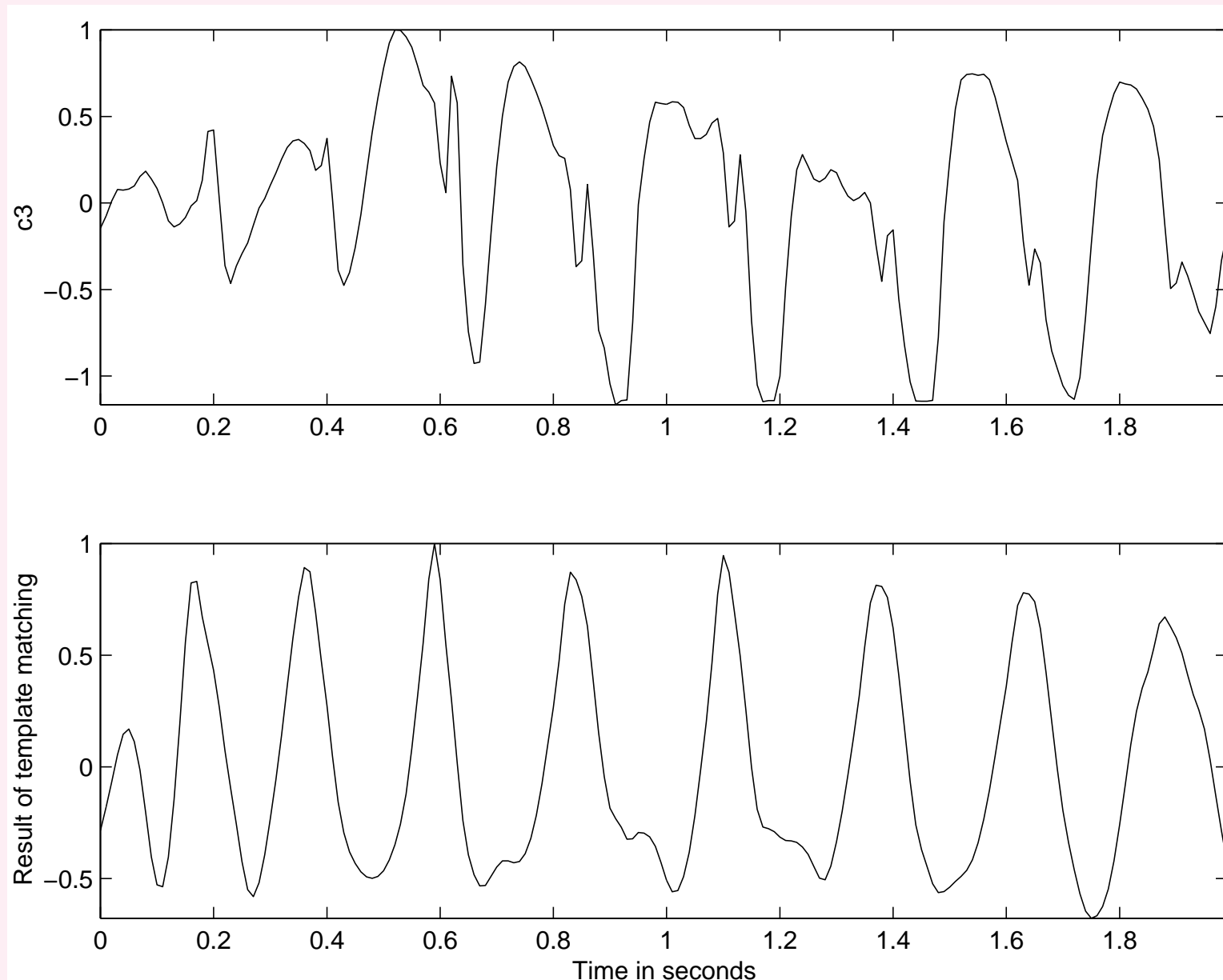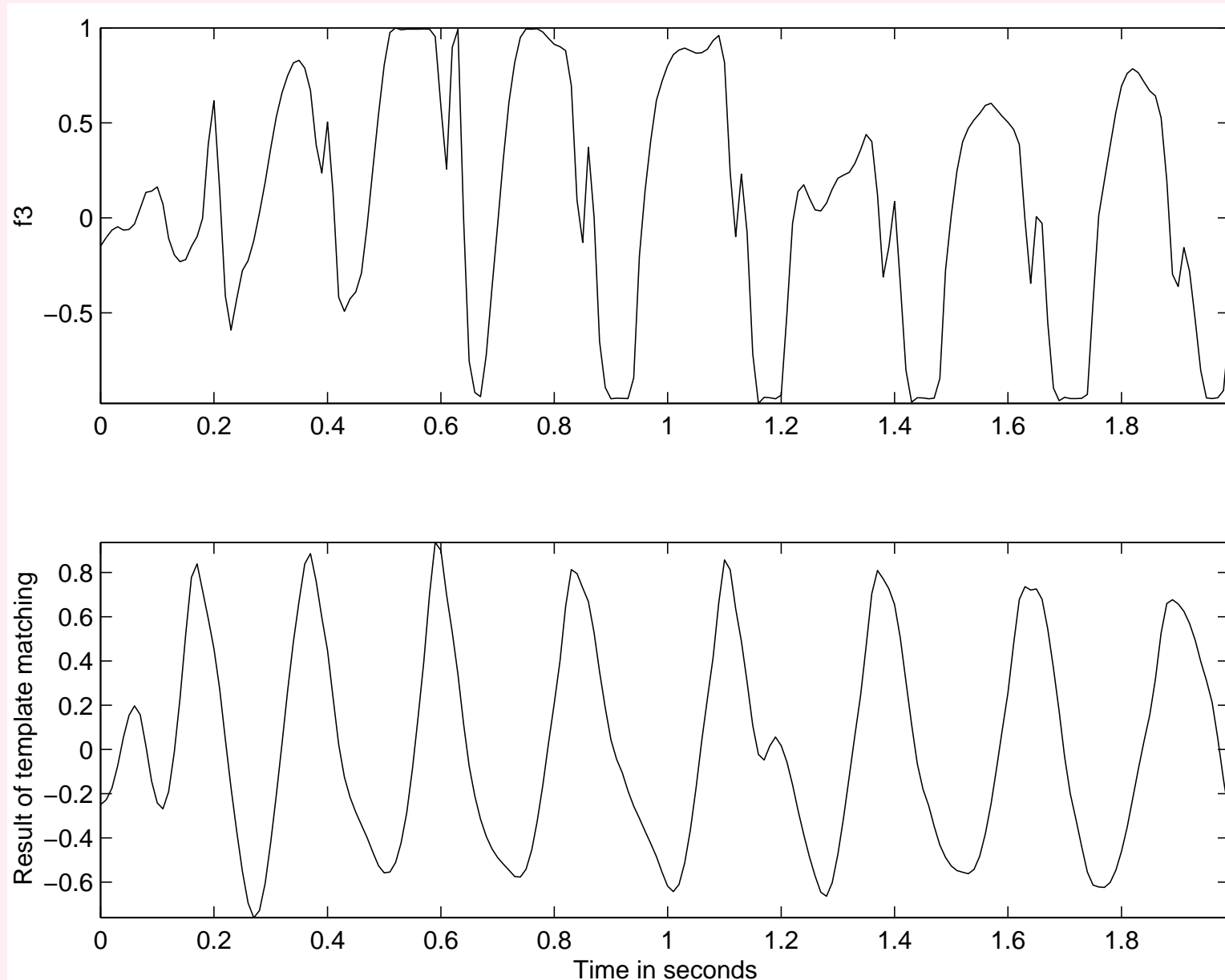
Figure 4.15: Upper trace: the f3 channel of the EEG signal shown in Figure 1.40. Lower trace: result of template matching. The spike-and-wave complex between $0.60\ s$ and $0.82\ s$ in the c3 channel (see Figure 4.14) was used as the template.

4.4.3 Detection of EEG rhythms related to seizure

Yadav et al. noted that the recurring nature of seizures of a given patient could be used to design patient-specific templates for the recognition of seizures.

In most patients, a few types of seizures tend to occur repeatedly, with related similar, though not identical, patterns in the EEG.

Yadav et al. suggested that it is possible to train a patient-specific seizure detector using previously identified templates.
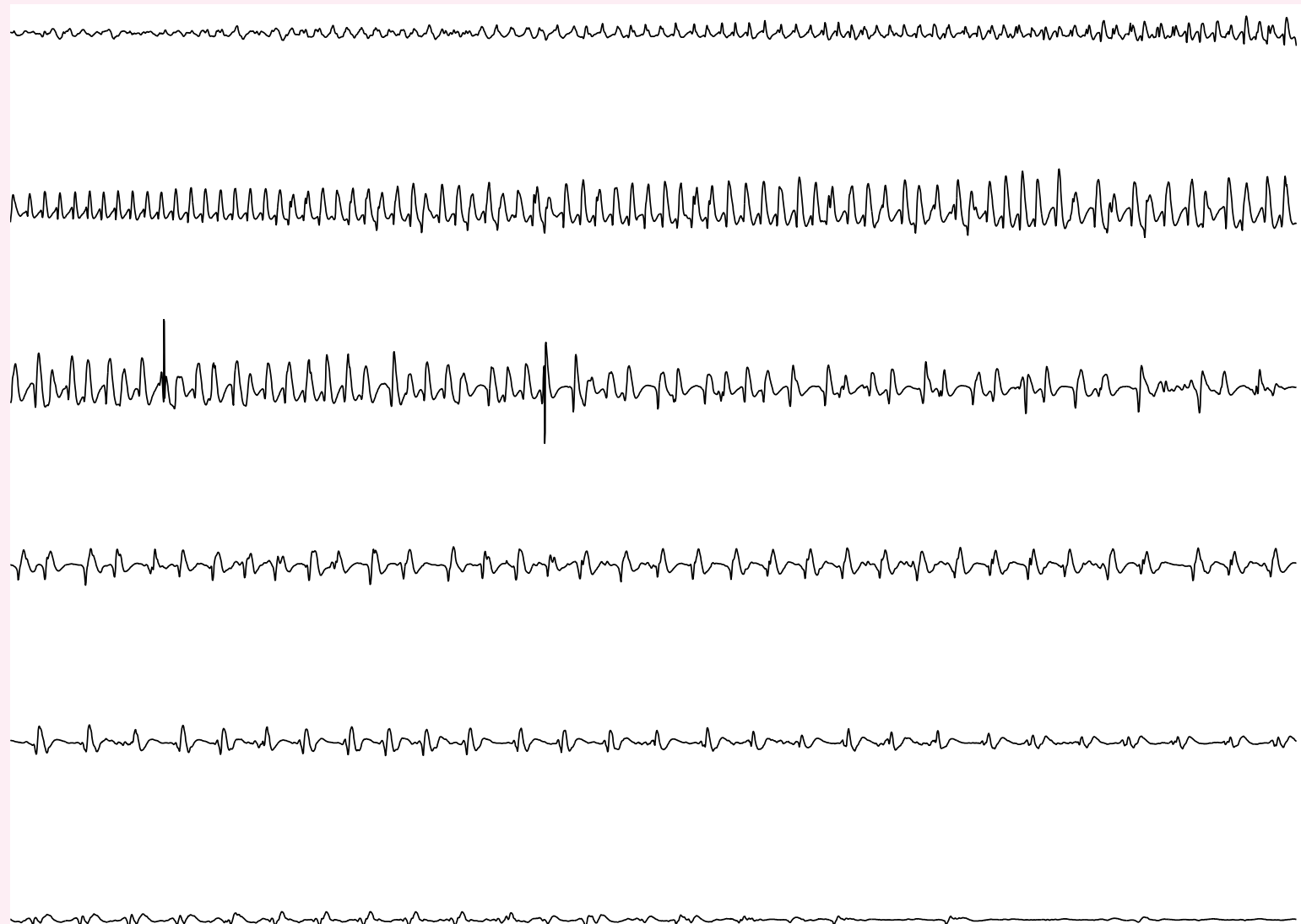
Figure 4.16: The evolution of various rhythms related to a seizure event as seen in an intracranial EEG signal. Each row represents a duration of 15 s and is a continuation of the preceding row. The minimum to maximum range of the signal shown is about 120 μV. Data courtesy of R. Agarwal.

4.5   Cross-spectral Techniques

Multiple peaks in ACF or CCF may cause

confusion in the detection of rhythms.

Fourier-domain equivalents of the ACF or the CCF —

PSD or CSD — permit easier and intuitive analysis

in the frequency domain than in the time domain.

Notion of rhythms easier with frequencies in cps or Hz

than with the corresponding inversely related periods.

© R.M. Rangayyan, IEEE/Wiley, 2nd Ed., 2015

4.5.1 Coherence analysis of EEG channels

Problem: *Describe a frequency-domain approach to study*

the presence of rhythms in multiple channels of an EEG.

Solution: PSD $S_{xx}(f)$ of a signal:

$$S_{xx}(f) = FT[\phi_{xx}(\tau)] = X(f)\, X^*(f) = |X(f)|^2. \quad (4.29)$$

CSD = FT[CCF] between two signals:

$$S_{xy}(f) = FT[\theta_{xy}(\tau)] = X^*(f)\, Y(f). \quad (4.30)$$

PSD displays peaks at frequencies corresponding to

periodic activities in the signal.

Facilitates the detection of rhythms in the EEG:

α rhythm indicated by a peak or multiple peaks

in the range $8 - 13 \; Hz$.

PSD also shows the presence of activity spread over specific

bands of frequencies: formants in speech, murmurs in PCG.

CSD exhibits peaks at frequencies present in

both of the signals being compared.

CSD may be used to detect rhythms present

in common between two channels of the EEG.

Normalized *magnitude coherence spectrum* of two signals:

$$\Gamma_{xy}(f) = \left[\frac{|S_{xy}(f)|^2}{S_{xx}(f)\ S_{yy}(f)} \right]^{1/2}. \qquad (4.31)$$

Phase of the coherence spectrum $\psi_{xy}(f) = \angle S_{xy}(f)$

represents average phase difference or time delay

between common frequency components in the two signals.

To evaluate the coherence spectrum, each PSD or CSD,

S_{xy}, S_{xx}, and S_{yy},

must be estimated using an averaging procedure

applied to several observations of the signals.

Coherence between EEG signals recorded from

different positions on the scalp depends upon

the structural connectivity or functional coupling

between the corresponding parts of the brain — *symmetry.*

4.6   The Matched Filter

When a sample observation or template of a

typical version of a signal event is available,

it is possible to design a filter that is *matched*

to the characteristics of the event.

If a signal that contains repetitions of the event

is passed through the *matched filter*, the output

should have peaks at the time instants of the events.

© R.M. Rangayyan, IEEE/Wiley, 2nd Ed., 2015

Matched filters are useful in the detection of signals of

known characteristics that are buried in noise.

They are designed to perform correlation between

the input signal and the signal template,

and hence are known as *correlation filters*.

4.6.1 Derivation of the transfer function of the matched filter

To derive the transfer function, $H(\omega)$, of the matched filter, let the signal $x(t)$ be the input to the matched filter.

$$X(\omega) = \int_{-\infty}^{\infty} x(t) \, \exp(-j\omega t) \, dt. \qquad (4.32)$$

Output $y(t) = \text{IFT of } Y(\omega) = X(\omega)H(\omega)$:

$$y(t) = \frac{1}{2\pi} \int_{-\infty}^{\infty} X(\omega) \, H(\omega) \, \exp(+j\omega t) \, d\omega$$

$$= \int_{-\infty}^{\infty} X(f) \, H(f) \, \exp(+j\, 2\pi \, f t) \, df. \quad (4.33)$$

Consider the presence of white noise at the input, with PSD

$$S_{\eta i}(f) = \frac{P_{\eta i}}{2},\tag{4.34}$$

where $P_{\eta i}$ is the average noise power at the input.

Then, the noise PSD at the output is

$$S_{\eta o}(f) = \frac{P_{\eta i}}{2} |H(f)|^2.\tag{4.35}$$

The average output noise power is

$$P_{\eta o} = \frac{P_{\eta i}}{2} \int_{-\infty}^{\infty} |H(f)|^2 \, df.\tag{4.36}$$

RMS value of noise in the absence of any signal $= \sqrt{P_{\eta o}}$.

Letting $t = t_0$ in Equation 4.33, the magnitude of the instantaneous output signal at $t = t_0$ is

$$M_y = |y(t_0)| = \left| \int_{-\infty}^{\infty} X(f) \; H(f) \; \exp(+j\,2\pi\,f t_0) \; df \right|.$$

$$(4.37)$$

The SNR at the output is $\dfrac{M_y}{\sqrt{P_{\eta o}}}$.

To derive the optimal transfer function of the matched filter, we could maximize the SNR, which is equivalent to maximizing the peak-power SNR

$$\frac{M_y^2}{P_{\eta o}} = \frac{instantaneous\ peak\ power\ of\ signal}{noise\ mean\ power}. \quad (4.38)$$

For a given signal $x(t)$, the total energy is a constant:

$$E_x = \int_{-\infty}^{\infty} x^2(t)\ dt = \int_{-\infty}^{\infty} |X(f)|^2\ df. \quad (4.39)$$

Consider the following ratio:

$$
\frac{M_y^2}{E_x \ P_{\eta o}} = \frac{\left| \int_{-\infty}^{\infty} H(f) \ X(f) \ \exp(+j \, 2\pi \, f t_0) \ df \right|^2}{\frac{P_{\eta i}}{2} \int_{-\infty}^{\infty} |H(f)|^2 \ df \ \int_{-\infty}^{\infty} |X(f)|^2 \ df} . \quad (4.40)
$$

E_x is a constant for a given input signal;

hence, maximizing the expression in Equation 4.40 is equivalent to maximizing the expression in Equation 4.38.

To determine the condition for maximization of the expression in Equation 4.40, recall Schwarz's inequality for two arbitrary complex functions $A(f)$ and $B(f)$:

$$\left| \int_{-\infty}^{\infty} A(f)\, B(f)\, df \right|^2 \leq \tag{4.41}$$

$$\left[\int_{-\infty}^{\infty} |A(f)|^2\, df \right] \left[\int_{-\infty}^{\infty} |B(f)|^2\, df \right].$$

For any two real functions $a(t)$ and $b(t)$:

$$\left[\int_{-\infty}^{\infty} a(t)\, b(t)\, dt \right]^2 \leq \left[\int_{-\infty}^{\infty} a^2(t)\, dt \right] \left[\int_{-\infty}^{\infty} b^2(t)\, dt \right].$$
$$\tag{4.42}$$

For any two vectors $\mathbf{a}$ and $\mathbf{b}$:

$$|\mathbf{a}.\mathbf{b}| \leq |\mathbf{a}|\,|\mathbf{b}|, \tag{4.43}$$

$$|\mathbf{a} + \mathbf{b}| \leq |\mathbf{a}| + |\mathbf{b}|. \tag{4.44}$$

In the inequalities stated above, equality is achieved

if $\mathbf{a} = K\,\mathbf{b}$, that is, $\mathbf{a}$ and $\mathbf{b}$ are collinear;

if $a(t) = K\,b(t)$; or if $A(f) = K\,B^*(f)$,

where K is a real constant.

The inequality in Equation 4.41 can be applied to Equation 4.40 by considering

$$A(f) = H(f),$$

$$B(f) = X(f)\,\exp(+j\,2\pi\,ft_0).$$

　　　　　　　　　　© R.M. Rangayyan, IEEE/Wiley, 2nd Ed., 2015

$$\frac{P_{\eta i} \, M_y^2}{2 \, E_x \, P_{\eta o}} \leq 1 \qquad\qquad (4.45)$$

because

$$\left| \int_{-\infty}^{\infty} X(f) \, H(f) \, \exp(+j \, 2\pi \, f t_0) \, df \right|^2 \quad (4.46)$$

$$\leq \int_{-\infty}^{\infty} |X(f)|^2 \, df \int_{-\infty}^{\infty} |H(f)|^2 \, df \, .$$

The LHS represents the instantaneous output power, M_y^2, evaluated in the Fourier domain.

Thus, the ratio in Equation 4.40 is maximized when equality is achieved, that is, $A(f) = K\,B^*(f)$ with the functions $A(f)$ and $B(f)$ as explained above, leading to the condition

$$
\begin{aligned}
H(f) &= K\;[X(f)\;\exp(+j\,2\pi\,ft_0)]^* \\
&= K\;X^*(f)\;\exp(-j\,2\pi\,ft_0), \qquad (4.47)
\end{aligned}
$$

which leads to maximal peak output SNR.

Taking the inverse Fourier transform of the last expression

$$
h(t) = K\;x[-(t - t_0)]. \qquad (4.48)
$$

Therefore, the impulse response of the matched filter is a scaled, reversed, and shifted version of the signal of interest.

Output of the matched filter:

$$y(t) = \int_{-\infty}^{\infty} X(f) \, H(f) \, \exp(+j \, 2\pi \, ft) \, df$$

$$= \int_{-\infty}^{\infty} X(f) \, K \, X^*(f) \, \exp(-j \, 2\pi \, ft_0) \, \exp(+j \, 2\pi \, ft) \, df$$

$$= K \int_{-\infty}^{\infty} |X(f)|^2 \, \exp[+j \, 2\pi \, f(t - t_0)] \, df$$

$$= K \, \phi_x(t - t_0). \tag{4.49}$$

Note: FT[ACF] = PSD.

$$FT[x(-t)] = X^*(f).$$

$$FT[x(t - \tau)] = \exp(-j \, 2\pi \, f \, \tau) \, X(f).$$

Illustration of application: Figure 4.17 shows a signal $x(n)$ composed of three events.

$$x(n) = 3\,\delta(n-5) + 2\,\delta(n-6) + \delta(n-7) \qquad (4.50)$$
$$+ \; 1.5\,\delta(n-16) + \delta(n-17) + 0.5\,\delta(n-18)$$
$$+ \; 0.75\,\delta(n-26) + 0.5\,\delta(n-27) + 0.25\,\delta(n-28).$$

$x(n)$ is composed of three occurrences of $g(n)$:

$$g(n) = 3\,\delta(n) + 2\,\delta(n-1) + \delta(n-2), \qquad (4.51)$$

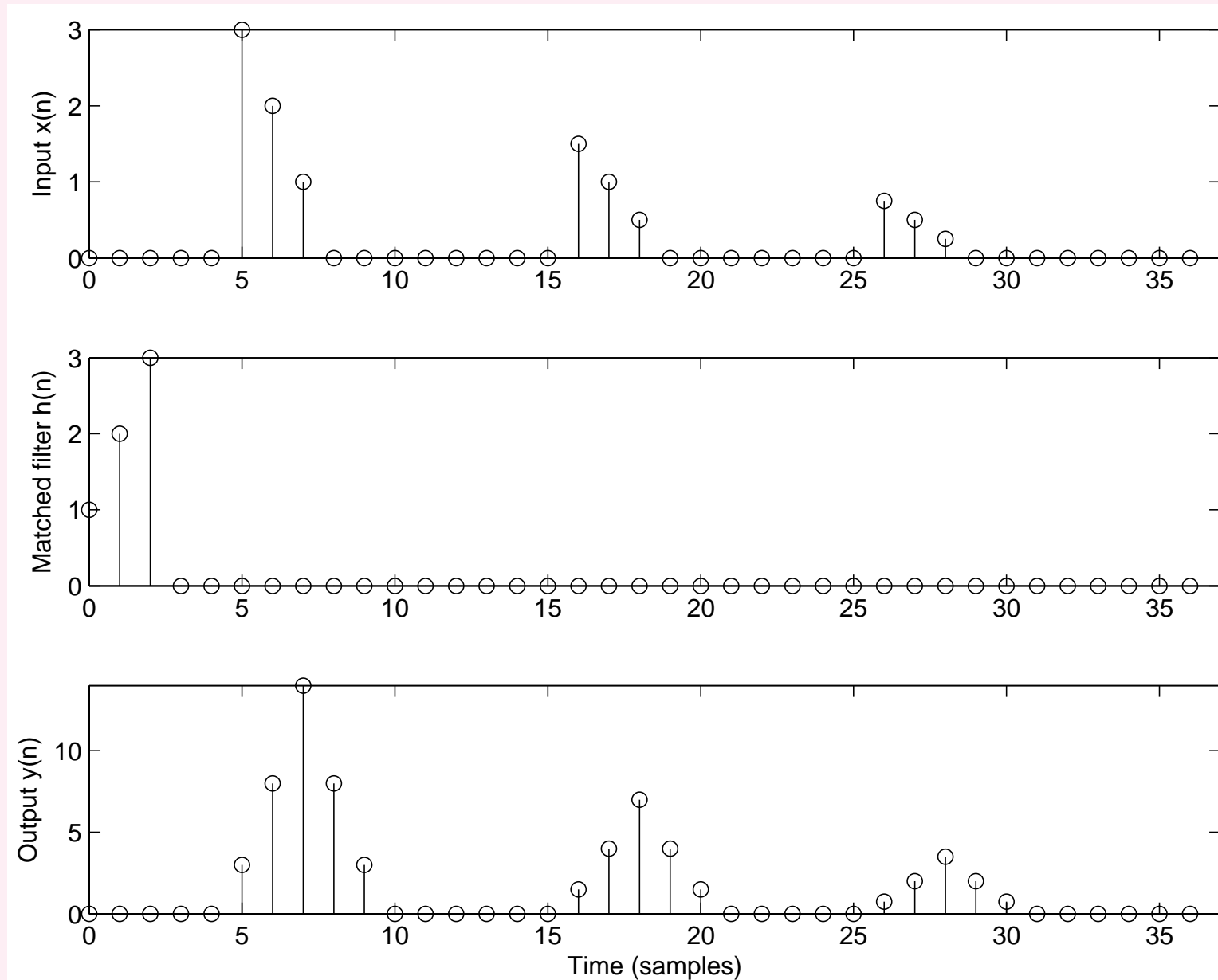$$x(n) = g(n-5) + 0.5\,g(n-16) + 0.25\,g(n-26). \quad (4.52)$$

Figure 4.17: Top: A test signal with three events. Middle: Impulse response of the matched filter. Bottom: Output of the matched filter with peaks at the locations of occurrence of the basic signal pattern.

If $g(n)$ is the basic pattern to be detected by the matched filter, we need the impulse response of the filter to be

$$h(n) = K\, g(-n + n_0).$$

K is a scale factor; n_0 is a delay for a causal $h(n)$.

In the present case, $n_0 = 2$ samples. Let $K = 1$. Then,

$$h(n) = \delta(n) + 2\,\delta(n-1) + 3\,\delta(n-2). \qquad (4.53)$$

4.6.2   Detection of EEG spike-and-wave complexes

Problem: *Design a matched filter*

to detect spike-and-wave complexes in an EEG signal.

A reference spike-and-wave complex is available.

Solution:

Let $x(t)$ be the given reference signal,

representing an ideal observation of the event of interest.

© R.M. Rangayyan, IEEE/Wiley, 2nd Ed., 2015

Let $X(f)$ be the Fourier transform of $x(t)$.

Consider passing $x(t)$ through an LTI filter

whose impulse response is $h(t)$;

the transfer function of the filter is $H(f) = FT[h(t)]$.

Output: $y(t) = x(t) * h(t)$ or $Y(f) = X(f) \, H(f)$.

The output energy is maximized when

$$H(f) = K \ X^*(f) \ \exp(-j2\pi f t_0), \qquad (4.54)$$

where K is a scale factor and

t_0 is a time instant or delay.

Optimal impulse response

$$h(t) = K \ x(t_0 - t). \qquad (4.55)$$

The transfer function of the matched filter is proportional to

the complex conjugate of the FT of the signal to be detected.

The impulse response is a *reversed* or *reflected* version

of the reference signal that is scaled and delayed.

A delay has to be added to make the filter causal.

Impulse response is a reversed version of $x(t)$; therefore

convolution performed by the matched filter $\equiv$ correlation:

output equal to cross-correlation of input and reference.

If the input contains the reference signal:
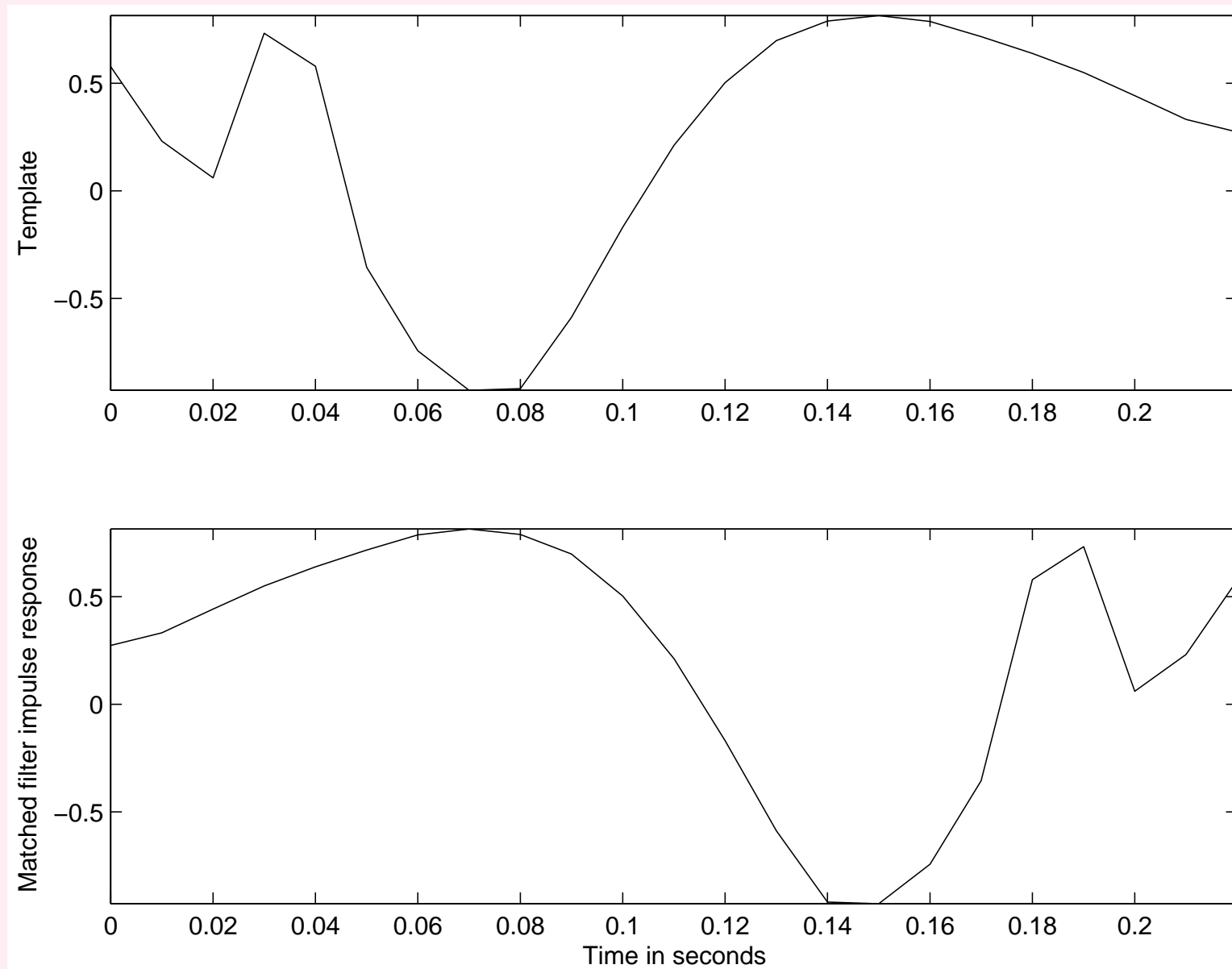
$$Y(f) = X(f)\,H(f) = X(f)\,X^*(f) = S_x(f). \qquad (4.56)$$

Figure 4.18: Upper trace: The spike-and-wave complex between $0.60\ s$ and $0.82\ s$ in the c3 channel of the EEG signal shown in Figure 1.40. Lower trace: Impulse response of the matched filter derived from the signal segment in the upper trace. Observe that the latter is a time-reversed version of the former.
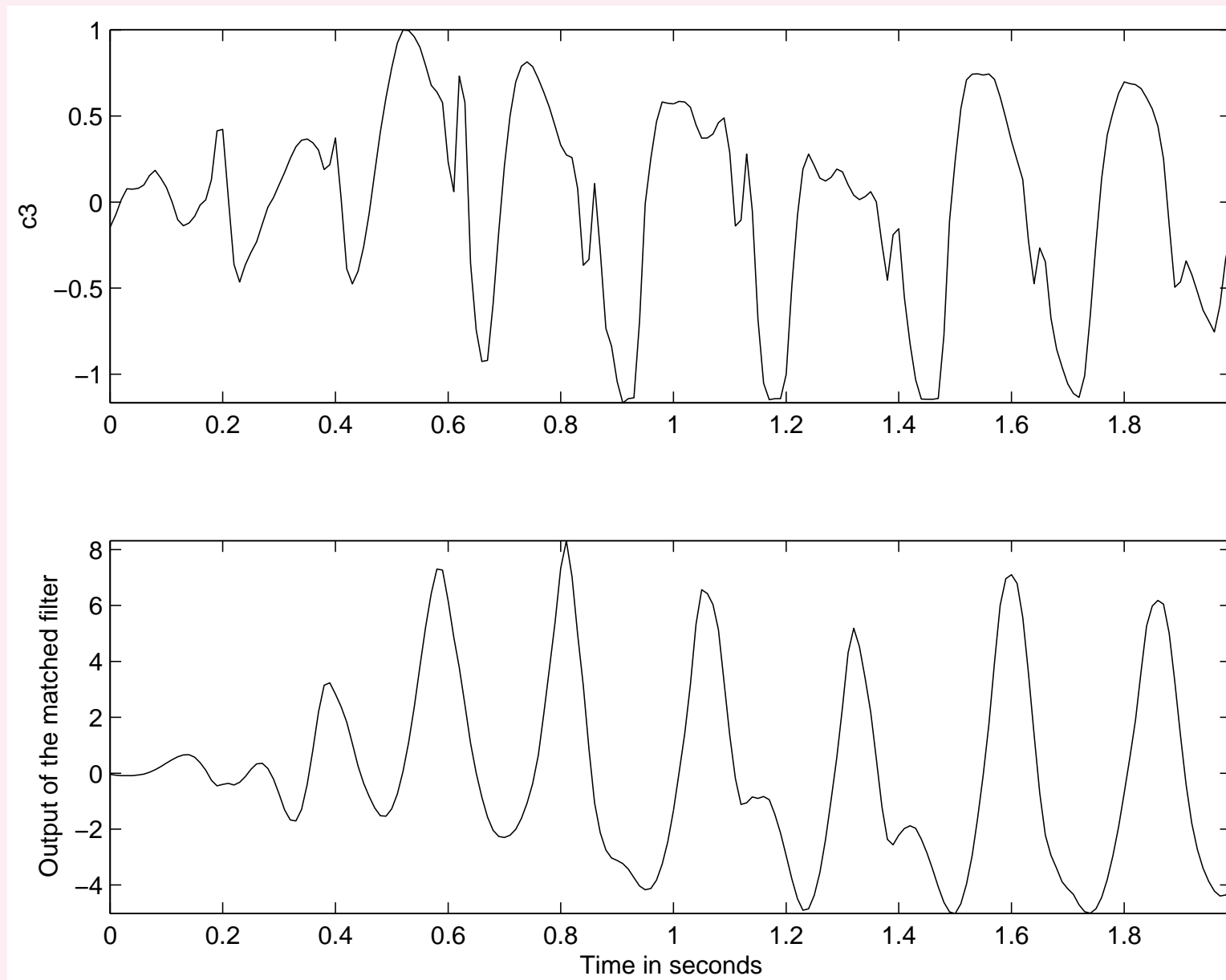
Figure 4.19: Upper trace: The c3 channel of the EEG signal shown in Figure 1.40, used as input to the matched filter in Figure 4.18. Lower trace: Output of the matched filter. See also Figure 4.14.
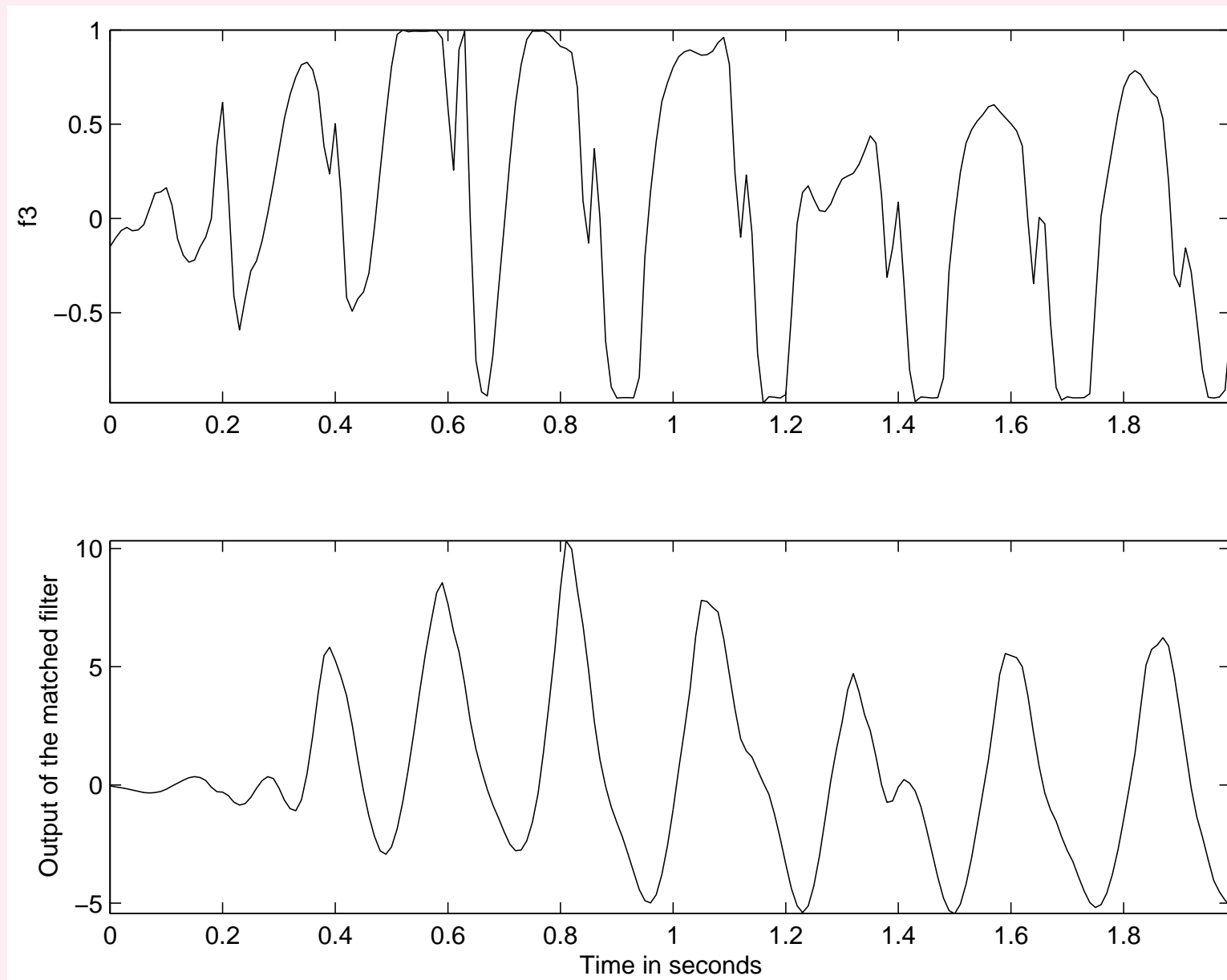
Figure 4.20: Upper trace: The f3 channel of the EEG signal shown in Figure 1.40, used as input to the matched filter in Figure 4.18. Lower trace: Output of the matched filter. See also Figure 4.15.

4.7   Detection of the P Wave

Detection of the P wave is difficult, as it is

small, has an ill-defined and variable shape, and could be

placed in a background of noise of varying size and origin.

Problem: *Propose an algorithm to*

detect the P wave in the ECG signal.

Solution 1: Hengeveld and van Bemmel.

1. QRS detected, deleted, and replaced with baseline.

2. Resulting signal bandpass filtered with

    $-3\ dB$ points at $3\ Hz$ and $11\ Hz$.

3. Search interval defined as

    $QT_{\max} = \frac{2}{9}RR + 250\ ms$.

4. Maximum and minimum values found in all

    three VCG leads from the end of the

    preceding T wave to the onset of the QRS.

5. Signal rectified and thresholded at 50% and 75% of the maximum to obtain a ternary (three-level) signal.

6. Cross-correlation of the result computed with a ternary template derived in a manner similar to the previous step from a representative set of P waves.

7. Peak in the cross-correlation corresponds to the P location in the original ECG.

The algorithm overcomes the dominance of the QRS

by first detecting the QRS and then deleting it.

Observe that the cross-correlation is computed

not with an original P wave, which could be obscure,

but with a ternary wave derived from the P wave,

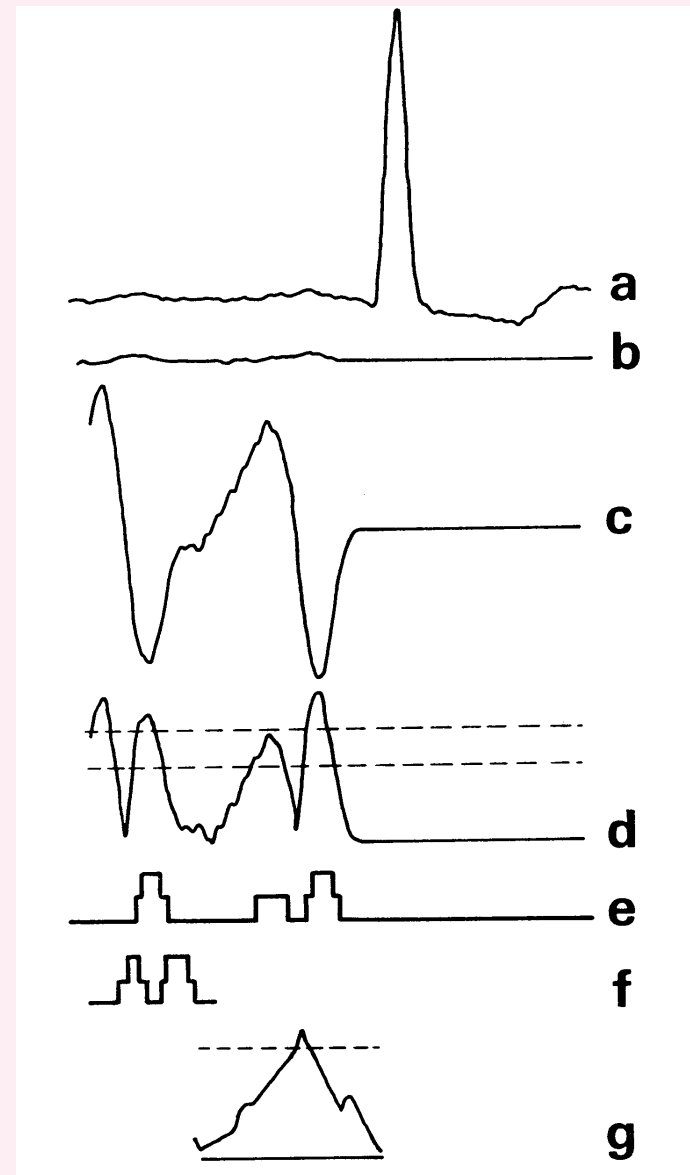which represents a simplified template of the P wave.

Figure 4.21: Illustration of the results at various stages of the Hengeveld and van Bemmel method for P wave detection. From top to bottom: (a) the original ECG signal; (b) after replacement of the QRS with the baseline; (c) after bandpass filtering; (d) after rectification, with the dashed lines indicating the thresholds; (e) the thresholded ternary signal; (f) the ternary P wave template; and (g) result of cross-correlation between the signals in (e) and (f). Reproduced with permission from S.J. Hengeveld and J.H. van Bemmel, Computer detection of P waves, *Computers and Biomedical Research*, 9:125–132, 1976. ©Academic Press.

Solution 2: Gritzali et al. proposed a common approach

to detect the QRS, T, and P waves in multichannel ECG

based upon the "length" transformation.

Given a set of ECG signals from N simultaneous channels

$x_1(t), x_2(t), \ldots, x_N(t)$, length transformation defined as

$$L(N, w, t) = \int_t^{t+w} \sqrt{\sum_{j=1}^{N} \left(\frac{dx_j}{dt}\right)^2} \; dt \; , \qquad (4.57)$$

w: width of time window for integration.

The procedure computes the total squared derivative

of the signals across the various channels available, and

integrates the summed quantity over a moving time window.

P and T expected to be well-defined in at least one channel.

QRS first detected by applying a threshold to $L(N, w, t)$,

with w set equal to the average QRS width.

End points of QRS marked by a pulse.

QRS complexes replaced by isoelectric baseline.

Procedure repeated with w equal to average T duration:

T waves detected and marked.

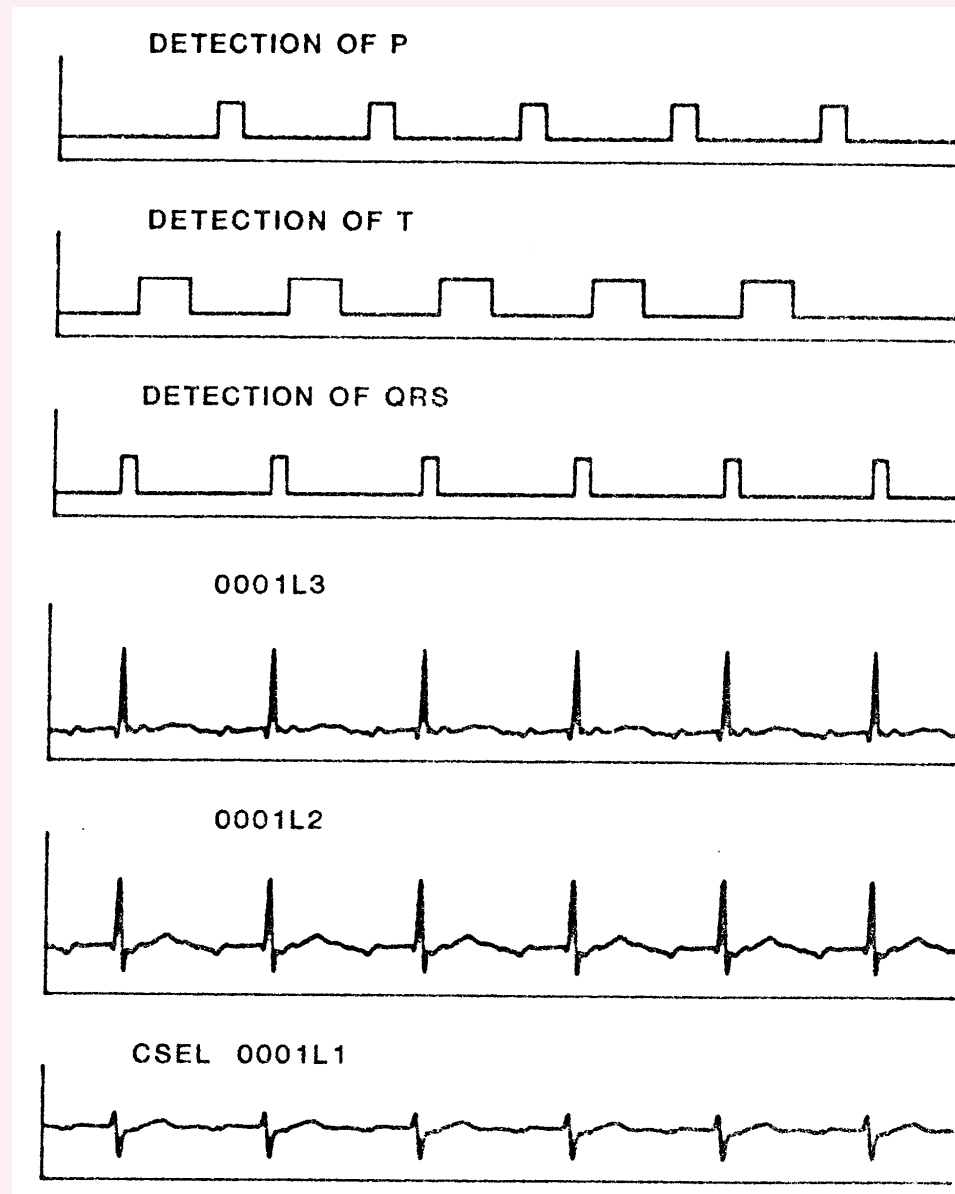Same steps repeated to detect P waves.

Figure 4.22: Detection of the P, QRS, and T waves in a three-channel ECG signal using the length transformation. The lower three traces show the three ECG channels. The upper three traces indicate the onset and end of the P, QRS, and T waves detected by the procedure in the form of pulse trains. The first P and the last T waves have not been processed. Reproduced with permission from F. Gritzali, G. Frangakis, G. Papakonstantinou, Detection of the P and T waves in an ECG, *Computers and Biomedical Research*, 22:83–91, 1989. ©Academic Press.

4.8   Homomorphic Filtering and the Complex Cepstrum

Linear filters are designed to separate signals that are

added together:

given $y(t) = x(t) + \eta(t)$, extract $x(t)$ only.

$$Y(\omega) = X(\omega) + \eta(\omega).$$

A linear filter will separate $X(\omega)$ and $\eta(\omega)$ if major portions of their energy are in different frequency bands.

Suppose that we are presented with a signal that is the

product of two signals: $y(t) = x(t)\, p(t)$.

Multiplication or convolution property of the FT:

$$Y(\omega) = X(\omega) * P(\omega).$$

$*$: convolution in the frequency domain!

How would we be able to separate $x(t)$ from $p(t)$?

Furthermore, suppose we have $y(t) = x(t) * h(t)$:

passage of the glottal pulse train or random excitation $x(t)$

through the vocal-tract system

with the impulse response $h(t)$.

$$Y(\omega) = X(\omega) \, H(\omega).$$

How would we attempt to separate $x(t)$ and $h(t)$?

4.8.1   Generalized linear filtering

Given that linear filters are well established and understood,

it is attractive to consider extending their application

to signals combined by operations other than addition.

Interesting possibility to achieve this:

convert the operation combining the signals to

addition by one or more transformations.

Assume that the transformed signals occupy

different portions of the transform space;

use linear filters to separate them.

Inverses of the transformations take us back

to the original space of the signals.

Homomorphic system for multiplied signals:

$$y(t) = x(t)\, p(t). \tag{4.58}$$

$$\log[y(t)] = \log[x(t)\, p(t)] = \log[x(t)] + \log[p(t)];$$

$$x(t) \neq 0,\ p(t) \neq 0\ \forall t. \tag{4.59}$$

$$Y_l(\omega) = X_l(\omega) + P_l(\omega); \tag{4.60}$$

subscript l: FT applied to log-transformed signal.

Assuming that the logarithmic transformation

has not affected the separability of the

Fourier components of the two signals,

a linear filter — lowpass, highpass, or bandpass —

may be applied to $Y_l(\omega)$ to separate them.

x → Input signal → [Logarithmic transform] → + → [Fourier transform] → + → [Linear filter] → + → [Inverse Fourier transform] → + → [Exponential transform] → x → Filtered signal
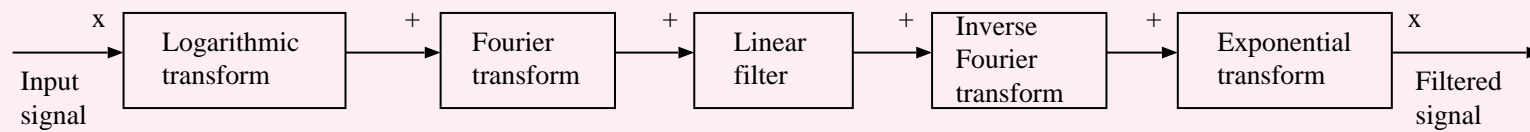
Figure 4.23: Operations involved in a multiplicative homomorphic system or filter. The symbol at the input or output of each block indicates the operation that combines the signal components at the corresponding step.

Useful in image processing: image modeled as the

product of an illumination function and a

transmittance or reflectance function.

The homomorphic filter facilitates

separation of the illumination function and

correction for nonuniform lighting: simultaneous

dynamic range compression and contrast enhancement.

4.8.2   Homomorphic deconvolution

Problem: *Propose a homomorphic filter to separate*

two signals that have been combined through convolution.

Solution: Convert convolution to addition.

$$y(t) = x(t) * h(t). \qquad (4.61)$$

$$Y(\omega) = X(\omega) H(\omega). \qquad (4.62)$$

$$\log[Y(\omega)] = \log[X(\omega)] + \log[H(\omega)]; \qquad (4.63)$$

$$X(\omega) \neq 0, \ H(\omega) \neq 0 \ \forall \omega.$$

$$\log_e[X(\omega)] = \hat{X}(\omega) = \log_e[|X(\omega)|] + j\angle X(\omega).$$
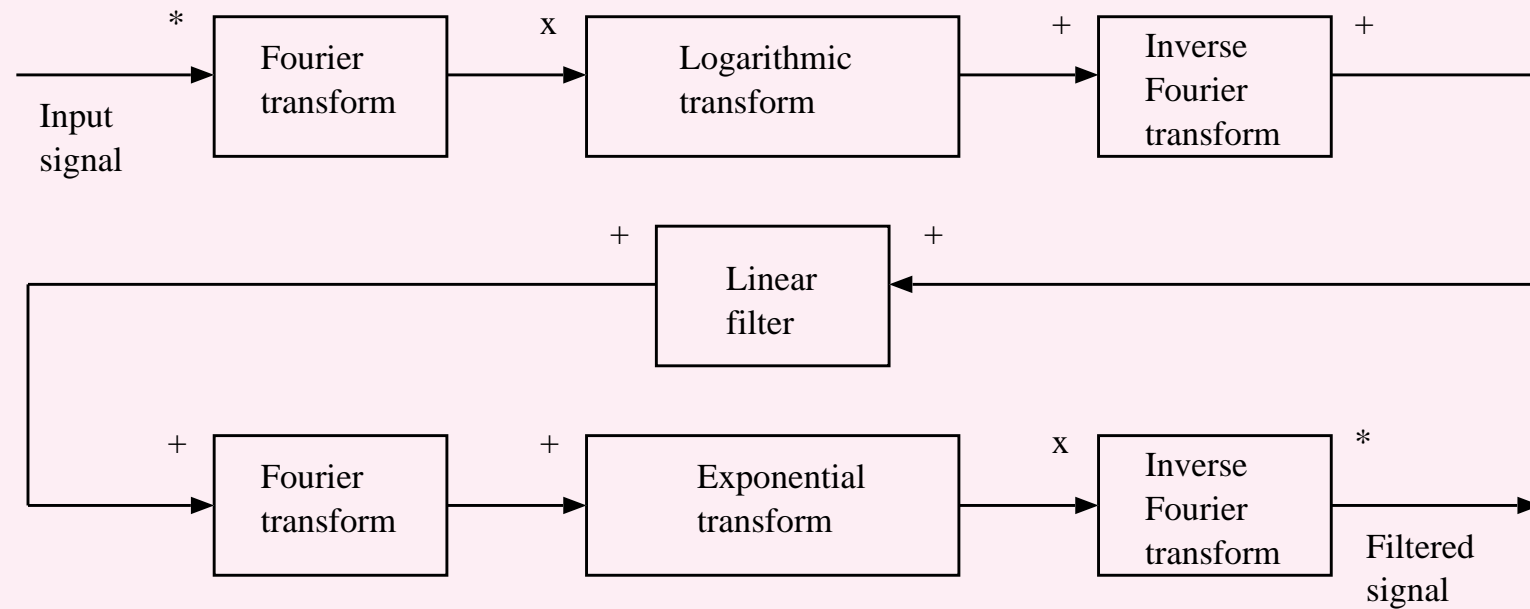
Figure 4.24: Operations involved in a homomorphic filter for convolved signals. The symbol at the input or output of each block indicates the operation that combines the signal components at the corresponding step.
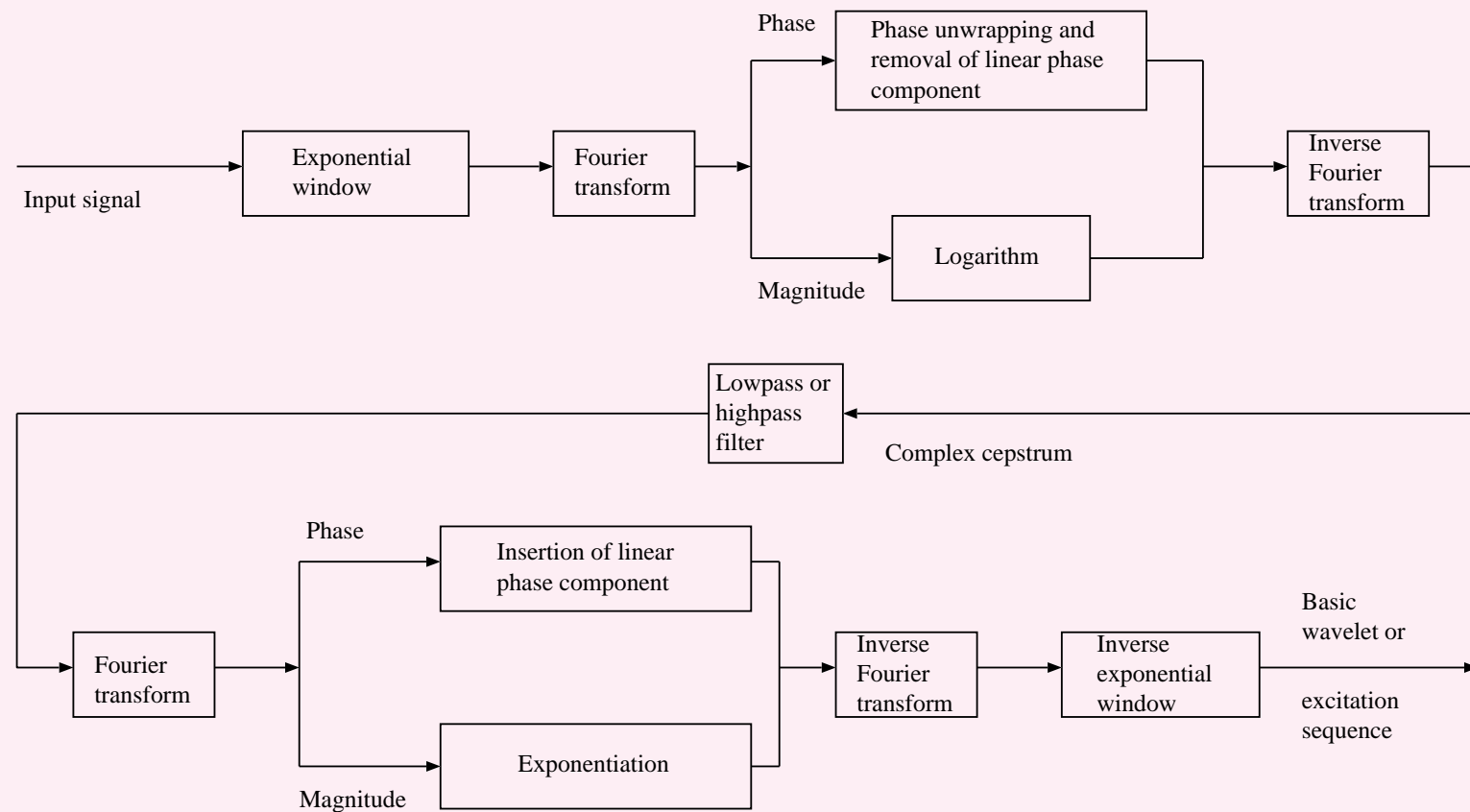
Figure 4.25: Detailed block diagram of the steps involved in deconvolution of signals using the complex cepstrum.

A linear filter may be used to separate the

transformed components of x and h,

assuming that they are separable in the transform space.

Inverses of the transformations: back to the original domain.

General formulation of the homomorphic filter is

in terms of the z-transform.

4.8.3　Extraction of the vocal-tract response

Problem: *Design a homomorphic filter*

to extract the basic wavelet corresponding to the

vocal-tract response from a voiced-speech signal.

Solution:

Voiced speech is generated by excitation of the vocal tract,

as it is held in a particular form, with a glottal waveform

that may be approximated as a series of pulses.

Voiced-speech signal: $y(n) = x(n) * h(n)$,

$x(n)$: glottal waveform or excitation sequence,

$h(n)$: impulse response of the vocal tract (basic wavelet).

Glottal excitation sequence: $x(n) = p(n) * g(n)$,

$p(n)$: train of ideal impulses (Dirac delta functions),

$g(n)$: a smoothing function —

this part will be neglected in our discussions.

The complex cepstrum: is the inverse z-transform of the

complex logarithm of the z-transform of the input signal.

"cepstrum": transposing the syllables of "spectrum".

$y(n)$: input signal; $Y(z)$ its z-transform;

complex cepstrum $\hat{y}(n)$ defined as

$$\hat{y}(n) = \frac{1}{2\pi j} \oint \log[Y(z)] \, z^{n-1} \, dz. \qquad (4.64)$$

Contour integral performs inverse z-transform;

evaluated within an annular region in the complex z-plane

where $\hat{Y}(z) = \log[Y(z)]$ is single-valued and analytic.

Unit of n in $\hat{y}(n)$ in the cepstral domain:

quefrency — switching the syllables in the term frequency.

Given $y(n) = x(n) * h(n)$, it follows that

$$\hat{Y}(z) = \hat{X}(z) + \hat{H}(z) \;\; or \;\; \hat{Y}(\omega) = \hat{X}(\omega) + \hat{H}(\omega). \quad (4.65)$$

The complex cepstra of the signals are related as

$$\hat{y}(n) = \hat{x}(n) + \hat{h}(n). \quad\quad (4.66)$$

The ˆ symbol over a function of z or ω:

complex logarithm of the corresponding function of z or ω.

ˆ symbol over a function of time (n):

complex cepstrum of the corresponding signal.

If $y(n)$ is real, its complex cepstrum $\hat{y}(n)$ is *real*;

the prefix *complex* indicates that the preceding

z and logarithmic transformations are complex functions.

The complex cepstrum is a function of time.

Important consideration in the evaluation of the

complex logarithm of $Y(z)$ or $Y(\omega)$: phase.

Phase spectrum computed as its principal value

in the range $0 - 2\pi$, given by $\tan^{-1}\left[\dfrac{imaginary\{Y(\omega)\}}{real\{Y(\omega)\}}\right]$,

will have discontinuities that will conflict with the

requirements of the inverse z-transformation or IFT.

$Y(\omega)$ needs to be separated into its

magnitude and phase components,

logarithmic operation applied to the magnitude,

the phase corrected to be continuous

by adding correction factors of $\pm 2\pi$

at discontinuities larger than π, and the

two components combined before inverse transformation.

Correcting phase spectrum as above: *phase unwrapping*.

Linear phase term in the spectrum of the input signal may

cause rapidly decaying oscillations in the cepstrum:

advisable to remove the linear phase term;

may be added to the filtered result, as a time shift.

■ ■ ■ ■ ■

The complex cepstrum of exponential sequences:

Exponential sequences: signals with a rational z-transform; their z-transforms are ratios of polynomials in z.

Such signals are effectively represented as weighted sums of exponentials in the time domain.

$$X(z) = A \, z^r \, \frac{\Pi_{k=1}^{M_I} \left(1 - a_k \, z^{-1}\right) \, \Pi_{k=1}^{M_O} \left(1 - b_k \, z\right)}{\Pi_{k=1}^{N_I} \left(1 - c_k \, z^{-1}\right) \, \Pi_{k=1}^{N_O} \left(1 - d_k \, z\right)} . \quad (4.67)$$

with $|a_k|, |b_k|, |c_k|, |d_k| < 1$.

The function $X(z)$ possesses

M_I zeros inside the unit circle:
a_k, $k = 1, 2, \ldots, M_I$;

M_O zeros outside the unit circle:
$1/b_k$, $k = 1, 2, \ldots, M_O$;

N_I poles inside the unit circle:
c_k, $k = 1, 2, \ldots, N_I$;

N_O poles outside the unit circle:
$1/d_k$, $k = 1, 2, \ldots, N_O$.

$$\hat{X}(z) = \log[X(z)] \qquad\qquad (4.68)$$

$$= \log[A] + \log[z^r]$$

$$+ \sum_{k=1}^{M_I} \log(1 - a_k\, z^{-1}) + \sum_{k=1}^{M_O} \log(1 - b_k\, z)$$

$$- \sum_{k=1}^{N_I} \log(1 - c_k\, z^{-1}) - \sum_{k=1}^{N_O} \log(1 - d_k\, z)\,.$$

For real sequences, A is real.

If $A > 0$, $\hat{x}(0) = \log[A]$.

The factor z^r indicates a delay or advance by r samples, depending upon the sign of r.

Recall the power series

$$\log(1+x) = x - \frac{x^2}{2} + \frac{x^3}{3} - \frac{x^4}{4} + \cdots, \quad if \ \ |x| < 1. \quad (4.69)$$

Thus, we have

$$\log(1 - \alpha \, z^{-1}) = -\sum_{n=1}^{\infty} \frac{\alpha^n}{n} z^{-n}, \quad if \ \ |z| > |\alpha|, \quad (4.70)$$

$$\log(1 - \beta \, z) = -\sum_{n=1}^{\infty} \frac{\beta^n}{n} z^{n}, \quad if \ \ |z| < |\beta^{-1}|. \quad (4.71)$$

Expanding all of the log terms in Equation 4.68 into their equivalent power series and taking the inverse z-transform,

$$\hat{x}(n) = \begin{cases} \log|A| & for \ \ n = 0; \\[2ex] -\Sigma_{k=1}^{M_I} \dfrac{a_k^n}{n} + \Sigma_{k=1}^{N_I} \dfrac{c_k^n}{n} & for \ \ n > 0; \quad (4.72) \\[2ex] \Sigma_{k=1}^{M_O} \dfrac{b_k^{-n}}{n} - \Sigma_{k=1}^{N_O} \dfrac{d_k^{-n}}{n} & for \ \ n < 0. \end{cases}$$

Properties of the complex cepstrum:

- The complex cepstrum, $\hat{x}(n)$, decays at least as fast as $1/n$. We have

$$|\hat{x}(n)| < K \left|\frac{\alpha^n}{n}\right|, \quad -\infty < n < \infty, \qquad (4.73)$$

  where $\alpha = \max(|a_k|, |b_k|, |c_k|, |d_k|)$, and K is a constant.

- $\hat{x}(n)$ will be of infinite duration even if $x(n)$ is of finite duration, and exists for $-\infty < n < \infty$, in general.

- If $x(n)$ is a minimum-phase signal, all of its poles and zeros are inside the unit circle in the z-plane. Then, $\hat{x}(n) = 0$ for $n < 0$; the complex cepstrum is causal.

- If $x(n)$ is a maximum-phase signal, it has no poles or zeros inside the unit circle in the z-plane. Then, $\hat{x}(n) = 0$ for $n > 0$; the complex cepstrum is anticausal.

With causal signals of finite energy, we need not consider poles on or outside the unit circle in the z-plane.

However, the z-transform of a finite-energy signal may have zeros outside the unit circle.

A composite mixed-phase signal may be separated

into its minimum-phase component by extracting the causal part ($n > 0$)

and maximum-phase component by extracting the anticausal part ($n < 0$)

of its complex cepstrum, followed by the inverse procedures.

Composite mixed-phase signal = convolution of

minimum-phase and maximum-phase components.

Effect of echoes or repetitions of a wavelet:

Consider a signal $y(n) = x(n) * h(n)$, where

$$x(n) = \delta(n) + a\,\delta(n - n_0), \qquad (4.74)$$

with a and n_0 being two constants.

$$y(n) = h(n) + a\ h(n - n_0). \qquad (4.75)$$

$$Y(z) = (1 + a\ z^{-n_0})\ H(z). \qquad (4.76)$$

Signal has two occurrences of the basic wavelet $h(n)$

at $n = 0$ and $n = n_0$.

a: magnitude of the second appearance of the basic wavelet,

called an *echo* in seismic applications,

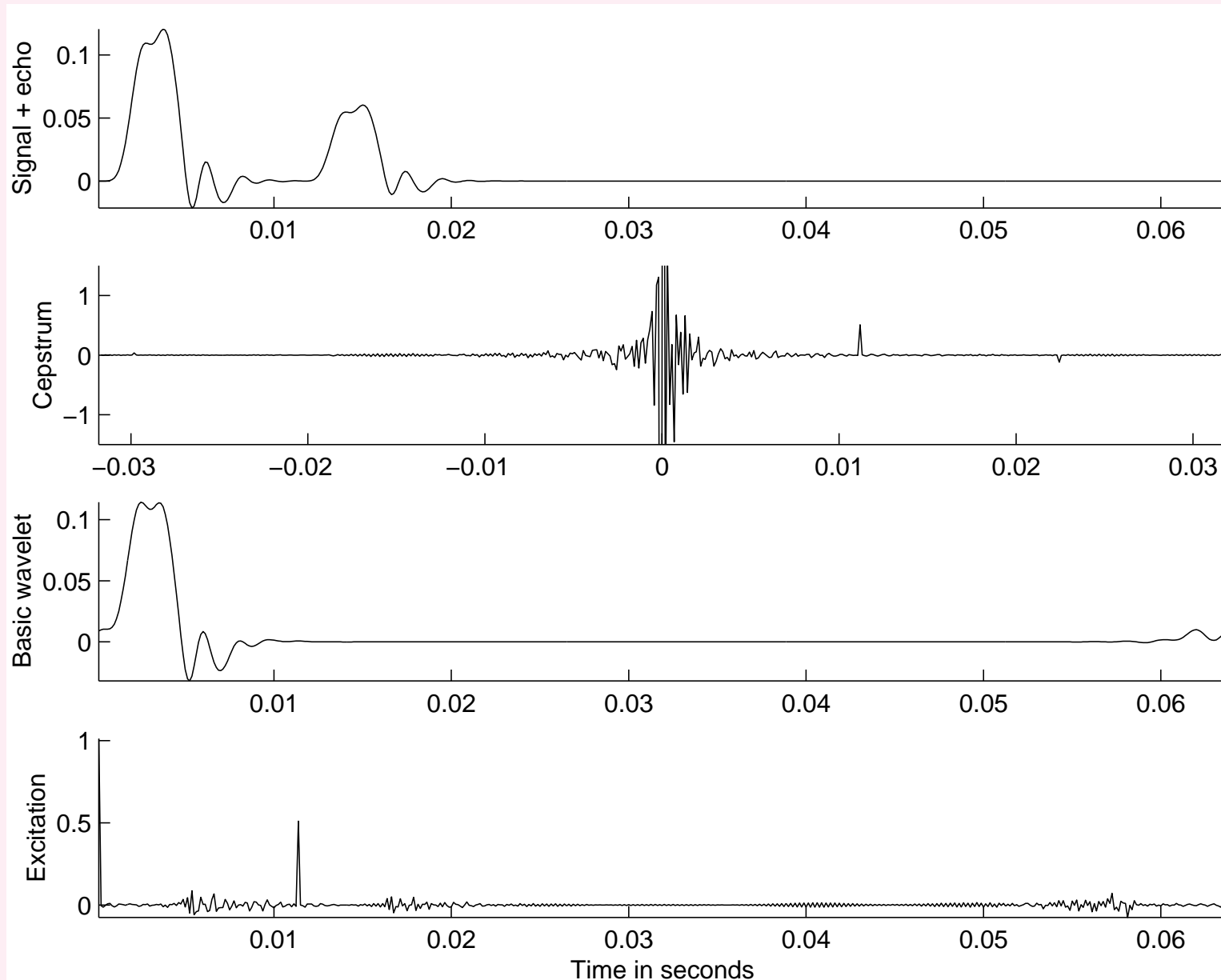n_0: delay of echo, or pitch in a voiced-speech signal.

Figure 4.26: From top to bottom: a composite signal with a wavelet and an echo; the complex cepstrum of the signal (the amplitude axis has been stretched to make the peaks at the echo time and its multiples more readily visible; values outside the range ± 1.5 have been clipped); the basic wavelet extracted by shortpass filtering the cepstrum; and the excitation sequence extracted by longpass filtering the cepstrum.

Echo: $a = 0.5$, $n_0 = 0.01125\ s$.

If the z-transform is evaluated on the unit circle,
we get the Fourier-transform-based expression

$$Y(\omega) = [1 + a \ \exp(-j\omega n_0)] \ H(\omega). \qquad (4.77)$$

Taking the logarithm, we have

$$\hat{Y}(\omega) = \hat{H}(\omega) + \log[1 + a \ \exp(-j\omega n_0)]. \qquad (4.78)$$

If $a < 1$, the log term may be expanded in a power series:

$$\hat{Y}(\omega) = \hat{H}(\omega) + a \exp(-j\omega n_0) - \frac{a^2}{2} \exp(-2j\omega n_0)$$

$$+ \frac{a^3}{3} \exp(-3j\omega n_0) - \cdots . \tag{4.79}$$

Taking the inverse Fourier transform:

$$\hat{y}(n) = \hat{h}(n) + a\,\delta(n - n_0) - \frac{a^2}{2}\,\delta(n - 2n_0)$$

$$+ \frac{a^3}{3}\,\delta(n - 3n_0) - \cdots . \tag{4.80}$$

The complex cepstrum of a signal with

a basic wavelet and an echo

= complex cepstrum of the basic wavelet

+ a series of impulses at echo delay and integral multiples.

Amplitudes of impulses proportional to echo amplitude (a)

and decay for the higher-order repetitions (if $a < 1$).

If there are multiple echoes or repetitions of a basic wavelet,

the cepstrum will possess multiple impulse trains.

Voiced-speech signal: location of first peak = pitch.

Assuming that the complex cepstrum of the basic wavelet

decays to negligible values before the first impulse

$a \, \delta(n - n_0)$ related to the echo, $\hat{h}(n)$ may be extracted

from the complex cepstrum $\hat{y}(n)$ of the composite signal

by a simple window that has unit value for $|n| < n_c < n_0$,

n_c being the cutoff point.

The inverse procedures will yield $h(n)$.

If $a \geq 1$, the complex cepstrum will have

a train of impulses on its negative time axis:

at $(n + kn_0), \ k = 1, 2, \ldots.$

An exponential weighting sequence may be used

to achieve the condition $a < 1$.

If the weighted signal satisfies the minimum-phase

condition, the cepstrum will be causal.

The power cepstrum: square of the inverse z-transform

of the logarithm of the squared magnitude of the z-transform

of the given signal.

In practice, z-transform replaced by the FFT.

Advantage: phase unwrapping not required.

The power cepstrum does not facilitate

separation of the components of the signal.

Evaluating the inverse z-transform on the unit circle

in the z-plane, the power cepstrum $\hat{y}_p(n)$

of a signal $y(n)$ is defined as

$$\hat{y}_p(n) = \left\{ \frac{1}{2\pi j} \oint \log |Y(z)|^2 \, z^{n-1} \, dz \right\}^2 . \qquad (4.81)$$

Consider $y(n) = x(n) * h(n)$.

$$|Y(z)|^2 = |X(z)|^2 \, |H(z)|^2.$$

$$\log |Y(z)|^2 = \log |X(z)|^2 + \log |H(z)|^2.$$

$$\hat{y}_p(n) = \hat{x}_p(n) + \hat{h}_p(n). \qquad (4.82)$$

$\hat{h}_p(n)$: power cepstrum of the basic wavelet.

$\hat{x}_p(n)$: power cepstrum of the excitation signal.

Cross-product term neglected: will be zero if the two

component power cepstra occupy nonoverlapping ranges

in the cepstral domain (quefrency).

Final squaring operation in Equation 4.81 may be omitted:

cross-term does not arise, and Equation 4.82 is valid.

© R.M. Rangayyan, IEEE/Wiley, 2nd Ed., 2015

Power cepstrum does not retain phase information.

Useful in the identification of the presence of echoes.

Power cepstrum related to complex cepstrum as

$$\hat{y}_p(n) = [\hat{y}(n) + \hat{y}(-n)]^2. \qquad (4.83)$$

Consider a signal with two occurrences of a basic wavelet:

$$y(n) = h(n) + a\, h(n - n_0).$$

$$|Y(z)|^2 = |H(z)|^2\, |1 + a\, z^{-n_0}|^2. \qquad (4.84)$$

Taking the logarithm and substituting $z = \exp(j\omega)$:

$$\log |Y(\omega)|^2 = \log |H(\omega)|^2 + \log[1 + a^2 + 2\,a\,\cos(\omega n_0)]$$

$$= \log |H(\omega)|^2 + \log(1 + a^2)$$

$$+ \log\left(1 + \frac{2a}{1 + a^2}\cos(\omega n_0)\right). \qquad (4.85)$$

Log (PSD) has sinusoidal components or ripples
due to the echo: difficulties in spectral analysis.

Amplitudes and frequencies of the ripples related to
amplitude a of the echo and its time delay n_0.

■ ■ ■ ■ ■

Illustration of application: Voiced-speech =

slow vocal-tract response * fast glottal pulse train.

Deconvolve to estimate vocal-tract response.

Shortpass filter the complex cepstrum; $n_c = 0.003125 \ s$.

Signal padded with zeros to twice its duration;

exponential weighting with $\alpha = 0.99$.

Facilitates spectral analysis without the

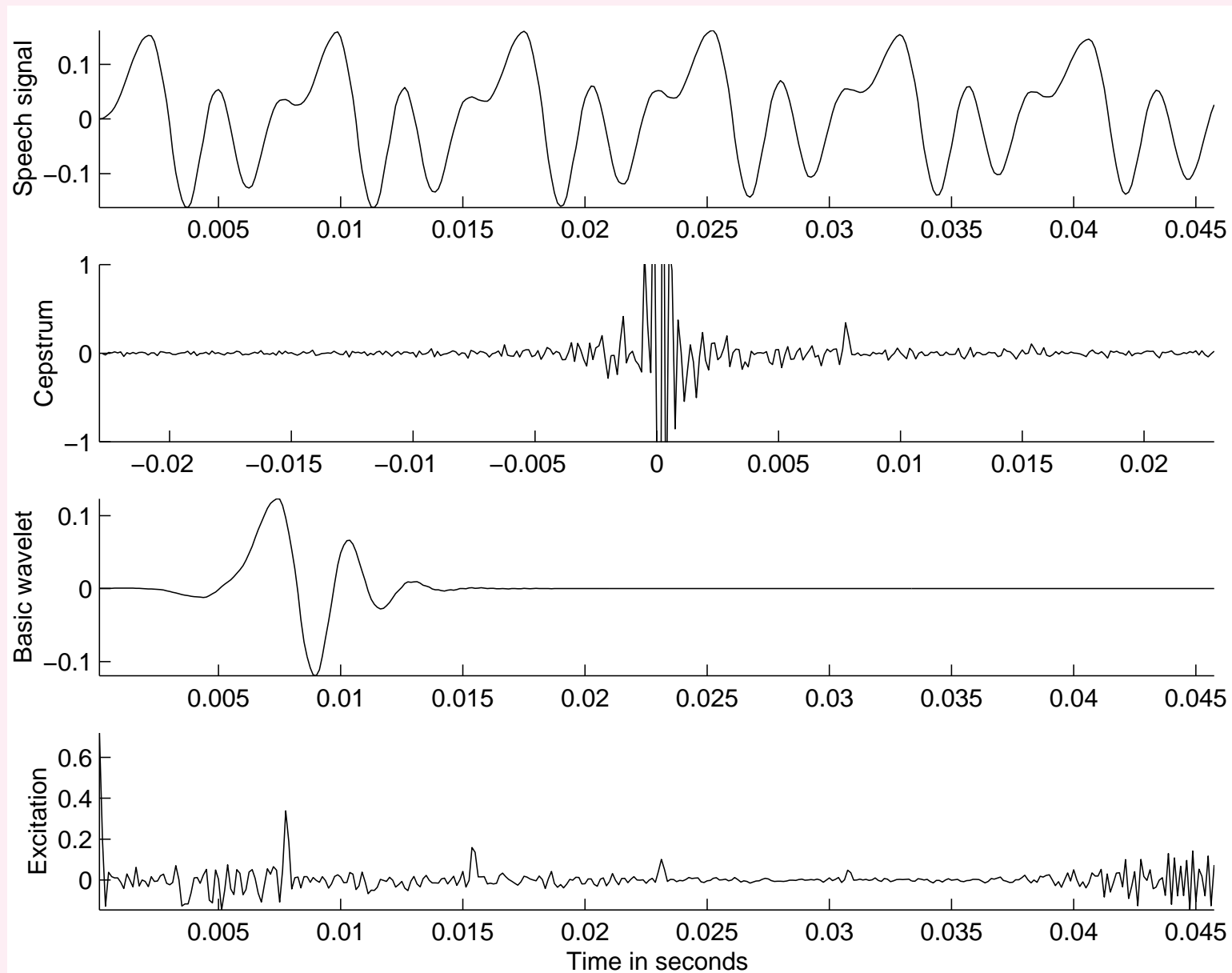effect of the quasiperiodic repetitions in the speech signal.

Figure 4.27: From top to bottom: a segment of a voiced-speech signal over six pitch periods (extracted from the signal shown in Figure 1.51 and lowpass filtered); the complex cepstrum of the signal (the amplitude axis has been stretched to make the peaks at the echo time and its multiples more readily visible; values outside the range ± 1.0 have been clipped); the (shifted) basic wavelet extracted by shortpass filtering the cepstrum; and the excitation sequence extracted by longpass filtering the cepstrum.

4.9   Application: ECG Rhythm Analysis

Problem: *Describe a method to measure the heart rate*

and average RR interval from an ECG signal.

Solution:
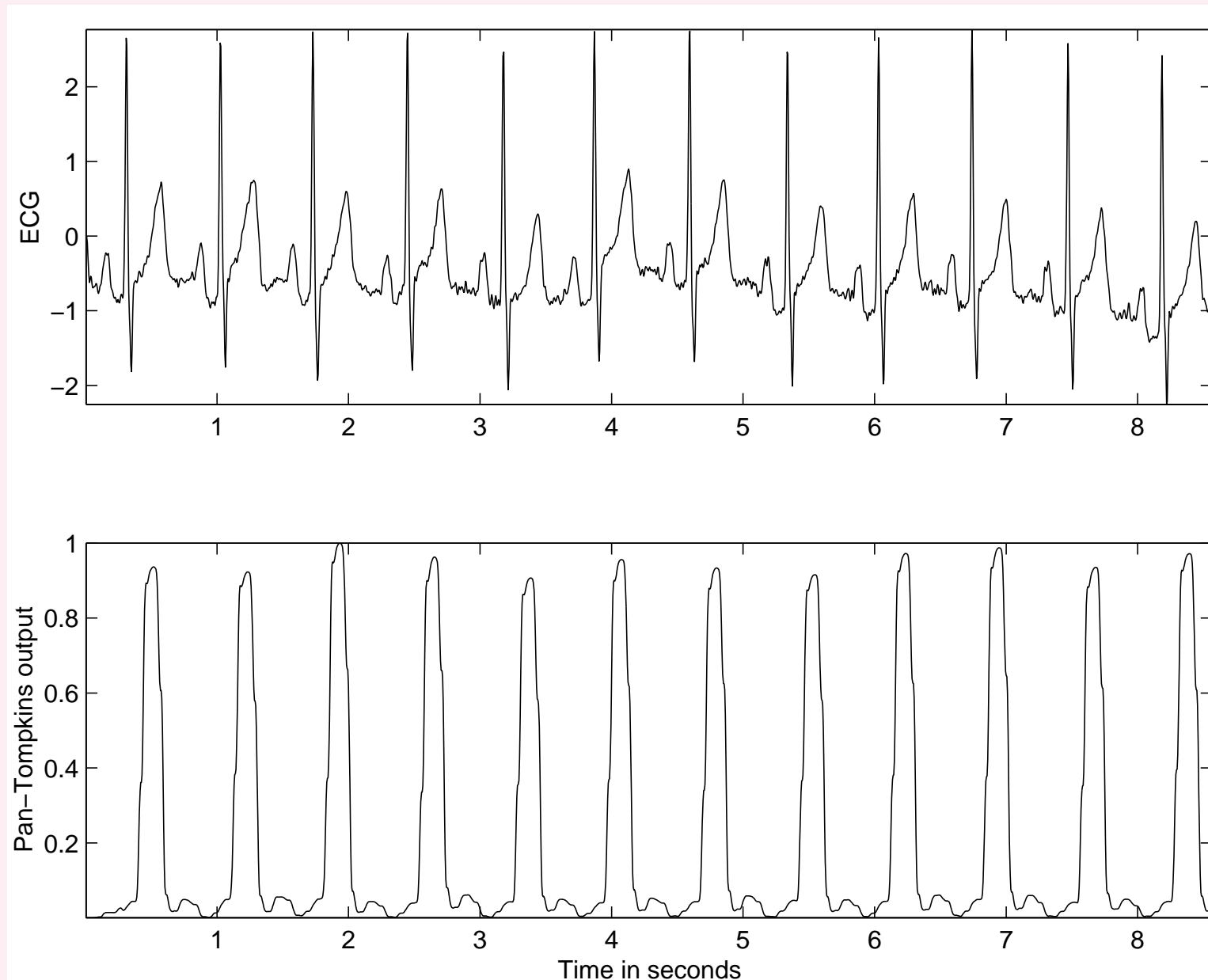
QRS detection using the Pan–Tompkins method.

Figure 4.28: Results of the Pan–Tompkins algorithm. Top: lowpass-filtered version of the ECG signal shown in Figure 3.5. Bottom: normalized result of the final integrator.

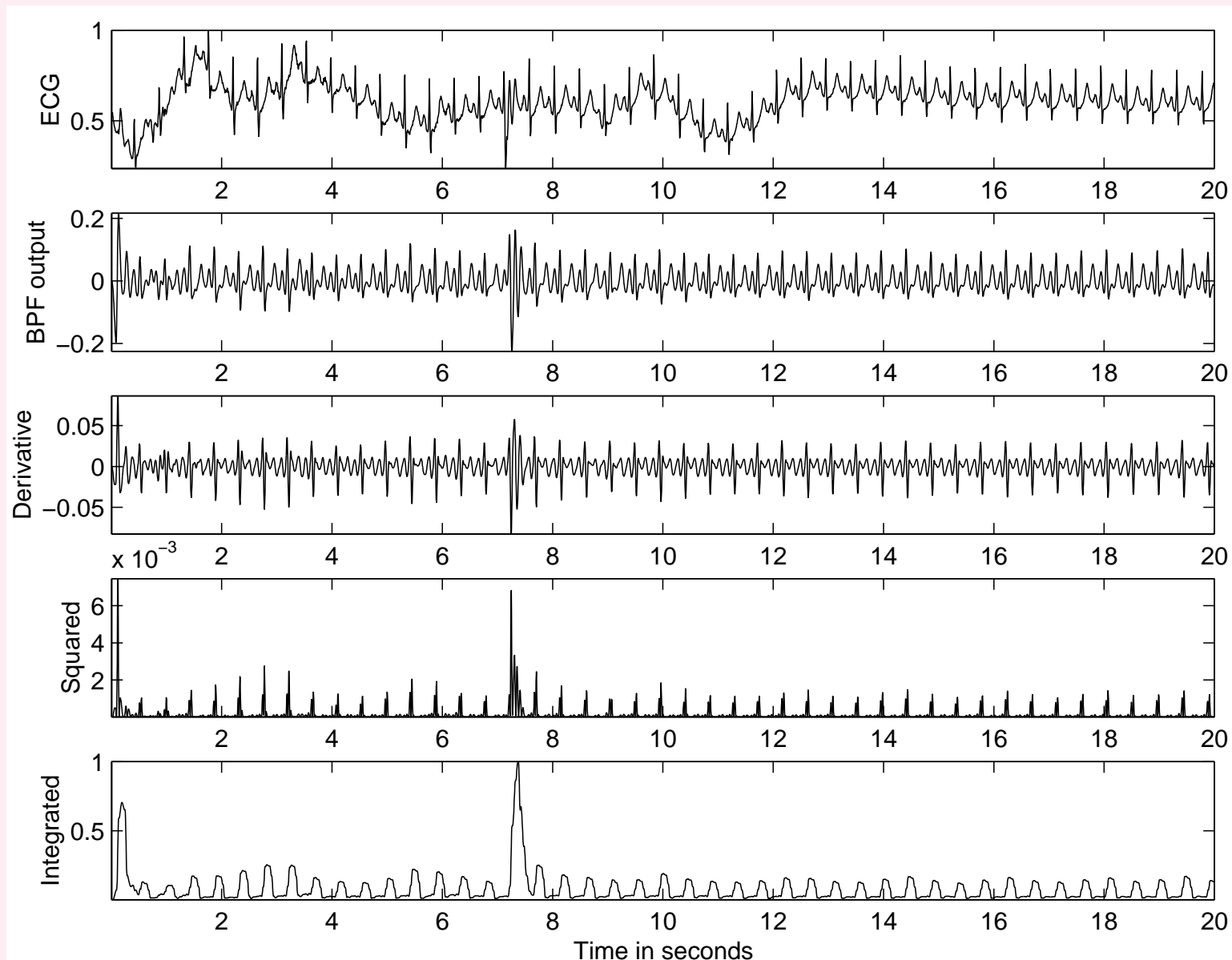Average RR interval $= 716\ ms$; effective heart rate $= 84\ bpm$.

Figure 4.29: Results of the Pan–Tompkins algorithm with a noisy ECG signal. From top to bottom: ECG signal sampled at $200\ Hz$; output of the bandpass filter (BPF); output of the derivative-based operator; the result of squaring; and normalized result of the final integrator.

Average RR interval $= 446.6\ ms$; effective heart rate $= 137\ bpm$.

4.10   Application: Identification of Heart Sounds

Problem: *Outline a signal processing algorithm*

to identify S1 and S2 in a PCG signal, and further

segment the PCG signal into its systolic and diastolic parts.

The ECG and carotid pulse signals are available

for reference.

Solution: Use ECG and carotid pulse signals to

demarcate the onset of S1 and S2 in the PCG.

Beginning of S1 in PCG = beginning of QRS in ECG.

Detect QRS using the Pan–Tompkins method.

Detection of the beginning of S2:

Let the heart rate be $HR\ bpm$.

Preejection period PEP = interval from the

beginning of QRS to onset of carotid upstroke.

Rate-corrected PEP: $PEPC = PEP + 0.4\ HR$,

with the periods in ms.

$PEPC$: $131 \pm 13\ ms$ for normal adults.

Ejection time ET = interval from

onset of carotid upstroke to dicrotic notch.

Rate-corrected ejection time in ms:

$$ETC = ET + 1.6\ HR,$$

range of $395 \pm 13\ ms$ for normal adult males and

$415 \pm 11\ ms$ for normal adult females.

Using $PEPC_{\max} = 144\ ms$ and $HR_{\min} = 60\ bpm$,

we get $PEP_{\max} = 120\ ms$.

With $HR_{\min} = 60\ bpm$ and $ETC_{\max} = 425\ ms$,

we get $ET_{\max} = 325\ ms$.

With these parameters, the maximum interval

between QRS and dicrotic notch is $380\ ms$.

Procedure proposed by Lehner and Rangayyan

for detection of the dicrotic notch:

search the output of the second-derivative-based method

in a $500\ ms$ interval after the QRS (Section 4.3.3).

After the dicrotic notch is detected, subtract the time delay

between the beginning of S2 and D.

Average S2 – D delay: $42.6\ ms$; SD: $5.0\ ms$.

Procedure to segment a PCG signal into its

systolic and diastolic parts:

1. Use Pan–Tompkins method to locate the QRS complexes in the ECG.

2. Identify one period of PCG as the interval between two successive QRS locations.
   Subtract the delay introduced by the filters in the Pan–Tompkins method.

3. Use the Lehner and Rangayyan method to detect the dicrotic notch in the carotid pulse.

4. Standardized S2 – D delay = mean plus two SD = $52.6\ ms$.

   Subtract the delay from the detected dicrotic notch Location to obtain the onset of S2.

5. S1 – S2 interval is the systolic part of the PCG cycle.

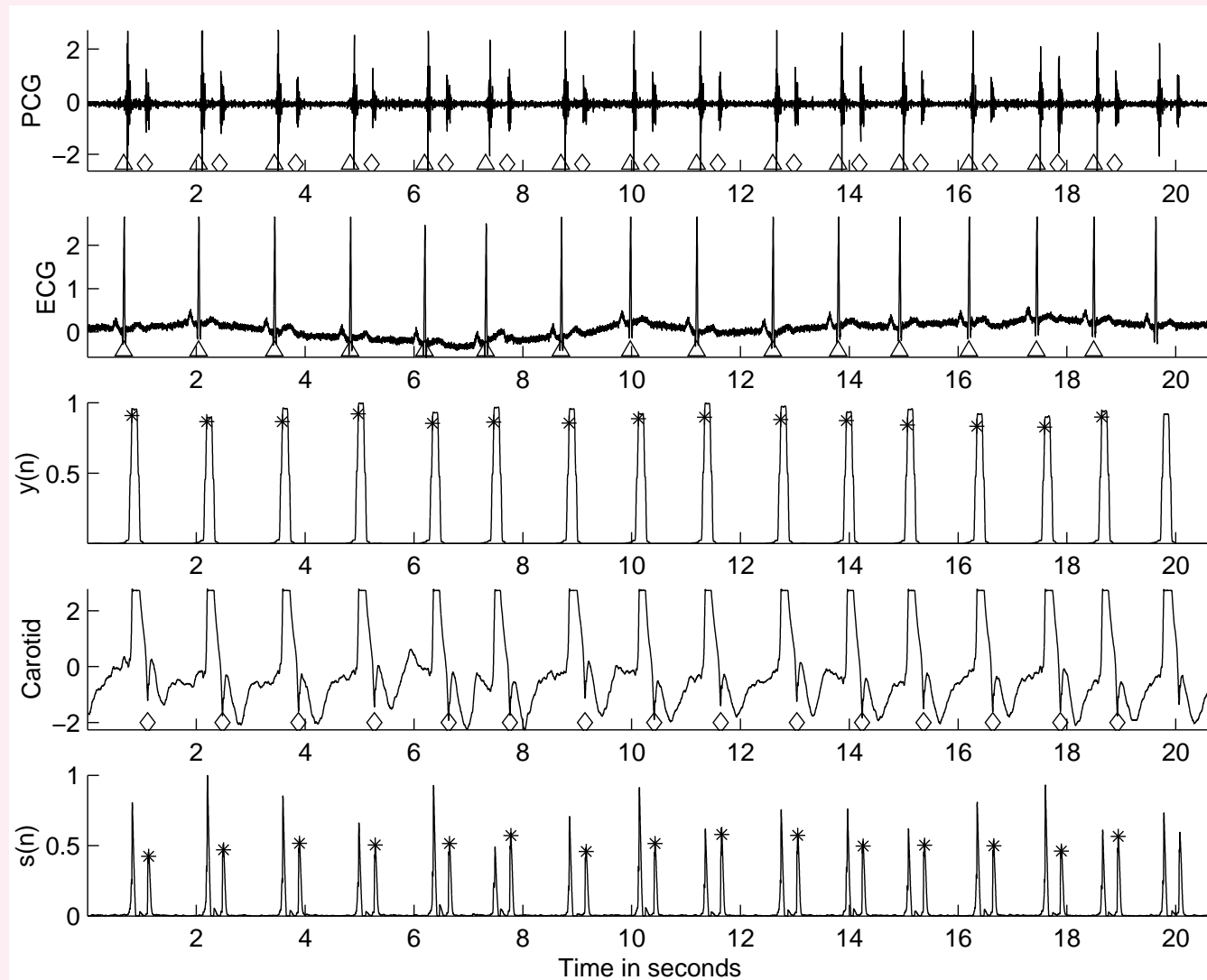6. Interval between S2 and next S1 is the diastolic part.

Figure 4.30: Results of segmentation of a PCG signal into systolic and diastolic parts using the ECG and carotid pulse signals for reference. From top to bottom: the PCG signal of a normal subject (male subject, 23 years); the ECG signal; $y(n)$, the output of the Pan–Tompkins method for detection of the QRS after normalization to the range $(0, 1)$; the carotid pulse signal; $s(n)$, the output of the Lehner and Rangayyan method for detection of the dicrotic notch, normalized to the range $(0, 1)$. The peaks detected in the outputs of the two methods have been identified with $*$ marks. The QRS and D positions have been marked with the triangle and diamond symbols, respectively. The S1 and S2 positions are marked on the PCG trace with triangles and diamonds, respectively. The last cardiac cycle was not processed.
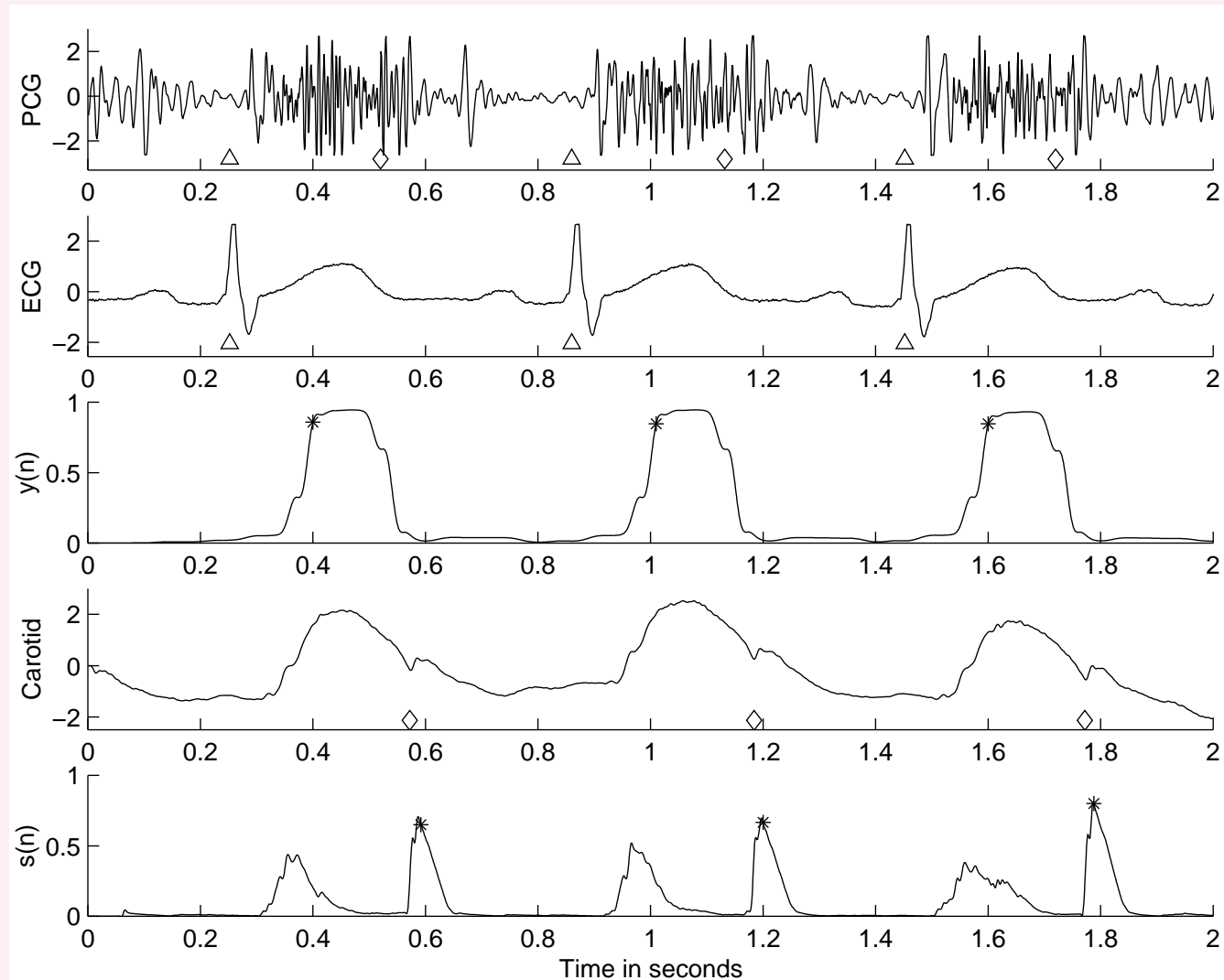
Figure 4.31: Results of segmentation of a PCG signal into systolic and diastolic parts using the ECG and carotid pulse signals for reference. From top to bottom: the PCG signal of a patient with a split S2, systolic ejection murmur, and opening snap of the mitral valve (female patient, 14 months); the ECG signal; $y(n)$, the output of the Pan–Tompkins method for detection of the QRS; the carotid pulse signal; $s(n)$, the output of the Lehner and Rangayyan method for detection of the dicrotic notch. The peaks detected in the outputs of the two methods have been identified with $*$ marks. The QRS and D positions have been marked with the triangle and diamond symbols, respectively. The S1 and S2 positions are marked on the PCG trace with triangles and diamonds, respectively.

4.11   Application: Aortic Component of S2

A2 caused by closure of aortic valve at end of systole.

P2 caused by closure of pulmonary valve.

Relative timing of A2 and P2 depends upon the

pressure differences across the corresponding valves in the

left and right ventricular circulatory systems.

     © R.M. Rangayyan, IEEE/Wiley, 2nd Ed., 2015

In a normal individual, timing of P2 varies with respiration;

the timing of A2 is independent of respiration.

Pulmonary pressure decreased during inspiration,

leading to a delayed closure of the pulmonary valve and

increased (audible and visible) gap between A2 and P2.

Gap closed; A2, P2 overlap during expiration (normally).

A2 and P2 have individual durations of about $50\ ms$.

Normal inspiratory A2 – P2 gap $\sim 30 - 40 \ ms$;

abnormal splits as long as $100 \ ms$ have been recorded.

Split in S2 $> 40 \ ms$ during sustained expiration: abnormal.

Complete right bundle-branch block could cause

delayed activation of the right ventricle:

delayed pulmonary valve closure, delayed P2, split S2.

Other conditions causing split S2: pulmonary stenosis,

atrial septal defect, ventricular septal defect.

Left bundle-branch block: delayed contraction of the

left ventricle, delayed aortic valve closure

(w.r.t. right ventricle and the pulmonary valve),

A2 appears after P2 — *reversed splitting*.

Aortic insufficiency and abnormally early closure of the

pulmonary valve also cause reversed splitting of S2.

Identification of A2 and P2 could assist in the

diagnosis of several cardiovascular defects and diseases.

Problem: *Given that the second heart sound S2*

is made up of an aortic component A2 and a

pulmonary component P2 with variable temporal

relationships, propose a method to detect only A2.

Solution:

Detect dicrotic notch in the carotid pulse signal.

Detect the beginning of S2.

Direct relationship between aortic valve closure,

aortic incisura, and consequently the dicrotic notch.

Detect and segment S2 over several cardiac and

respiratory cycles.

Perform synchronized averaging of S2:

A2 appears at the same instant in every S2 segment;

strengthened by synchronized averaging.

P2 appears at different times;

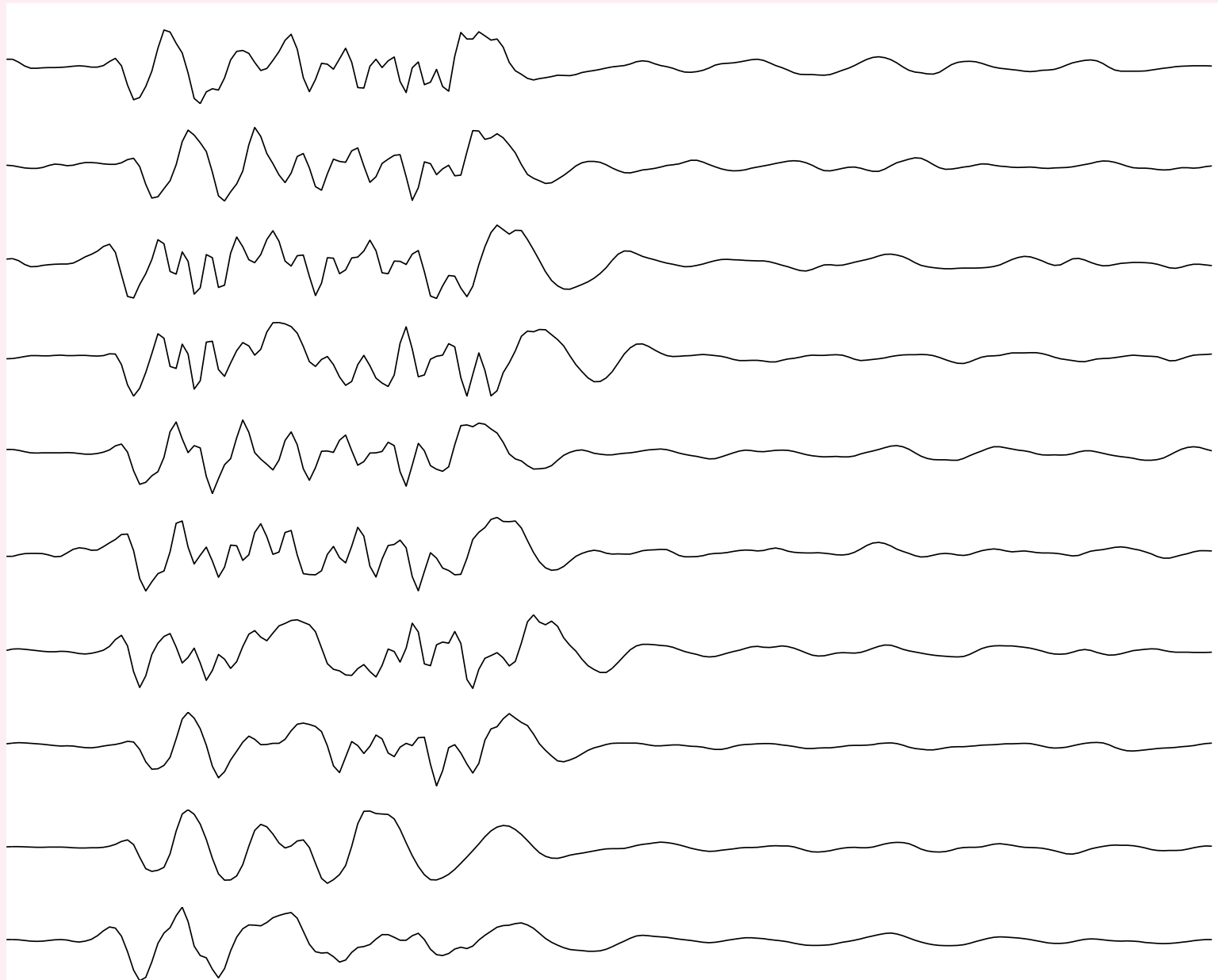cancelled or suppressed by averaging.

Figure 4.32: Synchronized averaging of S2 to detect A2 and suppress P2. The figure displays nine consecutive segments of S2 (duration = $300\ ms$) of a patient (female, 7 years) with atrial septal defect leading to a variable split in S2. The trace at the bottom is the average of S2 over 21 consecutive beats.

5

Analysis of Waveshape and Waveform Complexity

Some biomedical signals, e.g., the ECG and carotid pulse,

have simple and recognizable waveshapes, which are

modified by abnormal events and pathological processes.

EMG, PCG, VAG: no identifiable waveshapes.

EMG: complex interference patterns of several SMUAPs.

PCG: vibration waves with no specific waveshapes.

The waveform complexity in the EMG and the PCG varies

in relation to physiological and pathological phenomena.

Analyzing the waveform complexity of such signals may

assist in understanding of the processes they reflect.

5.1   Problem Statement

Explain how waveshapes and waveform complexity

in biomedical signals relate to the characteristics

of the underlying physiological and

pathological phenomena.

Propose techniques to parameterize and analyze

the signal features you identify.

5.2   Illustration of the Problem with Case Studies

5.2.1   The QRS complex in the case of bundle-branch block

The His bundle and its branches conduct the

cardiac excitation pulse from the AV node to the ventricles.

A block in one of the bundle branches causes asynchrony

between the contraction of the left and the right ventricles.

This causes a staggered summation of the action potentials

of the myocytes of the left and the right ventricles

over a longer-than-normal duration.

The result is a longer and possibly jagged QRS complex.

5.2.2   *The effect of myocardial ischemia and infarction on QRS waveshape*

Occlusion of a coronary artery or a branch due to

deposition of fat, calcium, etc. results in reduced

blood supply to a portion of the cardiac musculature:

the part of the myocardium served by the affected artery

suffers from ischemia or lack of blood supply.

Prolonged ischemia could lead to myocardial infarction:

the deceased myocytes cannot contract any more,

and no longer produce action potentials.

Action potential of an under-nourished ventricular myocyte:

smaller amplitude and shorter duration.

ST segment either elevated or depressed,

T wave may be inverted.

5.2.3 Ectopic beats

Ectopic beats generated by cardiac tissues that possess

abnormal pacing capabilities.

Ectopic beats originating in the atria: altered P waveshape

due to different paths of propagation of the excitation pulse.

QRS complex of atrial ectopic beats will appear normal.

Ectopic beats originating on the ventricles (PVCs):

bizarre waveshapes due to different paths of conduction.

PVCs typically lack a preceding P wave.

PVCs triggered by ectopic foci close to the AV node

may possess near-normal QRS shape.

RR intervals of preceding beat (short) and

succeeding beat (compensatory pause) play important

roles in determining the nature of ectopic beats.

5.2.4   EMG interference pattern complexity

Motor units are recruited by two mechanisms —

spatial and temporal recruitment — to produce

increasing levels of contraction and muscular force output.

SMUAPs of the active motor units overlap and produce a

complex interference pattern.

Increasing complexity of EMG with

increasing level of contraction.

© R.M. Rangayyan, IEEE/Wiley, 2nd Ed., 2015

5.2.5   PCG intensity patterns

Vibration waves in PCG not amenable to visual analysis.

General intensity pattern of PCG over a cardiac cycle

recognizable by auscultation or visual inspection.

Cardiovascular diseases and defects alter the

relative intensity patterns of S1 and S2,

cause additional sounds or murmurs,

split S2 into two distinct components, etc.

Many diseases cause murmurs;

intensity pattern or envelope of murmurs could assist

in arriving at a specific diagnosis.

5.3   Analysis of Event-related Potentials

Most important parameter in a visual ERP:

timing or latency of the first major positivity P120.

Latencies of the troughs before and after P120,

called N80 and N145, are also of interest.

Amplitudes of ERP features of lesser importance.

5.4   Morphological Analysis of ECG Waves

ECG waveshape changed by many abnormalities:

myocardial ischemia or infarction,

bundle-branch block, and ectopic beats.

5.4.1 Correlation coefficient

Problem: *Propose a general index*

to indicate altered QRS waveshape.

You are given a normal QRS template.

Solution: Jenkins et al. used correlation coefficient

$$\gamma_{xy} = \frac{\Sigma_{n=0}^{N-1} \ x(n) \ y(n)}{\left[\Sigma_{n=0}^{N-1} \ x^2(n) \ \Sigma_{n=0}^{N-1} \ y^2(n)\right]^{1/2}} \cdot$$

Normal beat used as template to compute γ_{xy}

for each detected beat; see Figure 2.2.

Most normal beats: $\gamma_{xy} > 0.9$.

PVCs and beats with abnormal shape: lower values of γ_{xy}.

5.4.2   *The minimum-phase correspondent and signal length*

Most of the energy of a normal ECG signal is concentrated

within an interval of about $80\ ms$ in the QRS complex.

Normally isoelectric PQ, ST, and TP segments: no energy.

Certain abnormal conditions cause the QRS to widen

or the ST segment to bear a nonzero value:

energy of signal spread over a longer duration.

Problem: *Investigate the effect of the*

distribution of energy over the time axis

on a signal's characteristics.

Propose measures to parameterize the effects and

study their use in the classification of ECG beats.

Solution:

Signal $x(t)$: distribution of the amplitude

of a certain variable over the time axis.

$x^2(t)$: instantaneous energy of the signal.

$x^2(t), \ 0 \le t \le T$: energy distribution or density function.

Total energy of the signal:

$$E_x = \int_0^T x^2(t)\, dt. \qquad (5.1)$$

Facilitates definition of moments of the energy distribution.

Centroidal time:

$$t_{\bar{x}} = \frac{\int_0^T t\, x^2(t)\, dt}{\int_0^T x^2(t)\, dt}. \tag{5.2}$$

Dispersion of energy about the centroidal time:

$$\sigma_{t_{\bar{x}}}^2 = \frac{\int_0^T (t - t_{\bar{x}})^2\, x^2(t)\, dt}{\int_0^T x^2(t)\, dt}. \tag{5.3}$$

Similarity between the equations above and

Equations 3.1 and 3.3: normalized function

$$p_x(t) = \frac{x^2(t)}{\int_0^T x^2(t)\, dt} \qquad (5.4)$$

treated as a PDF.

Other moments may also be defined to characterize and

study the distribution of $x^2(t)$ over the time axis.

Minimum-phase signals:

Distribution of energy of a signal over its duration

related to its amplitude spectrum and phase spectrum.

Notion of minimum phase useful in analyzing

the distribution of energy over the time axis.

© R.M. Rangayyan, IEEE/Wiley, 2nd Ed., 2015

A signal $x(n)$ is a minimum-phase signal if both the signal

and its inverse $x_i(n)$ are one-sided signals —

completely causal or anticausal — with finite energy:

$$\sum_{n=0}^{\infty} x^2(n) < \infty,$$

$$\sum_{n=0}^{\infty} x_i^2(n) < \infty.$$

Note: The inverse of a signal is defined such that

$x(n) * x_i(n) = \delta(n)$; equivalently, $X_i(z) = \frac{1}{X(z)}$.

Important properties of a minimum-phase signal:

- For a given amplitude spectrum, there exists one and only one minimum-phase signal.

- Of all finite-energy, one-sided signals with identical amplitude spectra, the energy of the minimum-phase signal is optimally concentrated toward the origin, and the signal has the smallest phase lag and phase-lag derivative at each frequency.

- The z-transform of a minimum-phase signal has all poles and zeros inside the unit circle in the z-plane.

- The complex cepstrum of a minimum-phase signal is causal.

■ ■ ■ ■ ■ ■

Minimum-phase and maximum-phase components:

A signal $x(n)$ that does not satisfy

the minimum-phase condition,

referred to as a composite signal or a mixed-phase signal,

may be split into its minimum-phase component

and maximum-phase component

by filtering its complex cepstrum $\hat{x}(n)$.

To obtain the minimum-phase component,

the causal part of the complex cepstrum is chosen as

$$\hat{x}_{\min}(n) = \begin{cases} 0 & n < 0 \\ 0.5\,\hat{x}(n) & n = 0 \\ \hat{x}(n) & n > 0 \end{cases}. \qquad (5.5)$$

The inverse procedures yield the

minimum-phase component $x_{\min}(n)$.

Maximum-phase component obtained by application of the

inverse procedures to the anticausal part of the cepstrum:

$$\hat{x}_{\max}(n) = \begin{cases} \hat{x}(n) & n < 0 \\ 0.5\,\hat{x}(n) & n = 0 \\ 0 & n > 0 \end{cases}. \qquad (5.6)$$

      © R.M. Rangayyan, IEEE/Wiley, 2nd Ed., 2015

The minimum-phase and maximum-phase components

of a signal satisfy the following relationships:

$$\hat{x}(n) = \hat{x}_{\min}(n) + \hat{x}_{\max}(n), \tag{5.7}$$

$$x(n) = x_{\min}(n) * x_{\max}(n). \tag{5.8}$$

The minimum-phase correspondent (MPC):

A mixed-phase signal may be converted to a

minimum-phase signal that has the same spectral magnitude

as the original signal by filtering the complex cepstrum as

$$\hat{x}_{MPC}(n) = \begin{cases} 0 & n < 0 \\ \hat{x}(n) & n = 0 \\ \hat{x}(n) + \hat{x}(-n) & n > 0 \end{cases} \qquad (5.9)$$

and applying the inverse procedures.

The *minimum-phase correspondent* or MPC

possesses optimal concentration of energy around the origin

under the constraint imposed by the magnitude spectrum

of the original mixed-phase signal.

Observe that $\hat{x}_{MPC}(n) = 2 \times$ even part of $\hat{x}(n)$ for $n > 0$.

This leads to a simpler procedure to compute the MPC:

Assume $\hat{X}(z) = \log X(z)$ to be analytic over the unit circle.

$$\hat{X}(\omega) = \hat{X}_R(\omega) + j\hat{X}_I(\omega);$$

R and I indicate the real and imaginary parts.

$\hat{X}_R(\omega)$ and $\hat{X}_I(\omega)$ are the log-magnitude and

phase spectra of $x(n)$.

Now, IFT of $\hat{X}_R(\omega)$ = even part of $\hat{x}(n)$,

defined as $\hat{x}_e(n) = [\hat{x}(n) + \hat{x}(-n)]/2$.

Thus, we have

$$\hat{x}_{MPC}(n) = \begin{cases} 0 & n < 0 \\ \hat{x}_e(n) & n = 0 \\ 2\,\hat{x}_e(n) & n > 0 \end{cases} . \qquad (5.10)$$

Thus we do not need to compute the complex cepstrum,

which requires the unwrapped phase spectrum of the signal,

but need only to compute a *real cepstrum*

using the log-magnitude spectrum.

Furthermore, given that PSD = FT of ACF, we have

$$\log \left[FT \left\{ \phi_{xx}(n) \right\} \right] = 2 \, \hat{X}_R(\omega).$$

It follows that, in the cepstral domain,

$\hat{\phi}_{xx}(n) = 2\,\hat{x}_e(n)$, and therefore

$$\hat{x}_{MPC}(n) = \begin{cases} 0 & n < 0 \\ 0.5\,\hat{\phi}_{xx}(n) & n = 0 \\ \hat{\phi}_{xx}(n) & n > 0 \end{cases}, \qquad (5.11)$$

where $\hat{\phi}_{xx}(n)$ is the cepstrum of the ACF $\phi_{xx}(n)$ of $x(n)$.

Signal length: different from signal duration!

SL relates to how the energy of a signal is

distributed over its duration.

SL depends upon both magnitude and phase spectra.

For one-sided signals, minimum SL implies

minimum phase; the converse is also true.

General definition of SL of a signal $x(n)$:

$$SL = \frac{\Sigma_{n=0}^{N-1} \, w(n) \, x^2(n)}{\Sigma_{n=0}^{N-1} \, x^2(n)}. \qquad (5.12)$$

$w(n)$: nondecreasing, positive weight function; $w(0) = 0$.

Definition of $w(n)$ depends upon the application and

the desired characteristics of SL.

Samples of the signal away from the origin $n = 0$

receive progressively heavier weighting by $w(n)$.

Definition of SL: normalized moment of $x^2(n)$.

If $w(n) = n$: SL= centroidal time instant of $x^2(n)$.

For a given amplitude spectrum and hence total energy,

the minimum-phase signal has its energy

optimally concentrated near the origin $\rightarrow$ lowest SL.

Signals with increasing phase lag have their

energy spread over a longer time duration:

larger SL due to the increased weighting by $w(n)$.

Illustration of application: Normal QRS vs PVCs.

Duration of normal QRS-T waves $\sim 350 - 400 \ ms$.

QRS $\sim 80 \ ms$ due to rapid and coordinated depolarization

of the ventricular motor units via the Purkinje fibers.

PVCs have QRS-T complexes that are wider than normal:

energy distributed over longer span within the total duration,

due to slower and disorganized excitation sequences

triggering the ventricular muscle fibers.

Ectopic triggers may not be conducted

via the Purkinje system;

may be conducted through the ventricular muscle cells.

PVCs lack an isoelectric ST segment.

Murthy and Rangaraj proposed the application of SL

to classify ECG beats as normal or ectopic (PVC).

To overcome ambiguities in the detected onset of each beat:

SL of the MPC of segmented ECG signals (P-QRS-T).

208 beats of a patient: 132 out of 155 normals and

48 out of 53 PVCs were correctly classified;

one beat missed by the QRS detection algorithm.
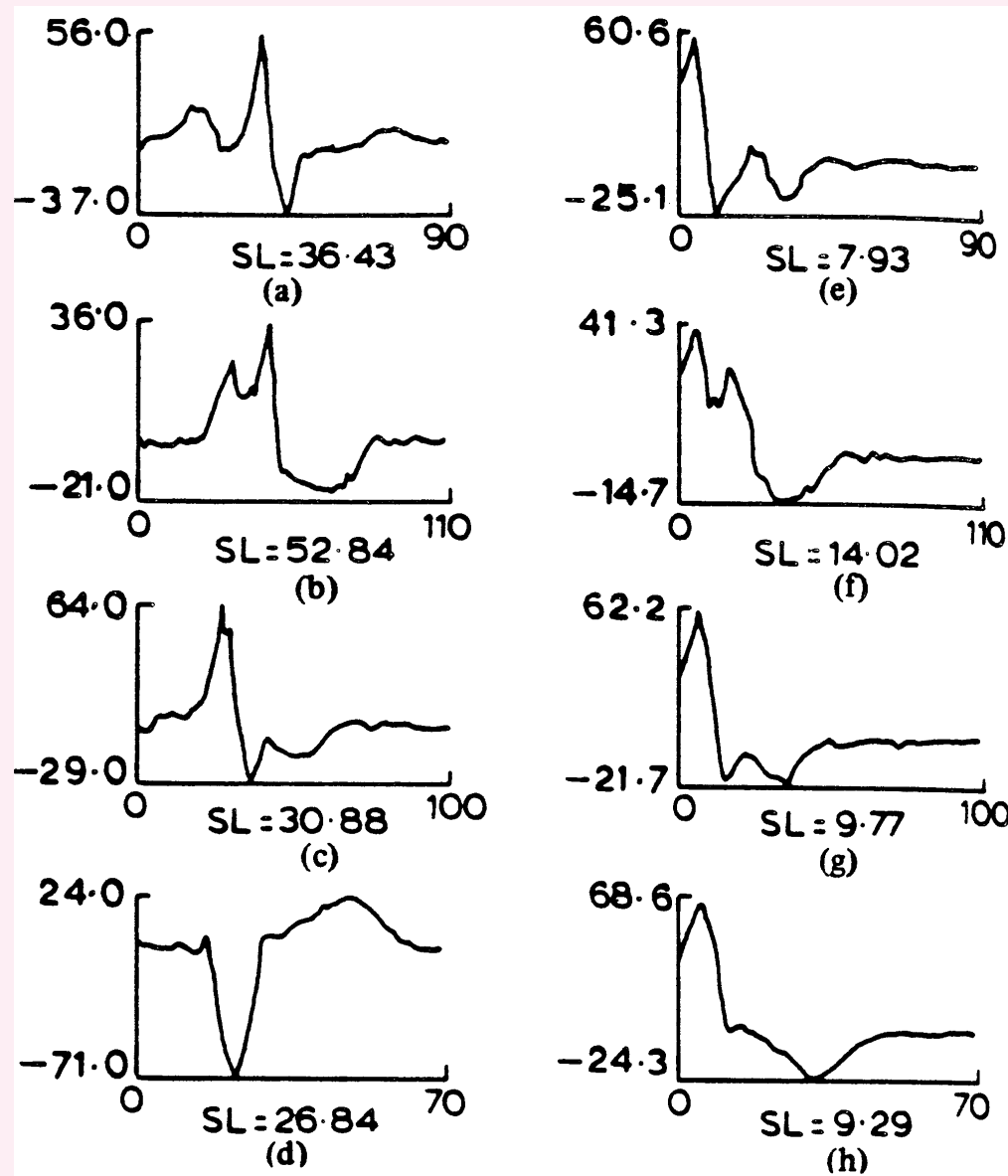
Figure 5.1: (a) A normal ECG beat and (b) – (d) three ectopic beats (PVCs) of a patient with multiple ectopic foci. (e) – (h) MPCs of the signals in (a) – (d). The *SL* values of the signals are also indicated. Note that the abscissa is labeled in samples, with a sampling interval of 10 *ms*. The ordinate is not calibrated. The signals have different durations and amplitudes although plotted to the same size. Reproduced with permission from I.S.N. Murthy and M.R. Rangaraj, New concepts for PVC detection, *IEEE Transactions on Biomedical Engineering,* 26(7):409–416, 1979. ©IEEE.
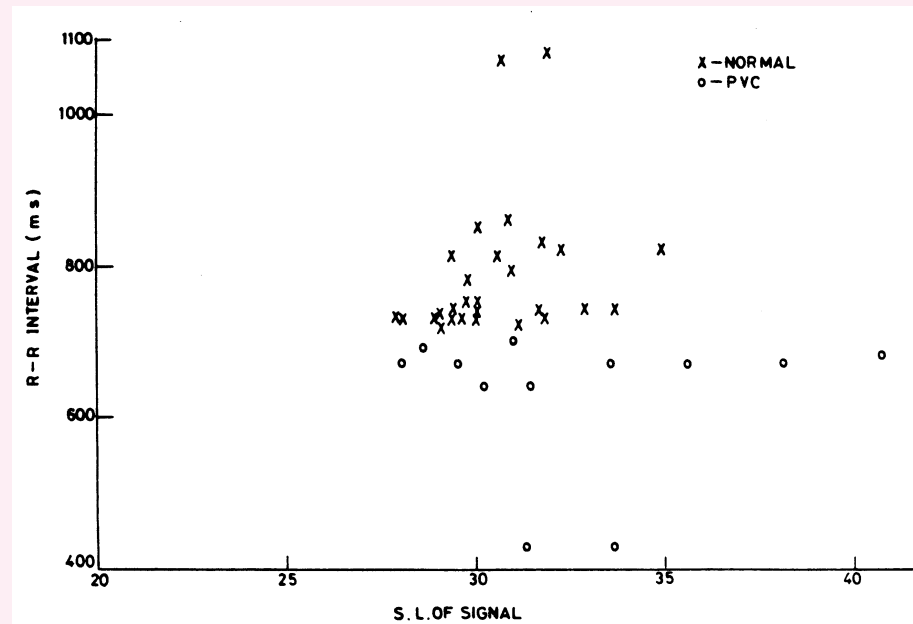
(a)
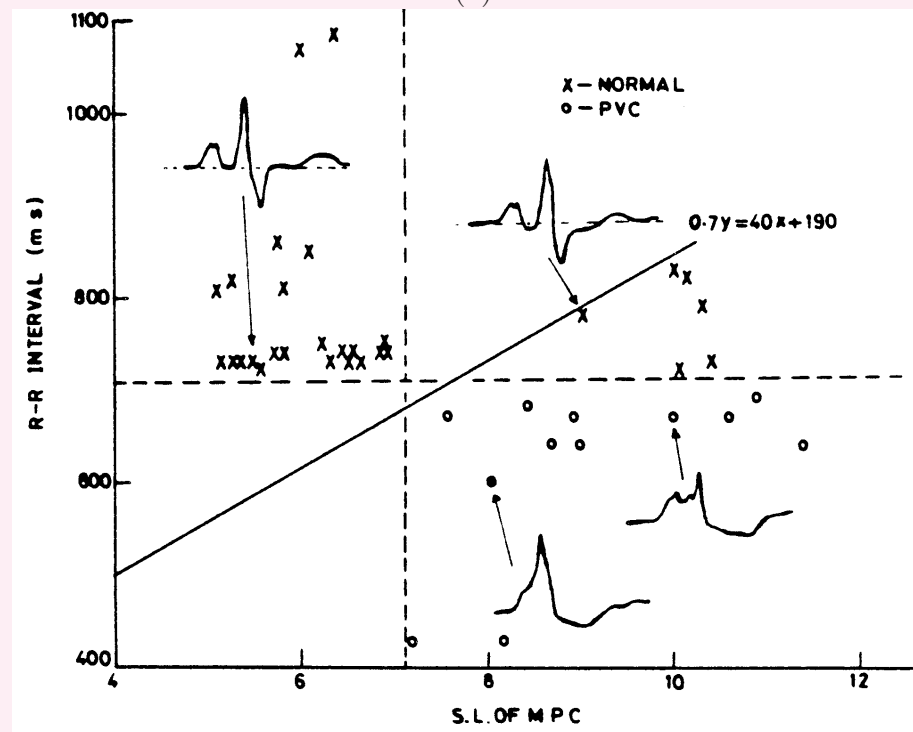
(b)

Figure 5.2: (a) Plot of RR and SL values of several beats of a patient with multiple ectopic foci (as in Figure 5.1). (b) Same as (a) but with the SL of the MPCs of the signals. A few representative ECG cycles are illustrated. The linear discriminant (decision) function used to classify the beats is also shown. Reproduced with permission from I.S.N. Murthy and M.R. Rangaraj, New concepts for PVC detection, *IEEE Transactions on Biomedical Engineering,* 26(7):409–416, 1979. ©IEEE.

5.4.3　ECG waveform analysis

Measures such as correlation coefficient and SL

provide general parameters to compare waveforms.

Detailed analysis of ECG waveforms requires several

features or measurements for categorization of various

QRS shapes and correlation with cardiovascular diseases.

ECG waveform depends upon the lead used:

sets of features derived for multiple-lead ECGs.

Steps for ECG waveform analysis:

1. Detection of ECG waves, primarily the QRS complex,

   and possibly the P and T waves.

2. Delimitation of wave boundaries,

   including the P, QRS, and T waves.

3. Measurement of interwave intervals, such as

   RR, PQ, QT, ST, QQ, and PP intervals.

4. Characterization of the morphology (shape) of the waves.

5. Recognition of isoelectric segments expected

   (PQ and ST).

Cox et al. proposed four measures to characterize
QRS complexes:

1. *Duration* — duration or width of QRS.

2. *Height* — maximum minus minimum amplitude of QRS.

3. *Offset* — positive or negative vertical distance
   from midpoint of baseline to center of QRS complex.

   Baseline: line connecting temporal boundary points of
   QRS complex.

   Center: midpoint between highest and lowest
   QRS amplitude.

4. *Area* — area under QRS waveform rectified w.r.t.
   straight line through midpoint of baseline.
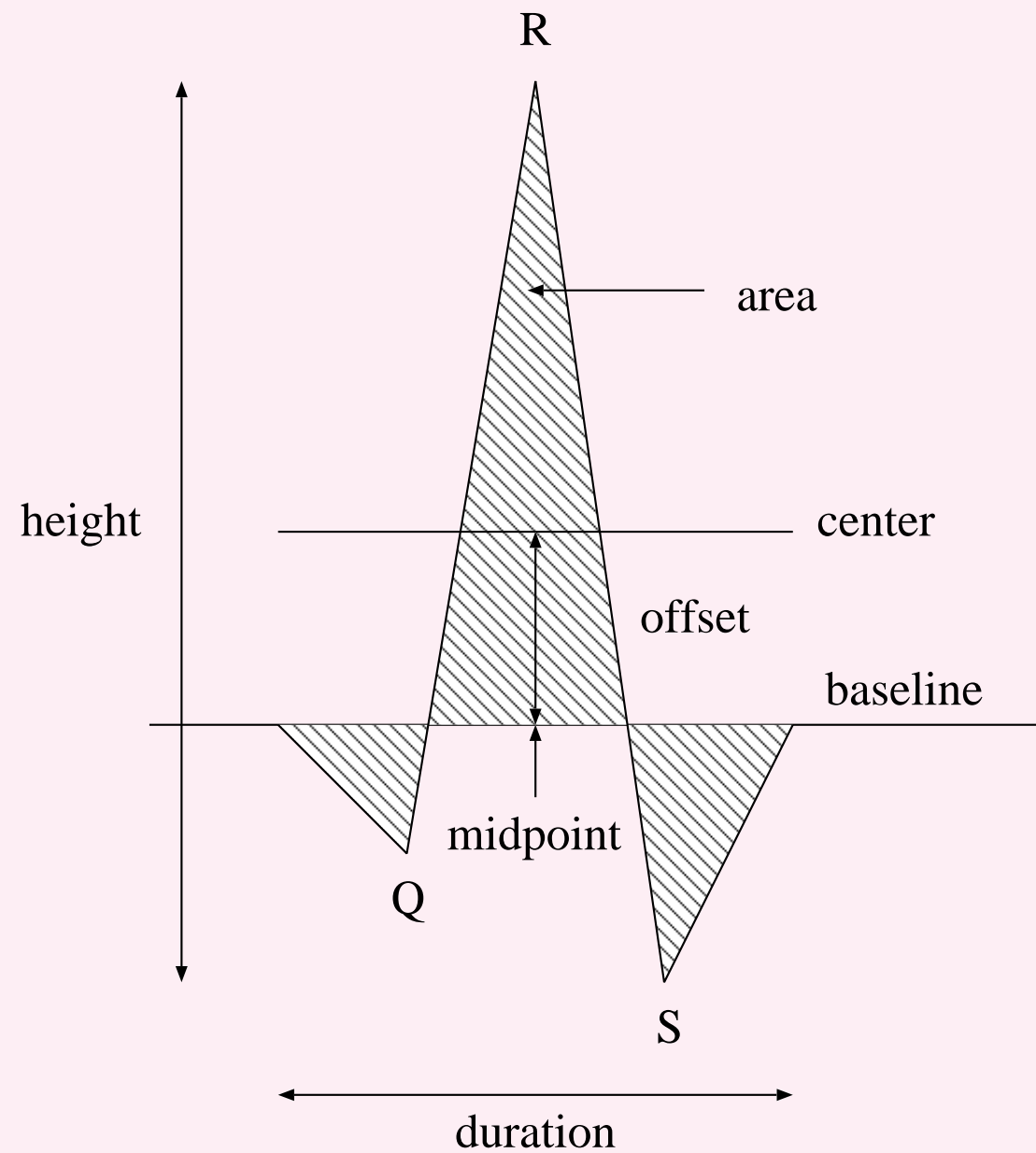
Figure 5.3: ECG waveform features used by Cox et al. and Nolle.

"Argus:" Arrhythmia Guard System.

QRS complexes divided into 16 dynamic families.

Families $00, 01, 02, 04, 06,$ and 10: normal beats.

Clinical tests of Argus with over $50,000$ beats:

85% of $45,364$ normal beats detected & classified correctly;

78% of $4,010$ PVCs detected & classified correctly;

0.04% of normal beats missed; 5.3% of PVCs missed;

38 normals ($< 0.1\%$ of the beats) falsely labeled as PVCs.
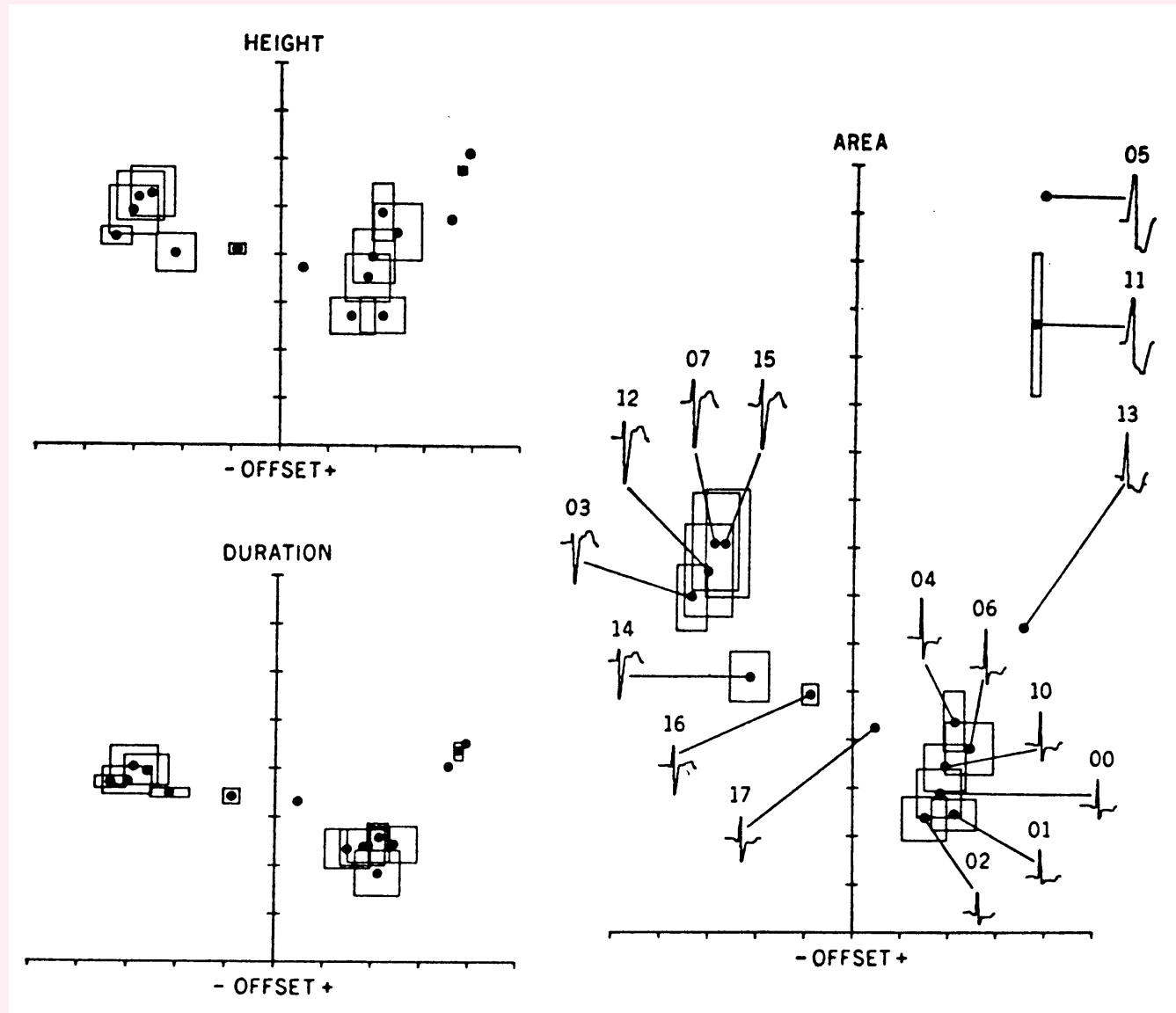
Figure 5.4: Use of four features to catalog QRS complexes into one of 16 dynamic families of similar complexes enclosed by four-dimensional boxes. The waveforms of typical members of each family are shown in the area-versus-offset feature plane. The family numbers displayed are in the octal (base eight) system. The families labeled 00, 01, 02, 04, 06, and 10 were classified as normal beats, with the others being PVCs or border-line beats. Reproduced with permission from J.R. Cox, Jr., F.M. Nolle, and R.M. Arthur, Digital analysis of the electroencephalogram, the blood pressure wave, and the electrocardiogram, *Proceedings of the IEEE,* 60(10):1137–1164, 1972. ©IEEE.

5.5   Envelope Extraction and Analysis

Signals with complex patterns, such as the EMG and PCG,

may not permit direct analysis of their waveshape.

Intricate high-frequency variations may not be of interest;

general trends in level of the overall activity useful:

the *envelope* of the signal carries important information.

Problem: *Formulate algorithms to extract the envelope*

of an EMG or PCG signal to facilitate analysis of

trends in the level of activity or energy in the signal.

Solution:

Obtain the absolute value of the signal at each instant:

perform full-wave rectification.

© R.M. Rangayyan, IEEE/Wiley, 2nd Ed., 2015

Rectification creates abrupt discontinuities at instants when

signal values change sign: at zero-crossings.

Discontinuities create high-frequency components of

significant magnitude: need lowpass filter with

low bandwidth in the range of $0 - 10$ or $0 - 50 \; Hz$

to obtain smooth envelopes of EMG and PCG signals.

MA filter useful for lowpass filtering.

Basic definition of time-averaged envelope:

$$y(t) = \frac{1}{T_a} \int_{t-T_a}^{t} |x(t)| \, dt, \qquad (5.13)$$

where T_a is the duration of the MA window.

Lehner and Rangayyan applied a weighted MA filter to the

squared PCG signal: smoothed energy distribution curve

$$E(n) = \sum_{k=1}^{M} x^2(n - k + 1) \, w(k), \qquad (5.14)$$

where $x(n)$ is the PCG signal,

$w(k) = M - k + 1$, and $M = 32$ with $f_s = 1,024 \, Hz$.

Observe: difference between energy and power is

division by the time interval; scale factor ignored.

© R.M. Rangayyan, IEEE/Wiley, 2nd Ed., 2015

Envelope: total averaged activity within averaging window.

Filter: balance between the need to smooth discontinuities

and the requirement to maintain good sensitivity

to represent relevant changes in signal level or amplitude.

Procedure known as envelope detection or

amplitude demodulation.

5.5.1 Amplitude demodulation

Amplitude modulation (AM) of signals for

radio transmission:

multiplication of the signal $x(t)$ to be transmitted

by an RF carrier $\cos(\omega_c t)$, where ω_c is the carrier frequency.

AM signal $y(t) = x(t) \, \cos(\omega_c t)$.

If the exact carrier wave used at the transmitting end

were available at the receiving end (including phase),

synchronous demodulation possible by

multiplying the received signal $y(t)$ with the carrier.

Demodulated signal:

$$x_d(t) = y(t) \ \cos(\omega_c t) = x(t) \ \cos^2(\omega_c t)$$

$$= \frac{1}{2} \ x(t) + \frac{1}{2} \ x(t) \ \cos(2\omega_c t). \qquad (5.15)$$

AM component at $2\omega_c$ removed by a lowpass filter,

leaving the desired signal $x(t)$.

If $x(t)$ is always positive, or a DC bias is added,

the envelope of the AM signal is equal to $x(t)$.

Asynchronous demodulation possible —

just need to follow the envelope of $y(t)$;

does not require the carrier.

© R.M. Rangayyan, IEEE/Wiley, 2nd Ed., 2015

Carrier frequency ω_c is far greater than

the maximum frequency present in $x(t)$:

positive envelope of $y(t)$ extracted by

half-wave rectification.

Lowpass filter with an appropriate time constant

to "fill the gaps" between the peaks of the carrier wave

gives a good estimate of $x(t)$.

Complex demodulation: The given signal is

demodulated to derive the time-varying amplitude and

phase characteristics for each frequency (band) of interest.

$$x(t) = a(t) \ \cos[\omega_o t + \psi(t)] + x_r(t). \qquad (5.16)$$

ω_o: frequency of interest,

$a(t)$ and $\psi(t)$: time-varying amplitude and phase at ω_o;

$x_r(t)$: remainder after component at ω_o removed.

Assume that $a(t)$ and $\psi(t)$ vary slowly

in relation to the frequencies of interest.

$x(t)$ expressed in terms of complex exponentials:

$$x(t) = \frac{1}{2} a(t) \{\exp\{j[\omega_o t + \psi(t)]\}$$

$$+ \exp\{-j[\omega_o t + \psi(t)]\}\} + x_r(t). \qquad (5.17)$$

In complex demodulation, the signal is shifted in frequency

by $-\omega_o$ via multiplication with $2\exp(-j\omega_o t)$, to obtain

$$
\begin{aligned}
y(t) &= 2\,x(t)\,\exp(-j\omega_o t) \quad\quad\quad\quad\quad\quad\quad (5.18)\\
&= a(t)\,\exp[j\psi(t)] + a(t)\,\exp\{-j[2\omega_o t + \psi(t)]\}\\
&\quad + 2\,x_r(t)\,\exp(-j\omega_o t).
\end{aligned}
$$

Second term centered at $2\omega_o$, third term centered at ω_o;

only first term placed at DC.

A lowpass filter may be used to extract the first term:

$$y_o(t) \approx a(t) \exp[j\psi(t)]. \qquad (5.19)$$

The desired entities may then be extracted as

$a(t) \approx |y_o(t)|$ and $\psi(t) \approx \angle y_o(t)$.

Frequency resolution depends upon the bandwidth

of the lowpass filter used.

The procedure may be repeated at every frequency

or frequency band of interest.

Result: envelope of the signal for the specified frequency

or frequency band.

In biomedical signals such as the PCG and the EMG,

there is no underlying RF carrier wave in the signal:

the envelope rides on relatively high-frequency

acoustic or electrical activity with a composite spectrum.

5.5.2　Synchronized averaging of PCG envelopes

ECG and PCG: good signal pair for synchronized averaging.

One could average the PCG over several cardiac cycles

with the ECG as the trigger.

However, the PCG is not amenable to direct

synchronized averaging: the vibration waves may

interfere in a destructive manner and cancel one another.

Karpman et al. proposed to rectify the PCG signal,

smooth the result using a lowpass filter, and then

perform synchronized averaging of the envelopes

using the ECG as the trigger.
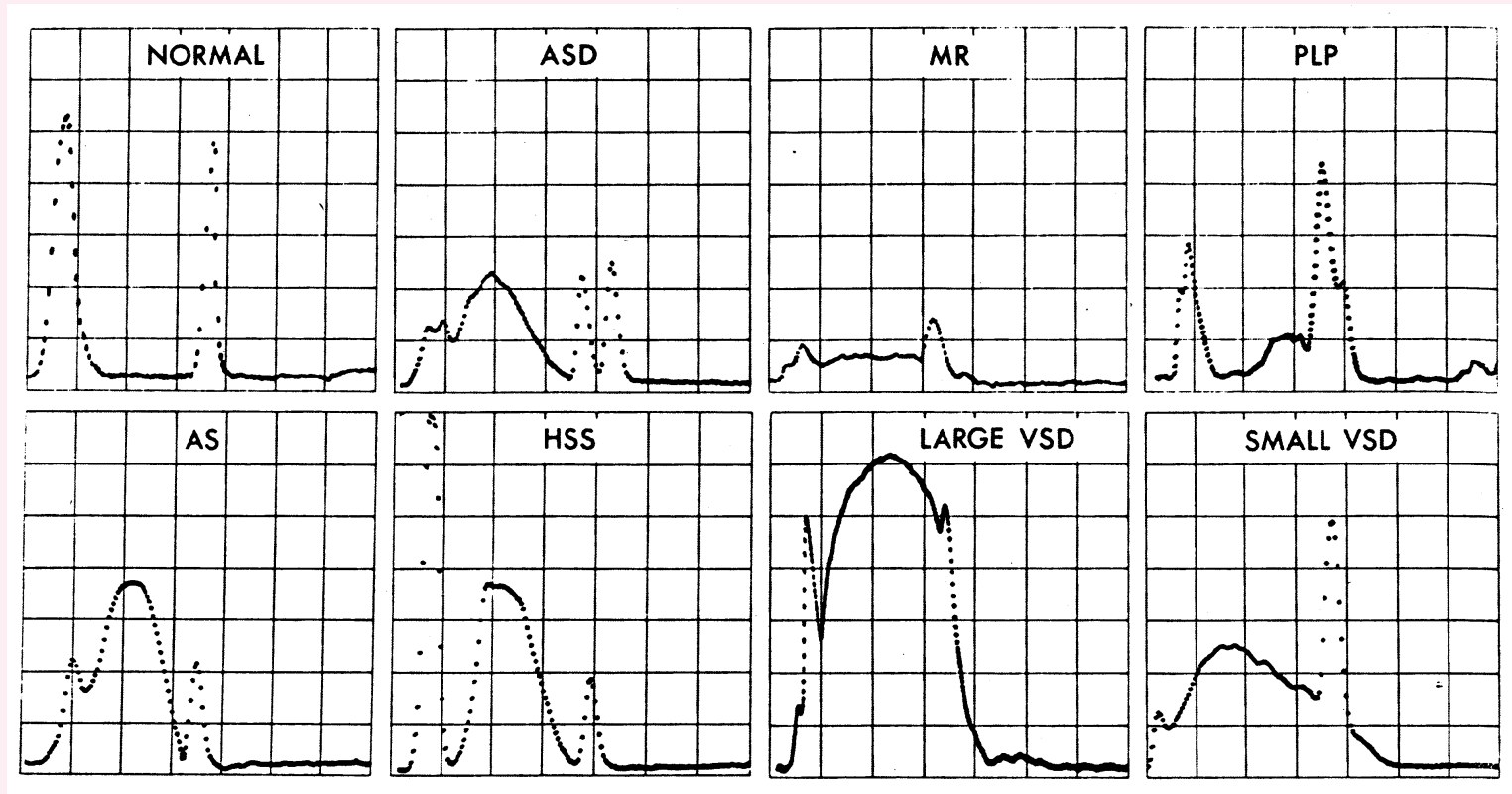
Figure 5.5: Averaged envelopes of the PCG signals of a normal subject and patients with systolic murmur due to aortic stenosis (AS), atrial septal defect (ASD), hypertrophic subaortic stenosis (HSS), rheumatic mitral regurgitation (MR), ventricular septal defect (VSD), and mitral regurgitation with posterior leaflet prolapse (PLP). Reproduced with permission from L. Karpman, J. Cage, C. Hill, A.D. Forbes, V. Karpman, and K. Cohn, Sound envelope averaging and the differential diagnosis of systolic murmurs, *American Heart Journal,* 90(5):600–606, 1975. ©American Heart Association.
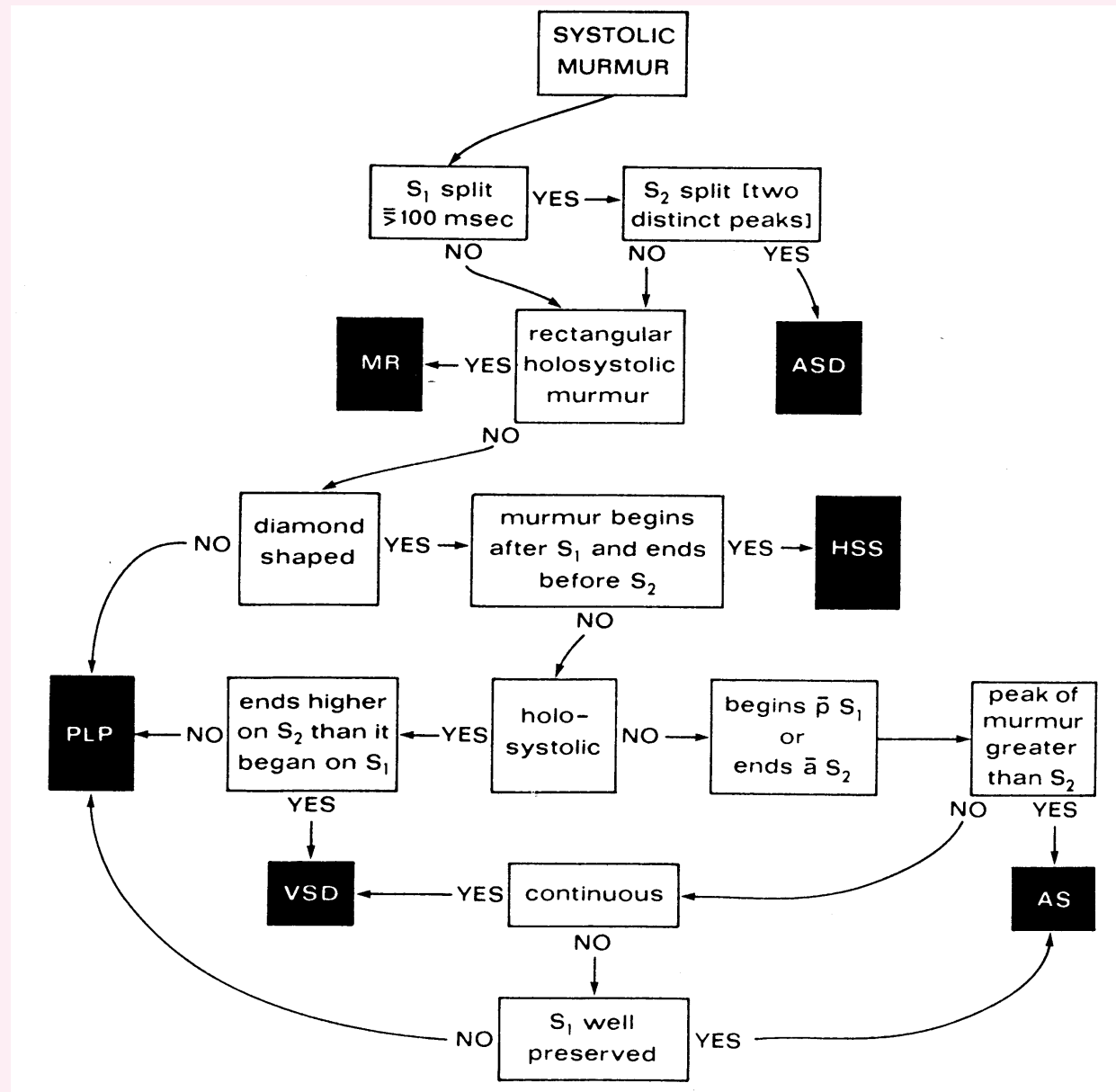
Figure 5.6: Decision tree to classify systolic murmurs based upon envelope analysis. For details on the abbreviations used, refer to the text or the caption of Figure 5.5. $\bar{p}S_1$: after S_1; $\bar{a}S_2$: before S_2. Reproduced with permission from L. Karpman, J. Cage, C. Hill, A.D. Forbes, V. Karpman, and K. Cohn, Sound envelope averaging and the differential diagnosis of systolic murmurs, *American Heart Journal,* 90(5):600–606, 1975. ©American Heart Association.

5.5.3   *The envelogram*

Sarkady et al.: *envelogram estimate* —

magnitude of the analytic signal $y(t)$ formed using the

PCG $x(t)$ and its Hilbert transform $x_H(t)$ as

$$y(t) = x(t) + jx_H(t). \qquad (5.20)$$

An analytic function is a complex function of time

having a Fourier transform that is zero for $f < 0$.

The Hilbert transform of a signal is defined as

the convolution of the signal with $\frac{1}{\pi t}$:

$$x_H(t) = \int_{-\infty}^{\infty} \frac{x(\tau)}{\pi(t-\tau)} \, d\tau. \qquad (5.21)$$

The Fourier transform of $\frac{1}{\pi t}$ is $-j\, sgn(\omega)$, where

$$sgn(\omega) = \begin{cases} -1, & \omega < 0 \\ 0, & \omega = 0 \\ 1, & \omega > 0 \end{cases} . \qquad (5.22)$$

Then, $Y(\omega) = X(\omega)[1 + sgn(\omega)]$.

$Y(\omega)$ is a one-sided or single-sideband function of ω

containing positive-frequency terms only.

Algorithm of Sarkady et al. to obtain
the envelogram estimate:

1. Compute the DFT of the PCG signal.

2. Set the negative-frequency terms to zero;
   $X(k) = 0$ for $\frac{N}{2} + 2 \leq k \leq N$,
   with the DFT indexed $1 \leq k \leq N$ as in MATLAB.

3. Multiply the positive-frequency terms,
   $X(k)$ for $2 \leq k \leq \frac{N}{2} + 1$, by 2;
   the DC term $X(1)$ remains unchanged.

4. Compute the inverse DFT of the result.

5. The magnitude of the result gives the
   envelogram estimate.

The complex demodulation procedure of Sarkady et al.

yields a high-resolution envelope of the input signal.

Envelograms and PSDs of PCG signals over single cycles

tend to be noisy; affected by respiration and muscle noise.

Sarkady et al.: synchronized averaging of envelograms

and PSDs of PCGs over several cardiac cycles.
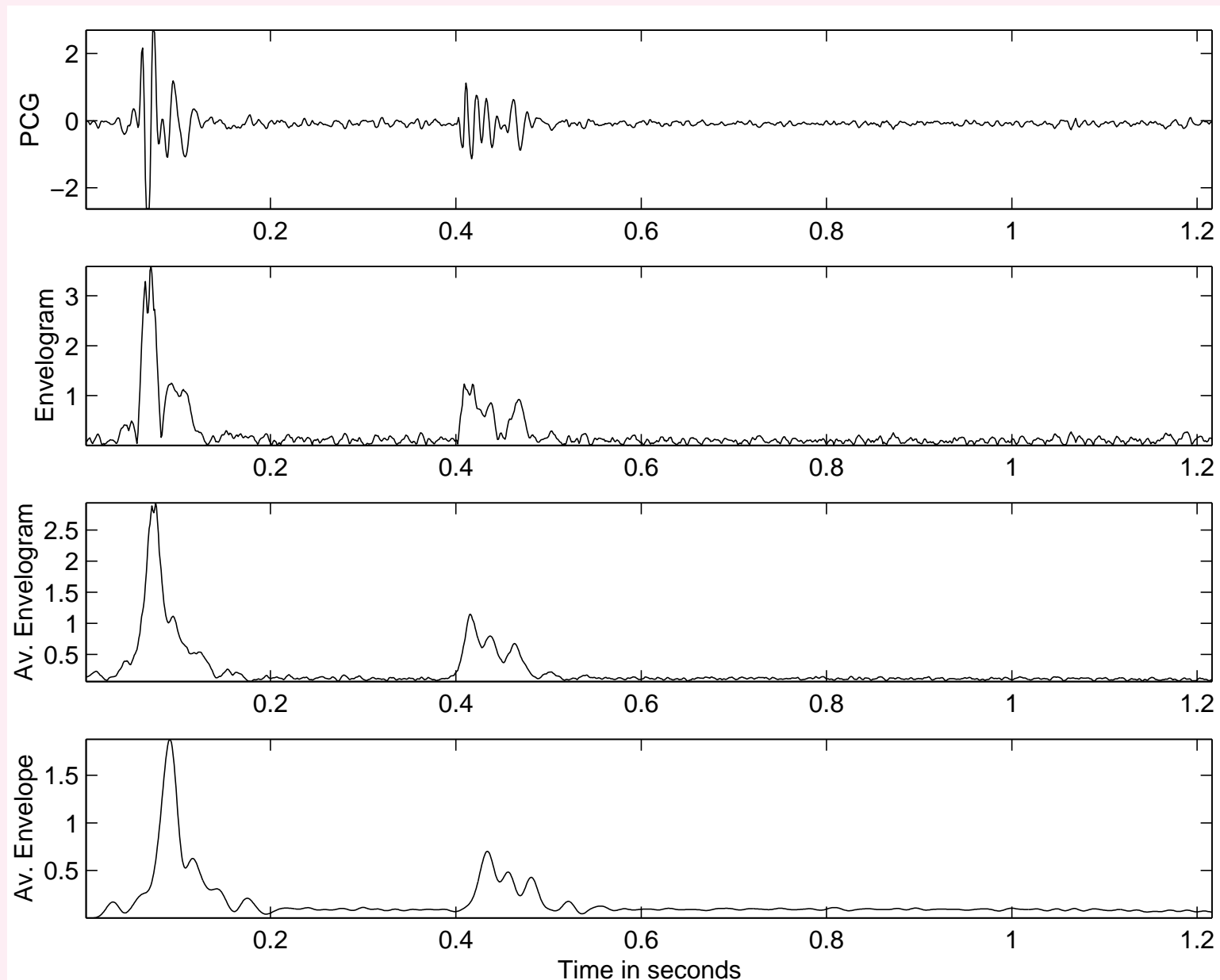
Figure 5.7: Top to bottom: PCG signal of a normal subject (male, 23 years); envelogram estimate of the signal shown; averaged envelogram over 16 cardiac cycles; averaged envelope over 16 cardiac cycles. The PCG signal starts with S1. See Figure 4.30 for an illustration of segmentation of the same signal.
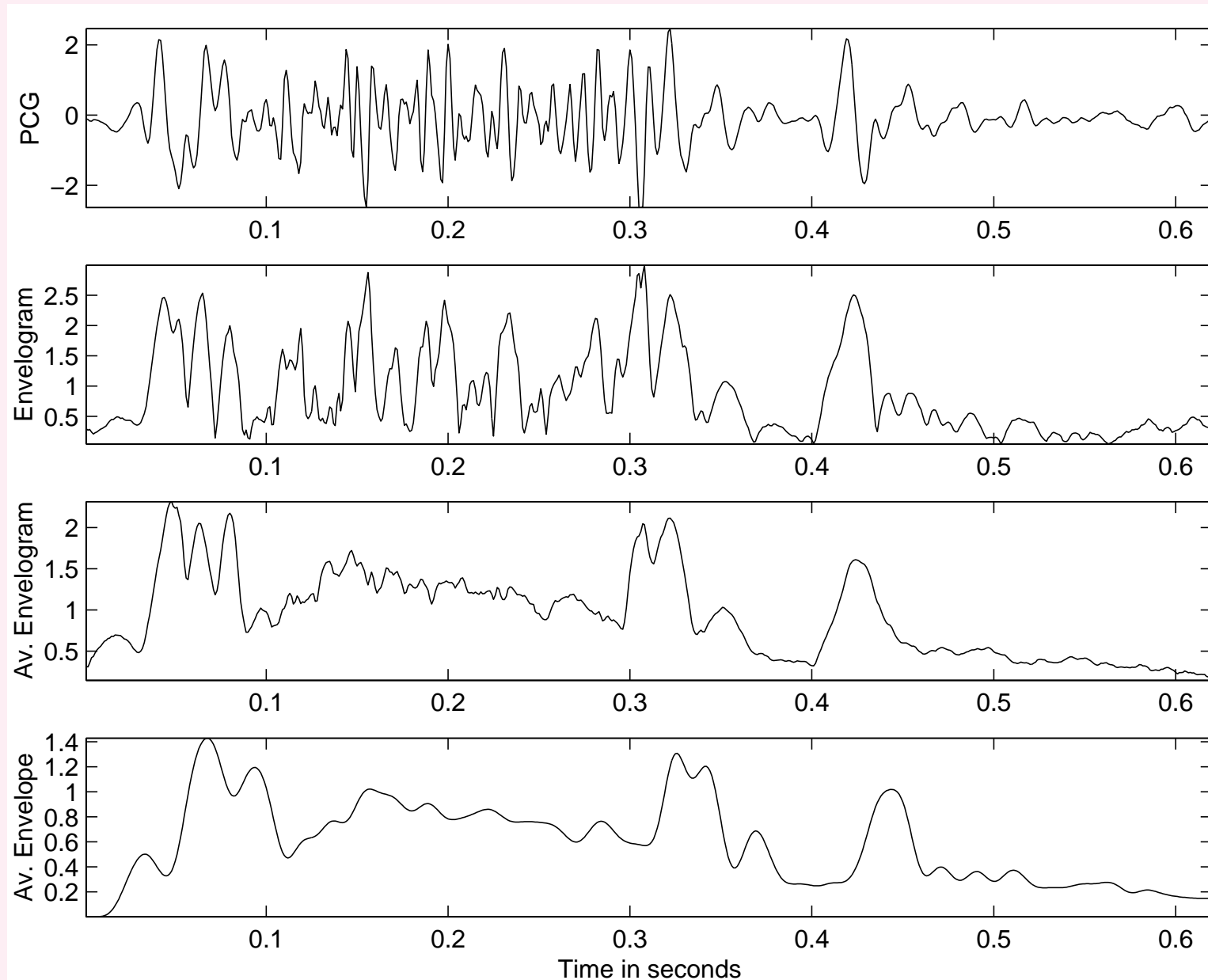
Figure 5.8: Top to bottom: PCG signal of a patient (female, 14 months) with systolic murmur (approximately $0.1 - 0.3 \, s$), split S2 ($0.3 - 0.4 \, s$), and opening snap of the mitral valve ($0.4 - 0.43 \, s$); envelogram estimate of the signal shown; averaged envelogram over 26 cardiac cycles; averaged envelope over 26 cardiac cycles. The PCG signal starts with S1. See Figure 4.31 for an illustration of segmentation of the same signal.

5.6   Analysis of Activity

Problem: *Propose measures of waveform complexity or*

activity to analyze the extent of variability

in signals such as the PCG and EMG.

Solution: Samples of a given EMG or PCG signal

may be treated as a random variable x.

Variance $\sigma_x^2 = E[(x - \mu_x)^2]$:

averaged measure of the variability or *activity*

of the signal about its mean.

If the signal has zero mean, or is so preprocessed,

$\sigma_x^2 = E[x^2]$: variance = average power.

SD = RMS value.

RMS value: indicator of the level of activity about the mean.

5.6.1 The RMS value

RMS value of $x(n)$ over total duration of N samples:

$$RMS = \left[\frac{1}{N} \sum_{n=0}^{N-1} x^2(n) \right]^{\frac{1}{2}}. \qquad (5.23)$$

Global measure of signal level (related to power):

not useful for the analysis of trends in nonstationary signals.

Running estimate of RMS value over a

causal window of M samples:

$$RMS(n) = \left[\frac{1}{M} \sum_{k=0}^{M-1} x^2(n-k)\right]^{\frac{1}{2}}. \qquad (5.24)$$

Useful indicator of average power as a function of time:

short-time analysis of nonstationary signals.

Duration of the window M needs to be chosen

in accordance with the bandwidth of the signal; $M << N$.

Gerbarg et al.: power versus time curves of PCG signals;

average power in contiguous segments of duration $10\ ms$.

Used to identify systolic and diastolic segments of the PCG:

diastolic segments expected to be

longer than systolic segments.

Gerbarg et al. also computed ratios of the mean power of the

last third of systole to the mean power of systole

and also to a certain "standard" noise level.

Ratio also computed of mean energy of systole to

mean energy of PCG over the complete cardiac cycle.

$78 - 91\%$ agreement between computer classification

and clinical diagnosis of mitral regurgitation.

5.6.2 Zero-crossing rate

Intuitive indication of "busy-ness" of a signal

provided by the number of times it crosses the

zero-activity line or some other reference level.

ZCR: number of times the signal crosses the

zero-level within a specified interval.

ZCR increases as the high-frequency content

of the signal increases;

affected by DC bias, baseline wander,

low-frequency artifacts.

Advisable to measure ZCR of the derivative of the signal;

similar to turning points in the test for randomness.

ZCR used in practical applications:

Saltzberg and Burch — relationship between ZCR and

moments of PSDs, application to EEG analysis.

Speech signal analysis — speech versus silence decision;

to discriminate between voiced and unvoiced sounds.

PCG analysis — detection of murmurs.

Jacobs et al.:

ZCR for normal versus abnormal classification

of PCG signals using the ECG as a trigger.

Decision limit of 20 zero-crossings in a cardiac cycle.

Correct-classification rates of 95% for normals ($58/61$) and

94% for abnormals ($77/82$).

Yokoi et al.: maximum amplitude and ZCR

in $8\ ms$ segments of PCG signals sampled at $2\ kHz$.

Correct-classification rates of

98% with $4,809$ normal subjects;

76% with $1,217$ patients with murmurs.

5.6.3　*Turns count*

Willison: analyze level of activity in EMG signals by

determining number of spikes in interference pattern.

Instead of counting zero-crossings, Willison's method

investigates the significance of every change in phase

— direction or slope — of the EMG signal called a *turn*.

Turns greater than $100 \ \mu V$ are counted; threshold avoids

counting insignificant fluctuations due to noise.

　　　　　　　　© R.M. Rangayyan, IEEE/Wiley, 2nd Ed., 2015

Turns count similar to counting turning points

in the test for randomness, but

robust in the presence of noise due to the threshold.

Not directly sensitive to SMUAPs, but significant

phase changes caused by superimposed SMUAPs counted.

EMG signals of subjects with myopathy:

higher turns counts than those of normal subjects

at comparable levels of volitional effort.
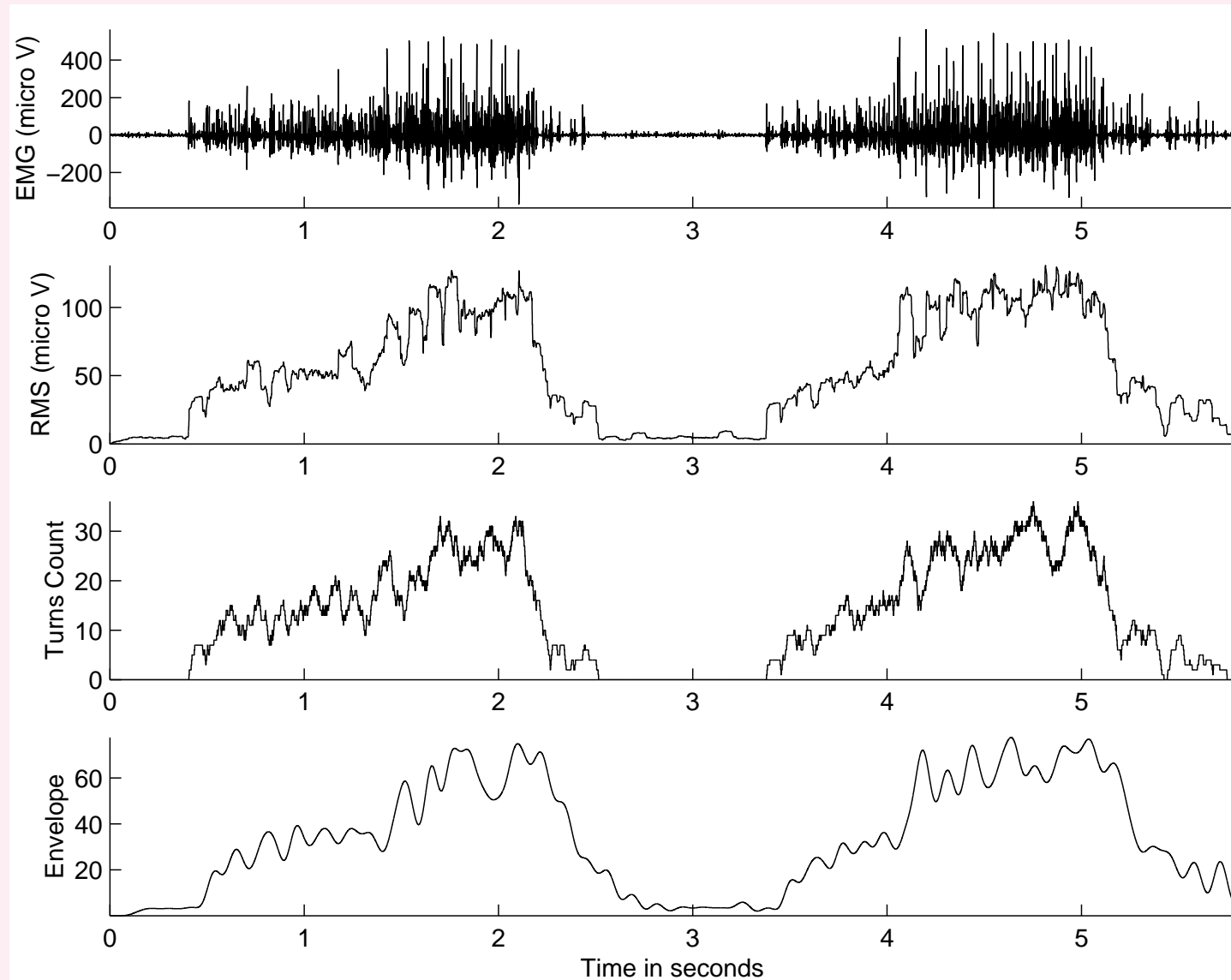
Figure 5.9: Top to bottom: EMG signal over two breath cycles from the crural diaphragm of a dog recorded via implanted fine-wire electrodes; short-time RMS values; turns count using Willison's procedure; and smoothed envelope of the signal. The RMS and turns count values were computed using a causal moving window of $70\ ms$ duration. EMG signal courtesy of R.S. Platt and P.A. Easton, Department of Clinical Neurosciences, University of Calgary.

Envelope: absolute value of the signal (equivalent to full-wave rectification) followed by a Butterworth lowpass filter of order $N = 8$ and cutoff frequency $f_c = 8\ Hz$.
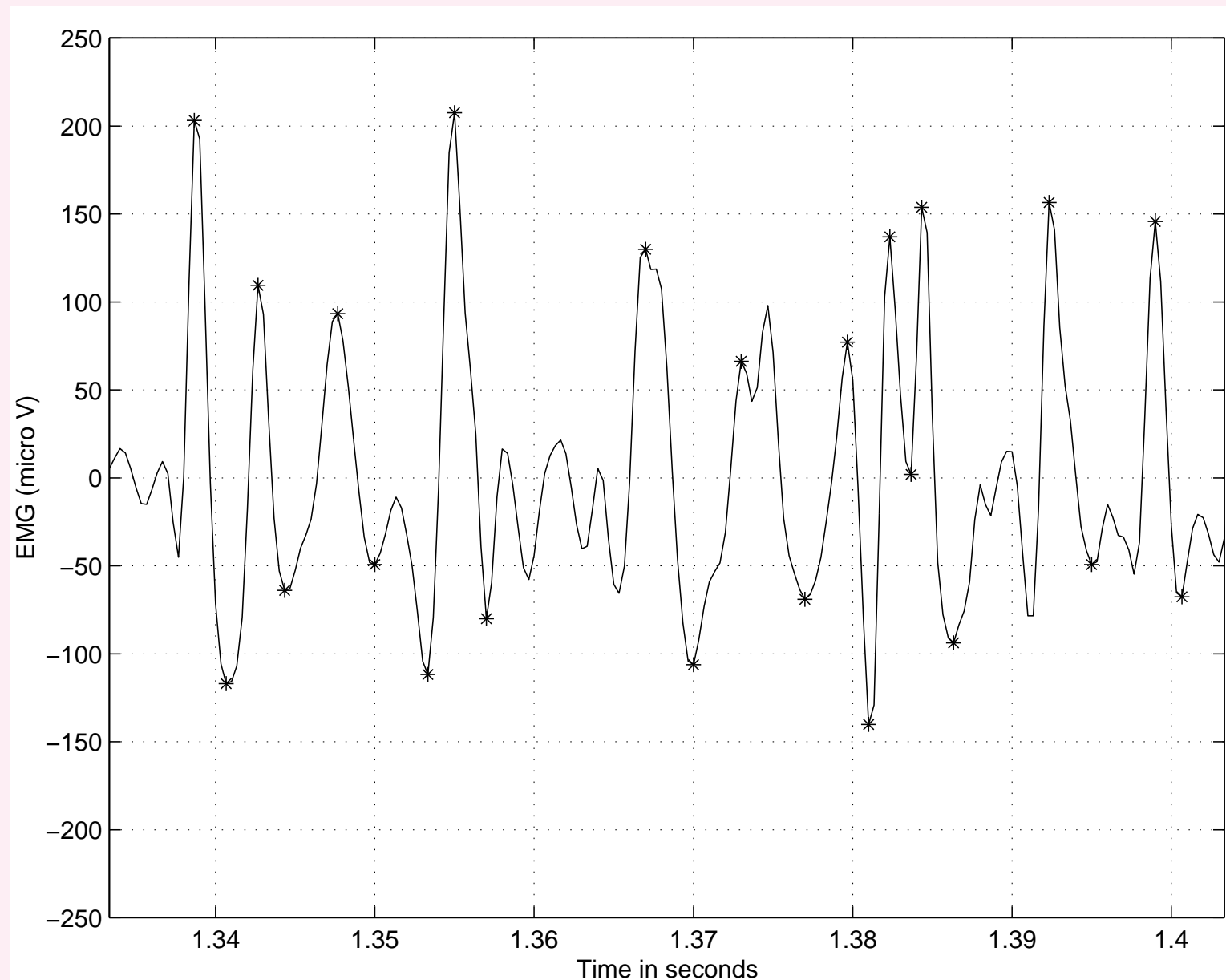
Figure 5.10: Illustration of the detection of turns in a $70\ ms$ window of the EMG signal in Figure 5.9. Threshold = $100\ \mu V$. The segments of the signal between pairs of '*' marks have been identified as significant turns.

5.6.4   Form factor

Based upon variance as a measure of signal activity,
Hjorth proposed a method for the analysis of EEG waves.

Segments of duration $\sim 1\ s$ analyzed using
three parameters:

Activity = variance σ_x^2 of signal segment x.

Mobility M_x:

$$M_x = \left[\frac{\sigma_{x'}^2}{\sigma_x^2}\right]^{\frac{1}{2}} = \frac{\sigma_{x'}}{\sigma_x}. \qquad (5.25)$$

x': first derivative of x.

Complexity or *form factor FF*:

$$FF = \frac{M_{x'}}{M_x} = \frac{\sigma_{x''}/\sigma_{x'}}{\sigma_{x'}/\sigma_x}. \tag{5.26}$$

x'': second derivative of the signal.

Complexity or FF of a sinusoidal wave = unity.

Complexity values increase with the extent of

variations in the signal.

Hjorth described the mathematical relationships between

activity, mobility, complexity, and PSD of a signal;

applied them to model EEG signal generation.

Binnie et al.: application of FF and spectrum analysis to

EEG analysis for the detection of epilepsy.

FF based upon the first and second derivatives

of the signal and their variances: sensitive to noise.

5.7 Application: Parameterization of Normal and Ectopic ECG Beats

Problem: *Develop a parameter to discriminate*

between normal ECG waveforms and ectopic beats (PVCs).

Solution:

Ectopic beats have bizarre and complex waveshapes.

Form factor FF parameterizes waveform complexity:

a value that increases with complexity.
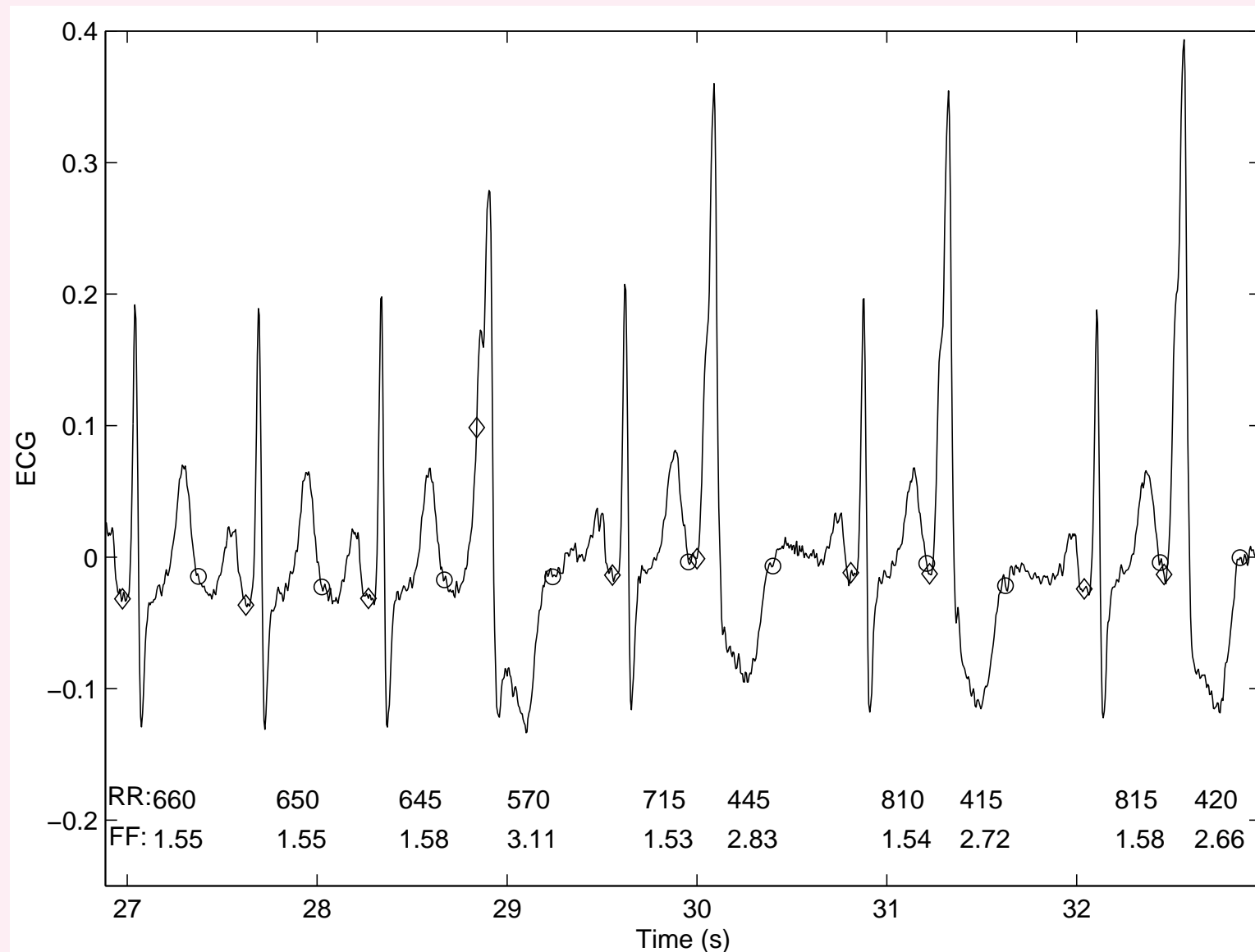
Figure 5.11: Segment of the ECG of a patient (male, 65 years) with ectopic beats. The diamond and circle symbols indicate the starting and ending points, respectively, of each beat obtained using the Pan-Tompkins algorithm for QRS detection. The RR interval (in ms) and form factor FF values are printed for each beat.

Each beat segmented at points $160\ ms$ before and $240\ ms$ after the detected marker point.

5.8   Application: Analysis of Exercise ECG

Problem: *Develop an algorithm to analyze*

changes in the ST segment of the ECG during exercise.

Solution:

Hsia et al.: ECG analysis performed as part of

radionuclide ventriculography (gated blood-pool imaging).

Nuclear medicine images obtained of the left ventricle

before and after exercise on a treadmill or bicycle ergometer.

Images obtained at different phases of the cardiac cycle by

gating the radionuclide (gamma ray) emission data

with the ECG; image data for each phase

averaged over several cardiac cycles.

Analysis of exercise ECG complicated: baseline artifacts

caused by the effects of respiration,

skin resistance changes due to perspiration, and

soft tissue movement affecting electrode contact.

Detection of changes in ST segment in the presence of

such artifacts poses a major challenge.

Main parameter used by Hsia et al.: correlation coefficient.

$$\gamma_{xy} = \frac{\Sigma_{n=0}^{N-1} \left[x(n)\right]\left[y(n) - \Delta\right]}{\sqrt{\Sigma_{n=0}^{N-1} \left[x(n)\right]^2 \; \Sigma_{n=0}^{N-1} \left[y(n) - \Delta\right]^2}} \; . \qquad (5.27)$$

$x(n)$: template generated by averaging 20 QRS complexes;
$y(n)$: ECG signal being analyzed;

Δ : baseline correction factor =
difference between baseline of $y(n)$ and baseline of $x(n)$;

$N =$ duration (number of samples) of template and signal.

$\gamma_{xy} < 0.85$: abnormal beat.

Beats with abnormal morphology, such as PVCs rejected.

ST reference point defined as

$$R + 64 \ ms + \max(4, \frac{200 - HR}{16}) \times 4 \ ms$$

or $S + 44 \ ms + \max(4, \frac{200 - HR}{16}) \times 4 \ ms$.

R or S: position of R or S of the present beat in ms,

HR: heart rate in bpm.

Elevation or depression of the ST segment by more than

$0.1 \ mV$ with reference to the baseline reported.

5.9   Application: Quantitative Analysis of EMG versus Force

Problem: *Propose methods for parametric analysis of the variations in the EMG signal with respect to the force exerted by a muscle.*
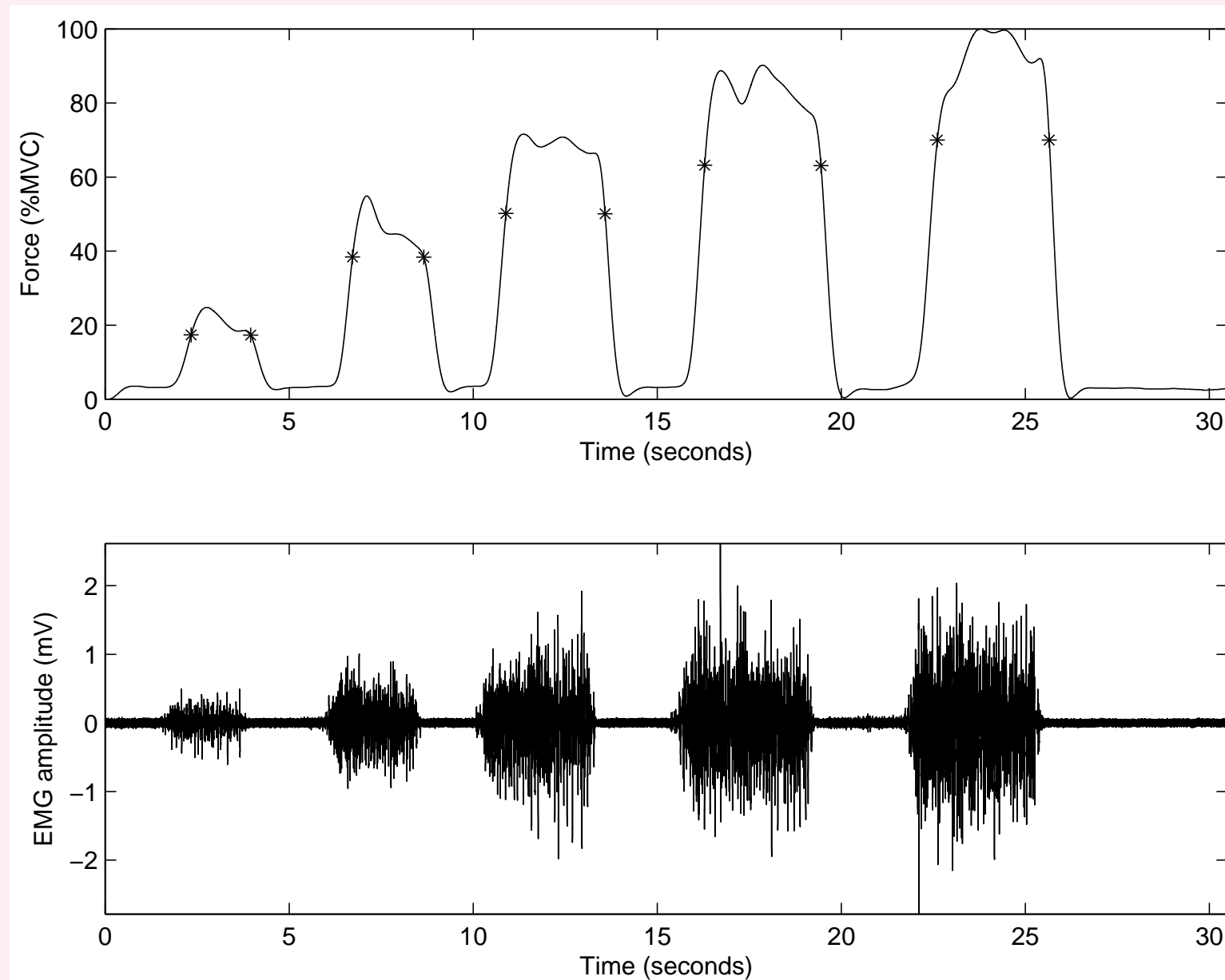
Figure 5.12: Force and EMG signals recorded from the forearm muscle of a subject using surface electrodes. The portions of muscular contraction have been automatically identified in the force signal and delimited by the '*' marks.
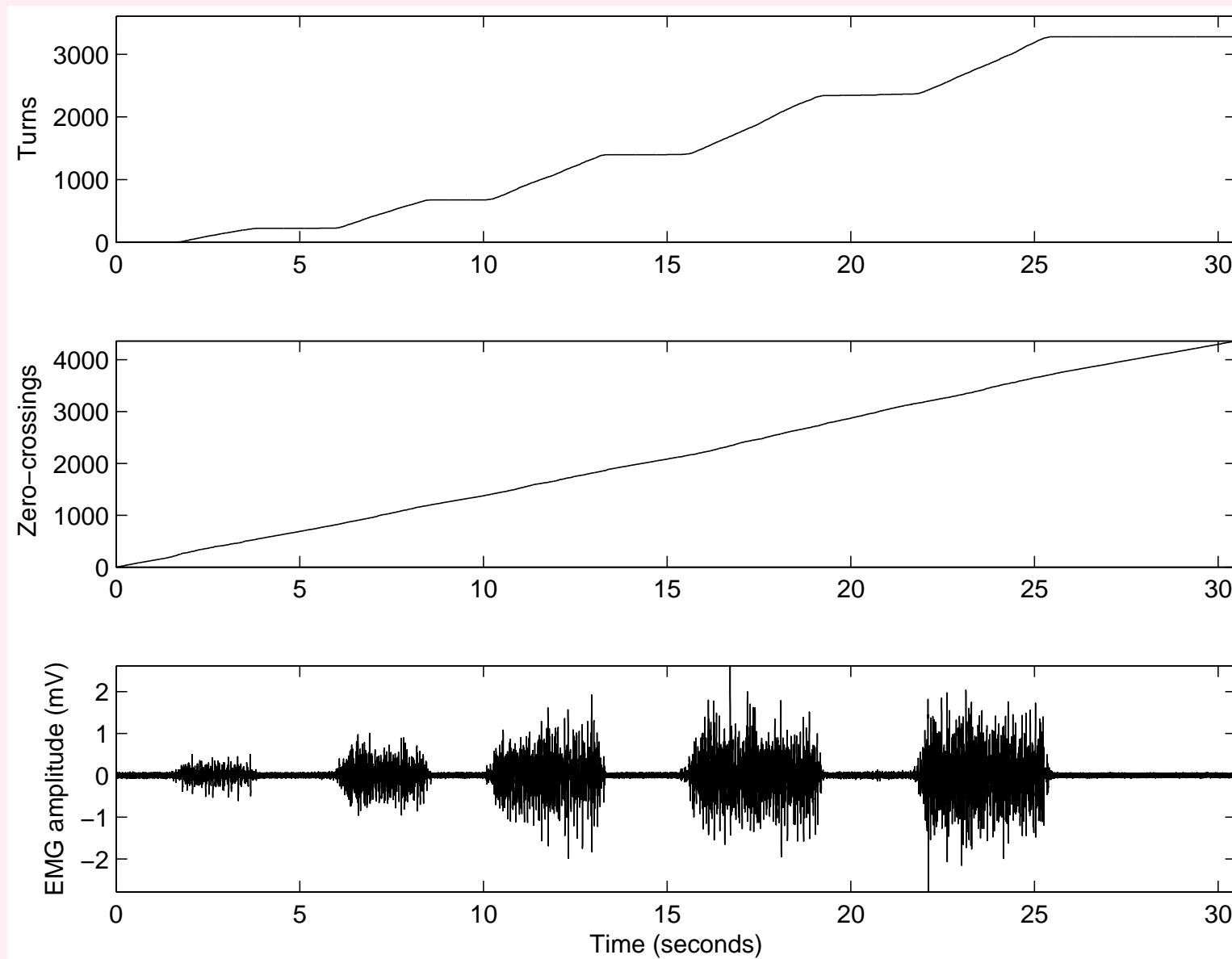
Figure 5.13: Bottom to top: EMG signal, cumulative count of zero-crossings, and cumulative number of significant turns. See also Figure 5.12.

To obtain a measure of fit between each parameter and force, the correlation coefficient was computed as

$$r^2 = \frac{\left[\sum_{n=1}^{n=N} x(n)\, y(n) - N\,\bar{x}\,\bar{y}\right]^2}{\left[\sum_{n=1}^{n=N} x^2(n) - N\,\bar{x}^2\right]\left[\sum_{n=1}^{n=N} y^2(n) - N\,\bar{y}^2\right]}, \quad (5.28)$$

$N = $ number of samples of x or y representing the variables RMS, ZCR, TCR, or force ($N = 5$ in the present study);

$\bar{x}$ is the mean of x.

ZCR: limited variation and low correlation with force.

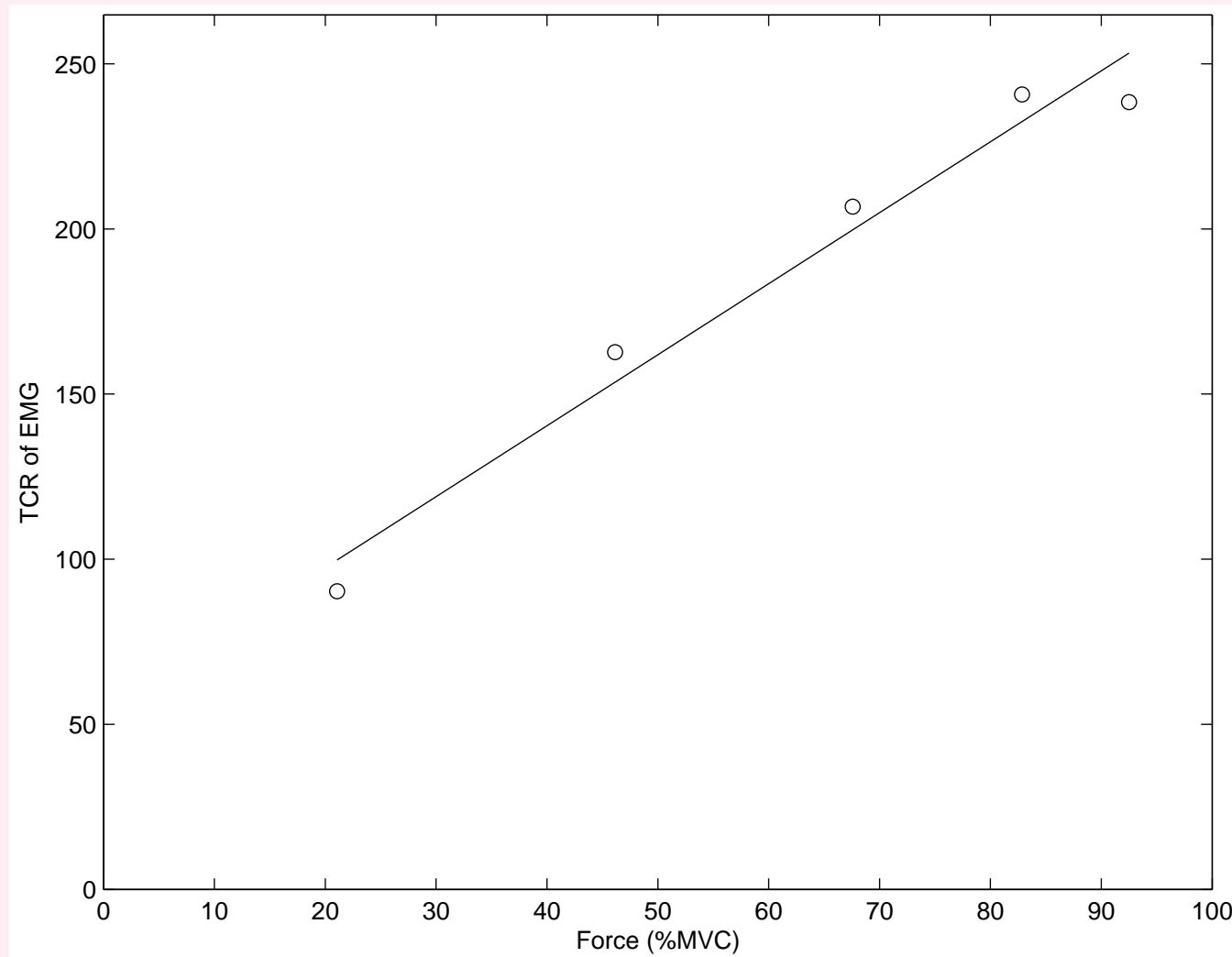RMS, TCR: high correlation, linear behavior w.r.t. force.
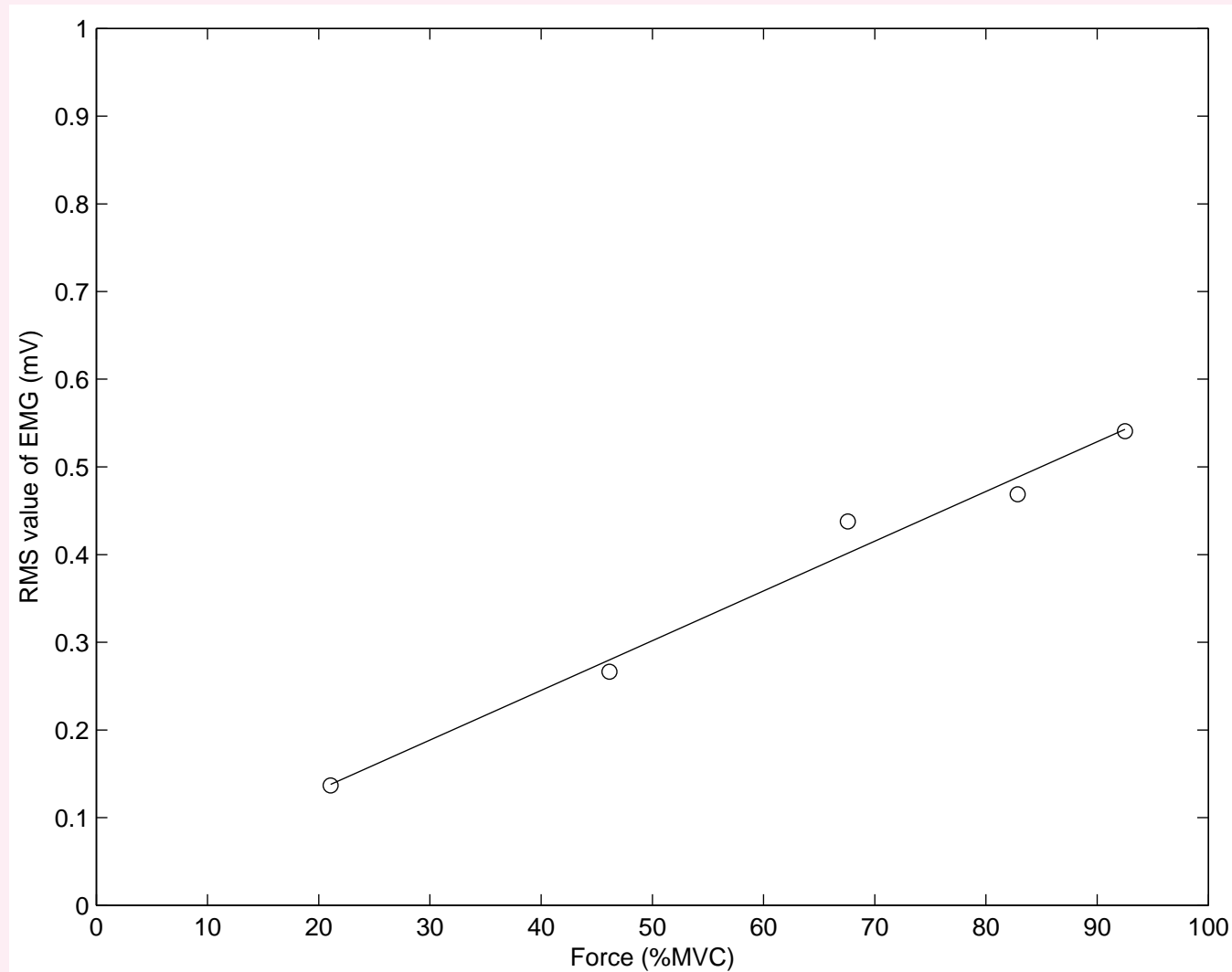
Figure 5.14: Variation of the RMS value of the EMG signal in Figure 5.12 with the average muscular force exerted in each of the five periods of contraction. The '∘' marks indicate the measured values and the straight line indicates the computed linear model. $r^2 = 0.98$.
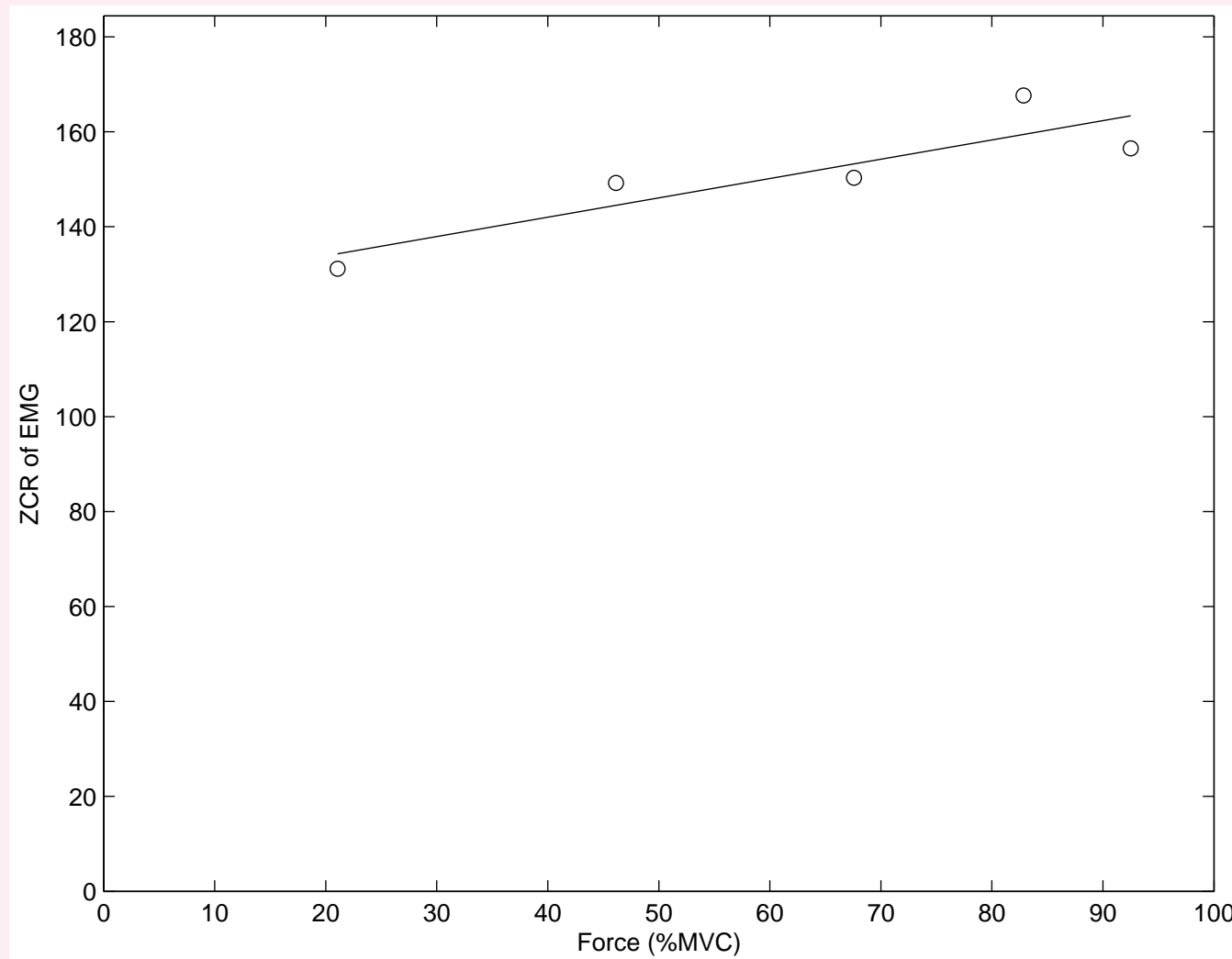
Figure 5.15: Variation of the ZCR value of the EMG signal in Figure 5.12 with the average muscular force exerted in each of the five periods of contraction. The '∘' marks indicate the measured values and the straight line indicates the computed linear model. $r^2 = 0.78$.

Figure 5.16: Variation of the TCR value of the EMG signal in Figure 5.12 with the average muscular force exerted in each of the five periods of contraction. The '○' marks indicate the measured values and the straight line indicates the computed linear model. $r^2 = 0.97$.

5.10 Application: Analysis of Respiration

Problem: *Propose a method to*

relate EMG activity to airflow during inspiration.

Solution: Platt et al. recorded EMG signals from a

pair of electrodes mounted $2\ mm$ apart between

fibers in the third left parasternal intercostal muscle

about $2\ cm$ from the edge of the sternum of a dog.

Crural diaphragm EMG obtained via fine-wire electrodes

sewn in-line with the muscle fibers, placed $10\ mm$ apart.

The dog breathed through a snout mask;

pneumotachograph used to measure airflow.

Envelope obtained by smoothing full-wave-rectified EMG.

Modified Bessel filter: severely attenuated frequencies

beyond $20\ Hz$ with gain $< -70\ dB$.
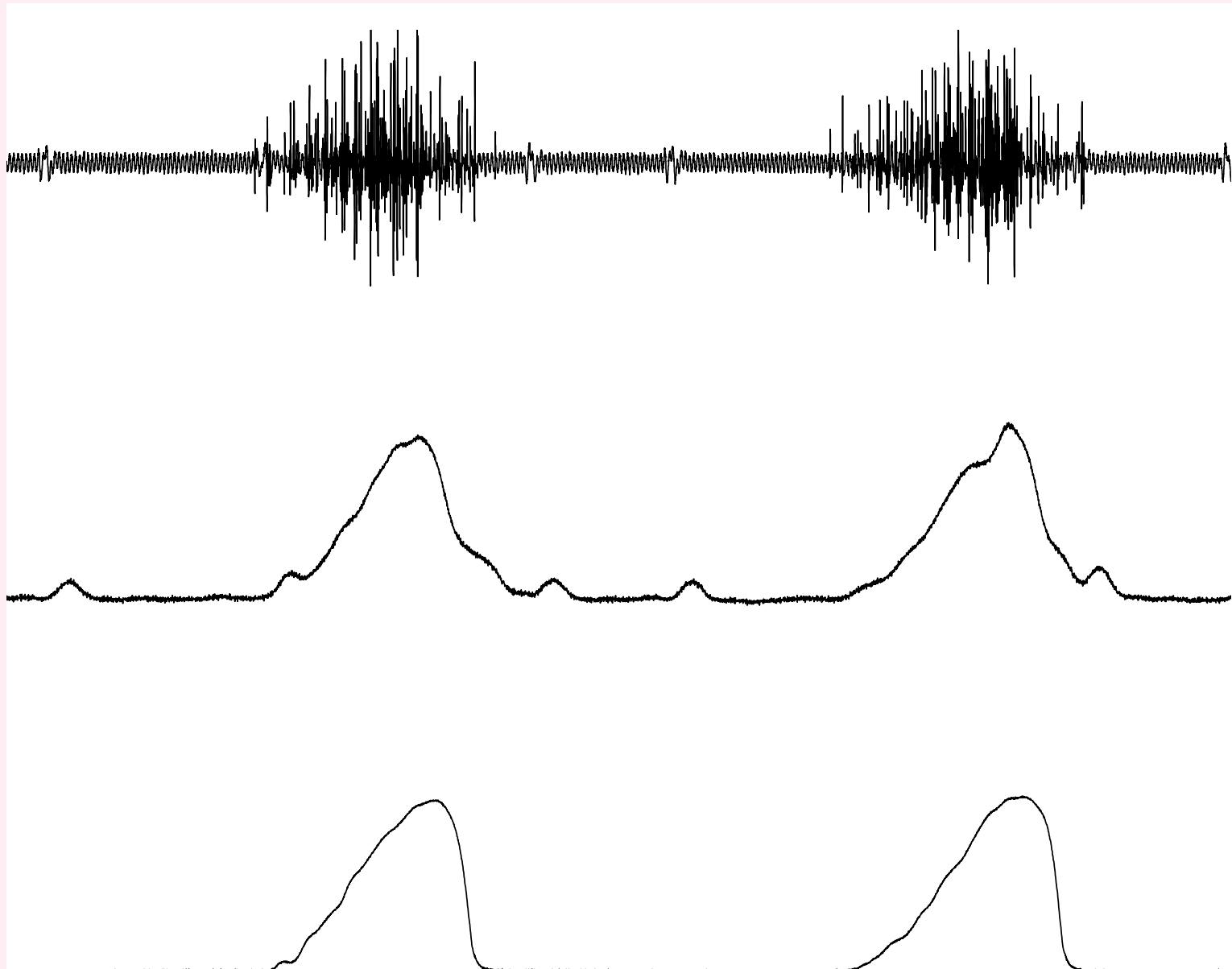
Figure 5.17: Top to bottom: EMG signal over two breath cycles from the parasternal intercostal muscle of a dog recorded via implanted electrodes; EMG envelope obtained with the modified Bessel filter with a time constant of $100~ms$; and inspiratory airflow. The duration of the signals plotted is $5~s$. The several minor peaks appearing in the envelope are related to the ECG which appears as an artifact in the EMG signal. Data courtesy of R.S. Platt and P.A. Easton, Department of Clinical Neurosciences, University of Calgary.
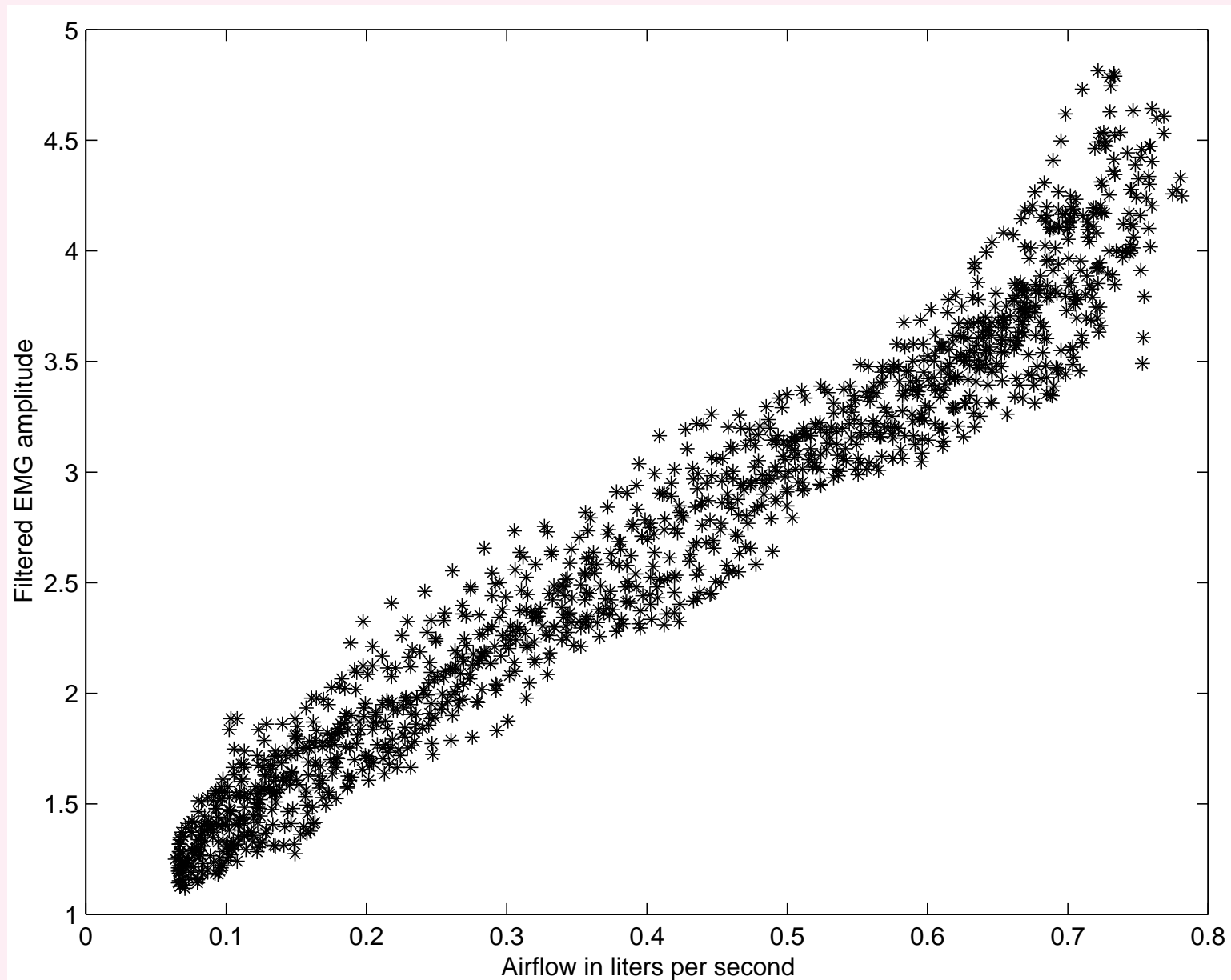
Figure 5.18: Correlation between EMG amplitude from Bessel-filtered envelope versus inspiratory airflow. The EMG envelope was filtered using a modified Bessel filter with a time constant of $100 \ ms$. Data courtesy of R.S. Platt and P.A. Easton, Department of Clinical Neurosciences, University of Calgary.

5.11 Application: Electrical and Mechanical Correlates of Muscular Contraction

Problem: *Derive parameters from the electrical*

and mechanical manifestations of muscular activity

that correlate with the level of contraction or force.

Solution: Zhang et al. studied the usefulness of simultaneously recorded EMG and VMG signals in the analysis of muscular force.

Subjects performed isometric contraction

of the rectus femoris (thigh) muscle

(with no movement of the associated leg)

to different levels of torque with a Cybex II dynamometer.

Four levels of contraction: 20%, 40%, 60%, and 80%

of MVC at three knee-joint angles: $30°$, $60°$, and $90°$.

Each contraction held for a duration of about $6\ s$;

rest between experiments to prevent muscle fatigue.

VMG signal recorded using a Dytran 3115a accelerometer;

surface EMG signals recorded using $Ag - AgCl$ electrodes.

VMG signals filtered to $3 - 100\ Hz$;

EMG signals filtered to $10 - 300\ Hz$.

VMG and EMG sampled at $250\ Hz$ and $1,000\ Hz$.

RMS values computed for each contraction level over $5\ s$.

Almost-linear trends of RMS values of

both EMG and VMG with muscular contraction:

useful in analysis of muscular activity.

EMG RMS vs force relationships vary

from muscle to muscle.
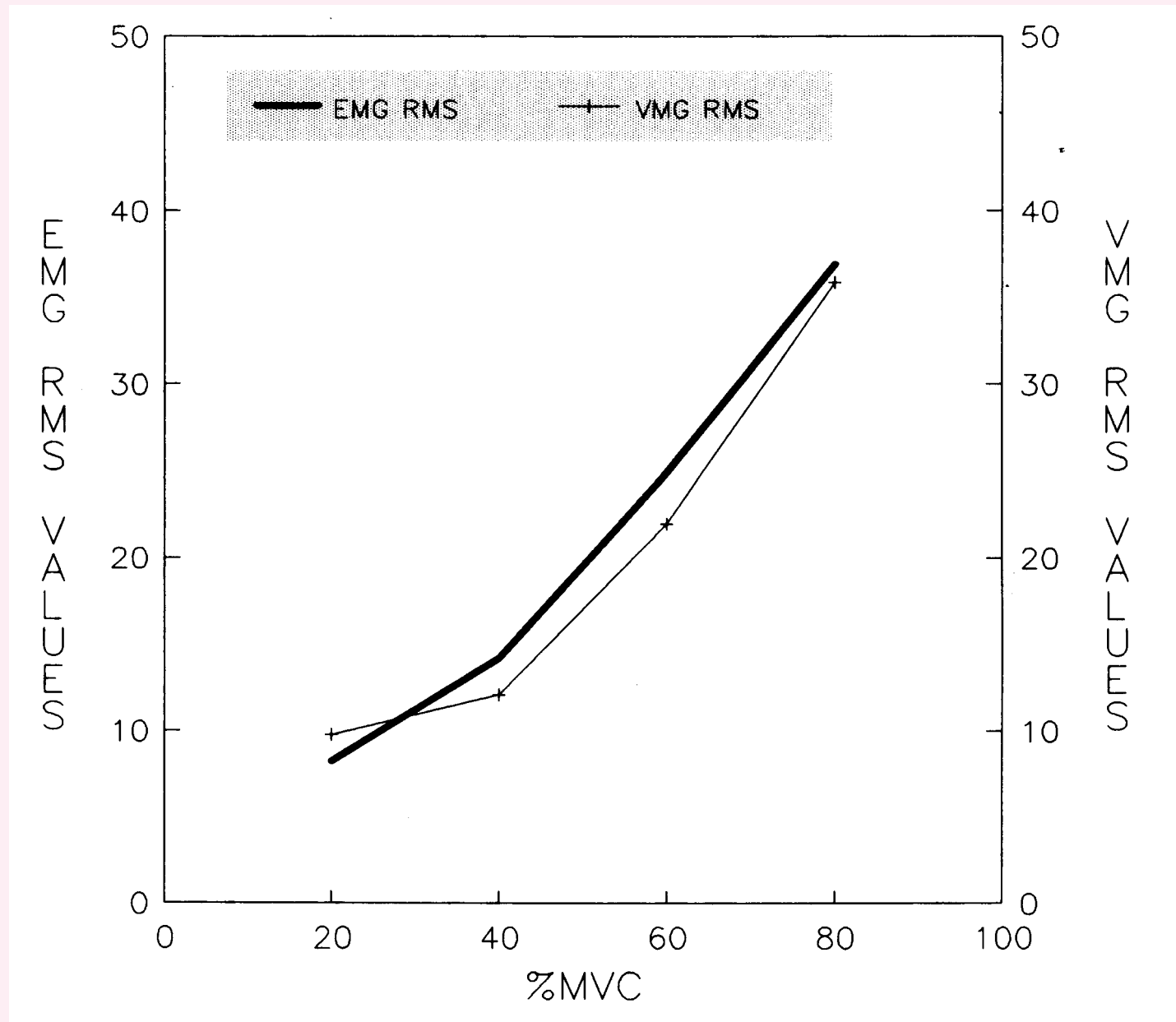
Figure 5.19: RMS values of the VMG and EMG signals for four levels of contraction of the rectus femoris muscle at 60° knee-joint angle averaged over four subjects. Reproduced with permission from Y.T. Zhang, C.B. Frank, R.M. Rangayyan, and G.D. Bell, Relationships of the vibromyogram to the surface electromyogram of the human rectus femoris muscle during voluntary isometric contraction, *Journal of Rehabilitation Research and Development,* 33(4): 395–403, 1996. ©Department of Veterans Affairs.
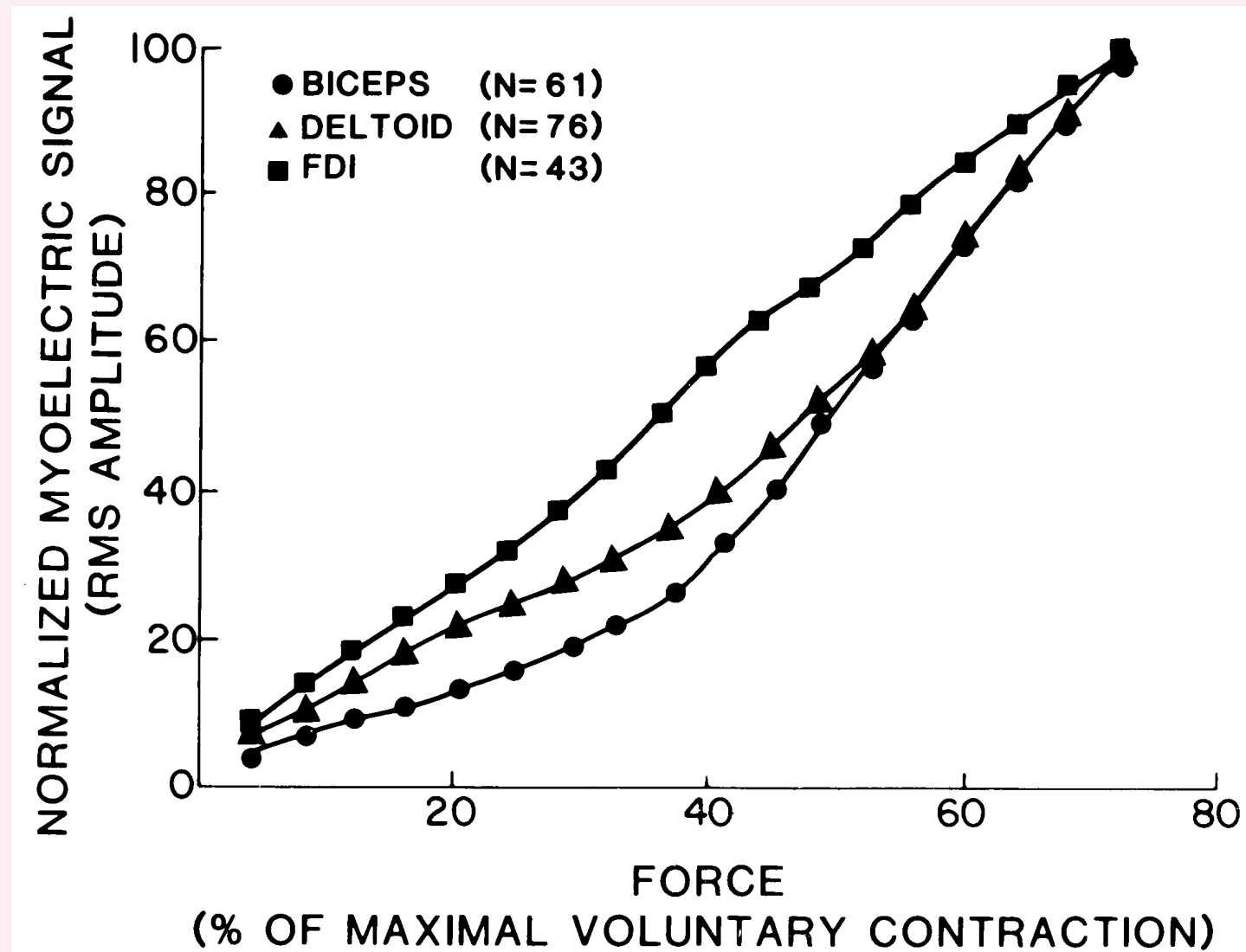
Figure 5.20: EMG RMS value versus level of muscle contraction expressed as a percentage of the maximal voluntary contraction level (%MVC) for each subject. The relationship is displayed for three muscles. FDI: first dorsal interosseus. N: number of muscles in the study. Reproduced with permission from J.H. Lawrence and C.J. de Luca, Myoelectric signal versus force relationship in different human muscles, *Journal of Applied Physiology,* 54(6):1653–1659, 1983. ©American Physiological Society.

5.12   Application: Statistical Analysis of VAG Signals

Problem: *Explore the use of statistical parameters that characterize variability for parametric representation and classification of VAG signals.*

Solution: A normal knee joint has smooth cartilage surfaces and produces almost no sound or vibration.

Under pathological conditions, the cartilage surfaces are eroded and could generate additional sounds.

The statistics of the variability of normal and abnormal VAG signals could be different.

5.12.1 Acquisition of knee-joint VAG signals

The data set consists of 89 signals, with 51 from normal volunteers and 38 from subjects with knee-joint pathology.

Each subject sat on a rigid table in a relaxed position with the leg to be tested being freely suspended in air.
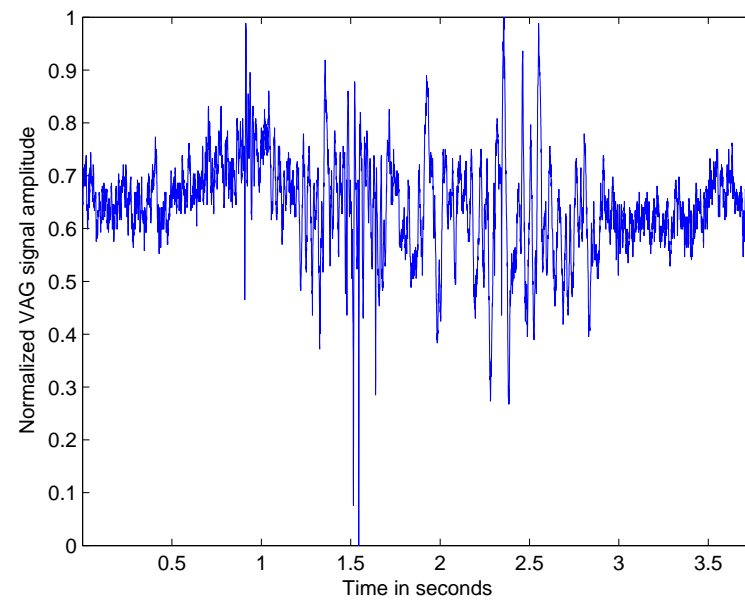
VAG signal recorded with an accelerometer at the midpatella position of the knee, as the subject swung the leg $135°$ (full flexion) to $0°$ (full extension) and back to $135°$ in $4\ s$.

First half of signal: extension; second half: flexion.

Signal filtered $10\ Hz$ to $1\ kHz$; digitized at $2\ kHz$.
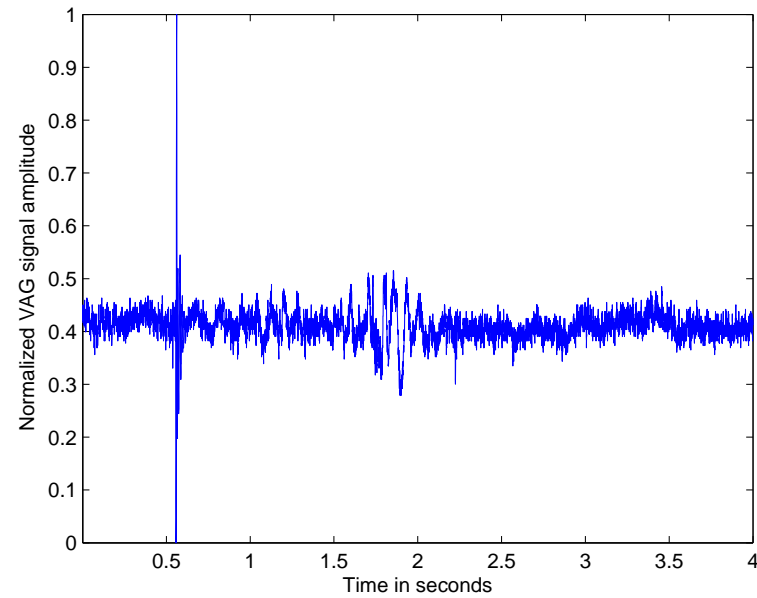
(a)

(b)

Figure 5.21: VAG signal of (a) a normal subject and (b) a subject with knee-joint pathology. Reproduced from R.M. Rangayyan and Y.F. Wu, Screening of knee-joint vibroarthrographic signals using probability density functions estimated with Parzen windows, *Biomedical Signal Processing & Control*, January 2010, 5(1):53–58, with permission from Elsevier. ©Elsevier.

5.12.2   Estimation of the PDFs of VAG signals

Rangayyan and Wu: models of the PDFs of VAG signals were derived using the Parzen-window approach.

A histogram was computed by combining all of the normal signals into one group: $h_n(x_l)$, with x_l, $l = 0, 1, 2, \ldots, L - 1$, representing the L bins used to quantize the range of the values of the signal x.

$L = 100$ bins used to represent the normalized range of $[0, 1]$ for the VAG signal values.

Similarly, a histogram $h_a(x_l)$ was obtained by pooling together all of the abnormal signals.

Each histogram was normalized by dividing by the total number of samples in the population to have unit area.

A Gaussian fit was obtained for each of the two histograms, denoted as $g_n(x_l)$ and $g_a(x_l)$.

Consider a set of independent samples, $Z = \{z_1, z_2, \dots, z_K\}$, with an unknown PDF $p(z)$.

A nonparametric estimate of $p(z)$ from Z is provided by

$$\hat{p}(z) = \frac{1}{K} \sum_{k=1}^{K} \kappa(z - z_k), \qquad (5.29)$$
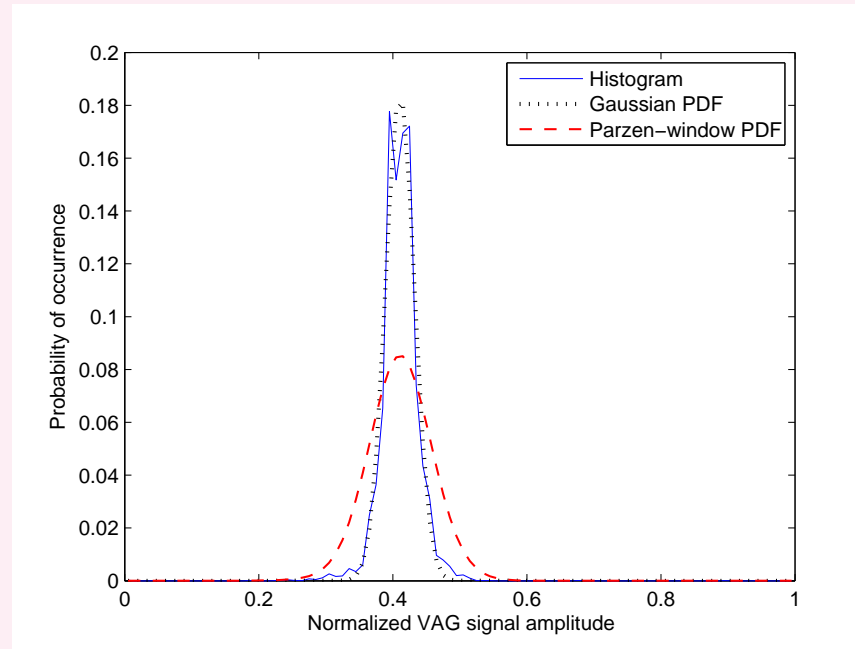
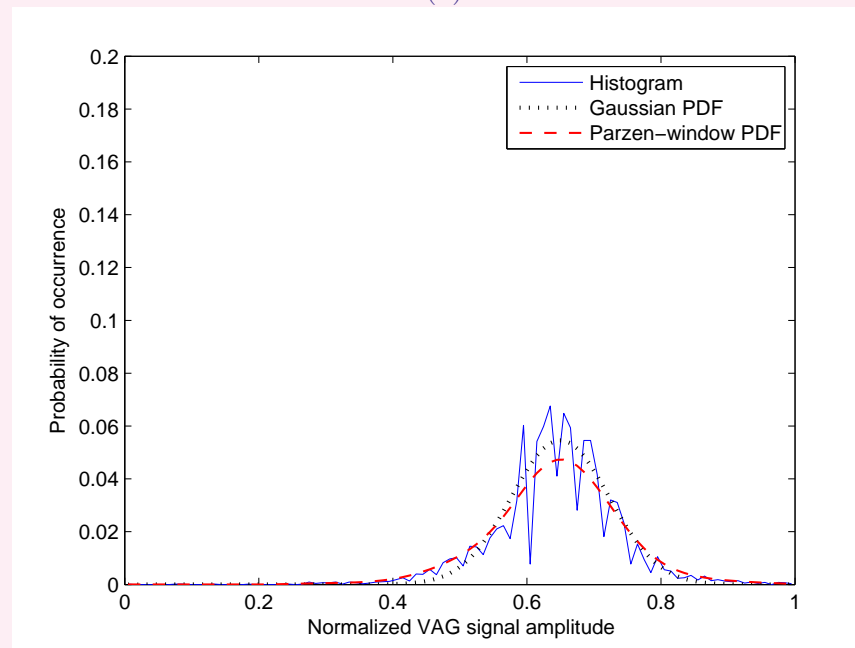where κ is a window or kernel that integrates to unity.

$$\kappa(z - z_k) = \frac{1}{\sigma_P \sqrt{2\pi}} \exp\left[-\frac{(z - z_k)^2}{2\,\sigma_P^2}\right]. \qquad (5.30)$$

The Parzen-window PDF was estimated using the quantized values of the signals, x_l, $l = 0, 1, 2, \ldots, L - 1$, with $L = 100$ levels, in the normalized range $[0, 1]$.

Experiments were conducted with the value of the parameter σ_P in Equation 5.30 varying over the range $[0.01, 0.1]$ in steps of 0.01; the final value was set equal to 0.04.
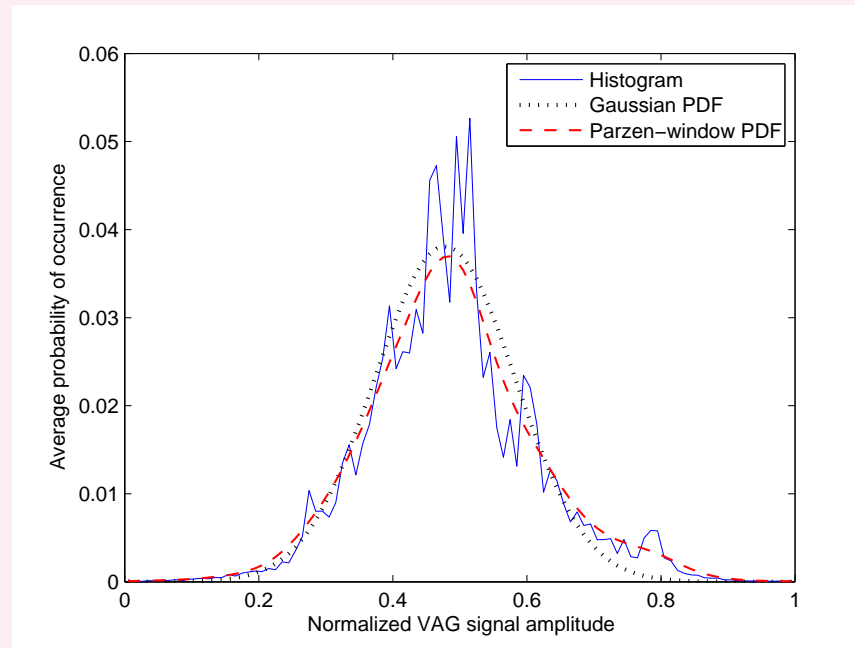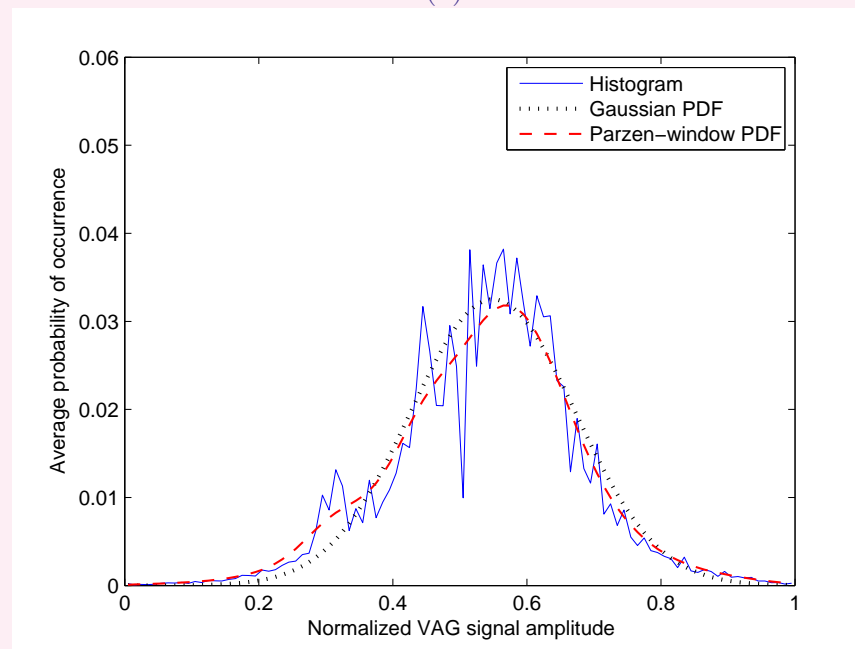
(a)

(b)

Figure 5.22: Nonparametric Parzen-window estimates of the PDFs of the VAG signals in Figure 5.21: (a) of a normal subject and (b) of a patient with knee-joint pathology. The amplitude has been normalized to the range $[0, 1]$. The figure also shows the normalized histogram and the Gaussian fit for each case. The parameters of the Gaussian fit are (a) mean $= 0.4107$, $SD = 0.0216$; and (b) mean $= 0.6499$, $SD = 0.0730$. Reproduced from R.M. Rangayyan and Y.F. Wu, Screening of knee-joint vibroarthrographic signals using probability density functions estimated with Parzen windows, *Biomedical Signal Processing & Control*, January 2010, 5(1):53–58, with permission from Elsevier. ©Elsevier.

(a)

(b)

     © R.M. Rangayyan, IEEE/Wiley, 2nd Ed., 2015

Figure 5.23: Nonparametric Parzen-window estimates of the PDFs of VAG signals: (a) derived from VAG signals of 51 normal volunteers and (b) derived from VAG signals of 38 subjects with knee-joint pathology. The amplitude has been normalized to the range $[0, 1]$. The figure also shows the normalized histogram and the Gaussian fit for each case. The parameters of the Gaussian fit are (a) mean $= 0.4778$, $SD = 0.1047$; and (b) mean $= 0.5495$, $SD = 0.1227$. Reproduced from R.M. Rangayyan and Y.F. Wu, Screening of knee-joint vibroarthrographic signals using probability density functions estimated with Parzen windows, *Biomedical Signal Processing & Control*, January 2010, 5(1):53–58, with permission from Elsevier. ©Elsevier.

The following observations were made from the PDFs of the normal and abnormal VAG signals:

- In general, the Parzen-window PDFs are closer to the normalized histograms of the VAG signals than the corresponding Gaussian models. The closeness of the fit depends upon the value of σ_P used.

- Abnormal signals have higher probabilities of occurrence of higher values within the range $[0, 1]$.

- It should be possible to classify VAG signals using parameters derived from their PDFs.

- The models suggest different underlying signal-generation processes or statistical models for normal and abnormal VAG signals.

5.12.3   Screening of VAG signals using statistical parameters

VAG signals related to knee-joint pathology possess a larger extent of variability over the duration of a swing cycle of the leg than normal VAG signals.

Rangayyan and Wu used FF, skewness, kurtosis, entropy, adaptive turns count, and the variance of MS for screening of VAG signals.

Various statistical measures may be computed based upon the moments of the PDF of a given signal, $p_x(x_l)$, with x_l, $l = 0, 1, 2, \ldots, L - 1$.

The kth central moment of the PDF $p_x(x_l)$ is defined as

$$m_k = \sum_{l=0}^{L-1} (x_l - \mu)^k \, p_x(x_l), \qquad (5.31)$$

where μ is the mean value, given by

$$\mu = \sum_{l=0}^{L-1} x_l \, p_x(x_l). \qquad (5.32)$$

See Section 3.2.1 for related statistical parameters.

The Kullback–Leibler distance or divergence (KLD) between two PDFs $p_1(x_l)$ and $p_2(x_l)$ is

$$KLD(p_1, p_2) = \sum_{l=0}^{L-1} p_2(x_l) \, \ln\left[\frac{p_2(x_l)}{p_1(x_l)}\right]. \qquad (5.33)$$

Rangayyan and Wu computed the KLD between the PDF estimated for the signal to be classified and the PDF models for the normal and abnormal VAG signals.

The leave-one-out (LOO) method was used: the signal to be classified was left out of the procedure to obtain the Parzen-window model for the corresponding class.

Using the KLD obtained with the Parzen-window models, a normal-versus-abnormal classification accuracy of 73% was obtained with the data set of 89 VAG signals.

Sensitivity and specificity of screening: 68.42% and 76.47%.

The use of KLD with the Gaussian models resulted in poorer performance, with overall accuracy of 69.7%.

Note that the Gaussian model does not facilitate the characterization of asymmetric or skewed PDFs.

Pattern classification using the set of parameters (KLD, K, H, μ, σ) led to an overall accuracy of 77.5%, sensitivity of 71.1%, and specificity of 82.4% using radial basis functions (RBF) with LOO.

Given the nonstationary nature of VAG signals, it would be advantageous to compute parameters using segments of VAG signals instead of their full duration.

5.13   Application: Fractal Analysis of the EMG in Relation to Force

Problem: *Can fractal analysis be applied to characterize the variations in an EMG signal with respect to the force exerted by a muscle?*

Solution: Several biomedical systems and signals exhibit varying levels of complexity in their characteristics that vary across different states of health and disease.

The fractal dimension (FD) can be used to represent such complexity in a quantitative manner.

5.13.1   Fractals in nature

The term "fractal" was coined by Mandelbrot to represent patterns that possess self-similarity at several scales.

Self-similarity: substructure that resembles superstructure.

Under several levels of magnification, a fractal appears to have the same form.

A Euclidean form, such as a square or a triangle, does not retain its original form when magnified.

Examples of fractals: fern, broccoli, cauliflower,
Cantor bar, Koch curve, Sierpinski triangle, Hilbert curve.

Natural objects may not possess self-similarity at all scales.

A real-life pattern does not possess infinite levels of detail or granularity.

A natural pattern, when magnified, may appear similar but not exactly identical to its original unmagnified form: statistical self-similarity.

5.13.2   *Fractal dimension*

Consider a self-similar pattern that exhibits a number of self-similar parts represented by the variable a, at the reduction factor of $1/s$.

The self-similarity dimension (D) is defined in a power-law:

$$a = \frac{1}{s^D}.\qquad(5.34)$$

$$D = \frac{\log(a)}{\log(1/s)}.\qquad(5.35)$$

$D =$ slope of plot of log of the number of self-similar parts, $\log(a)$, versus log of the reduction factor, $\log(1/s)$.

■ ■ ■ ■ ■

The ruler method: Using rulers of different length, the total length of a pattern or signal can be estimated to different levels of accuracy.

If a large ruler is used, the small details in the given pattern are ignored.

As smaller rulers are used, finer details get measured.

The measured or estimated length increases and improves in accuracy as the size of the ruler decreases.

Let u be the length measured with a ruler of size s.

The precision of measurement is represented by $1/s$.

A fractal is expected to satisfy the power law

$$u = c\,\frac{1}{s^d}\,, \tag{5.36}$$

where c is a constant of proportionality and $FD = 1 + d$.

$$\log(u) = \log(c) + d\,\log(1/s)\,. \tag{5.37}$$

The slope d of a plot of $\log(u)$ versus $\log(1/s)$ provides an estimate of FD as $FD = 1 + d$.

If we let $u = ns$, where n is the number of times the ruler is used to measure the length u with the ruler of size s, then

$$\log(n) = \log(c) + (1 + d)\,\log(1/s)\,. \qquad (5.38)$$

The slope of a plot of $\log(n)$ versus $\log(1/s)$ directly provides an estimate of FD.

The box-counting method: Partition the pattern or signal space into square boxes of equal size and count the number of boxes that contain a part of the signal.

Repeat the process by partitioning the signal space into smaller and smaller squares.

Plot the log of the number of boxes counted against the log of the magnification index for each stage of partitioning.

$FD =$ slope of the straight line fitted to the plot.

■ ■ ■ ■ ■

Higuchi's method: FD of a signal by computing measures of the length of the signal using multiple versions of the signal reconstructed for varying measurement intervals.

Given a signal $x(n)$, $n = 1, 2, \ldots, N$, create new signals

$$x_k(m) = x(m), x(m+k), x(m+2k), \ldots, \quad (5.39)$$

$$x\left(m + \lfloor \frac{N-m}{k} \rfloor k\right),$$

for various values of k, where k and m are integers with $m = 1, 2, \ldots, k$.

m represents the initial point and k is the interval between the points of $x_k(m)$.

The length of each derived signal is computed as

$$L(m,k) = \frac{1}{k}\frac{N-1}{k\left\lfloor\frac{N-m}{k}\right\rfloor} \sum_{i=1}^{\left\lfloor\frac{N-m}{k}\right\rfloor} |x(m+ik) - x[m+(i-1)k]|$$

$$(5.40)$$

$$L(k) = \frac{1}{k}\sum_{m=1}^{k} L(m,k). \qquad (5.41)$$

The slope of a straight-line fit to a log–log plot of $L(k)$ against $1/k$ gives the FD of the original signal.

5.13.3   Fractal analysis of physiological signals

Fractal properties have been observed in several
physiological structures and processes.

Many anatomical structures have fractal-like appearance,
such as the coronary arteries, venous branching patterns,
bronchial trees, certain muscle fiber bundles, and the
His–Purkinje network in the ventricles.

5.13.4   Fractal analysis of EMG signals

The EMG signal in Figure 1.20 was filtered with a Butterworth lowpass filter of 6th order and cutoff frequency of $300 \ Hz$.

Segments of duration $1 \ s$ were cut for each level of contraction to estimate FD using Higuchi's method.
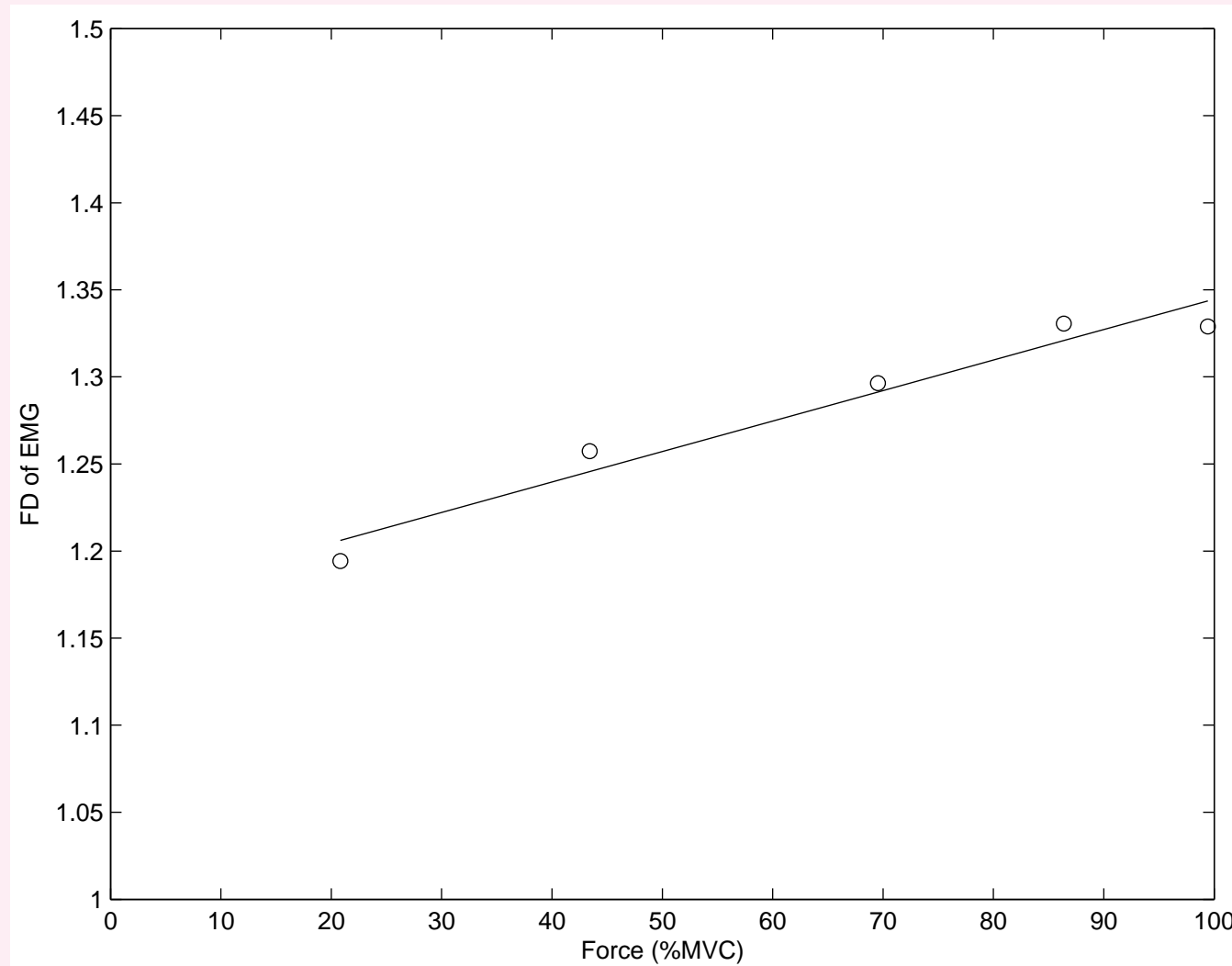
Figure 5.24: Variation of FD with the level of muscle contraction for the EMG signal shown in Figure 1.20; $r^2 = 0.95$. Figure courtesy of Faraz Oloumi.

5.14   Remarks

We have studies methods to derive parameters from segments of biomedical signals.

The parameters considered were designed with the aim of discriminating between different types of waveshapes, or representing change in waveform complexity through the course of a physiological or pathological process.

Various parameters can help in distinguishing between normal and ectopic ECG beats,

and serve as quantities correlated with physiological activity, such as respiration and muscular contraction.

In most practical applications, a single parameter or a couple of measures may not adequately serve the purposes of signal analysis or diagnostic decision making.

A single parameter such as FF or SL may assist in distinguishing some types of PVCs from normal ECG beats;

however, several cardiovascular diseases and defects may cause changes in the ECG signal that may lead to similar variations in the FF or SL values.

A practical application would need to maintain a broad scope of analysis and use several parameters to detect various possible abnormalities.

6

Frequency-domain Characterization of Signals and Systems

Many biomedical systems exhibit innate rhythms and

periodicity: more readily expressed and appreciated

in terms of frequency than time units.

Cardiac rhythm more conveniently expressed in

beats per minute,

a measure of frequency of occurrence or rate of repetition,

than in terms of duration of a beat or

interval between beats in seconds (RR interval).

Cardiac rhythm expressed as $72\ bpm$ more easily

understood than the corresponding RR interval as $0.833\ s$.

EEG rhythm conveyed more readily by description in

cycles per second or in *Hertz (Hz)*

than a time-domain description:

alpha rhythm having a frequency of $11.5 \, Hz$

versus the equivalent period of $0.087 \, s$.

PCG: interesting example of a signal with

multiple frequency-domain features.

Beat-to-beat periodicity or rhythm.

Heart sounds within a cardiac cycle exhibit *resonance*.

Multicompartmental nature of the cardiac system:

multiple resonance frequencies: composite *spectrum* of

several dominant or resonance frequencies.

Constrained flow of blood through an orifice (septal defect)

or across a stenosed valve acting as a baffle

leads to turbulence: *wideband noise*.

Need to consider the distribution of the signal's energy or

power over a wide band of frequencies:

leads to the notion of the power *spectral density* function.

6.1   Problem Statement

Investigate the potential use of the Fourier spectrum and

parameters thereof in the analysis of biomedical signals.

Identify physiological and pathological processes that could

modify the frequency content of the corresponding signals.

Outline the signal processing tasks needed to perform

spectral analysis of biomedical signals and systems.

6.2 Illustration of the Problem with Case Studies

6.2.1 The effect of myocardial elasticity on heart sound spectra

The first and second heart sounds — S1 and S2 —

are typically composed of low-frequency components,

due to the fluid-filled and elastic nature of the

cardiohemic system.

■ ■ ■ ■ ■

Sakai et al. processed recorded heart sound signals by using

tunable bandpass filters, with a bandwidth of $20\ Hz$,

tuned over the range $20 - 40\ Hz$ to $400 - 420\ Hz$, and

estimated the frequency distributions of S1 and S2.

Heart sound spectra maximum in the $20 - 40\ Hz$ band;

S1: peaks at lower frequencies than those of S2;

S2: "gentle peaking" between $60\ Hz$ and $220\ Hz$.

Gerbarg et al.: computer program to simulate a filter bank.

Obtained averaged power spectra of S1 and S2 of

$1,000$ adult males, 32 high-school children,

and 75 patients in a hospital.

Averaged PSDs of S1 and S2:

peak power in the range $60 - 70\ Hz$,

power levels lower than $-10\ dB$ beyond $150\ Hz$.

PSD of S2: more high-frequency energy than S1.

Yoganathan et al.: FFT analysis of S1 and S2.

Spectra of $250\ ms$ windows with S1 averaged over 15 beats.

Spectrum of S1:

peaks in a low-frequency range ($10 - 50\ Hz$)

and a medium-frequency range ($50 - 140\ Hz$).

■ ■ ■ ■ ■

Spectrum of S2: peaks in low-frequency ($10 - 80\ Hz$),

medium-frequency ($80 - 220\ Hz$),

and high-frequency ranges ($220 - 400\ Hz$).

Spectral peaks related to resonance and the

elastic properties of heart muscles.

Adolph et al.: dynamic spectrum analyzer to study

frequency content of S1 during isovolumic contraction.

Center frequency of filter with $20\ Hz$ bandwidth

varied from $30\ Hz$ to $70\ Hz$, in steps of $10\ Hz$.

Outputs of filters averaged over 10 consecutive beats.

Ratios of the average peak voltage of the filtered outputs

to that of full S1 during isovolumic contraction computed.

Adolph et al. hypothesized that frequency content of S1

during isovolumic contraction should depend on

relative contributions of mass and elasticity of left ventricle.

Mass of left ventricle with blood content remains

constant during isovolumic contraction.

Frequency content of S1 decreases in case of diseases

that reduce ventricular elasticity: myocardial infarction.
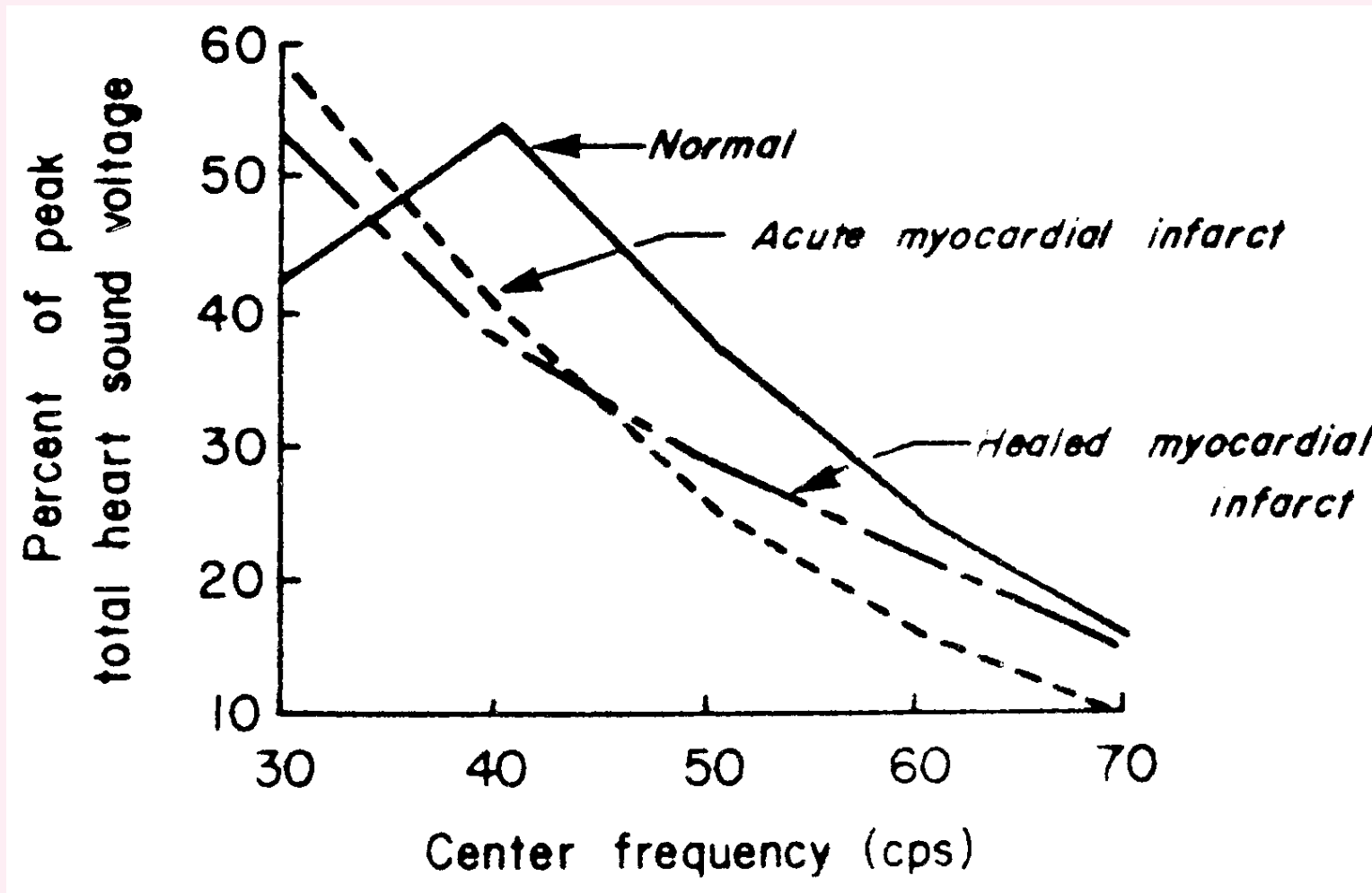
Figure 6.1: First heart sound spectra for normal, acute myocardial infarct, and healed myocardial infarct cases. The latter two cases exhibit an increased percentage of low-frequency components. Reproduced with permission from R.J. Adolph, J.F. Stephens, and K. Tanaka, The clinical value of frequency analysis of the first heart sound in myocardial infarction, *Circulation,* 41:1003–1014, 1970. ©American Heart Association.

■ ■ ■ ■ ■

6.2.2   Frequency analysis of murmurs to diagnose valvular defects

Cardiovascular valvular defects and diseases cause

high-frequency, noise-like sounds known as murmurs.

Yoshimura et al.: tunable bandpass filter with cutoff

$18 - 1,425 \ Hz$ to process recorded PCG signals.

Diastolic *rumble* of mitral stenosis: $20 - 200 \ Hz$.

Diastolic *blow* of aortic regurgitation: $200 - 1,600 \ Hz$.

van Vollenhoven et al.:

tunable bandpass filter, $50\ Hz$ bandwidth,

center frequency tunable in steps of $50\ Hz$.

$100\ ms$ window in diastolic phase of recorded PCG signals.

Murmur of mitral stenosis: limited to less than $400\ Hz$.

Aortic insufficiency combined with mitral stenosis:

more high-frequency energy in the range $300 - 1,000\ Hz$.

Sarkady et al.:

synchronized averaging of PSDs of PCG signals

over several cardiac cycles computed using the FFT.

Johnson et al.:

FFT-based PSDs of systolic murmur (aortic stenosis).

PSDs of systolic windows of duration $86, 170,$ and $341\ ms$,

averaged over 10 cardiac cycles.

Hypothesis: higher murmur frequencies generated

as the severity of aortic stenosis increases.

Trans-aortic-valvular systolic pressure gradient measured

with catheterization and cardiac fluoroscopy:

$10 - 140 \; mm \; of \; Hg.$

Spectral power ratios computed with the bands

$25 - 75 \; Hz :$ constant area (CA) related to normal sounds,

$75 - 150 \; Hz :$ predictive area (PA) related to murmurs.
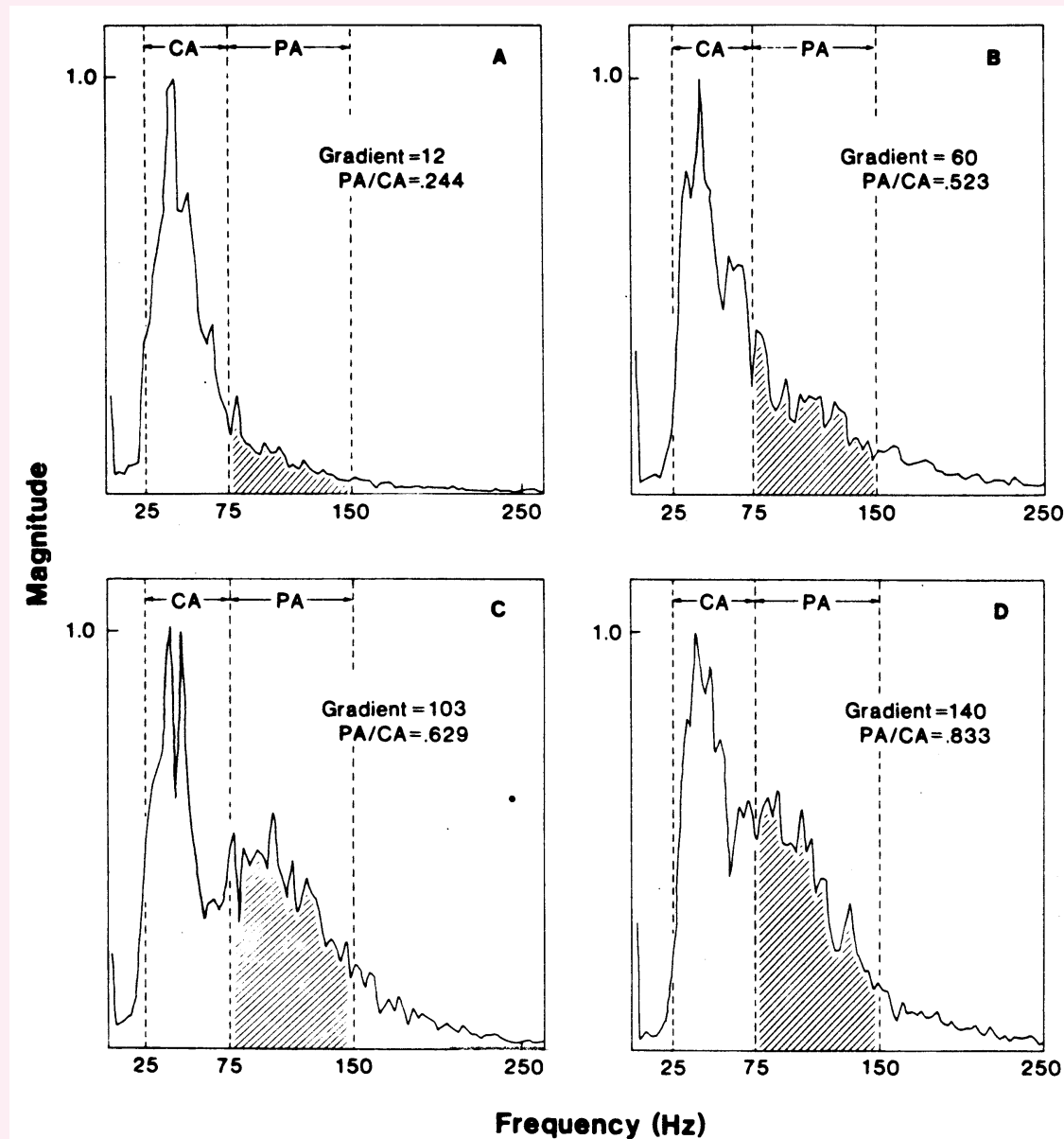
Figure 6.2: Averaged and normalized PSDs of four patients with aortic stenosis of different levels of severity. Each PSD is segmented into two parts: a constant area CA and a predictive area PA. The transvalvular systolic pressure gradient (measured via catheterization in $mm\ of\ Hg$) and the PA/CA spectral power ratio are shown for each case. Reproduced with permission from the American College of Cardiology: G.R. Johnson, R.J. Adolph, and D.J. Campbell, Estimation of the severity of aortic valve stenosis by frequency analysis of the murmur, *Journal of the American College of Cardiology,* 1(5):1315–1323, 1983 ©Elsevier Science.

6.3   Estimation of the Power Spectral Density Function

Consider a signal with N samples:

$x(n)$, $n = 0, 1, 2, \ldots, N - 1$.

To compute the time-averaged ACF

$\phi_{xx}(m)$ for a delay of m samples,

we need to form the product $x(n)\, x(n \pm m)$

and sum over the available range of data samples.

True ACF: $\phi_{xx}(m) = E[x(n)\, x(n + m)]$.

We may sum from $n = 0$ to $n = N - 1$ when computing

$\phi_{xx}(0)$ with $x(n)\, x(n) = x^2(n)$.

However, when computing $\phi_{xx}(1)$ with $x(n)\, x(n+1)$,

we can only sum from $n = 0$ to $n = N - 2$.

Linear shift of m samples to compute $\phi_{xx}(\pm m)$:

m samples of one signal drop out of the window of analysis

indicated by the overlap between the

two versions of the signal.
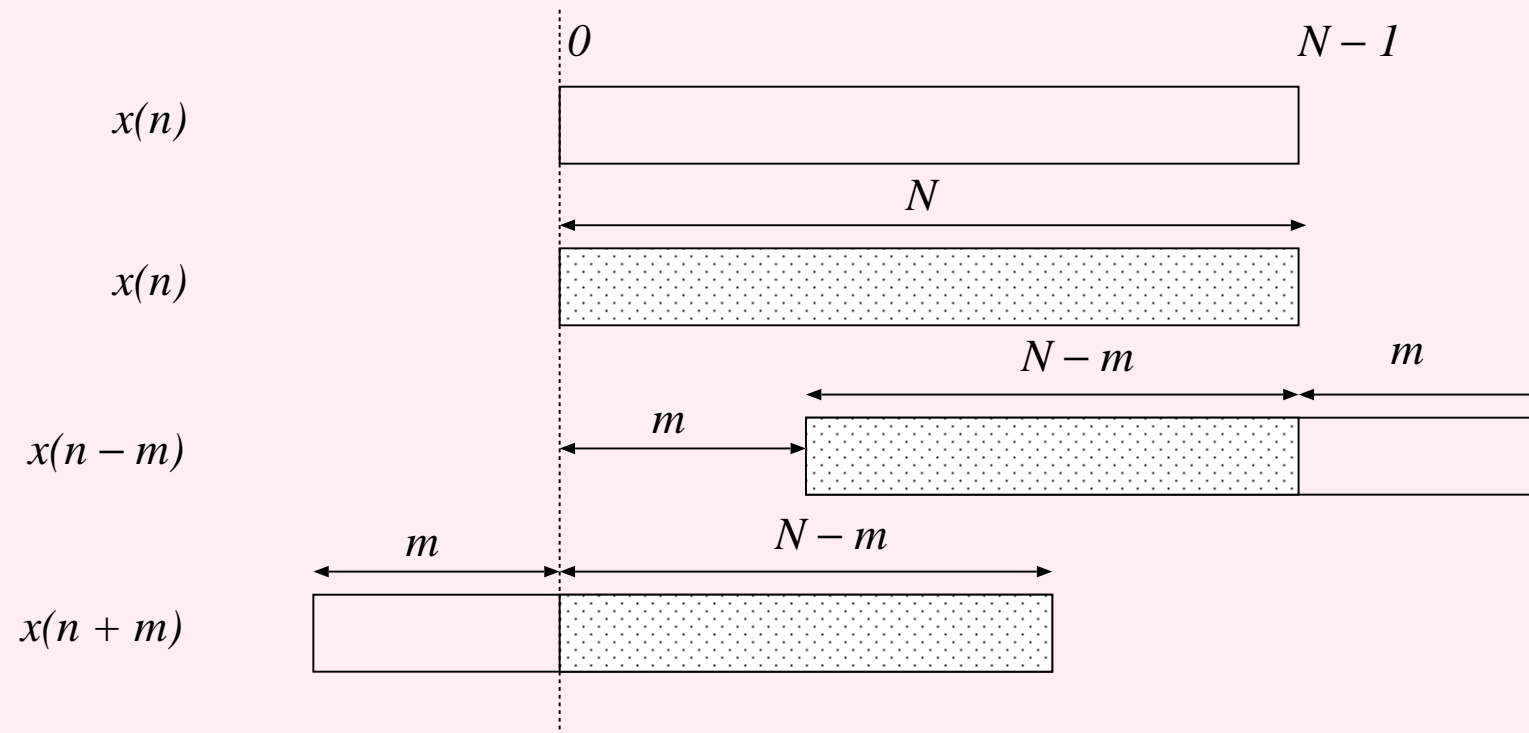
Figure 6.3: The effect of shifting in the computation of the ACF or CCF: as the shift increases, the number of available pairs of samples is reduced.

Only $N - |m|$ pairs of data samples available to estimate

ACF for delay of $\pm m$ samples.

Sample-mean estimate of ACF:

$$\phi_1(m) = \frac{1}{N - |m|} \sum_{n=0}^{N-|m|-1} x(n) \; x(n+m). \qquad (6.1)$$

Oppenheim and Schafer:

$\phi_1(m)$ is a consistent estimate of $\phi_{xx}(m)$.

Zero bias and variance that tends to zero as $N \to \infty$.

Variance of estimate exceptionally large as $m \to N$:

very few nonzero pairs of samples available

to compute the ACF.

Alternative definition of ACF:

ignore lack of $|m|$ nonzero pairs of samples,

apply the same scale factor for all delays:

$$\phi_2(m) = \frac{1}{N} \sum_{n=0}^{N-|m|-1} x(n)\, x(n+m). \qquad (6.2)$$

Upper limit of summation could be $N - 1$:

no effect on the result.

First or last $|m|$ samples of $x(n)$

will not overlap with $x(n + m)$:

result in zero product terms.

Oppenheim and Schafer: $\phi_2(m)$ has bias $= \frac{m}{N} \phi_{xx}(m)$.

Bias tends to actual value being estimated as $m \to N$.

Variance almost independent of m,

tends to zero as $N \to \infty$.

Both ACF estimates asymptotically unbiased;

bias of $\phi_2(m)$ tends to zero as $N \to \infty$.

Good estimates of ACF if N is large and $m << N$.

ACF estimates $\phi_1(m)$ and $\phi_2(m)$ interrelated:

$$\phi_2(m) = \frac{N - |m|}{N} \; \phi_1(m). \qquad (6.3)$$

$\phi_2(m)$ is a scaled version of $\phi_1(m)$.

Scaling factor is a function of m: referred to as a *window*.

6.3.1   The periodogram

PSD and ACF: Fourier transform pair.

$$S_2(\omega) = \sum_{m=-(N-1)}^{N-1} \phi_2(m) \, \exp(-j\omega m). \qquad (6.4)$$

Fourier transform of $x(n)$, $n = 0, 1, 2, \ldots, N - 1$:

$$X(\omega) = \sum_{n=0}^{N-1} x(n) \, \exp(-j\omega n). \qquad (6.5)$$

$$S_2(\omega) = \frac{1}{N}\, |X(\omega)|^2 \,. \tag{6.6}$$

PSD estimate $S_2(\omega)$: *periodogram* of $x(n)$.

Oppenheim and Schafer:

$S_2(\omega)$ is a biased estimate of the PSD, with

$$E[S_2(\omega)] = \sum_{m=-(N-1)}^{N-1} \frac{N - |m|}{N}\, \phi_{xx}(m)\ \exp(-j\omega m). \tag{6.7}$$

FT of $\phi_1(m)$: a different estimate of PSD.

$$S_1(\omega) = \sum_{m=-(N-1)}^{N-1} \phi_1(m) \, \exp(-j\omega m). \qquad (6.8)$$

$$E[S_1(\omega)] = \sum_{m=-(N-1)}^{N-1} \phi_{xx}(m) \, \exp(-j\omega m). \qquad (6.9)$$

$S_1(\omega)$ is a biased estimate of the PSD.

The two estimates $S_2(\omega)$ and $S_1(\omega)$ may be seen as the

Fourier transforms of windowed ACFs.

Window function for $\phi_2(m)$:

triangular function or Bartlett window.

$$w_B(m) = \begin{cases} \frac{N-|m|}{N}, & |m| < N \\ 0, & otherwise \end{cases}. \qquad (6.10)$$

Window function for $\phi_1(m)$: rectangular function.

$$w_R(m) = \begin{cases} 1, & |m| < N, \\ 0, & otherwise \end{cases} . \qquad (6.11)$$

The windows have a duration of $(2N - 1)$ samples.

ACF multiplied with window $\longrightarrow$

PSD convolved with FT of window:

leads to spectral leakage and loss of resolution.

FT of Bartlett and rectangular windows:

$$W_B(\omega) = \frac{1}{N}\left[\frac{\sin(\omega N/2)}{\sin(\omega/2)}\right]^2, \qquad (6.12)$$

$$W_R(\omega) = \frac{\sin[\omega(2N-1)/2]}{\sin(\omega/2)}. \qquad (6.13)$$

Oppenheim and Schafer: periodogram has a

variance that does not approach zero as $N \to \infty$;

variance of the order of σ_x^4 regardless of N.

The periodogram is not a consistent estimate of the PSD.

6.3.2   The need for averaging

Common approach to reduce the variance of an estimate:

average over a number of statistically independent estimates.

A number of periodograms may be computed

over multiple observations of a signal and

averaged to obtain a better estimate of the PSD.

It is necessary for the process to be stationary,

at least over the period over which the

periodograms are computed and averaged.

Problem: *How can we obtain an averaged periodogram*

when we are given only one signal record of finite duration?

Solution: Bartlett method to average

periodograms of segments of the given signal record.

1. Divide given data $x(n)$, $n = 0, 1, 2, \ldots, N-1$,

   into K segments of M samples each:

$$x_i(n) = x(n+(i-1)M), \quad 0 \leq n \leq M-1, \quad 1 \leq i \leq K.$$
$$(6.14)$$

2. Compute the periodogram of each segment as

$$S_i(\omega) = \frac{1}{M} \left| \sum_{n=0}^{M-1} x_i(n) \, \exp(-j\omega n) \right|^2, \quad 1 \leq i \leq K.$$
$$(6.15)$$

   FT: DFT using the FFT.

3. If ACF $\phi_{xx}(m)$ negligible for $|m| > M$,

   the periodograms of the K segments with M samples

   each may be assumed to be mutually independent.

   Bartlett estimate $S_B(\omega)$ of the PSD = sample mean

   of the K independent observations of the periodogram:

$$S_B(\omega) = \frac{1}{K} \sum_{i=1}^{K} S_i(\omega). \qquad (6.16)$$

Oppenheim and Schafer: expected value of the

Bartlett estimate $S_B(\omega)$ = convolution of true PSD $S_{xx}(\omega)$

with the FT of the Bartlett window.

Bias, spectral smearing, and leakage:

loss of spectral resolution.

Variance tends to zero as number of segments K increases:

consistent estimate of the PSD.

Stationary signal of fixed duration of N samples: limitations

on the number of segments K that we may obtain.

Variance of PSD estimate decreases as K is increased:

but as M decreases, the main lobe of the FT of the

Bartlett window widens; frequency resolution lost.

Cyclostationary signals such as the PCG offer a

unique and interesting approach to synchronized averaging

of periodograms over a number of cycles,

without trade-off between reduction of variance and

loss of spectral resolution.

6.3.3   The use of windows: Spectral resolution and leakage

Bartlett procedure: ensemble averaging approach to

reduce the variance of the periodogram.

Another approach: to obtain a smooth spectrum,

convolve periodogram $S(\omega)$ with filter or

smoothing function $W(\omega)$ in the frequency domain

(similar to the use of an MA filter in the time domain).

Smoothed estimate $S_s(\omega)$:

$$S_s(\omega) = \frac{1}{2\pi} \int_{-\pi}^{\pi} S(\nu) \, W(\omega - \nu) \, d\nu. \qquad (6.17)$$

ν: temporary variable for integration.

PSD: nonnegative function.

Condition on the smoothing function $W(\omega)$:

$W(\omega) \geq 0, \, -\pi \leq \omega \leq \pi.$

Oppenheim and Schafer:

variance of smoothed periodogram reduced by the factor

$$\frac{1}{N} \sum_{m=-(M-1)}^{M-1} w^2(m) = \frac{1}{2\pi N} \int_{-\pi}^{\pi} W^2(\omega) \, d\omega, \qquad (6.18)$$

with reference to variance of original periodogram.

N: total number of samples in signal.

$(2M - 1)$: number of samples in smoothing window.

Rectangular window: variance-reduction factor of $\sim \frac{2M}{N}$.

Bartlett window: variance-reduction factor of $\sim \frac{2M}{3N}$.

Smoothing of spectrum and reduction of variance achieved

at the price of loss of frequency resolution.

Periodogram = FT of ACF estimate $\phi(m)$:

convolution operation in frequency domain in Equation 6.17

equivalent to multiplying $\phi(m)$ with $w(m) = \text{IFT}\,[W(\omega)]$.

Same PSD estimate as $S_s(\omega)$ obtained by

applying a window to the ACF estimate and

taking the Fourier transform of the result.

ACF is an even function: window should also be even.

Welch's method to average modified periodograms:

Given signal is segmented as in the Bartlett procedure,

but a window is applied to the original signal segments.

Periodograms of windowed segments:

$$S_{Wi}(\omega) = \frac{1}{M E_w} \left| \sum_{n=0}^{M-1} x_i(n) \; w(n) \; \exp(-j\omega n) \right|^2,$$

$$(6.19)$$

$$i = 1, 2, \ldots, K.$$

E_w = average power of window, duration = M samples:

$$E_w = \frac{1}{M} \sum_{n=0}^{M-1} w^2(n). \qquad (6.20)$$

Welch PSD estimate $S_W(\omega)$ =

average of modified periodograms:

$$S_W(\omega) = \frac{1}{K} \sum_{i=1}^{K} S_{Wi}(\omega). \qquad (6.21)$$

Welch showed that, if the segments are not overlapping,

the variance of the averaged modified periodogram is

inversely proportional to K, the number of segments used.

Spectral window convolved with the PSD in the frequency

domain is proportional to the squared magnitude of the

Fourier transform of the time-domain data window applied:

any type of data window may be used.

Commonly used data windows:

causal, length $= N$ samples, defined for $0 \le n \le N - 1$.

Rectangular:
$$w(n) = 1. \tag{6.22}$$

Bartlett (triangular):
$$w(n) = \begin{cases} \frac{2n}{N-1}, & 0 \le n \le \frac{N-1}{2}, \\ \\ 2 - \frac{2n}{N-1}, & \frac{N-1}{2} \le n \le N - 1. \end{cases} \tag{6.23}$$

Hamming:

$$w(n) = 0.54 - 0.46 \, \cos\left(\frac{2\pi n}{N-1}\right). \qquad (6.24)$$

von Hann:

$$w(n) = \frac{1}{2}\left[1 - \cos\left(\frac{2\pi n}{N-1}\right)\right]. \qquad (6.25)$$

Blackman:

$$w(n) = 0.42 - 0.5 \, \cos\left(\frac{2\pi n}{N-1}\right) + 0.08 \, \cos\left(\frac{4\pi n}{N-1}\right). \quad (6.26)$$
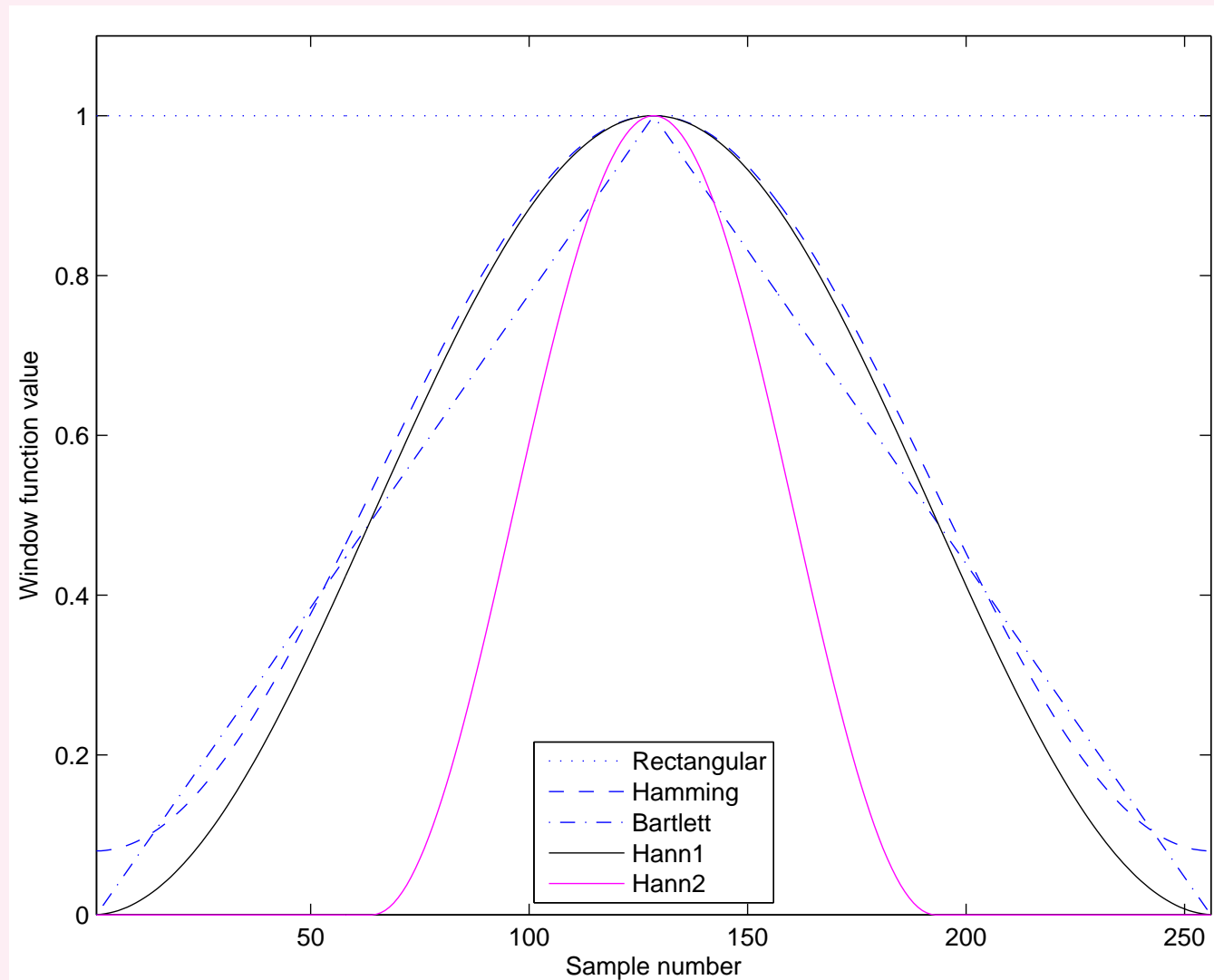
Figure 6.4: Commonly used window functions: rectangular, Bartlett, Hamming, and Hann windows with $N = 256$ (Hann1), and Hann window with $N = 128$ samples (Hann2). All windows are centered at the 128th sample.

Advantage of tapered windows

(all of the above, except rectangular):

ends of given signal reduced to zero (except Hamming).

No discontinuities in the periodic version of the signal

encountered in DFT-based procedures.

All window functions above are symmetric (even) functions:

linear phase; zero phase if window centered at the origin.
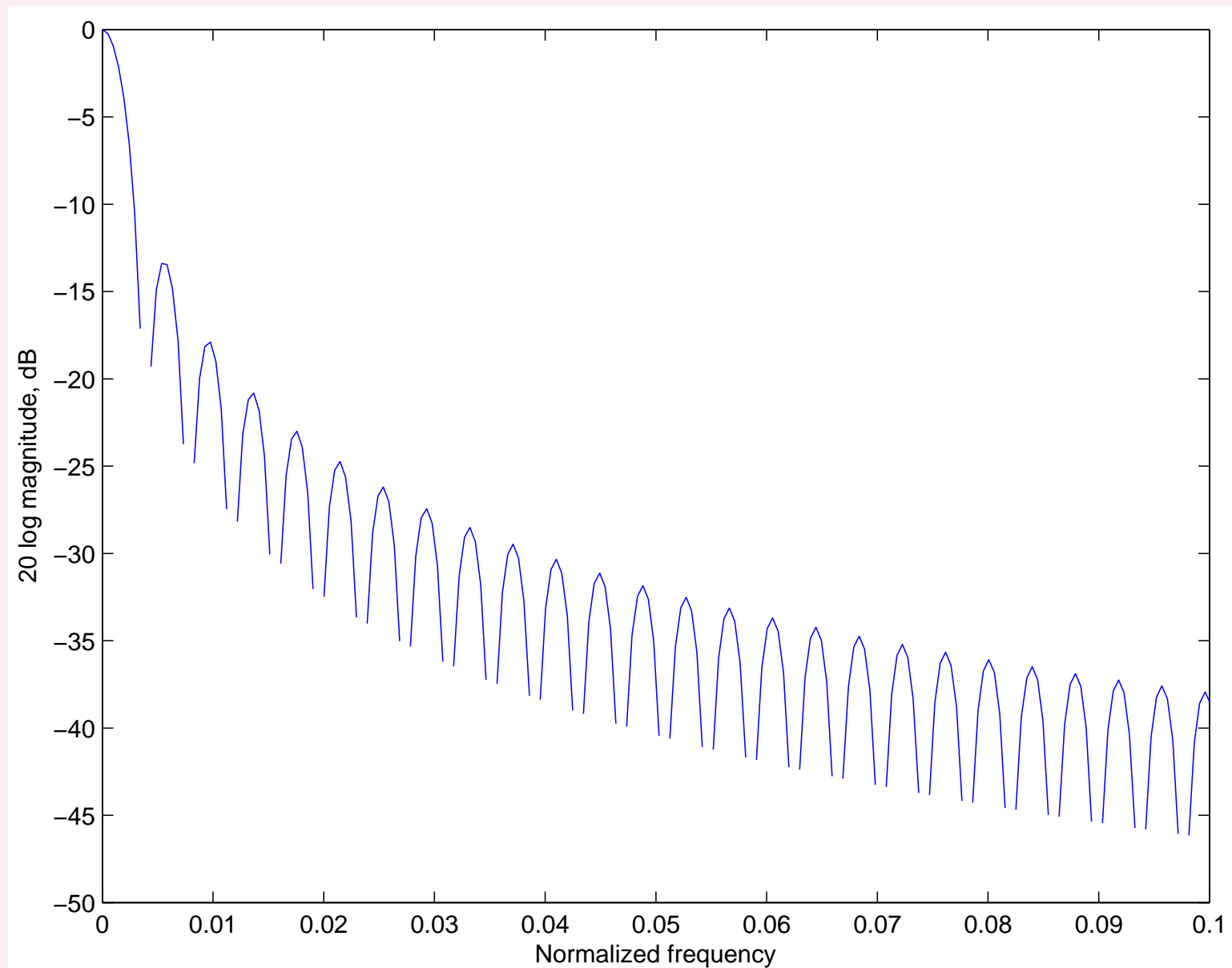
Figure 6.5: Log-magnitude frequency response of the rectangular window illustrated in Figure 6.4. The window width is $N = 256$ samples.
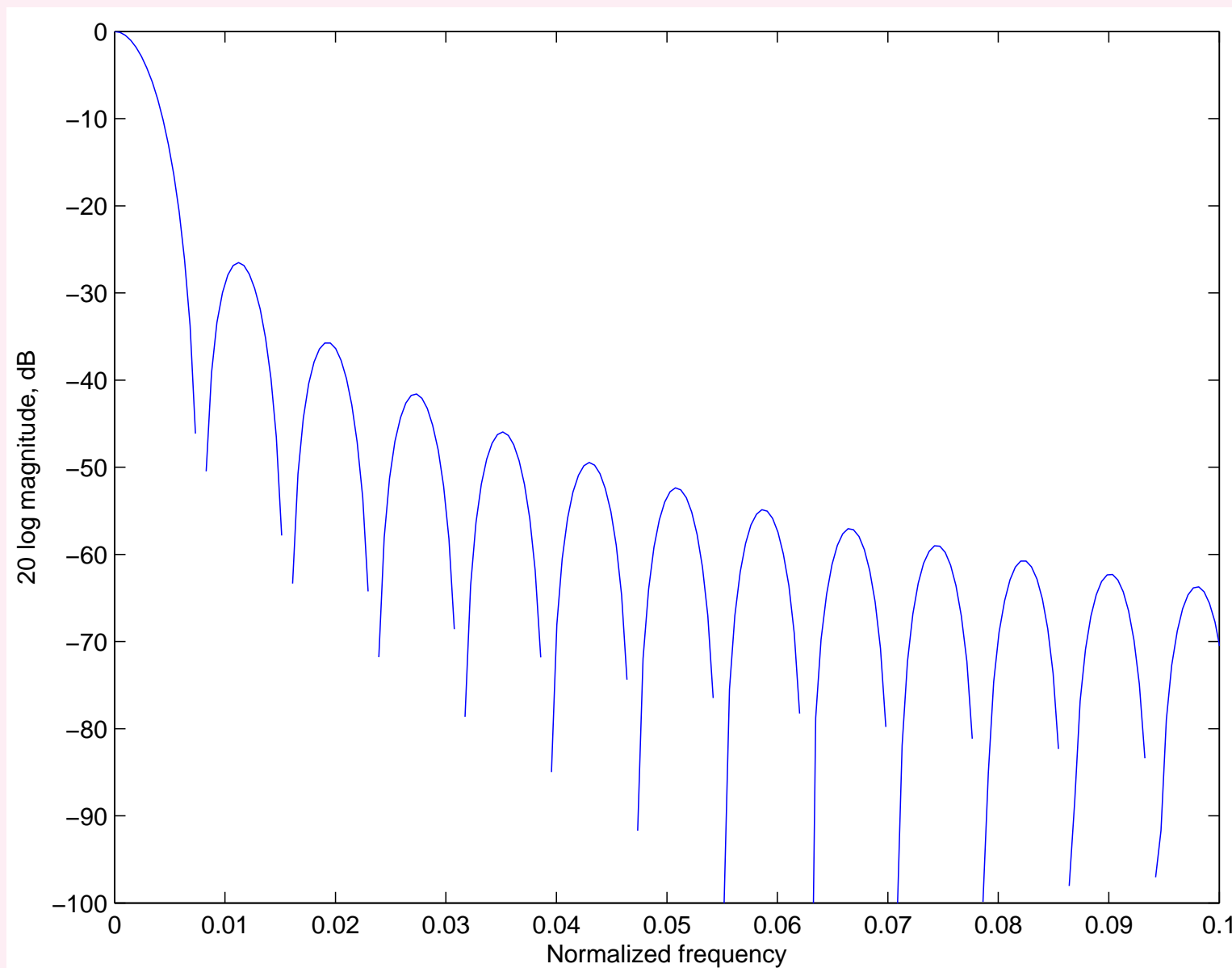
Figure 6.6: Log-magnitude frequency response of the Bartlett window illustrated in Figure 6.4. The window width is $N = 256$ samples.
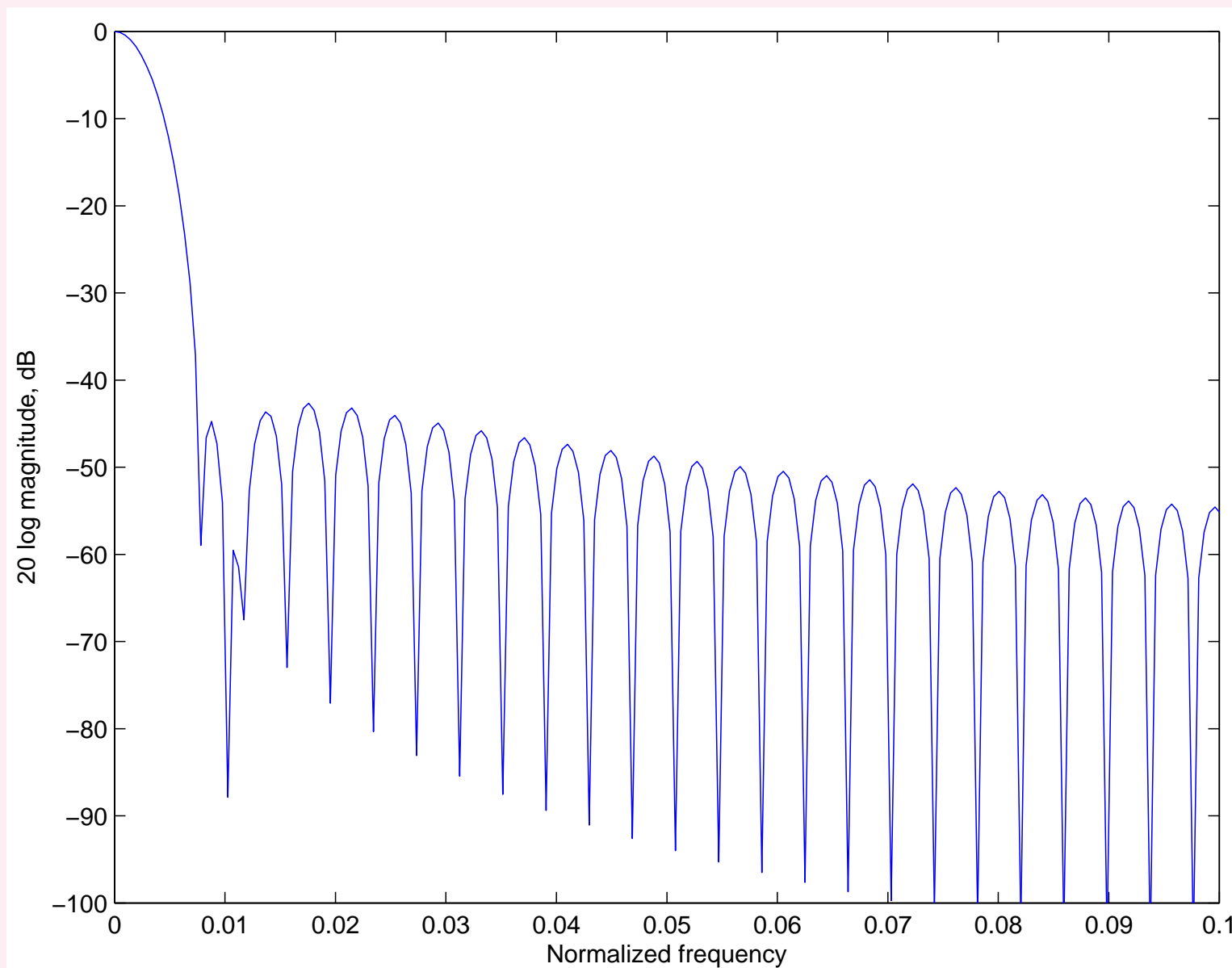
Figure 6.7: Log-magnitude frequency response of the Hamming window illustrated in Figure 6.4. The window width is $N = 256$ samples.
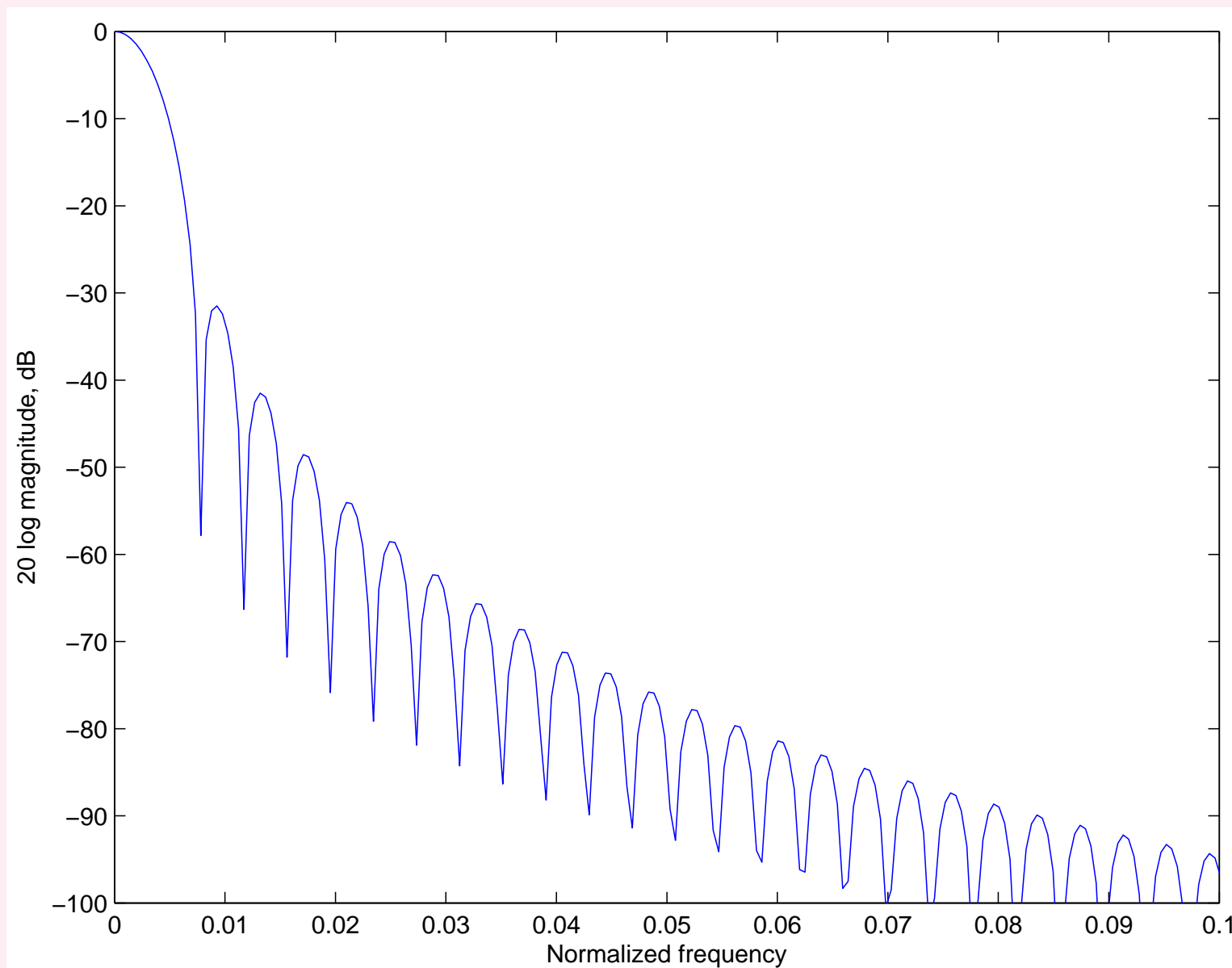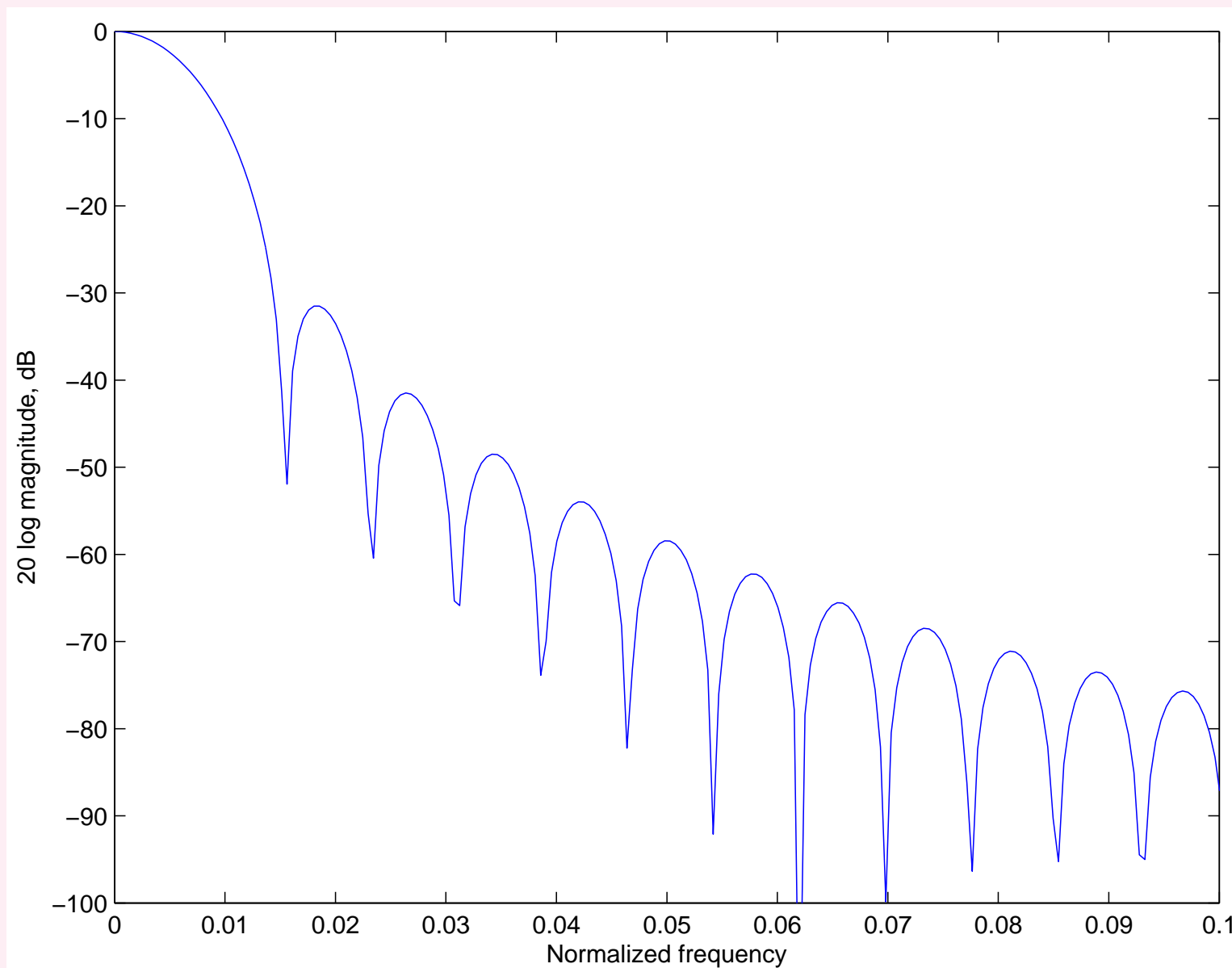
Figure 6.8: Log-magnitude frequency response of the Hann1 window illustrated in Figure 6.4. The window width is $N = 256$ samples.

Figure 6.9: Log-magnitude frequency response of the Hann2 window illustrated in Figure 6.4. The window width is $N = 128$ samples.

Rectangular window: narrowest main lobe of width $\frac{4\pi}{N}$.

Main lobe wider $= \frac{8\pi}{N}$ for Bartlett, Hann, and Hamming

windows; widest for Blackman window $= \frac{12\pi}{N}$.

Reduction in window width leads to

increase in the main-lobe width.

The wider the main lobe, the greater is the

spectral smoothing: severe loss of spectral resolution.

Rectangular window: highest peak side-lobe $= -13\ dB$.

Bartlett, Hann, Hamming, and Blackman windows:

peak side-lobe $-25\ dB$, $-31\ dB$, $-41\ dB$, and $-57\ dB$.

Higher side-lobes cause more spectral leakage and

result in a distorted spectrum.

Reduction of leakage with tapered windows comes at the

price of increased main-lobe width: more smoothing and
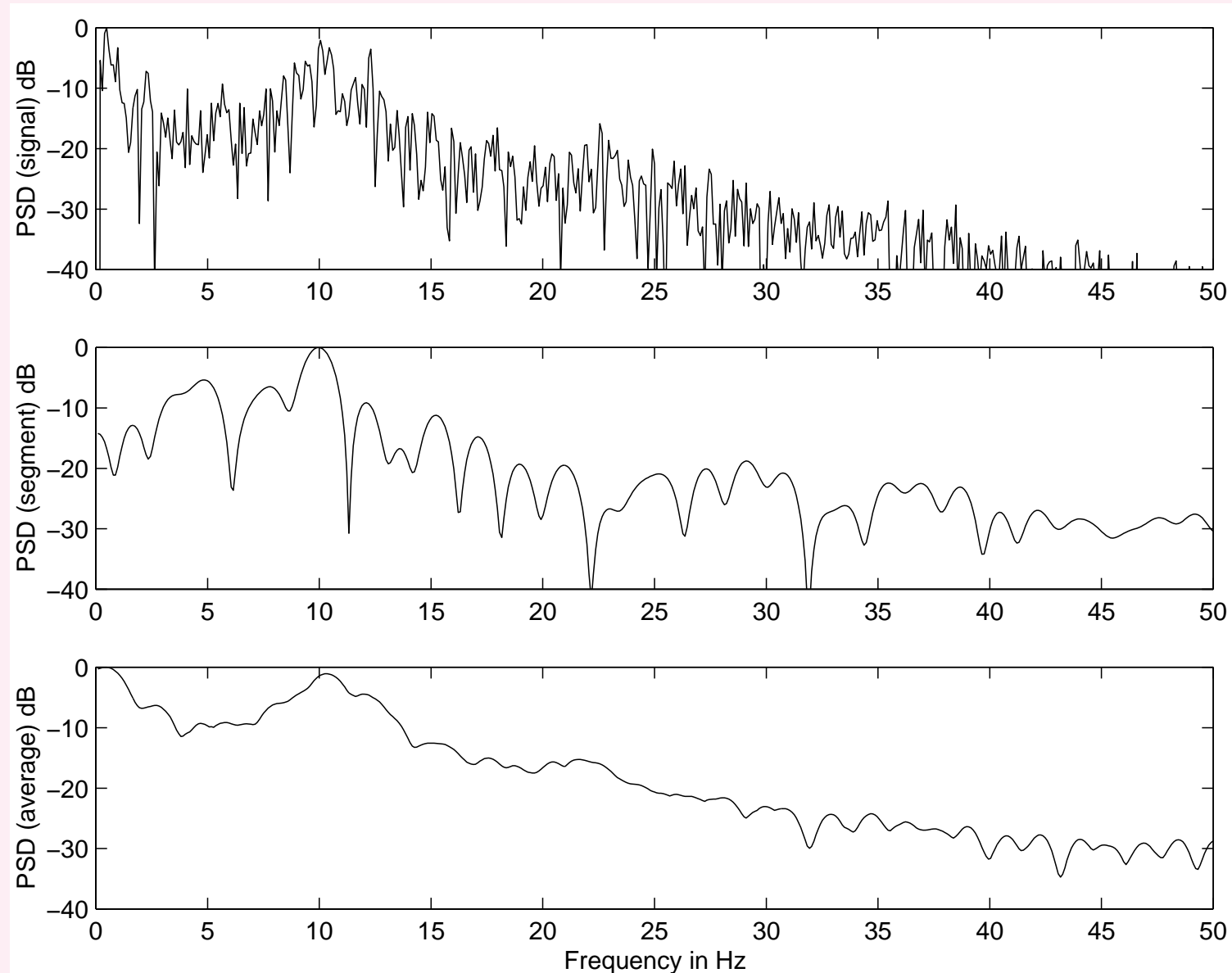
loss of spectral resolution.

■ ■ ■ ■ ■

Figure 6.10: Bartlett PSD estimate of the o2 channel of the EEG signal in Figure 1.39. Top trace: PSD of the entire signal. Middle trace: PSD of the 11th segment. Bottom trace: Averaged PSD using $K = 11$ segments of the signal. The rectangular window was (implicitly) used in all cases. Number of samples in the entire signal: $N = 750$. Number of samples in each segment: $M = 64$. All FFT arrays were computed with $L = 1,024$ samples. Sampling frequency $f_s = 100 \ Hz$.
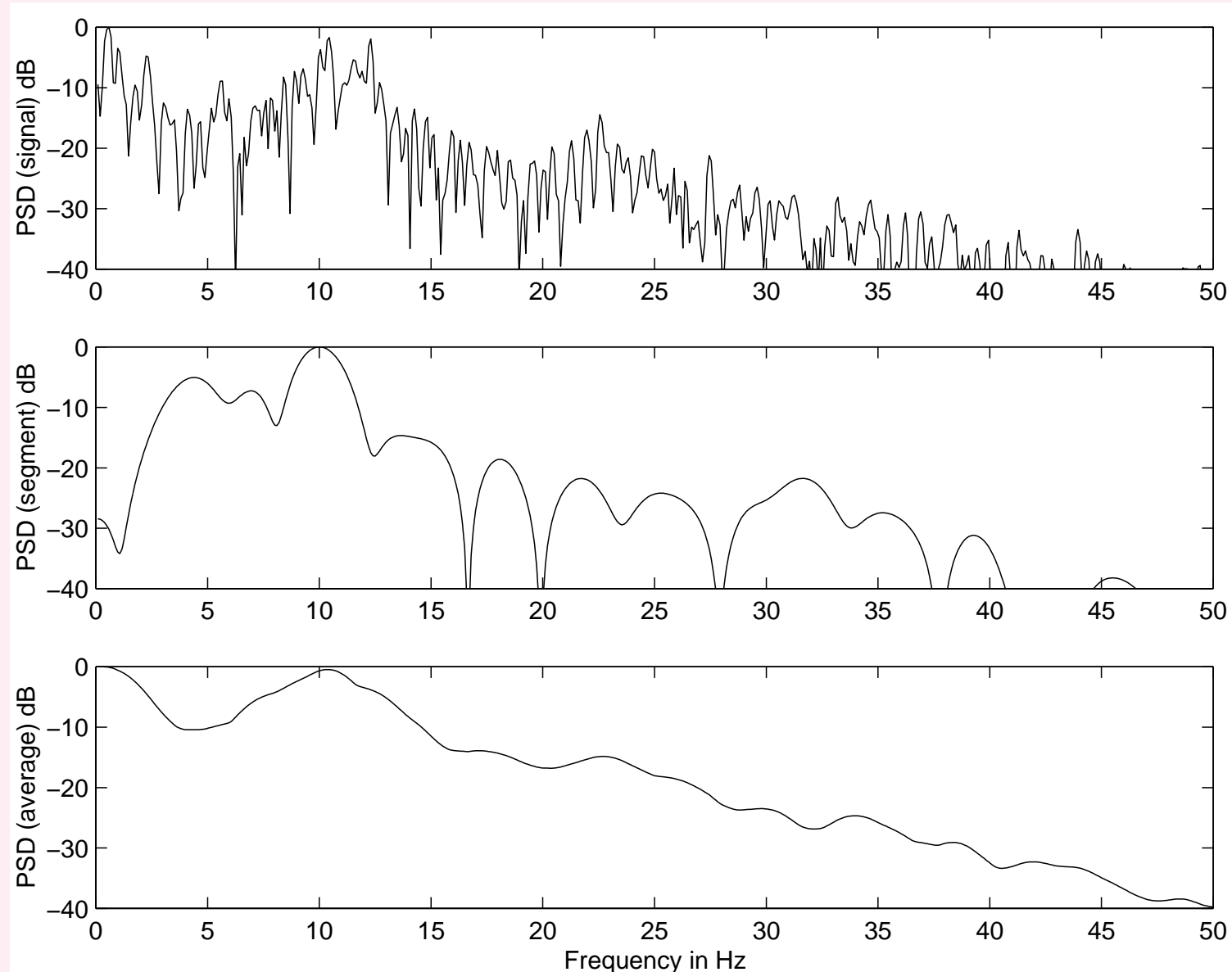
Figure 6.11: Welch PSD estimate of the o2 channel of the EEG signal in Figure 1.39. Top trace: PSD of the entire signal. Middle trace: PSD of the 11th segment. Bottom trace: Averaged PSD using $K = 11$ segments of the signal. The Hann window was used in all cases. Number of samples in the entire signal and the size of the Hann window used in computing the PSD of the entire signal: $N = 750$. Number of samples in each segment and the size of the Hann window used in the averaged periodogram method: $M = 64$. All FFT arrays were computed with $L = 1,024$ samples. Sampling frequency $f_s = 100\ Hz$.

Hann window: smoothing of spurious peaks in PSD.

Wider main-lobe of Hann window's frequency response:

more severe loss of frequency resolution (smoothing).

Averaged PSD in the lowest trace of Figure 6.11 illustrates

benefit of Hann window: reduced power for $f > 30 \ Hz$.

Lower side-lobe levels of Hann window: less leakage

(as compared to the rectangular window).

6.3.4   Estimation of the ACF

Good estimates of ACF required in applications such as

design of the optimal Wiener filter and

estimation of the statistics of stochastic processes.

After a PSD estimate has been obtained (Bartlett or Welch)

take the inverse Fourier transform → estimate of ACF.

We may also fit a smooth curve or a parametric model —

exponential or Laplacian — to the PSD or ACF.

$$\phi_2(m) = \frac{1}{N} \sum_{n=0}^{N-|m|-1} x(n)\, x(n+m). \qquad (6.27)$$

ACF is an even function: need to compute only for $m > 0$.

ACF estimate $= \frac{1}{N} \times$ linear convolution of $x(n)$ with $x(-n)$.

DFT $[x(n)] = X(k) \rightarrow$ DFT $[x(-n)] = X^*(k)$.

Convolution in time $\equiv$ multiplication in frequency:

obtain $X(k)\, X^*(k) = |X(k)|^2$, take its inverse DFT.

DFT: circular convolution, not linear convolution.

Pad $x(n)$ with at least $M - 1$ zeros;

M: largest lag for which the ACF is desired.

Compute DFT with at least $L = N + M - 1$ samples;

N: number of samples in the original signal.

Include the above steps in averaged periodogram procedure,

take inverse DFT of final PSD estimate $\rightarrow$ estimate of ACF.

Divide by $\frac{1}{N}$, or divide by $\phi_{xx}(0)$ to get normalized ACF.

6.3.5 Synchronized averaging of PCG spectra

PCG: nonstationary signal.

Amount of blood in each cardiac chamber and

state of contraction of cardiac muscles

change continuously during each cardiac cycle.

S2 usually has more high-frequency content than S1.

PSD of normal PCG changes within about $300 \ ms$.

Valve opening or closing sounds: short duration $\sim 10\ ms$;

transients with high-frequency character.

Murmurs add another dimension of nonstationarity:

frequency content well beyond that of normal heart sounds.

PSD of abnormal PCG could change within $100\ ms$.

Individual epochs of S1, S2, valve snaps, and murmurs of

limited durations of $\sim 10 - 300\ ms$.

Cannot perform segmented averaging (Bartlett or Welch).

The transmission characteristics of the chest wall

change during breathing.

PCG at various locations on the chest are subject to

different transmission-path effects.

Adult subjects may cooperate in PCG signal acquisition by

holding their breath or performing other maneuvers:

no possible with infants and young children in poor health.

Problem: *Propose a method to obtain averaged*

PSD estimates of the systolic and diastolic heart sounds.

Solution: Cyclostationarity of PCG — unique approach

to average functions of PCG segments corresponding to the

same phase of the cardiac cycle cut from multiple beats.

Nonstationarity of the signal within a cardiac cycle:
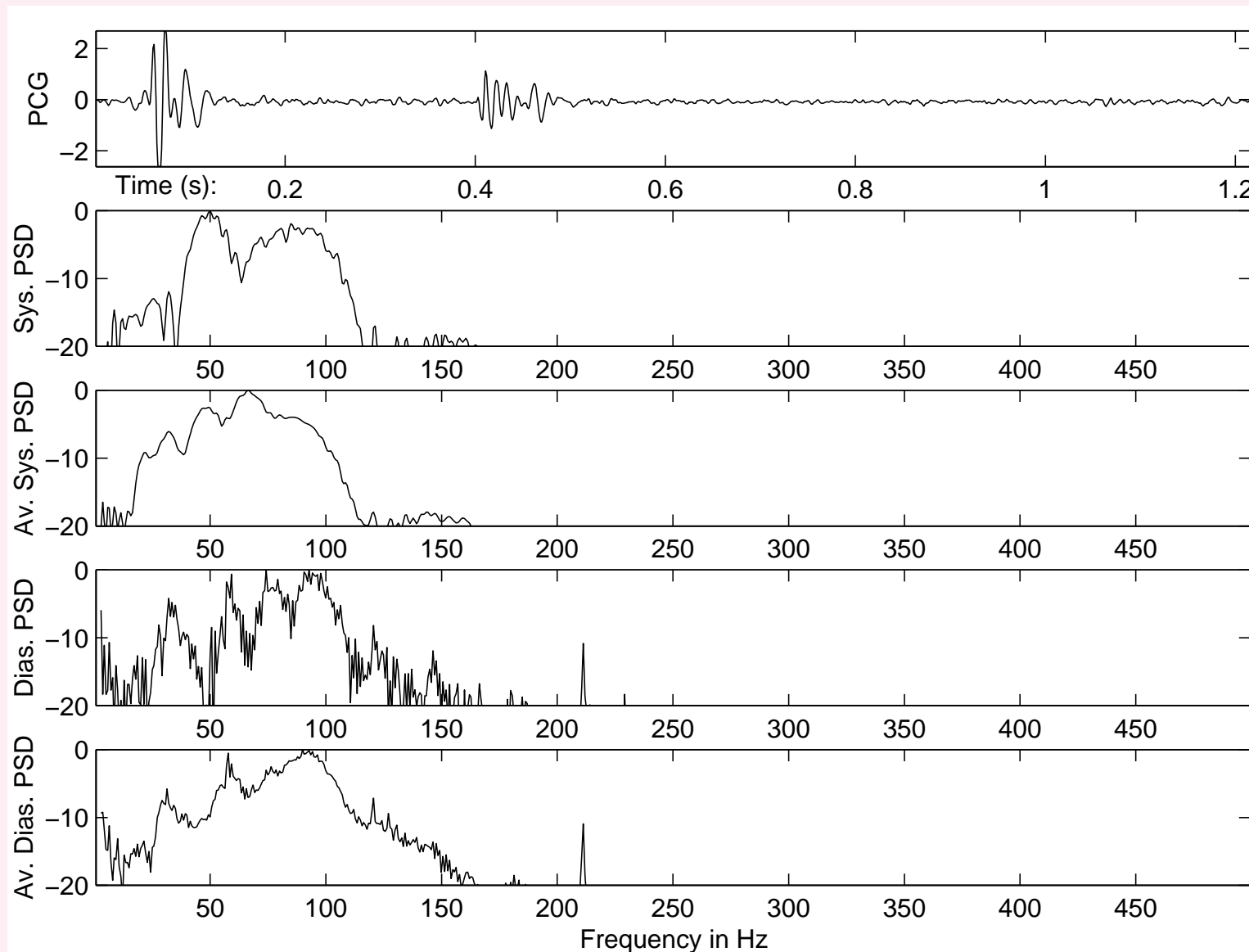
need to segment phases of PCG cycles.

Figure 6.12: Top to bottom: A sample PCG signal over one cardiac cycle of a normal subject (male, 23 years; see also Figures 4.30 and 5.7); periodogram of the systolic portion of the signal (approximately $0 - 0.4\ s$); averaged periodogram of the systolic parts of 16 cardiac cycles segmented as illustrated in Figure 4.30; periodogram of the diastolic portion of the signal shown in the first plot (approximately $0.4 - 1.2\ s$); averaged periodogram of the diastolic parts of 16 cardiac cycles. The periodograms are on a log scale (dB).
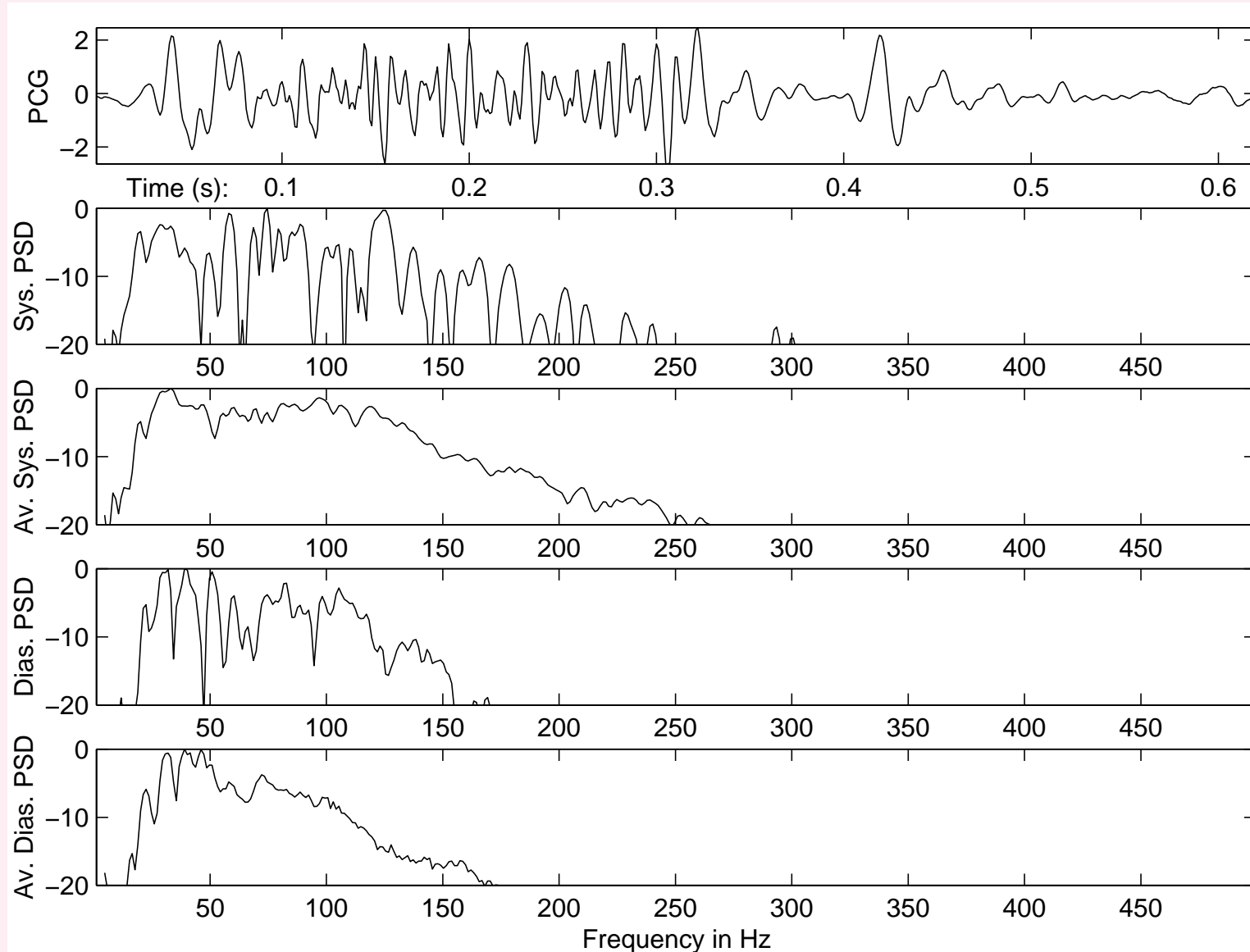
Figure 6.13: Top to bottom: A sample PCG signal over one cardiac cycle of a patient with systolic murmur, split S2, and opening snap of the mitral valve (female, 14 months; see also Figures 4.31 and 5.8); periodogram of the systolic portion of the signal (approximately $0 - 0.28\ s$); averaged periodogram of the systolic parts of 26 cardiac cycles segmented as illustrated in Figure 4.31; periodogram of the diastolic portion of the signal shown in the first plot (approximately $0.28 - 0.62\ s$); averaged periodogram of the diastolic parts of 26 cardiac cycles. The periodograms are on a log scale (dB).

6.4 Measures Derived from Power Spectral Density Functions

PSD: density function of signal amplitude

or power versus frequency.

Facilitates *nonparametric* and general spectral analysis.

Problem: *Derive parameters or measures from a Fourier*

spectrum or PSD that can help in the characterization

of the spectral variations or features contained therein.

Solution:

PSD is a nonnegative function as well as a density function:

Treat it as a PDF and compute statistics using moments.

Detect peaks corresponding to resonance,

measure their bandwidth or quality factor,

derive measures of concentration of power in

specific frequency bands of interest or concern.

PSD is nonparametric:

but we may derive several parameters that,

while not completely representing the entire PSD,

may facilitate the characterization of

physiological and/or pathological phenomena.

6.4.1   Moments of PSD functions

Area under the PSD = total signal power or energy $\neq 1$.

Normalize all moments by total energy of the signal E_x:

$$E_x = \sum_{n=0}^{N-1} |x(n)|^2 = \frac{1}{N} \sum_{k=0}^{N-1} |X(k)|^2 \qquad (6.28)$$

$$= \frac{1}{2\pi} \int_0^{2\pi} |X(\omega)|^2 \, d\omega = \int_{f_n=0}^{1} |X(f_n)|^2 \, df_n.$$

Frequency f_n: normalized as $f_n = f/f_s$; $0 \le f_n \le 1$.

Replace $|X(.)|^2$ in the above expressions by $S_{xx}(.)$.

In all definitions of moments of PSDs:

$$S_{xx}(k) = \frac{1}{N} |X(k)|^2.$$

$X(k)$: DFT of $x(n)$; $S_{xx}(k)$: PSD of $x(n)$.

Measure of concentration of signal power over its

frequency range: mean frequency $\overline{f}$ = first-order moment

$$\overline{f_n} = \frac{2}{E_x} \int_{f_n=0}^{0.5} f_n \, S_{xx}(f_n) \, df_n. \qquad (6.29)$$

$$\overline{f_{Hz}} = \frac{f_s}{N} \frac{2}{E_x} \sum_{k=0}^{N/2} k \, S_{xx}(k). \qquad (6.30)$$

Median frequency $f_{med} =$

frequency that splits the PSD in half:

$$f_{med} = \frac{m}{N} \, f_s \quad with \ the \ largest \ m \ such \ that \quad (6.31)$$

$$\frac{2}{E_x} \sum_{k=0}^{m} S_{xx}(k) < \frac{1}{2}; \quad 0 \le m \le \frac{N}{2}.$$

Higher-order statistics:

- Variance f_{m2} = second-order moment using $(f_n - \overline{f_n})^2$:

$$f_{m2} = \frac{2}{E_x} \int_{f_n=0}^{0.5} (f_n - \overline{f_n})^2 \, S_{xx}(f_n) \, df_n. \qquad (6.32)$$

$$f_{m2} = \left(\frac{f_s}{N}\right)^2 \frac{2}{E_x} \sum_{k=0}^{N/2} (k - \overline{k})^2 \, S_{xx}(k). \qquad (6.33)$$

$\overline{k} = N \, \overline{f_{Hz}} / f_s$ = frequency sample index
corresponding to $\overline{f_{Hz}}$.

© R.M. Rangayyan, IEEE/Wiley, 2nd Ed., 2015

▪ Skewness:

$$skewness = \frac{f_{m3}}{(f_{m2})^{3/2}}. \qquad (6.34)$$

Third-order moment f_{m3} computed with $(f_n - \overline{f_n})^3$:

$$f_{m3} = \frac{2}{E_x} \int_{f_n=0}^{0.5} (f_n - \overline{f_n})^3 \, S_{xx}(f_n) \, df_n. \qquad (6.35)$$

$$f_{m3} = \left(\frac{f_s}{N}\right)^3 \frac{2}{E_x} \sum_{k=0}^{N/2} (k - \overline{k})^3 \, S_{xx}(k). \qquad (6.36)$$

- Kurtosis:

$$kurtosis = \frac{f_{m4}}{(f_{m2})^2}.\qquad (6.37)$$

Fourth-order moment f_{m4} computed with $(f_n - \overline{f_n})^4$:

$$f_{m4} = \frac{2}{E_x} \int_{f_n=0}^{0.5} (f_n - \overline{f_n})^4 \, S_{xx}(f_n) \, df_n.\qquad (6.38)$$

$$f_{m4} = \left(\frac{f_s}{N}\right)^4 \frac{2}{E_x} \sum_{k=0}^{N/2} (k - \overline{k})^4 \, S_{xx}(k).\qquad (6.39)$$

Mean frequency: measure of concentration of signal power;

could indicate resonance frequency

of unimodal distributions.

Multiple resonance frequencies: mean frequency not useful.

Multimodal PSDs: series of peak frequencies,

with measures of relative level, bandwidth, or quality factor.

Square-root of f_{m2}: measure of spectral spread.

Skewness = zero if PSD symmetric about mean frequency;

otherwise, indicates extent of asymmetry of distribution.

Kurtosis indicates if PSD is a long-tailed function.

6.4.2   *Spectral power ratios*

Fraction of signal power in a

frequency band of interest $(f_1 : f_2)$

$$E_{(f_1:f_2)} = \frac{2}{E_x} \int_{f=f_1}^{f_2} |X(f)|^2 \, df = \frac{2}{N E_x} \sum_{k=k_1}^{k_2} |X(k)|^2.$$

$$(6.40)$$

k_1 and k_2: DFT indices corresponding to f_1 and f_2.

May be computed for several frequency bands.

Johnson et al.: compared integral of magnitude spectrum of

systolic murmurs due to aortic stenosis

over the band $75 : 150\ Hz$ to that over the band $25 : 75\ Hz$.

Higher-frequency band: *predictive area* (PA)

of spectrum related to aortic stenosis.

Lower-frequency band: *constant area* (CA)

common to all systolic PCG signal segments.

$$\frac{PA}{CA} = \frac{\int_{f=f_2}^{f_3} |X(f)|\, df}{\int_{f=f_1}^{f_2} |X(f)|\, df}. \tag{6.41}$$

$f_1 = 25\ Hz,\ f_2 = 75\ Hz,\ f_3 = 150\ Hz.$

Figure 6.2:

$\frac{PA}{CA}$ ratio correlates well with severity of aortic stenosis.

Binnie et al.:

spectrum analysis of EEG for detection of epilepsy.

Partitioning or banding of EEG spectrum into not only the

traditional δ, θ, α, and β bands,

but also seven nonuniform bands:

$1 - 2, 2 - 4, 4 - 6, 6 - 8, 8 - 11, 11 - 14$, and $> 14\ Hz$.

Additional features related to the form factor used.

Study with 275 patients with suspected epilepsy:

90% of signals of patients with epilepsy

classified as abnormal;

86% of patients with EEGs classified as abnormal

had epilepsy.

6.5   Application: Evaluation of Prosthetic Heart Valves

Efficient opening and closing actions of cardiac valves

of paramount importance for proper pumping

of blood by the heart.

When native valves fail, they may be replaced by

mechanical prosthetic valves or by bioprosthetic valves.

Mechanical prosthetic valves prone to sudden failure

due to fracture of their components.

Bioprosthetic valves fail gradually due to tissue

degeneration and calcification: last for $7 - 12$ years.

Follow-up of the health of patients with prosthetic valves

requires periodic, noninvasive assessment of the

functional integrity of the valves.

Problem: *Deposition of calcium causes the normally*

pliant and elastic bioprosthetic valve leaflets to become stiff.

Propose a method to assess the functional integrity of

bioprosthetic valves.

Solution: Increased stiffness of a valve expected to lead to

higher-frequency components in opening/ closing sounds.

Durand et al. studied spectra of S1 to evaluate sounds

contributed by closure of porcine (pig) bioprosthetic valves

implanted in the mitral position in humans.

Normal S1 spectra: limited in bandwidth to about $100 \ Hz$.

Degenerated bioprosthetic valves: significant spectral

energy in the range $100 - 250 \ Hz$.

Spectral parameters used by Durand et al.:

first and second dominant peak frequencies;

median frequency;

bandwidth and quality factor of dominant peak;

integrated mean area above $-20\ dB$;

highest frequency at $-3\ dB$;

total area and RMS value of spectrum;

area and RMS value in the bands

$20 - 100, 100 - 200, 200 - 300\ Hz$.

Normal versus degenerated valve classification

accuracy: 98%.
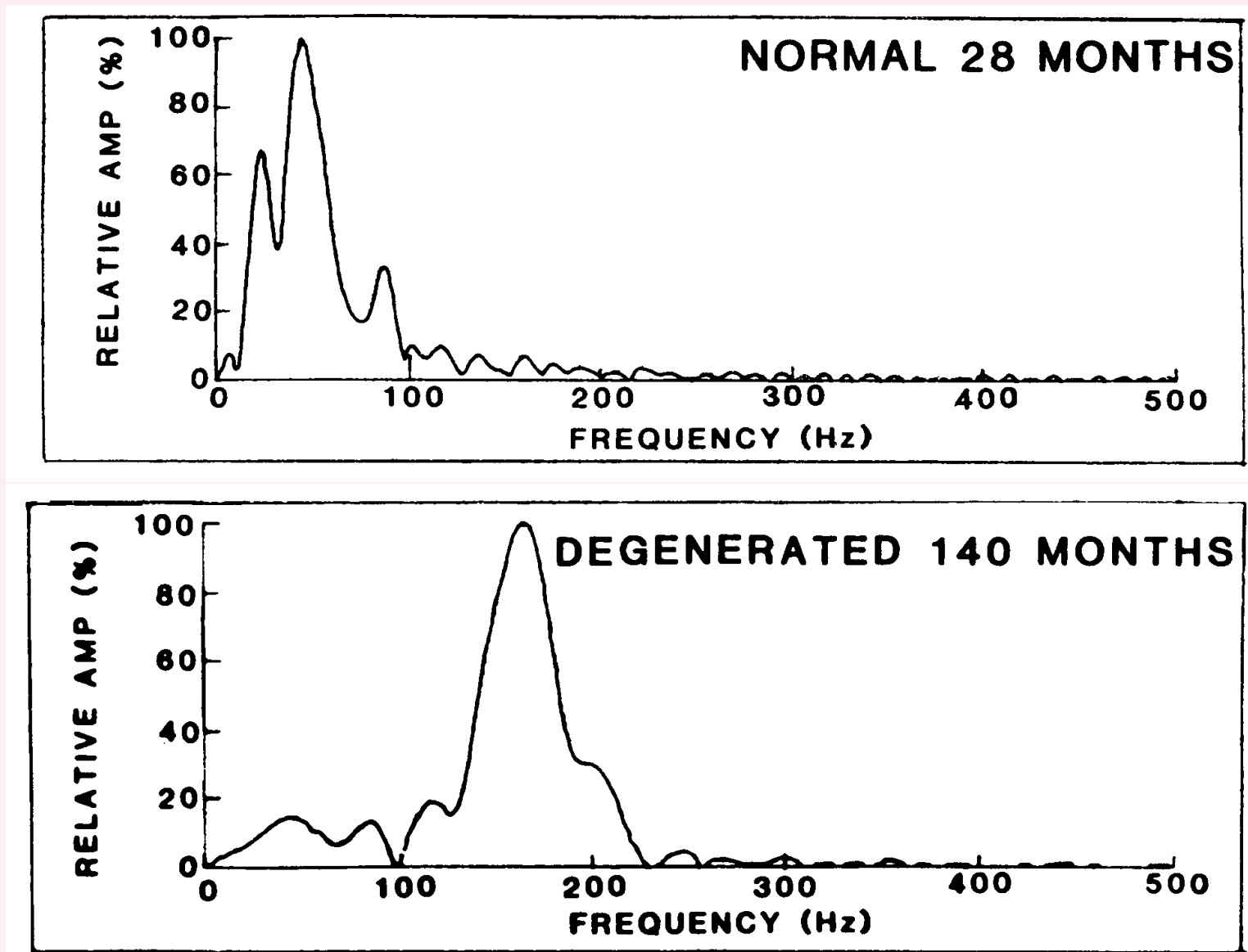
Figure 6.14: First heart sound spectra in the case of normal and degenerated porcine bioprosthetic valves implanted in the mitral position. Reproduced with permission from L.G. Durand, M. Blanchard, G. Cloutier, H.N. Sabbah, and P.D. Stein, Comparison of pattern recognition methods for computer-assisted classification of spectra of heart sounds in patients with a porcine bioprosthetic valve implanted in the mitral position, *IEEE Transactions on Biomedical Engineering,* 37(12):1121–1129, 1990 ©IEEE.

6.6   Application: Fractal Analysis of VAG Signals

Problem: *Knee-joint VAG signals exhibit varying levels of waveform complexity depending upon the state of the cartilage covering the joint surfaces. Given that fractals demonstrate complex patterns depending upon certain parameters, can fractal analysis assist in parametric representation and classification of VAG signals?*

Solution: Normal knee joints with smooth cartilage surfaces produce little sound or vibration.

When the cartilage surfaces are eroded or damaged, additional sounds could be generated.

6.6.1   *Fractals and the* $1/f$ *model*

Wiener's geometric model of physical fractional Brownian motion (fBm) has been used as the basis for algorithms to generate fractals.

The unpredictable variation of a quantity, V, over time, t, is viewed as a noise process, $V(t)$.

The PSD, $P_V(f)$, is used to estimate the power of fluctuations at a given frequency, f, and also of the variations over a time scale of the order of $1/f$.

A time-varying quantity, $V(t)$, with its PSD, $P_V(f)$, varying as $1/f^\beta$, is referred to as $1/f$ noise:

inverse power law or the $1/f$ model.

The PSD of a noise process represented by Brownian motion or random walk varies as $1/f^2$;
the power decreases quadratically with frequency.

The trace of such a signal is a fractal curve.

The FD of the signal related is to the slope, β, of the best fitting line to its PSD on a log–log scale.

fBm models have been extended to 2D for the synthesis of Brownian surfaces and 3D to generate Brownian clouds.

Figure 6.15: examples of signals, $V_H(t)$, generated as functions of an arbitrary time variable, t, using fBm.

The scaling of the traces is characterized by the scaling parameter H, or the Hurst coefficient, $0 \leq H \leq 1$.

High value of H close to 1: a relatively smooth signal.

A lower value of H produces a rougher trace.

Changes in V, $\Delta V = V(t_2) - V(t_1)$, related to differences in the time variable, $\Delta t = t_2 - t_1$, by the scaling law

$$\Delta V \propto (\Delta t)^H. \qquad (6.42)$$
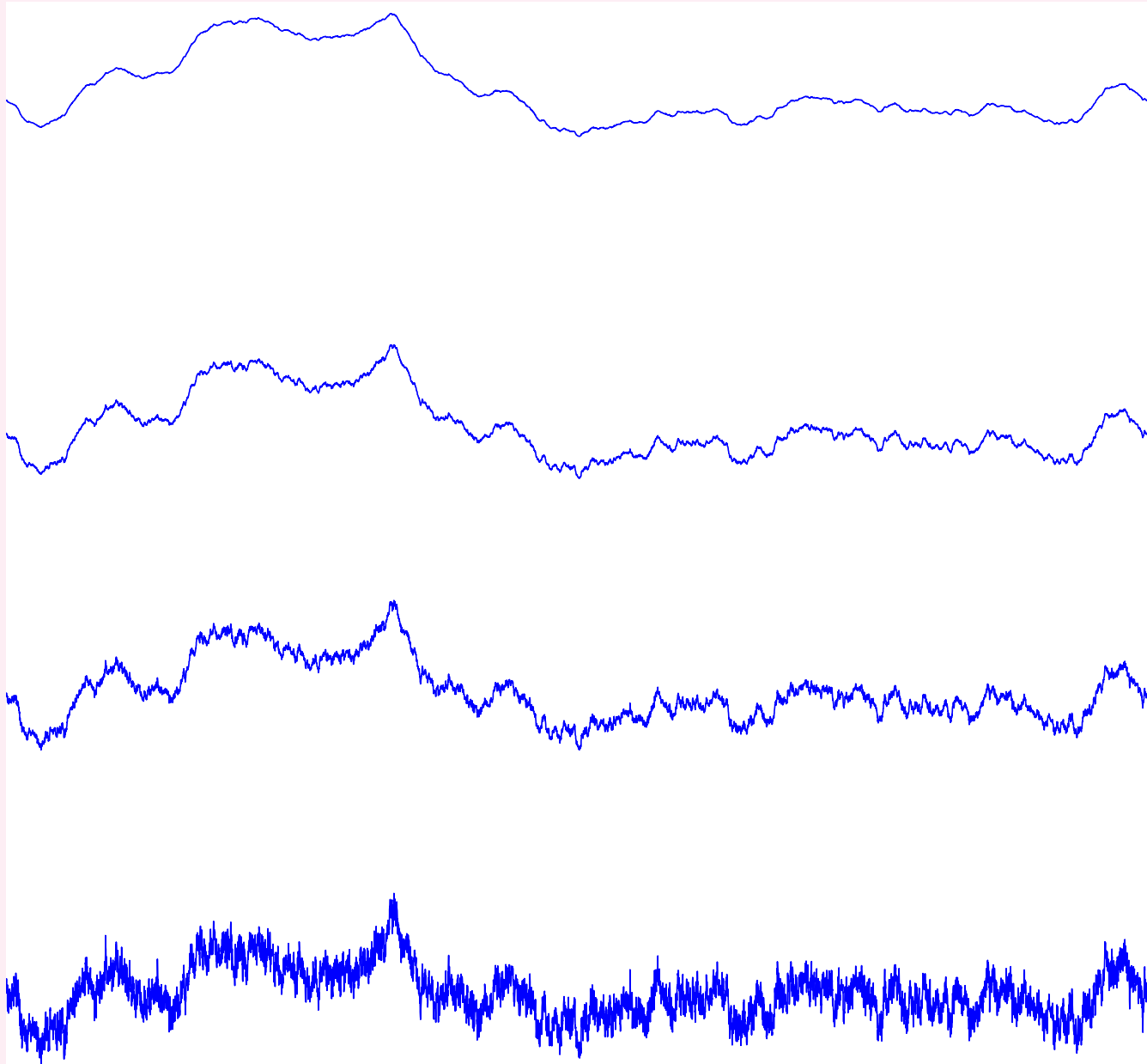
Figure 6.15: Examples of signals generated based on the fBm model for different values of H and FD. Top to bottom: $H = 0.9, 0.6, 0.4, 0.1$; model $FD = 1.1, 1.4, 1.6, 1.9$; estimated $FD = 1.103, 1.401, 1.600, 1.898$. Reproduced with permission from R.M. Rangayyan and F. Oloumi, Fractal analysis of knee-joint vibroarthrographic signals, Proceedings of the 10th IEEE International Conference on Information Technology and Applications in Biomedicine (ITAB 2010), Corfu, Greece, November 2010, pp 1–4. ©IEEE.

Self-similar patterns repeat themselves at various levels of magnification.

fBm traces repeat statistically only when t and V are magnified by different amounts.

If t is magnified by a factor r as rt, the value of V is magnified by the factor r^H and becomes $r^H V$.

Nonuniform scaling of this nature is known as self-affinity.

The zero-set of an fBm signal is the intersection of the signal with the horizontal axis.

The zero-set is a set of disconnected points with a topological dimension of zero and fractal dimension, D_0:

$$D_0 = 1 - H. \tag{6.43}$$

The FD of the signal is related to D_0 as

$$FD = D_0 + 1 \tag{6.44}$$

and to the scaling parameter, H, as

$$FD = 2 - H. \tag{6.45}$$

6.6.2 FD *via power spectral analysis*

A self-affine fBm function in an E-dimensional Euclidean space has its PSD $P_V(f) \propto 1/f^\beta$, with

$$FD = E + 1 - H, \qquad (6.46)$$

where

$$H = \frac{\beta - 1}{2}. \qquad (6.47)$$

The FD, in terms of the spectral component, β, for a 1D signal with $E = 1$, is

$$FD = \frac{5 - \beta}{2}. \qquad (6.48)$$

In the studies of Rangayyan and Oloumi, to estimate β, a Hann window was first applied to the given VAG signal.

The squared magnitude of the DFT of the windowed signal was used to obtain the PSD of the signal.

The slope of the best fitting line to the log–log plot of PSD was then determined.

The frequency range to obtain the linear fit was varied between $[10, 300]\ Hz$ and $[10, 380]\ Hz$.

6.6.3 Examples of synthesized fractal signals

Spectral synthesis by means of inverse Fourier filtering:

If a_k is the kth complex coefficient of the DFT, to obtain $P(f) \propto 1/f^{\beta}$, the condition is

$$E[|a_k|^2] \propto \frac{1}{k^{\beta}}, \qquad (6.49)$$

where k denotes the frequency index corresponding to f.

By randomly selecting coefficients that satisfy the stated condition and then taking their inverse DFT, we can obtain the corresponding signal in the time domain (Figure 6.15).

RMS error between the known and estimated values of FD by PSA for 110 synthesized signals: 0.0198.

With the box-counting method: RMS error $= 0.1387$.

With the ruler method: RMS error $= 0.2243$.

6.6.4   Fractal analysis of segments of VAG signals

The database used by Rangayyan and Oloumi consists of 89 VAG signals; see Section 5.12.1 for details.

Each signal normalized to the amplitude range $[0, 1]$ and resampled to $8,192$ samples by linear interpolation.

PSA method applied to each full VAG signal ($FD1$),

the first and second halves of the normalized duration ($FD1h$ and $FD2h$: extension and flexion),

and four segments with each spanning one quarter of the total duration ($FD1q, FD2q, FD3q,$ and $FD4q$).
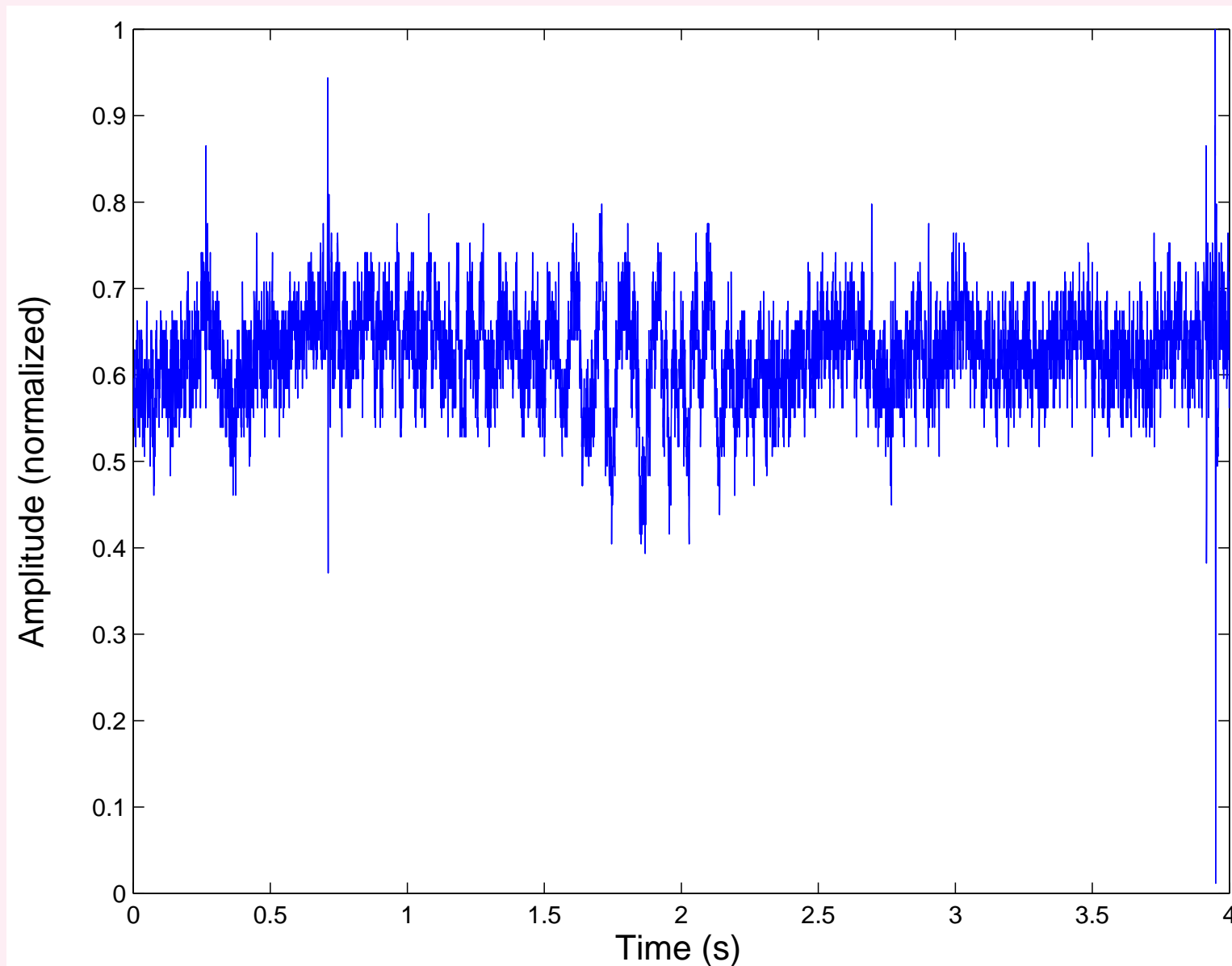
Figure 6.16: Example of a normal VAG signal. Reproduced with permission from R.M. Rangayyan and F. Oloumi, Fractal analysis of knee-joint vibroarthrographic signals, Proceedings of the 10th IEEE International Conference on Information Technology and Applications in Biomedicine (ITAB 2010), Corfu, Greece, November 2010, pp 1–4. ©IEEE.
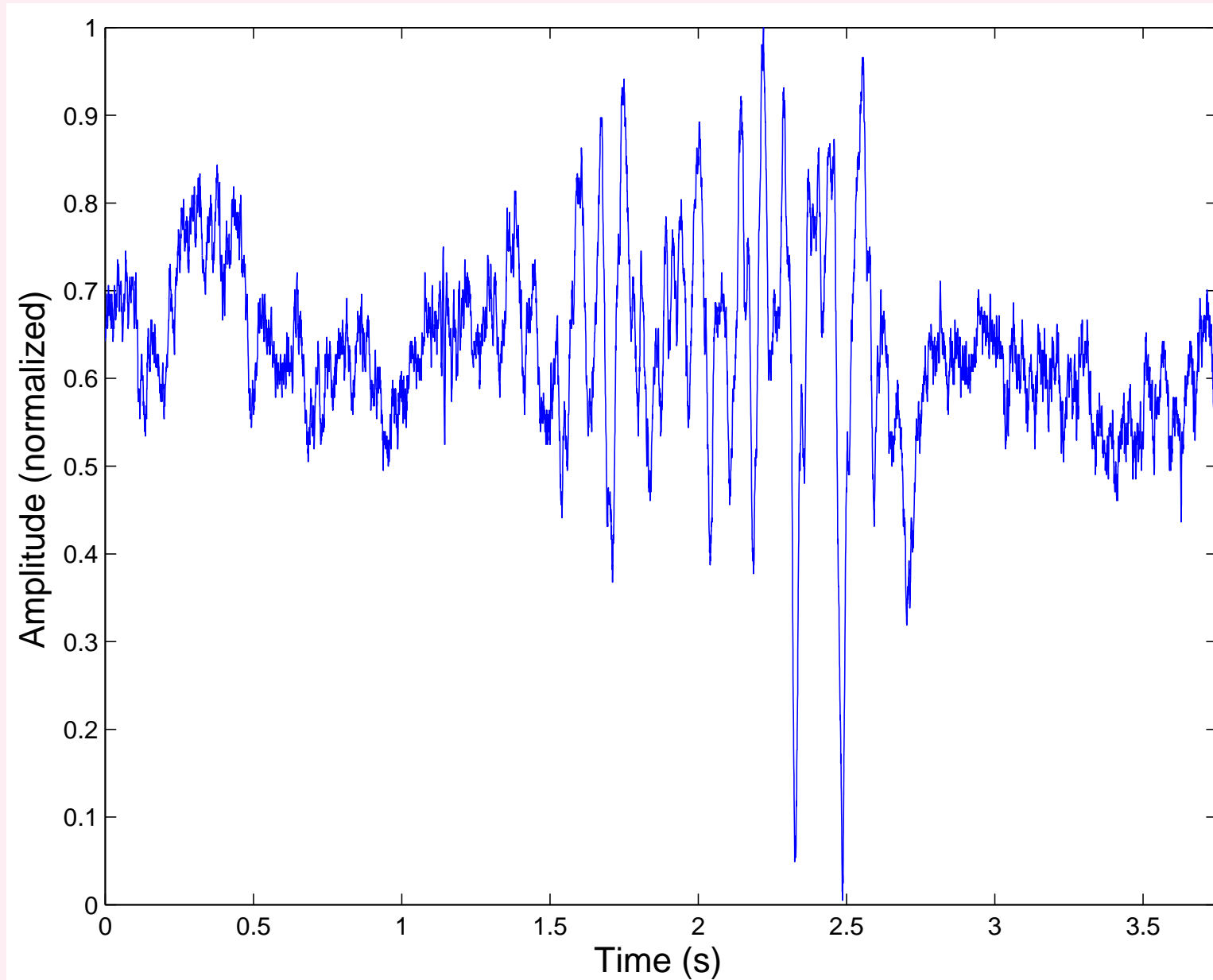
Figure 6.17: Example of an abnormal VAG signal. Reproduced with permission from R.M. Rangayyan and F. Oloumi, Fractal analysis of knee-joint vibroarthrographic signals, Proceedings of the 10th IEEE International Conference on Information Technology and Applications in Biomedicine (ITAB 2010), Corfu, Greece, November 2010, pp 1–4. ©IEEE.

Average and SD of $FD1$ for 51 normal signals:
1.8061 ± 0.2398,

for 38 abnormal VAG signals: 1.6695 ± 0.2226,

$A_z = 0.6872$, using the frequency range $[10, 300] \, Hz$.

With $FD1q$, $FD2q$, $FD3q$, and $FD4q$:

$A_z = 0.6546$, 0.7394, 0.5959, and 0.7023

using the frequency range $[10, 380] \, Hz$.

Combinations of FD with other features: $A_z = 0.92$ to 0.96.

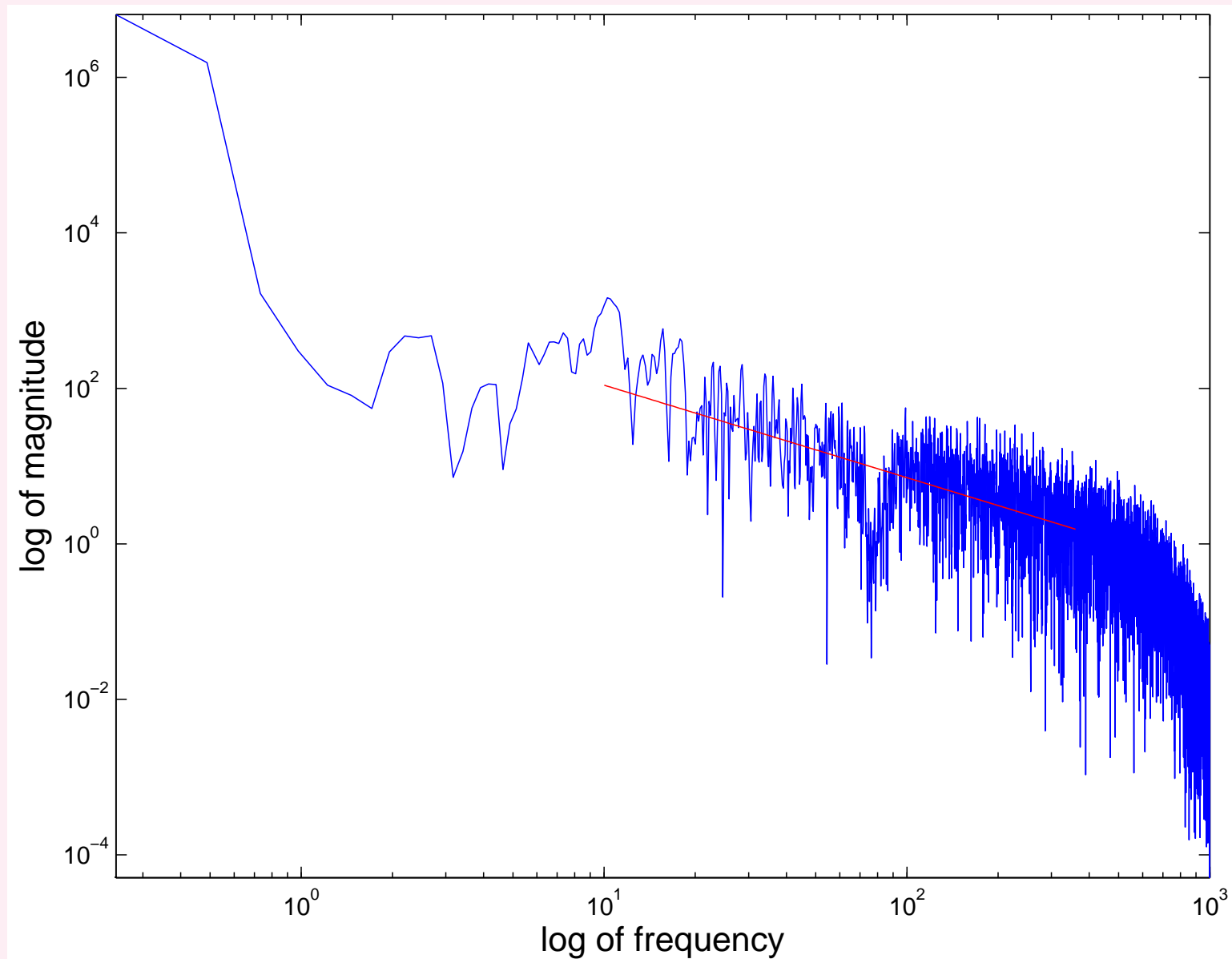Figure 6.18: PSD of the normal VAG signal in Figure 6.16 with the straight-line fit to the range $[10, 360]\ Hz$. $FD1 = 1.905$. Reproduced with permission from R.M. Rangayyan and F. Oloumi, Fractal analysis of knee-joint vibroarthrographic signals, Proceedings of the 10th IEEE International Conference on Information Technology and Applications in Biomedicine (ITAB 2010), Corfu, Greece, November 2010, pp 1–4. ©IEEE.
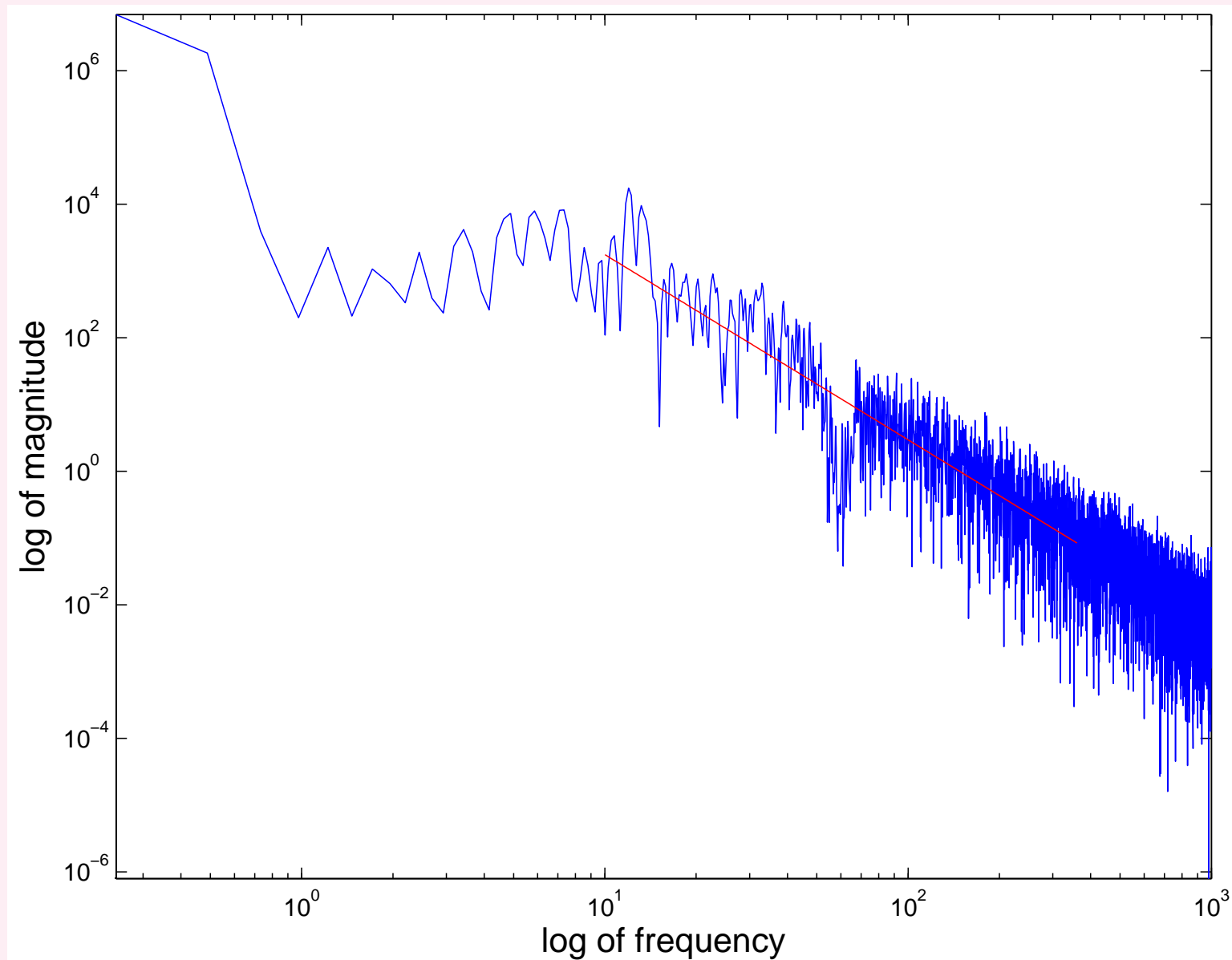
Figure 6.19: PSD of the abnormal VAG signal in Figure 6.17 with the straight-line fit to the range $[10, 360]\,Hz$. $FD1 = 1.113$. Reproduced with permission from R.M. Rangayyan and F. Oloumi, Fractal analysis of knee-joint vibroarthrographic signals, Proceedings of the 10th IEEE International Conference on Information Technology and Applications in Biomedicine (ITAB 2010), Corfu, Greece, November 2010, pp 1–4. ©IEEE.

6.7   Application: Spectral Analysis of EEG Signals

Problem: *Propose methods to obtain quantitative measures to characterize the spectral content of EEG signals and relate them to stages of sleep.*

Solution: A subject with eyes closed and being awake will typically demonstrate alpha waves in the EEG.

As the subject goes to sleep, the EEG rhythms are expected to shift to lower bands of theta and delta rhythms.

Episodes related to rapid eye movement (REM) and sleep spindles could contribute power in frequency bands that are higher than the theta and delta bands.
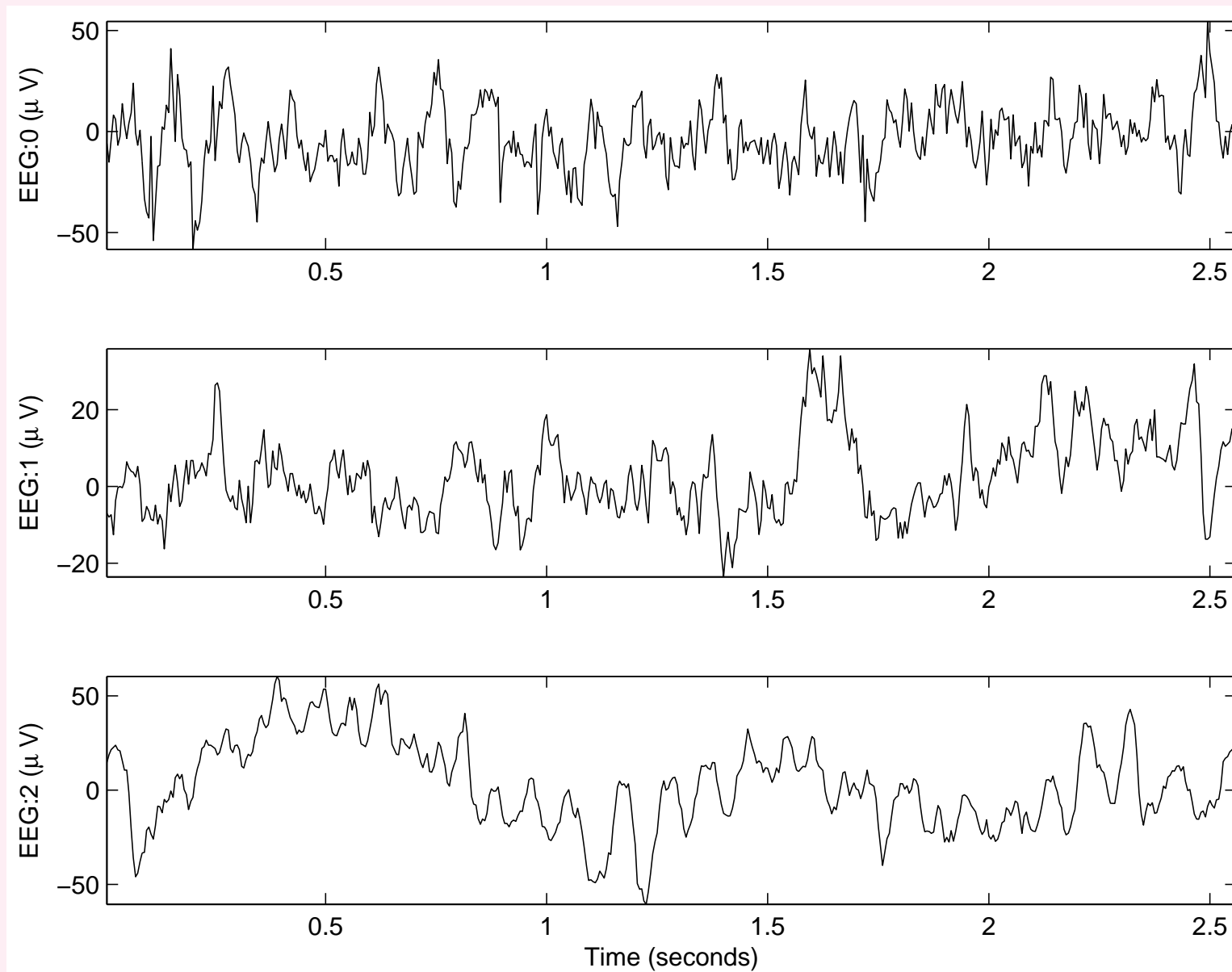
Figure 6.20: Top to bottom: Segments of the C3–A2 EEG channel of a subject during sleep in stages 0, 1, and 2. See also Figure 6.21. EEG data courtesy of R. Agarwal.

Agarwal and Gotman: The amount of low-frequency power in the delta and theta bands in relation to the power in the alpha band is a useful feature in sleep staging.

The Welch method of windowing signal segments and averaging their PSDs was applied to $5,988$-sample segments of the EEG signal.

Nonoverlapping segments of length 512 samples were obtained and the Hann window was applied before computing the DFT.

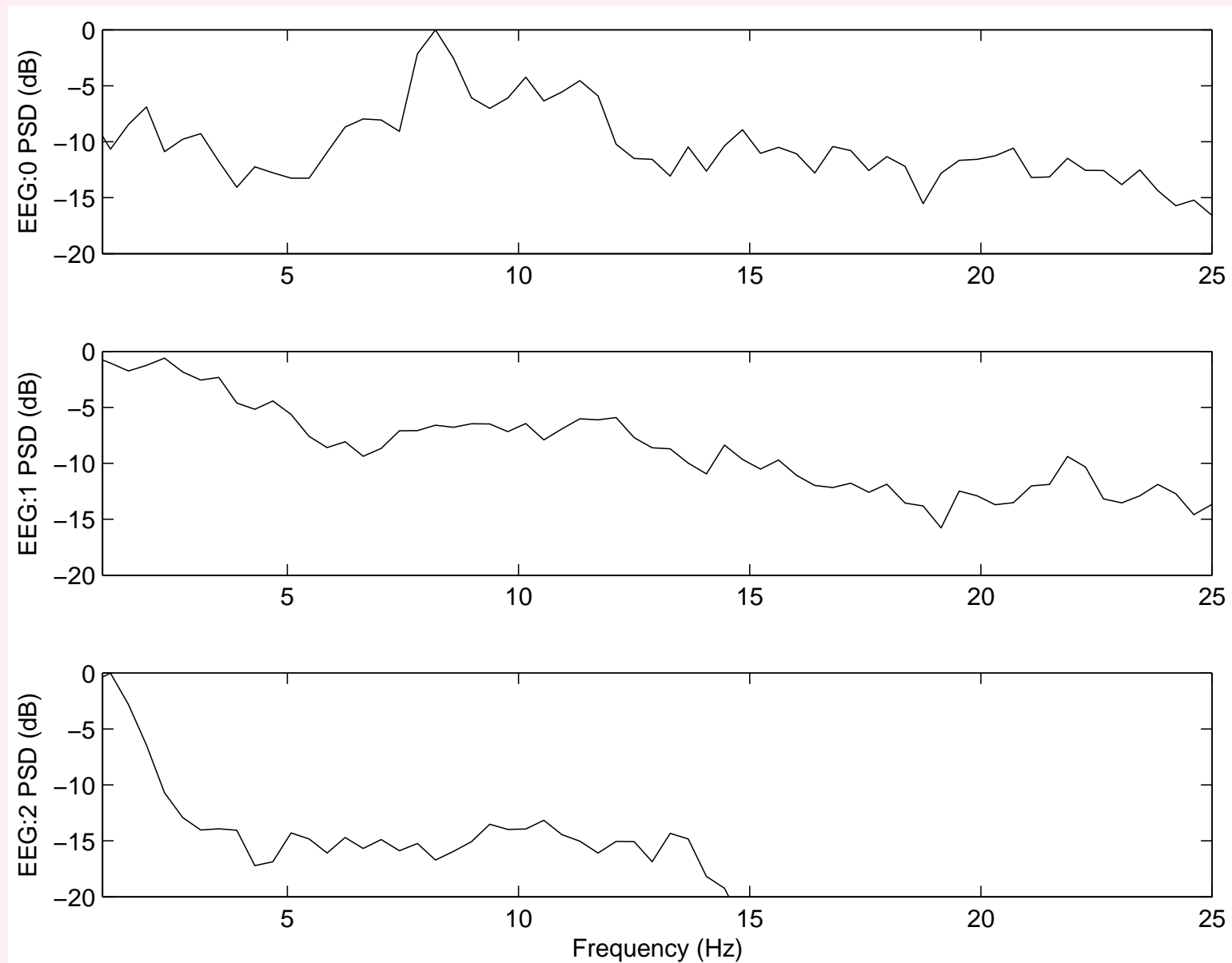The magnitude spectra of 10 segments were averaged.

Figure 6.21: Top to bottom: Average PSDs of segments of the C3–A2 EEG channel of a subject during sleep in stages 0, 1, and 2. Figure 6.20 shows sample segments used in the derivation of the PSDs.

Mean frequencies of the PSDs computed according to Equation 6.30 over $[0, 100]$ Hz.

For the PSDs illustrated in Figure 6.21, the mean frequencies are $20.21, 10.09,$ and 3.98 Hz:

downward trend over the sleep stages of 0, 1, and 2.

Agarwal and Gotman: alpha-to-slow-wave index ASI =

ratio of power in the alpha band (8.0 to 11 Hz) to the combined power in the delta (0.5 to 3.5 Hz) and theta (3.5 to 8.0 Hz) bands.

For the PSDs in Figure 6.21, ASI = $1.68, 0.21, 0.09$.

Figures 6.22 and 6.23 show cluster plots of the mean frequency and ASI for 702 segments of an overnight sleep EEG record with sleep stages of 0, 1, and 2.

Each segment: $5,988$ samples; $29.94\ s$; $f_s = 200\ Hz$.

Total EEG record $= 6\ h$ and $50\ min$.

Sleep stages 3 and 4 not present in the record;

such segments could be expected to possess lower values for the two spectral parameters.

Staging of sleep requires several parameters derived from not only multiple channels of the EEG signal but also additional channels of the EOG and EMG signals.
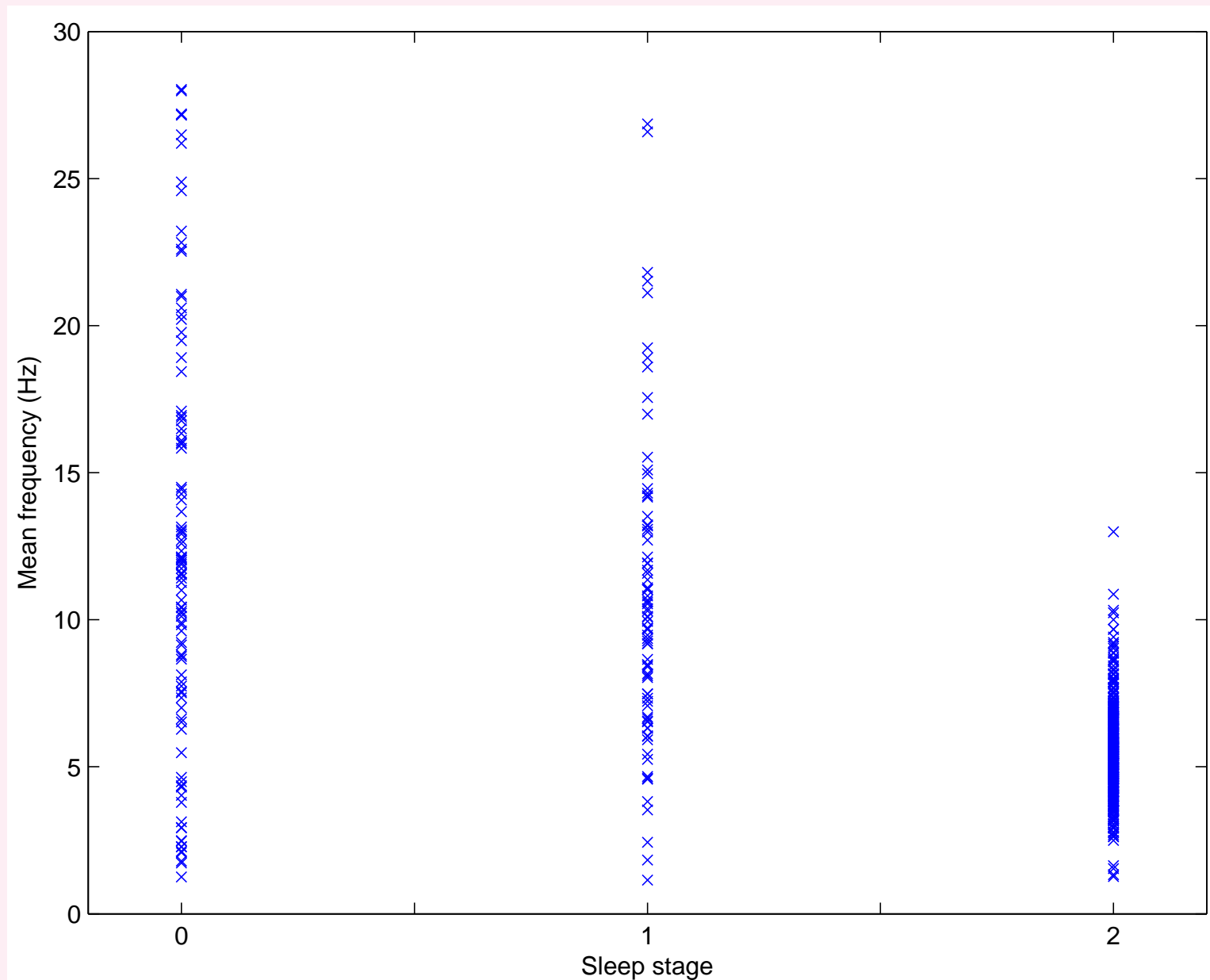
Figure 6.22: Cluster plot of mean frequency values for 702 EEG segments with sleep stages of 0, 1, and 2.
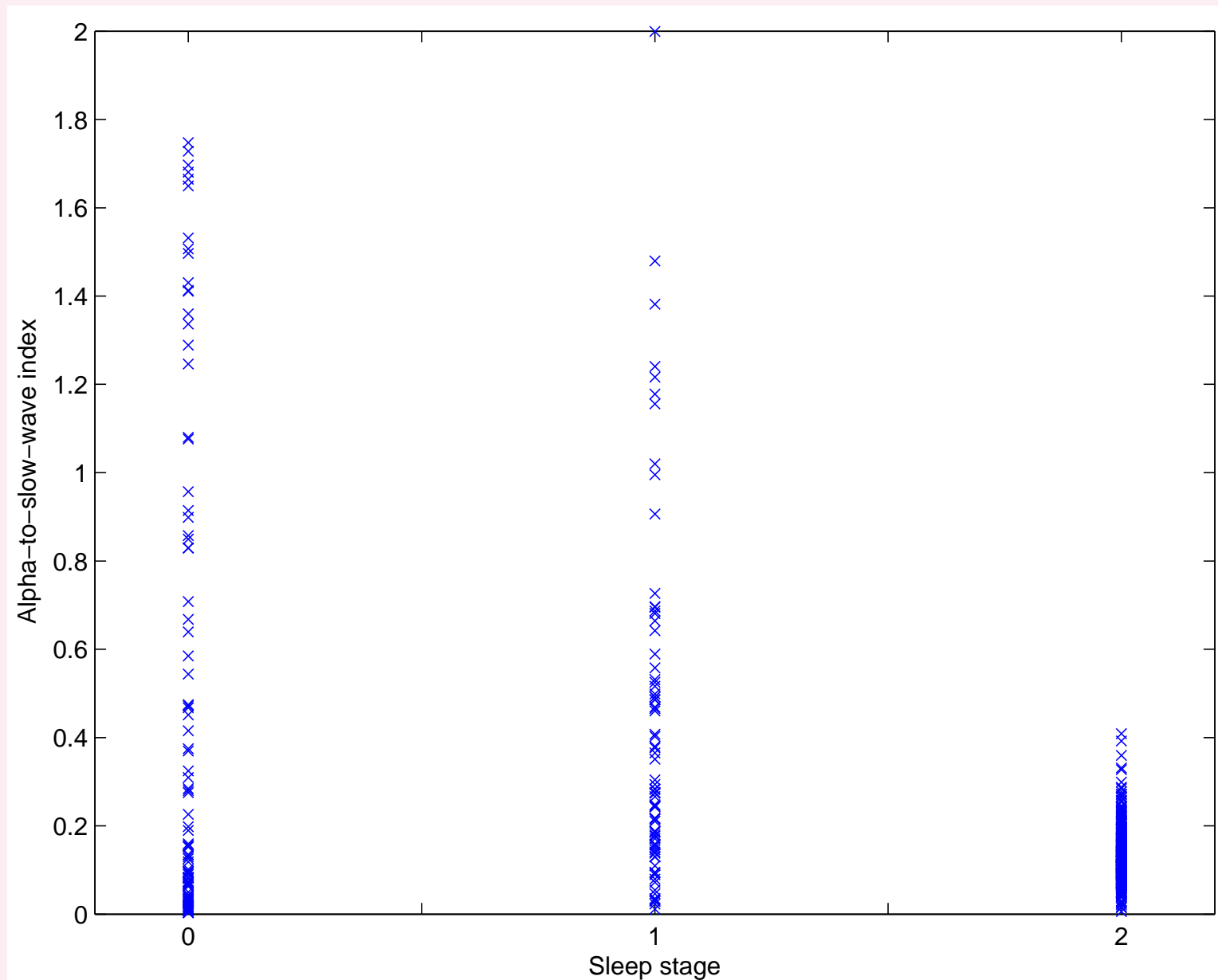
Figure 6.23: Cluster plot of the alpha-to-slow-wave index for 702 EEG segments with sleep stages of 0, 1, and 2.
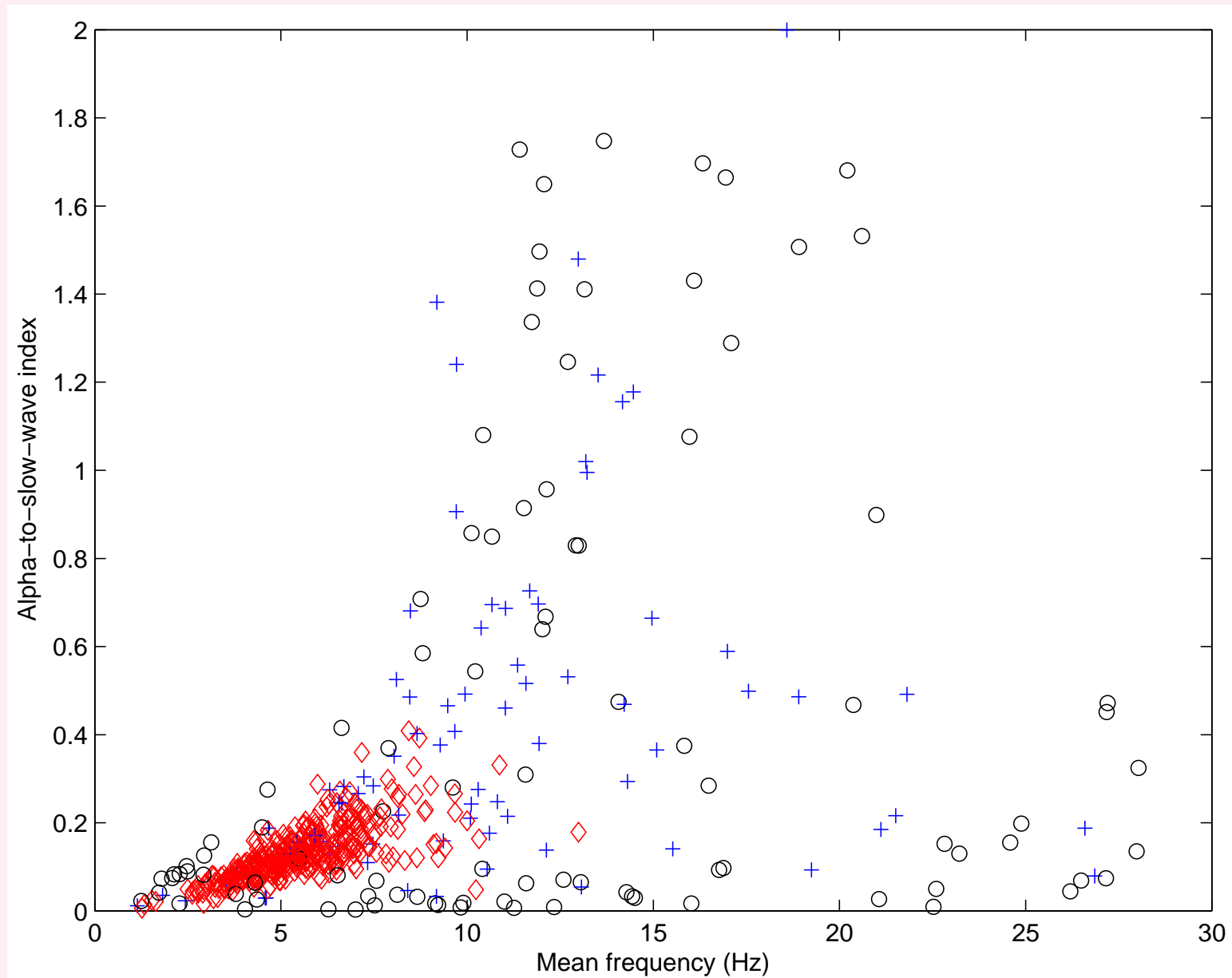
Figure 6.24: Cluster plot of the mean frequency and alpha-to-slow-wave index (ASI) for 702 EEG segments with sleep stages of 0 ('○' mark), 1 ('+' mark), and 2 (diamond mark).

6.8   Remarks

PSDs and their parameters enable us to view a signal from a different perspective than the time domain.

Signals that are not easy to interpret in the time domain may benefit from a move to the frequency domain.

PSDs and their parameters facilitate investigation of rhythms, resonance, and parameters that could be related to the physical characteristics of anatomical entities:

loss of elasticity of the myocardial muscles due to ischemia or infarction, the extent of aortic valvular stenosis, or the extent of calcification and stiffness of bioprosthetic valves.